MICROTUBULE REGULATION OF MITOCHONDRIAL BIOENERGETICS IN CARDIAC AND SKELETAL MUSCLES

SOFHIA VERENA RAMOS

A DISSERTATION SUBMITTED TO THE FACULTY OF GRADUATE STUDIES IN PARTIAL FULFILMENT OF THE REQUIREMENTS FOR THE DEGREE OF

DOCTOR OF PHILOSOPHY

GRADUATE PROGRAM IN KINESIOLOGY AND HEALTH SCIENCE
YORK UNIVERSITY
TORONTO, ONTARIO

July 2019

Abstract

A novel model of mitochondrial bioenergetic regulation has been proposed whereby microtubules may directly influence the permeability of ADP into the mitochondria to stimulate the production of ATP. Specifically, tubulin, the structural unit of microtubules, physically inserts into the voltage gated dependent anion channel (VDAC) embedded in planar lipid membranes which was speculated to prevent ADP/ATP cycling. Such regulation could be profound given ADP/ATP cycling kinetics determine the rate of oxidative phosphorylation and reactive oxygen species (ROS) emission – key mitochondrial functions that are critical to muscle cells. VDAC is also believed to be central to the formation of the mitochondrial permeability transition pore (mPTP) which releases pro-apoptotic factors that trigger cell death. To date, a direct measure of a tubulin-VDAC interaction has yet to be demonstrated in cardiac and skeletal muscles, particularly in relation to mitochondrial bioenergetics.

The primary objective of this thesis was to explore the tubulin-VDAC model of mitochondrial bioenergetic regulation in cardiac and skeletal muscles. This was achieved by employing pharmacological and genetic models of microtubule disorganization in an attempt to alter tubulin-VDAC interactions in relation to mitochondrial dysfunction. The results demonstrate that *in-vitro* paclitaxel treatment in extensor digitorum longus (EDL) muscle increases both α- and βII-tubulin-VDAC2 interaction while impairing some mitochondrial functions in partial support of the tubulin-VDAC model. The remaining data challenges this model. Specifically, cardiac muscle demonstrated a host of bioenergetic impairments *in-vitro* independent of a change in tubulin-VDAC interaction, while *in-vivo* treatment with paclitaxel, and vinblastine resulted in creatine independent mitochondrial impairments. Second, *in-vivo* paclitaxel administration surprisingly increased hind-limb torque and βII-tubulin-VDAC2

interaction in soleus while eliciting minor inhibitions of ADP-dependent bioenergetic functions. In contrast, *in-vivo* administration of vinblastine caused muscle weakness and mitochondrial dysfunction in both soleus and white gastrocnemius, but did not change tubulin-VDAC2 interactions. Lastly, EDL muscles isolated from D2.*mdx* mouse model of disorganized microtubules and muscle weakness did not show altered tubulin-VDAC interactions despite the presence of mitochondrial dysfunctions. Overall, this thesis is the first to identify a direct α- and βII-tubulin interaction with VDAC2 in cardiac and skeletal muscle. While the data presented are not always in support of this model it raises new questions that challenges the regulation of this physical interaction in ADP diffusion regulation.

Acknowledgements

Writing this thesis has been one of the most challenging and rewarding things that I have done in my academic career. None of this would have been possible without the support, guidance and friendship of my peers, friends and family. I feel very blessed and grateful for the love and support I've received throughout this entire degree and would like to take the time to acknowledge some of the people that have made this possible.

First and foremost, I'd like to thank my supervisor Christopher Perry. The first time I saw your presentation at OEP back in 2012 I knew that working with you would be an exciting roller-coaster ride. Thank you for your patience and guidance throughout the years. Even if I don't know much about mitochondria, I'll have a couple of good dad jokes in my back pocket. My experience in the Perry lab wouldn't have been the same without my amazing lab mates. During those long experimental days, staring at lines on screens I'm grateful to have had the company of Meghan Hughes. From all those Netflix shows we watched to our epic Easter Sunday pizza dinner, I wouldn't have wanted to share that with anyone else. To Patrick Turnbill, I honestly do think that we will eventually, through some feat of magic, end up working together again. Thank you for being a good friend and always lending an ear whether I want to vent about spilling an entire dish of newly isolated fibers all over the lab bench or discuss the newest nail fashion.

Secondly, I'd like to thank the amazing groups of friends I have. One of the attractive things about research is the amazing people you meet. From completing our MSc's and through PhD's/physiotherapy school, Paula, Laura, Kirsten and Leslie, thank you for always being there to talk science or just randomness when the science stops making sense. Also, to Phylicia, Shylo, and Miriam, thank you for listening to me spew incomprehensible science jargon over the last 7 years. Watching all of you ladies achieve your own individual goals has been motivational to me too. The support system we have created has tremendously helped me keep my cool when I feel like pulling all my hair out.

Lastly, I'd like to thank my family. I feel like the luckiest girl in the world to have the most supportive mother and grandmother; words cannot describe the gratitude I have to you both for your prayers and comfort throughout these 7 years of graduate school. To know what true love is, is to have your mother read your entire 200+ MSc and PhD theses, publications and listen to countless presentations about mitochondria and chemotherapy drugs with excitement. Thank you, mom, for all of your help, and your company, the long drives to St. Catherine's, 4am drop off to Pearson airport for conferences… I can't even list everything but I'm so grateful for everything you've done and continue to do. Any success I attain is because of the faith you both have in me. Also, to Micheal, Sara and Ashley, thank you for being the best siblings (sibling-in-law) anyone can ask for.

Table of Contents

List of tables

List of Figures

List of Supplemental figures

List of abbreviations

ADP	Adenosine diphosphate
ANT	Adenine nucleotide translocase
ATP	Adenosine triphosphate
Ca^{2+}	Calcium
Cr	Creatine
ctCK	Cytosolic creatine kinase
cyt c	Cytochrome c oxidase
DMD	Duchene muscular dystrophy
D2.mdx	mouse model of Duchene muscular dystrophy
e-	Electron
FDB	Flexor digitorum bravis
H+	proton
H_2O	Water
H_2O_2	Hydrogen peroxide
IMM	Inner mitochondrial membrane
IMS	Intermembrane space
O_2-	Superoxide
OMM	Outer mitochondrial membrane
OXPHOS	Oxidative phosphorylation
mPTP	Mitochondiral permeability transition pore
mtCK	Mitochondrial creatine kinase
PCr	Phosphocreatine
Pi	Inorganic phosphate
PLA	Proximity ligation assay
PmFB	Permeabilized muscle fiber bundle
ROS	Reactive oxygen species
VDAC	Voltage dependent anion channel
WT	Wild type

Introduction

Muscle is a very plastic tissue, able to adapt to various physiological conditions. This plasticity is partially due to the proper functioning of the mitochondria. Commonly known as the power house of the cell, mitochondria are primarily responsible for maintaining cell survival through the production of adenosine triphosphate (ATP), influencing cellular redox state through reactive oxygen species generation, or triggering cell death through the initiation of apoptosis. These cellular fates are governed, in part, by the ability of adenosine diphosphate (ADP) to permeate the outer-mitochondrial membrane (OMM) allowing its phosphorylation into a high energy ATP molecule, the energy 'currency' of the cell. ADP drives membrane potential-dependent oxidative phosphorylation which in turn determines the balance of reactive oxygen species (ROS) emission. ADP is able to cross the OMM through a channel protein embedded in the OMM known as the voltage dependent anion channel (VDAC). The process of ADP diffusion through the OMM was initially believed to be quite simple due to the abundance of pore proteins embedded in the OMM. A considerable amount of research has now highlighted the complexity of this process which may be regulated through various mechanisms.

In 1995, a new model was proposed which suggested that a cytoskeletal component could regulate mitochondrial ADP permeability (136). Through transmission electron microscopy, it was later discovered that tubulin, the dimeric component of microtubules, existed in close association with the mitochondria (20, 127). Since then, researchers have uncovered that the C-terminal tail (CTT) of tubulin physically inserts itself into VDAC, where phosphorylation, post-translational modifications or changes to mitochondrial membrane lipid composition, can influence tubulin-VDAC binding (125, 145). To date, the majority of this work has been completed using reconstructed planar lipid membranes. While this methodology is a great

physiological tool aiding the molecular understanding of this interaction, it places these proteins in isolation and therefore not mimicking the interactions between tubulin and VDAC that may occur under *in-vivo* conditions. Other groups examined this model using approaches that either removed tubulin by treating samples with trypsin, a non-specific protease, resulting in increased ADP-stimulated respiration or added tubulin to isolated mitochondrial preparations decreasing respiration, both highlighting the importance of tubulin regulation ADP permeability (40, 127). This introduces some limitations the understanding of the tubulin-VDAC model given the degree of mitochondrial-microtubule interactions are not preserved in these approaches nor was tubulin targeted specifically with general proteases.

To mitigate these limitations, the work completed in this thesis utilized *in-vitro* and *in-vivo* methodologies that better retained microtubule networks and mitochondrial morphology. In addition, pharmaceutical and genetic models of altered microtubule architectures were employed in an attempt to further reveal the contribution of the tubulin-VDAC model to mitochondrial bioenergetics in muscle. The pharmaceutical approach of applying microtubule stabilizers (paclitaxel) and destabilizers (vinblastine) to single fibres *in-vitro* or administered *in-vivo* will promote polymerization or depolymerisation of microtubules respectively. Interestingly, these microtubule targeted compounds are commonly used chemotherapies, which creates an intriguing opportunity to apply the tubulin-VDAC model of bioenergetic regulation to understand how microtubule-targeting chemotherapy may disrupt normal muscle metabolism. Concomitantly, this work will aid in determining the degree to which microtubule organization fundamentally regulates ADP-dependent mitochondrial bioenergetics in muscle. Considerations of muscle type and the effects of *in-vitro* vs *in-vivo* administration were considered in the experimental design (Chapters 4-7).

To further examine the contribution of the tubulin-VDAC model to mitochondrial bioenergetic regulation in muscle, this thesis utilized a model that is known to have a disorganized microtubule architecture. Duchenne muscular dystrophy is an X-linked disease characterized by the lack of dystrophin in the sarcolemma (5, 18). Dystrophin is required to anchor the intracellular and extracellular structural components of the cell, which includes microtubules (111). The disorganization of microtubules in the mouse (*mdx*) model of Duchenne muscular dystrophy is speculated to contribute to the intracellular impairments seen with this disease (111). Our lab has previously shown sever mitochondrial and whole muscle dysfunction in cardiac and skeletal muscles from a more severe mouse model of Duchenne muscular dystrophy (D2.*mdx*) (51, 52). What remains unknown is the contribution of an altered tubulin-VDAC interaction to these impairments in ADP-dependent mitochondrial bioenergetics.

These pharmacological and genetic models of altered microtubule organization represent new approaches to study the fundamental role of the tubulin-VDAC model and its contribution to mitochondrial bioenergetics in muscle, and may represent novel mechanisms to explain how disrupted muscle metabolism occurs in response to microtubule-targeting chemotherapy and in Duchenne muscular dystrophy. The main aims of this thesis are to 1) determine whether α-tubulin and βII-tubulin interact with VDAC2 in cardiac and skeletal muscles in rodent models 2) determine whether alterations in microtubule organization changes the amount of tubulin-VDAC interactions *in-vivo* and *in-vitro,* 3) determine whether mitochondrial bioenergetic changes are related to tubulin-VDAC model and lastly 4) relate mitochondrial bioenergetic changes to whole muscle functional capacity.

2. Literature Review

2.1 Overview of mitochondrial bioenergetics

2.1.1 Oxidative phosphorylation

Originally believed to be rod-shaped structures, mitochondria are composed of an outer mitochondrial membrane (OMM) containing specialized proteins and channels that regulate the transport of metabolites into the mitochondria and an inner mitochondrial membrane (IMM) where adenosine triphosphate (ATP) synthesis occurs. Between the OMM and the IMM is the inter mitochondrial membrane space (IMS) and in the center of the mitochondria is the matrix where metabolites are further reduced into reducing equivalents used as substrates for ATP synthesis. This was first proposed as the chemiosmotic theory, written by Dr. Peter Mitchell who elucidated the process of oxidative phosphorylation (87). Up until that point, researchers had already determined ATP to be the energy currency of the cell but the mechanism was unknown.

The production of ATP is completed through a series of redox reactions through the mitochondrial respiratory chain (OXPHOS) proteins embedded in the IMM (97) (Figure 2-1). The mitochondrial respiratory chain is composed of 5 complexes: complex I (NADH-UQ oxidoreductase), complex II (succinate dehydrogenase), complex III (UQH_2-cyt c oxidoreductase), complex IV (cytochrome c oxidase) and complex V (ATP synthase). The foods we consume (carbohydrates/sugars or fats) are taken up by the cell and broken down through glycolysis and β-oxidation to produce the high energy reducing equivalents NADH and $FADH_2$. These reducing equivalent then interact with complex I (NADH) or complex II ($FADH_2$) pumping protons through into the inter membrane space while simultaneously donating electrons that are passed through complexes I-IV to make H_2O at complex IV. The donation of electrons across the IMM creates a negative charge in the matrix of the mitochondria while the process of

pumping protons through to the inter mitochondrial membrane space creates the proton motive force. Protons that accumulate in the IMS create potential energy that is utilized by the motor of complex V allowing the phosphorylation of an ADP molecule to produce ATP.

$$ADP + Pi \text{ -----> } ATP$$

The transfer of electrons and proton motive force are predominately maintained by the concentration of adenosine diphosphate (ADP). ADP and Pi are the primary determinants of ATP synthase permeability to protons such that their kinetic concentrations dictate oxidative phosphorylation where a linear relationship exists between the amount of ADP provided and ATP produced (75). In a state of reduced [ADP], the proton motive force or membrane potential is increased slowing down the rate of ATP production and in turn, slows down the rate of electron transport. This can result in electrons slipping off complexes I and III, prematurely interacting with oxygen to produce superoxide (122). Also known as a reactive oxygen anion (O_2-), superoxide is highly reactive, capable of damaging proteins and cell membranes, ultimately leading to cell death. Understanding how ADP/ATP is transported through the mitochondria is crucial to understand how various metabolic states promote cell death or survival. The voltage dependent anion channel (VDAC) embedded in the OMM and adenine nucleotide translocase (ANT) embedded in the IMM are the two proteins responsible for the diffusion of ADP/ATP through the mitochondria and will be further discussed below (Section 2.2)

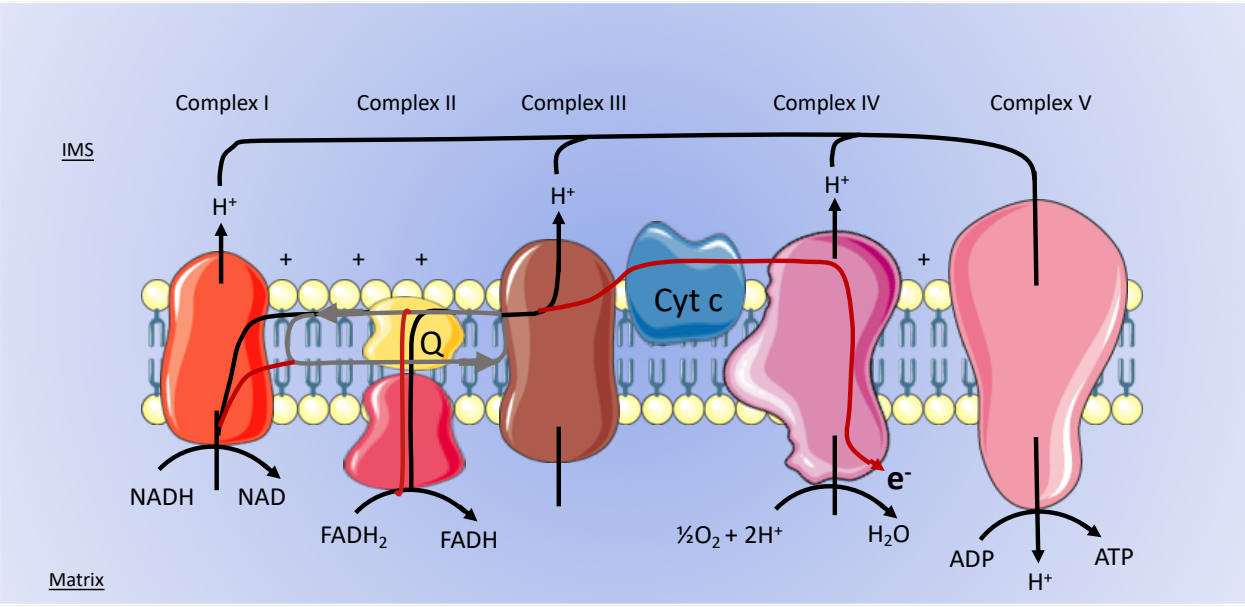

Figure 2-1. Schematic depiction of the mitochondrial electron transport chain. Embedded in the inner mitochondrial membrane (IMM) are complex I (NADH-UQ oxidoreductase), complex II (succinate dehydrogenase), Ubiquinone (Q), complex III (UQH_2-cyt c oxidoreductase), and complex IV (cytochrome c oxidase) where protons (H+) are pumped through to the intermembrane space (IMS) and electrons (e-) travel through the complexes. At complex V (ATP synthase), protons are pumped back into the mitochondrial matrix to make ATP.

2.1.2 Mitochondrial reactive oxygen species production and emission

A natural by-product of oxidative phosphorylation is the generation of reactive oxygen species (ROS) in the form of superoxide (O_2^-), a membrane impermeable, unstable, highly reactive free radical capable of reducing proteins, rendering them dysfunctional (1). A major source of free radical production occurs in the mitochondria where there are 11 reported sites of O_2- emission (172). In the absence of ADP, reducing equivalents continue to supply complexes with protons and electrons but do not complete oxidative phosphorylation. This results in an accumulation of protons in the IMS, decreasing the proton motive force, increasing the chances of an electron slip which in turn produces O_2-. Fortunately, mitochondria are equipped with endogenous superoxide dismutases to quickly scavenge O_2- free radicals, such as manganese superoxide dismutase (MnSOD), copper-zinc superoxide dismutase (CuZnSOD), both located within the mitochondrial matrix. These dismutases function to donate protons to O_2- to produce hydrogen peroxide (H_2O_2). While H_2O_2 is a type of ROS, it is a stable non-radical oxidant, able to permeate through lipid membranes and is an integral signaling molecule responsible for maintaining intracellular redox balance (30, 59). This is of particular interest as most experimental methods of measuring O_2- production can be done indirectly through the measurement of H_2O_2 emission, providing an overall redox status of the cell. When the amount of ROS produced exceeds the antioxidant capacity, the cell is considered to be in a state of oxidative stress. This can occur under pathological conditions where the rate ROS emission no longer functions for signaling purposes but can now damage intracellular proteins and organelle membranes leading to cell death. This is coupled with an decreased capacity for endogenous antioxidant systems (catalase, glutathione, thioredoxin) to buffer the increased ROS generation (59).

2.1.3 Energy transfer through cytosolic and mitochondrial creatine kinase

Cells in high energy demanding tissue such as the liver, brain, heart and skeletal muscles do not contain a reserve of ATP waiting on demand to be utilized. If depleted, this would result in a massive accumulation of metabolites and protons that would negatively impact the metabolic equilibrium. In order to provide and maintain an adequate energy balance, phosphagens are used to buffer intracellular energy. More specifically, creatine (Cr), and phosphocreatine (PCr) work with creatine kinase (CK) acting as an intracellular energy buffering system (Figure 1-3). This "system" is strategically placed in energy consuming locations within the cell to efficiently transport energy to its utilization sites and buffers the resulting metabolites to produce energy as needed. This is known as the creatine kinase system (165). There are various CK isoforms expressed in different quantities and locations depending on the tissue type and needs (166). In cardiac and skeletal muscle, the two predominate isoforms are cytosolic CK (ctCK) and mitochondrial CK (mtCK). mtCK is an octameric protein found embedded in between the IMM and OMM, attached to cardiolipin and indirectly attached to ANT on the IMM (72, 165) spanning the IMS, interacting with VDAC on the OMM (72, 140, 165). Together they catalyze the transfer of phosphates in the following reaction:

$$MgADP + PCr + H^+ \leftrightarrow MgATP + Cr \quad (165)$$

This is known as the more efficient method to transport energy through the mitochondrial membranes. Alternatively, ADP can passively diffuse through both VDAC and ANT to stimulate ATP production in a more inefficient manner. In the absence or inhibition of CK, ADP diffusion still occurs just at a significantly lower rate, reducing functional capacity which is exemplified by a recorded reduce sea urchin sperm flagellar motility further outlined below (155) (Figure 2-3).

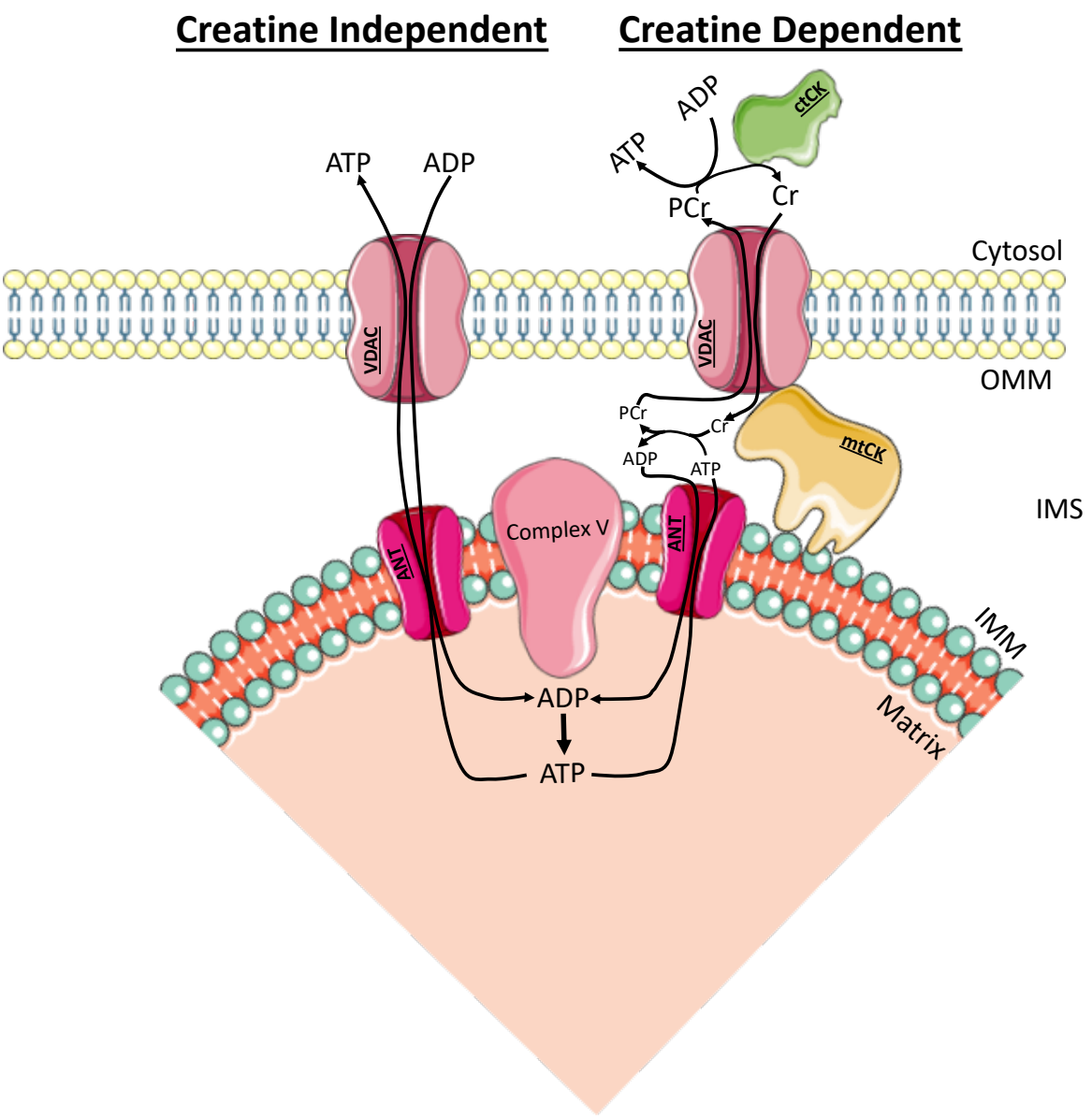

Figure 2-2. Creatine independent and dependent pathways of ADP/ATP transport through the mitochondria. Creatine independent pathway: Production of ATP at Complex V can directly diffuse through ANT and VDAC to the cytosol where ATP is utilized by various ATPases, generating ADP that can then diffuse back through VDAC and ANT providing ADP to complex V to maintain the production of ATP. Creatine dependent pathway: ATP produced at complex V is shuttled through ANT to the IMS where mtCK catalyzes the transfer of ATP's high energy phosphate to a Cr molecule creating PCr). PCr is then shuttled out through VDAC to ctCK where the high energy phosphate is transferred to an ADP molecule making ATP which can then be utilized by ATPases. The resulting Cr is shuttled back through VDAC to mtCK where the high energy phosphate transfer cycle occurs again (51, 52, 141).

2.1.4 Energy transfer through the mitochondrial interactosome

There is evidence that mitochondrial respiratory control, in cardiac cells, is regulated by the mitochondrial interactosome consisting of; ctCK located in the cytosol, outside of the mitochondria, VDAC embedded in the OMM with tubulin on the cytosolic side, mtCK anchored in the IMS, ANT embedded in the IMM and the proteins of the electron transport chain (OXPHOS), also embedded in the IMM (153). These mitochondrial interactosomes are believed to be situated in specific locations throughout the cell were energy is utilized forming intracellular energy units (ICEU) (134). While the majority of the work exploring ICEU's were completed in cardiac tissue, the same principles can be applied to skeletal muscles as mitochondria, mtCK and tubulin all appear to co-localize with muscle contractile units in a fiber type and tubulin isoform dependent manner (161).

The mitochondrial interactosome describes a model whereby reducing equivalents provide protons to the OXPHOS proteins generating free energy to drive motor of complex V, producing ATP which is then shuttled out into the IMS through ANT. The high energy phosphate on ATP is then transferred to a Cr molecule by CK, allowing the resulting ADP to cycle back through ANT to be re-phosphorylated in the matrix. The resulting PCr molecule is then shuttled out through VDAC on the OMM, interacting with ctCK catalyzing the transfer of the high energy phosphate from PCr onto an ADP yielding an ATP molecule that can then be used to provide energy to neighbouring ATPases. ADP and Cr is then quickly shuttled back into the IMS through VDAC where the entire cycle begins again (Figure 2-3).

As mentioned above this method of phosphate shuttling has been shown to be a more efficient way of transferring ATP through the double membranes of the mitochondria when compared to the diffusion of ATP and ADP alone. For this system to work effectively,

mitochondrial membrane potential needs to be maintained as prolonged VDAC closure will prevent ADP permeability, increasing membrane potential, which in turn increases the potential for ROS emission which can ultimately lead to mitochondrial dysfunction. Alternatively, if VDAC is maintained in an open confirmation, membrane potential will eventually dissipate also leading to mitochondrial dysfunction. Tubulin has been shown to be involved in the maintenance of membrane potential and therefore ADP permeability through the reversible closure of VDAC but the complete elucidation of how this occurs is currently unknown.

2.2 Proteins involved in ADP/ATP diffusion

2.2.1 Adenine Nucleotide Translocase (ANT)

ANT is a specialized protein embedded in the IMM responsible for the export of newly synthesized ATP and import of ADP from the cytoplasm to complex V. The kinetics of ATP/ADP cycling between mitochondria and cytoplasm are therefore determined, in part, by ANT permeability to these nucleotides on the inner mitochondrial membrane. In addition to its role in energy production, ANT is believed to contribute to mitochondrial proton leak or uncoupling where ANT1 knockout mice display a significant reduction in proton conductance in addition to a significant decrease in oxygen consumption (17). Although the mechanism of ANT's contribution to uncoupling remains unknown, a host of literature presents its importance for energy exchange. ANT is one of the most abundant proteins in mitochondria. Inhibition of ANT with carboxyatractyloside inhibits ATP transport by binding to the channel and blocking ATP/ADP diffusion in mitochondria isolated from cardiac tissue, outlining the importance of ANT in ADP supply (91).

There are 4 ANT isoforms all expressed in most tissue types (with the exception of ANT4) with a specific tissue distribution. ANT1 is most abundant in heart and skeletal muscles

(77), ANT2 is expressed in most tissue types with a potent expression in cardiac tissue and lower expression in skeletal muscle, ANT3 is ubiquitously expressed and ANT4 is exclusively expressed in testis (17, 79). ANT1 is expressed in both cardiac and skeletal muscle tissues where knockout studies reveal mitochondrial myopathy, highlighting its importance for proper mitochondrial function. As such, the remainder of this thesis will focus on the ANT1 isoform. In addition to its role in survival, ANT is believed to be involved in the initiation of cell death pathways which will be discussed further below.

2.2.2 Voltage Gated Dependent Anion Channel (VDAC)

The primary role of VDAC is to mobilize ADP from the cytosol into the IMM while transporting ATP from the IMM to the cytosol. There are three VDAC isoforms (VDAC1-3) where VDAC1 is expressed on both sarcolemma and OMM and VDAC2 and 3 are predominately found on the OMM. VDAC1 and 2 have a distinct distribution pattern on the OMM, where they are often found in groups or clusters while VDAC3 is uniformly distributed throughout the OMM. The VDAC proteins have a 75% sequence similarity (25, 95), structurally organized in barrels of 19 amphipathic β-strands and a N-terminal moiety, containing an α-helix segment (85), where protein-protein interactions are believed to occur (95). To further determine specific roles for the VDAC isoforms, knockout studies were completed. VDAC1 knockout induces changes to mitochondrial enzymes causing modifications to mitochondrial kinetics, compacted the mitochondrial cristae and enlarged the mitochondria (85, 95). VDAC3 knockout did not appear to cause dramatic impairments in mitochondrial function but it did increase male infertility, suggesting its involvement in reproductive success (85, 95). Interestingly, VDAC2 knockout resulted in embryonic death, highlighting its importance for survival (25). To an extent, the VDAC proteins appear to play redundant roles as VDAC1 knockout resulted with

dysfunctional mitochondria, unable to clear dysfunctional segments of the mitochondrial reticulum, while complete ablation of VDAC2 diminishes any redundancies with VDAC1 and 3, inhibiting the production of energy production and organelle survival (85). In addition, VDAC2 appears to have unique features when compared to the other two isoforms including an extension of 11 amino acids – believed to be on the α-helical portion of the N-terminus protruding outside of the pore – and it also has 9 cysteines, making it more susceptible to SH-oxidation when compared to the other VDAC isoforms. These factors have highlighted the uniqueness and importance of VDAC2 and is the VDAC isoform that will be focused for the remainder of this thesis.

One of the first elucidations of VDAC function was through the incorporation of VDAC into reconstructed planar lipid membranes where VDAC is isolated from mitochondria and added to synthetic membranes (139). It has been determined that – as the name suggests – the open or closed state of VDAC is dependent on the OMM membrane potential. Through these methodologies, researchers have been able to apply specific voltages to the OMM to manipulate the state of VDAC closure. At negative membrane potentials VDAC is mostly opened with a pore diameter of ~2-4nm allowing the transport of large molecules (~4-6kDa) through the OMM (85, 95, 123, 139). At positive membrane potentials, the VDAC pore is in a closed confirmation reducing the diameter to ~1.7-1.8nm, approximately half its size, no longer allowing the transport of most metabolites and proteins including nucleotides (123). The opened and closed state of VDAC was believed to be the only mechanism regulating ATP diffusion through VDAC, but even in the closed state, the channel can still be ~1.7nm opened which, in theory should allow metabolites and ATP through. It is not only the structural change in diameter that prevents ATP permeability, but the change in membrane potential that makes VDAC ion selective. As the

charge switches from negative to positive it creates an electrostatic barrier where in addition to a change in pore diameter, the channel becomes cation/anion selective (99, 123). At negative OMM potentials VDAC becomes anion selective and at positive OMM potentials VDAC becomes cation selective (85, 95, 123). In addition to the change in membrane potential and pore diameter, interactions with desmin, vimentin, tubulin and plectin appear to modulate mitochondrial function (132). Specifically, the cytoskeleton protein tubulin appears make a significant contribution to ADP permeability through VDAC, regulating bioenergetic processes.

2.2.3 Microtubules

Microtubules are hollow rod-like structures that span the length and width of cells (93, 100). They are composed of α- and β- tubulin dimers originating at microtubule organizing centers (MTOC) (100, 114). Through the hydrolysis of a GTP molecule, each tubulin dimer is bound to a successive one forming long protofilaments. The attachment of 3-4 protofilaments make up a mature microtubule. Microtubules are primarily known for their role in mitotic spindle formation during cell division and also known to provide an intracellular route for protein movement as well as providing structure and organization for the other intracellular organelle (46, 54). In striated muscle, microtubules originate from perinuclear golgi complexes growing from the plus end of the microtubule along the length of the fiber with the assistance from microtubule associated proteins (MAP) and end binding (EB) family proteins (93, 100). Unfortunately, in order to fully elucidate the role of microtubules, it would require methodologies capable of observing the spontaneous dynamic stability that microtubules are constantly under. Currently, fluorescently labeled tubulin molecules are below the level of resolution of most microscopes, making it particularly difficult to capture true *in-vivo* functions (163).

In skeletal muscle, microtubules contribute to providing the cell with structure, in addition to the thick and thin filaments that comprise the cytoskeleton. This structure is essential to maintain proper intracellular function through organelle placement and protein trafficking. Specifically, in skeletal muscle, microtubules are crucial to the maintenance of glucose metabolism as it provides a route for GLUT4 vesical translocation to the sarcolemma to allow for glucose diffusion into the cell (118). The dynamic stability of microtubules have also been speculated to contribute to force production where a shift towards stability or de-stability alters the ability of a cardiomyocytes to produce force (121). Although microtubules have been historically known only for their role in cell division, recent literature has highlighted its importance in overall metabolism.

Within the α- and β- class of tubulin isoforms, there are 8 different isotypes of α-tubulin and 10 different isotypes of β-tubulin each able of undergoing different post-translational modifications (PTM) including; acetylation, palmitoylation, phosphorylation, polyglutamylation, detyrosination, and polyglycylation, effectively changing each respective tubulin isoform type and function (46, 84, 93). In addition, γ-, η-, ξ-, ε-, and δ-tubulin isoforms also exist with a complete set of isotypes with their functions currently unknown (84). To further complicate the current understanding, tubulin isoform and isotype expression is varied amongst different tissue types and organisms presenting further difficulties in understanding their function (21, 84).

In skeletal muscle, in a more oxidative tissue such as the soleus, α-tubulin organization is composed of dense bundles that interlock around the nucleus forming long lines between nuclei while a more glycolytic tissue such as tensor fascial latae (TFL) display more individual microtubules not as densely organized as the soleus (16, 113). This fiber type specific organization of tubulin does not appear to be plastic as fiber types can be. Denervation of the

soleus and EDL muscles in Wistar rats results in a similar orthogonal microtubule organization in both tissues (113, 114) but when electrically stimulated in a manner to induce a change in fiber type, the EDL is able to mimic the dense microtubule organization seen in soleus but the soleus is unable to mirror the EDL's organization (114). This suggests that microtubule organization in each muscle fiber type may be specific to support the physiological demands of that tissue. Understanding microtubule organization is crucial in understanding microtubule and whole cell function as disruptions in microtubule dynamics has been shown to lead to cardiac and skeletal muscle dysfunction (78, 142). Microtubules are an integral component of all cells, interacting with cell membranes, golgi complex, endoplasmic reticulum and mitochondria (16, 20, 100, 111, 113, 114) where destabilization has been shown to reduce mitochondrial distance traveled and speed (54).

2.3 Tubulin regulation of VDAC permeability

Saetersdal and colleagues in 1990 were the first to report a close association of β-tubulin and mitochondria in isolated cardiomyocytes (131). Immunohistochemistry images reviled a dense microtubule network spread throughout the entire cell when it was originally believed that microtubules were only localized to the perinuclear region. Further investigation with the use of electron microscopy and immunogold labelling determined that microtubule organization appeared to be highly co-localized with mitochondria. In 1995, Saks and colleagues speculated the involvement of a cytoskeletal protein during oxidative phosphorylation (136). The comparison between isolated mitochondria to permeabilized muscle fiber bundles (PmFB) yielded significantly reduced oxygen consumption rates (136, 162). In isolated mitochondrial preparations, the tissue is homogenized and subjected to differential centrifugation, successfully disturbing all intracellular networks and potential protein interactions to isolate the mitochondrial

organelles. Comparatively, utilizing a PmFB preparation requires significantly less tissue, while also retaining most intracellular compartments – including the cytoskeleton – allowing for a more accurate depiction of what *in-vivo* conditions may be like (162). With the use of PmFB, researchers were able to determine that a cytoskeletal component, specifically tubulin, was able to limit the ability of ADP to diffuse into the mitochondria to stimulate oxygen consumption (127, 131, 136) (Figure 2-2).

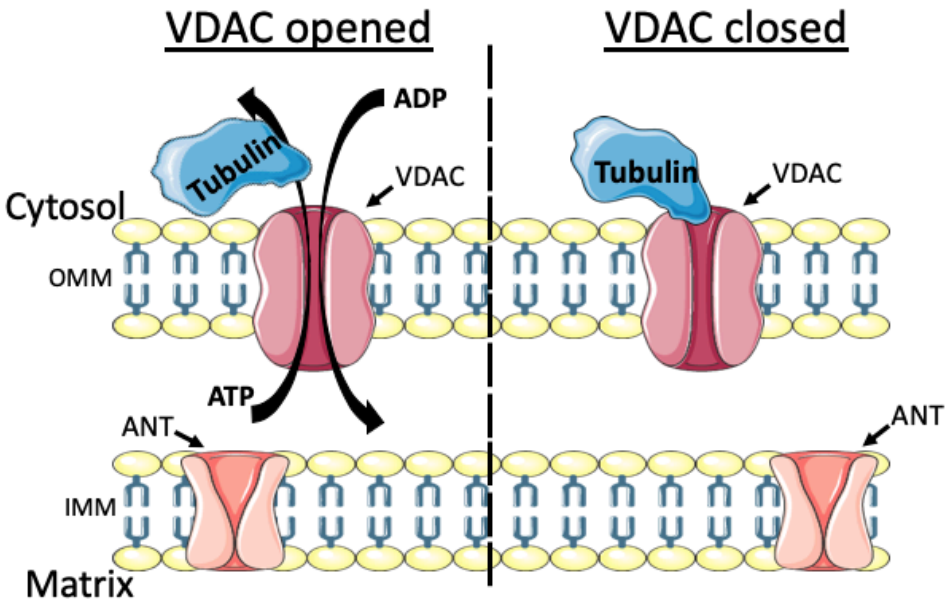

Figure 2-3. Schematic depiction of how the tubulin-VDAC interaction. It is hypothesized that when VDAC is in an opened conformation, ADP and ATP diffusion is permitted through the outer mitochondrial membrane (OMM) where ADP/ATP exchange can then occur through ANT embedded on the inner mitochondrial membrane (IMM). The closed confirmation of VDAC has been suggested to prevent any diffusion of ADP/ATP through the OMM. Schematic adapted from Rostovtseva et al., 2018 (127).

2.3.1 Reconstructed planar lipid membranes

The current model presents tubulin as a major regulator of ADP permeability through VDAC. Unfortunately, the exact mechanism of how this occurs *in-vivo* is currently unknown. Research completed to date has utilized reconstructed planar lipid membrane methodologies revealing the majority of what is known about the tubulin-VDAC interaction. These works show that it is solely the C-terminal tail of tubulin that is physically inserted into VDAC blocking its permeability (145). In addition, post-translational modifications (PTM), specifically detyrosination, increases the amount of tubulin-VDAC binding in a planar lipid membrane model (145). Phosphorylation of VDAC (146) and the manipulation of the OMM phospholipid content has also shown to alter this interaction (125). While this method of assessing tubulin-

VDAC interactions has proven to be extremely valuable in elucidating some mechanistic approaches of understanding this interaction, it is predominately completed in an isolated system. In these studies, VDAC and tubulin proteins are isolated from different tissues, where the isoform and isotypes are rarely specified (Table 2-1). In addition, it is possible that in the presence of other tubulin dimers, and protofilaments, microtubules may form which may alter the affinity of tubulin-VDAC binding.

2.3.2 In-vitro tissue analysis of tubulin and VDAC interactions

Studies in various human cancer cell lines have determined that tubulin is in an integral component of mitochondria. Electron microscopy images of mitochondria reveal traces of both α- and β-tubulin around the mitochondria (20). In addition, immunoprecipitation experiments isolating VDAC from the mitochondrial fraction yielded positive results when probed for tubulin (20). Analysis in striated muscle revealed that the addition of tubulin to isolated mitochondria decreases oxygen consumption while the removal of βII-tubulin increases oxygen consumption, strongly suggesting that tubulin is able to restrict the permeability of ADP by blocking VDAC (40, 127). The blocking action of tubulin on VDAC also corroborated with changes in membrane potential where at negative potentials the VDAC pore was open and with the addition of tubulin, membrane potentials became positive, effectively closing VDAC (127). This interaction was further supported by immunohistochemical images overlaying βII-tubulin with VDAC in cardiac, soleus and white gastrocnemius (WG) muscles harvested from rodents, displaying a close proximity of βII-tubulin with VDAC (161). These works strongly suggest that tubulin does in fact interact with VDAC but a direct protein-protein interaction had yet to be measured. In 2018, Rostovsteva and colleages were the first to identify a direct protein-protein interaction between βIII-tubulin with VDAC in a human neuroblastoma cell line (126) concluding that

perhaps the abundance of a tubulin isotype expressed in each respective tissue mediates the tubulin-VDAC interaction. To date, the direct interaction between tubulin and VDAC in cardiac and skeletal muscle has not been explored.

Table 2-1. Current literature measuring tubulin-VDAC interactions.

Author	Isoform/Isotype	Tissue	Methodology
Gonzales-Granillo et al., 2012	βII-tubulin	Cardiomyocytes	Trypsin
Carre et al., 2001	α- and β-tubulin	SK-N-SH, IMR-34 and A549 cells	Transmission Electron microscopy, co-immunoprecipitation
Maldonado et al., 2010	Tubulin	HepG2, A549 and UM-SCC-1 cells	Confocal microscopy – immunohistochemistry
Sheldon et al., 2015	PTM of α- and β-tubulin	---	Reconstructed planar lipid membrane
Rostovteva et al., 2008	CTT	---	Reconstructed planar lipid membrane
Gurnev et al., 2011	Tubulin	---	Reconstructed planar lipid membrane
Varikmaa et al., 2014	βII-tubulin	Soleus and white gastrocnemius	Confocal microscopy-co-localization
Rostovteva et al., 2018	βIII-tubulin	SK-N-SH	Proximity ligation assay

2.4 Mitochondrial-mediated apoptosis

Mitochondria are known as the "powerhouse of the cell" functioning to provide energy and promote survival. Concomitantly, mitochondria are also a major regulator of cell death where pathological conditions (cardiovascular disease, cancer, muscular dystrophies) present hostile intracellular environments where the cell's susceptibility to death is increased through swelling, dysfunction and permeabilization of mitochondria. This leads to the release of pro-apoptotic factors, initiating the cascade of mitochondrial derived cell death. A general overview of apoptosis is described below to provide further insight in understanding how VDAC may be involved in the initiation of apoptosis.

2.4.1 Apoptosis

Apoptosis, necrosis, mitotic catastrophe and autophagy are the main mechanism that lead to cell death (73). Focusing on apoptosis, it is defined by morphological changes including: cell

shrinkage, chromatin condensation, nuclear fragmentation and blebbing while functionally preventing ATP production, increasing ROS production and dissipating the mitochondrial membrane potential. There are two pathways in which apoptosis is stimulated 1) extrinsic pathway; mediated through the binding of a ligand to a cell membrane receptor which then stimulates a cascade of apoptotic events and 2) intrinsic pathway; mediated through increased mitochondrial permeability leading to the subsequent release of pro-apoptotic factors. Both pathways result in activating caspases which then cleave proteins causing the morphological and functional changes that occur during apoptosis. As VDAC is the most abundant protein on the OMM, responsible for the regulation of mitochondrial permeability, it is also believed to play a role in mediating mitochondrial induced cell death.

2.4.2 Mitochondrial permeability transition pore formation

Another mechanism of increased mitochondrial permeability is through the formation of the mitochondrial permeability transition pore (mPTP). Under pro-apoptotic stimulation this multi-complex protein channel forms a pore allowing water and solutes ~1.5kDa through, swelling the mitochondria and dissipating membrane potential (73, 128). Formation of the channel is stimulated by an increased calcium influx, pro-apoptotic protein binding (BcL-2 family) and some chemotherapies (73). Through the generation of cyclophilin D null mice, Baines and colleagues (2005) determined that cyclophilin D is a key regulator of the mPTP formation as null mice were resistant to in-vivo and in-vitro induction of mPTP (10, 27). The pore is speculated to be composed of VDAC, ANT, mtCK, HK and/or Bax (9, 73, 128). The exact components of the pore are highly debateable as under different experimental condition and in different tissues the presence of each protein appears to be optional (9, 73).

mPTP formation can be induced through elevated Ca^{2+} and ROS emission. Under conditions of elevated intracellular stress, cyclopilin D localizes from the matrix of the mitochondria to the IMM where it is believed to bind to ANT. Elevated intracellular calcium is then taken up into the mitochondria where it is speculated to bind to ANT – cycloplinin and induce a conformational change resulting in an IMM pore formation (10, 45). This then initiates the unrestricted flow of molecules through the mitochondria, such as the release of cytochrome c oxidase and other pro-apoptotic factors, initiating apoptosis. mPTP induction is also believed to be through elevated ROS production. Multiple measures of isolated rat cardiomyocytes subjected to ischemia-reperfusion injury to induce mPTP found elevated ROS production prior to changes in cytosolic calcium release and up until a loss in cell viability suggesting that ROS production precedes and may play more of a role in the induction mPTP (68).

2.4.3 The role of VDAC in mPTP formation

Under major speculation is VDAC as an integral component of the mPTP (9). VDAC was first speculated as an essential component of mPTP as isolation of cyclophilin D retained an ANT and VDAC interaction (31). In addition, reconstructed proteoliposomes embedded with VDAC, ANT and cyclophilin D demonstrated the characteristic mPTP opening and release of fluorescein with calcium stimulation (31). Closer observations presented doubt as the closed state of VDAC still appeared to be permeable to calcium (151). In addition, antibody and pharmacological inhibition of VDAC and mPTP has been questioned (9, 128). While there is a significant amount of evidence questioning the involvement of VDAC in mPTP formation, there has yet to be a physiological examination of VDAC knockout. Studies exploring knockout or knockdown of VDAC1 or 3 results with the other isoforms compensating for the subsequent knockout except VDAC2 where genetic manipulation does not sustain life (25, 85). To by-pass

this problem, Baines and colleagues (2007) isolated fibroblasts from VDAC1/3 knockout mice and then went on to knockdown VDAC2 to gain further insight of VDAC contribution to mPTP (11). Here they still discovered the release of cytochrome c oxidase, occurring quicker than in the presence of VDAC suggesting the formation of mPTP even in the absence of all VDAC isoforms. These authors suggest that the presence of VDAC may limit the induction of apoptosis through mPTP formation. While this work is very thorough, it does not discount that alternative mechanisms may be occurring *in-vivo* and in different tissues.

2.4.4 Bcl-2 family of proteins and hexokinase involvement in VDAC permeability

The Bcl-2 family of proteins contain members involved in the prevention of apoptosis (Bcl-2 and Bcl-X_L) and initiation of apoptosis (Bax, Bak, Bid and Bad) with the latter speculated to promote apoptosis through an interaction with VDAC (73, 128, 158). Specifically, planar lipid bilayer membranes embedded with VDAC displayed significantly increased VDAC activity with the addition of Bax/Bak, creating a channel 4-10fold larger than the open conformation of VDAC alone (147). A full delineation of Bax/Bak function is still up for debate as some labs have shown Bax/Bak form a pore independently on the OMM or others have shown that the mere swelling of the mitochondria is enough to cause breaks in the OMM allowing the release of cytochrome c oxidase and other pro-apoptotic factors, allowing the initiation of apoptosis (158). A limitation in this current model is the lack of specificity of VDAC isoforms used in experiments. It is generally believed that VDAC1 is more involved in the apoptotic activities of the cell (85, 95) but isoform specification is rarely defined (128, 147, 158).

Hexokinase is a rate limiting enzyme responsible for the commitment of glucose to glycolysis or the pentose pathway. Alternatively, research has shown that hexokinase is also involved in the suppression of apoptosis through an interaction with VDAC on the OMM.

Overexpression of hexokinase II inhibited cytochrome c oxidase release through competitive binding with Bax in HeLa cells (103). In addition, it has been speculated that the presence Bax is not necessary to prevent apoptosis (80). Lastly, others have also deduced that the VDAC closure caused by hexokinase binding increased mitochondrial swelling and membrane rupture, creating holes in the membrane allowing the release of cytochrome c oxidase to initiate apoptosis (73, 128, 158). Similarly to the BcL-2 family, a complete consensus has not been made regarding the role of hexokinase – considering both hexokinase isoforms – and VDAC permeability. It is interesting to note that both hexokinase and VDAC play a major role in cell survival by providing the cell with fuel for ATP production and energy transport respectively, while also contributing to the mediation of cell death through cytochrome c oxidase release.

2.5 Diseases and conditions of disorganized microtubules

2.5.1 Overview of cancer and chemotherapy

The world health organization has reported 9.6 million cancer cases in 2018 with this prevalence only expected to increase. In 2010, this placed an economic burden of 1.16 trillion dollars and can only be assumed to be larger now (57, 109). As these numbers continue to rise, lifestyle behaviours continue to worsen. Although there are some genetic influences in the development of cancer, the foods consumed and amount of physical activity can significantly increase an individual's chances of developing a tumor (57). The common goals in place for individuals diagnosed with cancer is to; 1) resect the tumor and "cure" the cancer, 2) prolong life and 3) improve their quality of remaining life. In addition to the side effects caused by the tumor, almost all treatment options involve the administration of cytotoxic compounds that not only target tumor cells, but all of the cells in the body causing new or exacerbating side effects seen

with this disease. Part of this thesis will explore how a specific class of chemotherapy alters cardiac and skeletal muscle mitochondrial bioenergetic function.

One of the major complications for individuals receiving cancer treatment and even after surviving treatment is the development of fatigue. Fatigue can manifest as psychological, physical or both and have debilitating effects on quality of life. A study completed on women diagnosed with breast cancer reported reduced strength and endurance, flexibility, and grip strength following unilateral treatment (48) resulting with reduced quality of life. A major strength to this study was the comparison between the treated and untreated arms or upper bodies that allowed for an internal control. A common limitation in this particular type of cancer literature is being unable to determine whether an individual is experiencing the symptoms due to the tumor itself or due to the treatment they've received. Jacobsen and colleagues (1999) attempted to overcome this limitation by determining levels of fatigue following various treatment cycles. Through questionnaires and home assessments, there was a significant increase in severity of symptoms and distress throughout treatment cycles (cycles 1-4) (56). The most commonly reported symptoms were sleep problems, muscle weakness, emotional upset and mouth sores (56). Of particular interest is the resulting muscle weakness that occurs from chemotherapy treatment. Developing a better understanding of how these chemotherapeutic drugs effects muscles may uncover why muscle weakness is a major symptom and aid in the development of better treatment strategies.

2.5.2 Overview of the different types of chemotherapies

2.5.2.1 Basic overview of the cell cycle

Originally, the term chemotherapy was classically known as a drug to treat a disease. More recently, it has been specifically used in the context of cancer treatment. There are many

classes of chemotherapies all with the common goal of preventing tumor cell division. As such, these chemotherapies are designed to prevent cell division. Both cancerous and non–cancerous cells undergo a process known as mitosis in order to divide and maintain life. This process occurs in 5 phases and can be thought of as a cycle where each cell produces 2 new cells that eventually go through the cycle producing even more cells (Figure 2-4). This process begins in the G0 or resting phase where non-dividing/dormant cells wait for an external stimulation to initiate division. Upon stimulation, the cell enters the G1-phase where it begins to duplicate intracellular proteins and grows in size so that it is capable of splitting into two cells which is quickly followed by the S-phase where DNA is copied making new DNA for the new cell. The G2-phase is known as the regulating check point where proteins double check that the DNA was copied correctly leading to the last step known as the M-phase, where microtubules form into mitotic spindles allowing the physical split of one cell into two (2, 83). Understanding the cell cycle is crucial as some chemotherapy drugs are developed to targeted a specific phase of the cell cycle to inhibit tumor growth (Figure 2-4).

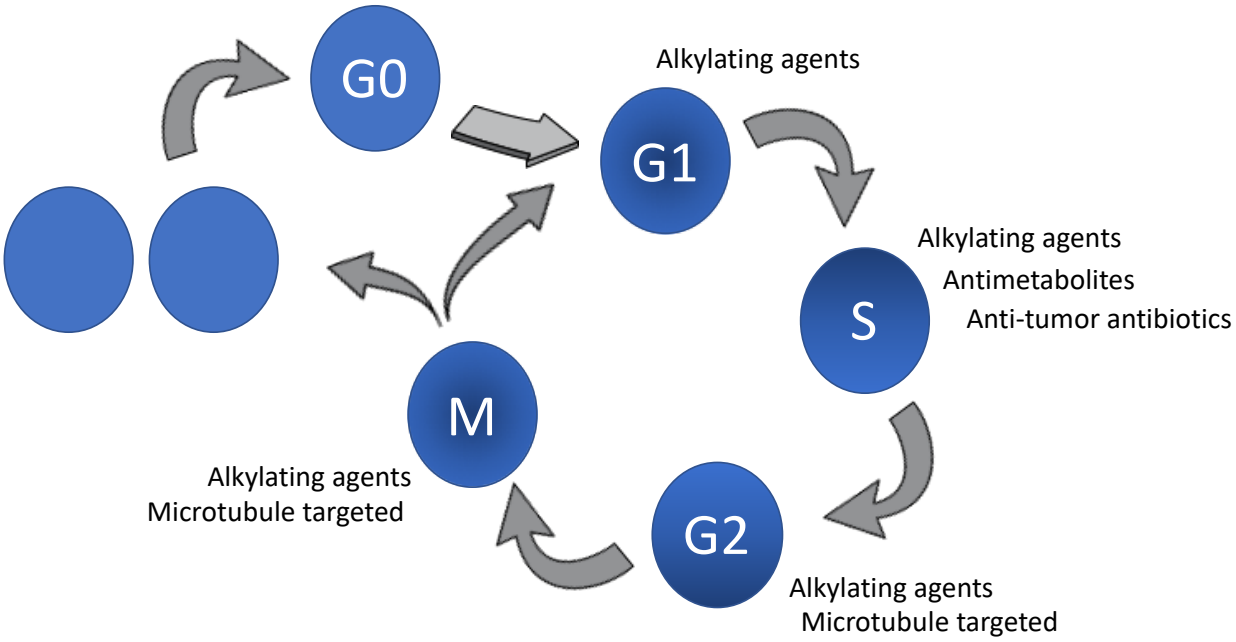

Figure 2-4. Representative schematic of the mitotic cell cycle. Dormant mitotic cells are found in the G0-phase awaiting external or internal stimulus to begin dividing. In the G1-phase, the cell grows while intracellular proteins are duplicated in preparation for division, quickly followed by the S-phase where new copy genetic materials are made. The G2-phase is a check-point to ensure no errors were made during duplication while mitotic spindle formation begins. Lastly, during the M-phase microtubules fully form mitotic spindles and divide the cell into two new cells. These newly divided cells can directly re-enter the cell cycle or remain dormant in the G0-phase. Chemotherapies are often designed to target specific phases of the cell cycle, all with the goal of inhibiting cell division.

2.5.2.2 Alkylating agents

This class of chemotherapy drugs inhibits tumor cell growth by attaching alkyl groups to the quinine base of DNA, introducing errors to the DNA during all phases of the cell cycle ultimately causing the cell to die (24). A major side effect of this therapy is the development of leukemia as the damage to the DNA occurs to both rapidly dividing cancerous and non-cancerous cells. Common alkylating agents are nitrogen mustards, nitrosoureas and alkyl sulfonates.

2.5.2.3 Antimetabolites

Through competitive inhibition, antimetabolites interfere with the replication of DNA and RNA during the S-phase of the cell cycle (58). This is especially advantageous in killing cancer cells as they divide at a much faster rate than normal cells.

2.5.2.4 Anti-tumor antibiotics

Anti-tumor antibiotics inhibit tumor cells from replicating by interfering with the enzymes involved in DNA replication and RNA production. These drugs physically insert themselves between the strands of DNA inhibiting replication. A subclass of anti-tumor antibiotics called topoisomerase inhibitors are also able to inhibit DNA replication by inhibiting topoisomerase II, preventing the separation of DNA for replication. One of the most common and successful anti-tumor antibiotics are anthracyclines, capable of sequestering to the nucleus causing DNA/RNA damage while also increasing ROS production. A common side effect with the use of anthracyclines is cardiotoxicity which limits the amount that each patient can receive.

2.5.2.5 Targeted therapies

As the knowledge of tumor cell metabolism increase, so do the advancement of treatment strategies. Targeted therapies are designed to mostly target tumor cells while leaving the majority

of healthy cells intact. These types of therapies are often used in conjunction with classic chemotherapies. One such type of therapy is hormone therapy aimed to alter the action or production of male and female hormones to successfully slow the growth of breast, prostate and uterine cancers dependent on hormones for growth. Another type of targeted therapy is immune therapy designed to either stimulate the body's natural immune response to target and fight tumor cells or are exogenously administered as antibiotics to target tumor cells. Lastly, in 2010 the first cancer vaccine was developed (Provenge®) to treat prostate cancer similarly to endogenous immune therapy shown to significantly extend life by 50% compared to control (22).

2.5.3 Microtubule targeted chemotherapy

The remainder of this thesis will specifically focus on mitotic inhibitors. These drugs are plant alkaloids often derived from natural products that have extreme cytotoxic effects. They specifically target the M phase of the cell cycle to prevent mitosis. Mitotic inhibitors, or microtubule targeted compounds are often used to treat lung and breast cancers, myelomas, lymphomas and leukemia. As mentioned above, a major consequence of these drugs is that they are not tumor cell specific, therefore they are successful at targeting and killing tumor cells but they are also successful at killing healthy cells. There are 4 types of microtubule targeted compounds designed to inhibit microtubule dynamics 1) Epothilones; inhibiting the transition from G2-phase to the M-phase by binding αβ-dimers stabilizing microtubules causing cell cycle arrest 2) Estramustine; a combination of estrogen and nitrogen mustards designed for the treatment of prostate cancer. This class of mitotic inhibitor is not often used 3) Taxanes; function by stabilizing αβ-dimers during the M-phase of the cell cycle preventing cell division ultimately causing cell death and lastly 4) Vinca alkaloids; prevent β-tubulin polymerization during the M-

phase of the cell cycle (129). This thesis will specifically focus on the taxane paclitaxel and the vinca alkaloid vinblastine.

2.5.3.1 Paclitaxel

Taxol, originally discovered by botanist Arthur Barclay and further isolated by Mansukn Wani and Monroe Wall, was found to have highly toxic properties specifically useful for killing cancer cells. Taxol is extracted from the bark of pacific yew tree, Taxus brevifolia, but unfortunately it is slow growing and, in the 1980's, was quickly becoming extinct as bark removal ultimately kills the tree. The synthetic form of taxol, paclitaxel, was then derived and is what is currently used for the treatment of some cancers (169). Paclitaxel inhibits the dynamic stability of microtubules by binding to αβ-dimers, preventing depolymerisation and encouraging polymerization. Specifically, paclitaxel binds to 31 amino acids on the N-terminal tail of β-tubulin, a site specific to only paclitaxel (130). A 5 minute incubation with paclitaxel in human T lymphocytes is sufficient to see the first bundles of polymerized microtubule appear, while 2 hours has been shown to be where cell cycle arrest begins to occurs (90). A result of microtubule stabilization during the G2-M phase of the cell cycle is the subsequent initiation of apoptosis activated through various pathways in different mitotic cell types (23, 90, 129, 173).

Paclitaxel induced apoptosis in cancer cells appears to occur in a multi-pathway manner where activation of certain apoptotic pathway differs depending on tumor type. Canine mammary gland tumor cells treated with paclitaxel increased ROS formation paired with decreased SOD activity. This was coupled with increased Bax and cytochrome c oxidase expression both resulting with increased caspase 3 activation, ensuing apoptosis (117). Following a 2-hour incubation with paclitaxel, human T lymphocyte cells displayed increased phosphorylation of BcL-2 followed by increased caspase 3 activation during the G2-M phase of

the cell cycle, also suggesting the initiation of apoptosis (90). There is an abundance of literature with the aim to understand how paclitaxel targets phases of the cell cycle to induce apoptosis and tumor cell death but unfortunately, there is limited knowledge on how this occurs in non-mitotic cardiac and skeletal muscles.

2.5.3.2 Vinblastine

There are three main types of vinca alkaloids; vinblastine, vincristine and vendesine (moudi et al.,). Vinca alkaloids binds to formed microtubules (~16 binding sites along the length of a microtubule) and has shown to inhibiting growth at the plus end of axonemal seeds while also promoting destabilization at the minus end (61, 62, 101). This thesis will primarily focus on the use of vinblastine to alter microtubule organization. Vinblastine was first discovered as an intended therapy for diabetes by Robert Noble and Charles Beer at the University of Western Ontario (98). Vinblastine is extracted from the *catharanthus roseus* plant and is now commonly utilized for chemotherapy treatment due to its cytotoxic properties (12, 61, 92).

In addition to inhibiting cell division by depolymerizing microtubules, vinblastine has shown to have a serious of intracellular effects all contributing to the fatality of the cell. Upon mitotic arrest, vinblastine has shown to induce apoptosis through various pathways. In KB-3 human carcinoma cells, vinblastine treatment was shown to induce apoptosis though a BcL-2 activated pathway (160) while in human cervical carcinoma, apoptosis was induced through c-Jun N-terminal protein pathway (JNK) (69). Lastly, mitochondria isolated from A375 and BLM melanoma cells treated with vinblastine resulted with the induction of apoptosis measured through dissipated mitochondrial membrane potential, cytochrome c oxidase release, and caspase 3 and 9 activation (143). It is evident that there is a link between altering microtubule architecture and initiating apoptosis through mitochondrial and non-mitochondrial induced

pathways but the mechanism remains unknown. Moreover, the effects on non-mitotic tissues also remain unexplored.

2.5.4 Potential impairments to muscle function in response to microtubule manipulation

Skeletal muscle is the largest organ in our body primarily responsible for locomotion and maintaining metabolism. As most chemotherapeutic therapies, specifically mitotic inhibitors, are not cell specific, they not only target and kill tumor cells but also target muscle cells. This presents an advantageous model to attempt to understand how microtubules may be involved in regulating non-mitotic cardiac and skeletal muscle metabolism and in-turn muscle function. Cardiac and skeletal muscle are non-mitotic, raising the question whether microtubule targeted drugs play a role in cardiotoxicity and muscle weakness seen following chemotherapy. As discussed, the known functions of microtubules in skeletal muscle are protein trafficking and organelle and protein movement/placement (54). The role of the tubulin-VDAC interaction has not been fully put to question as the model is still "novel". Current research exploring the effects of mitotic inhibitors on skeletal muscle focus more on the neurological effects. Direct administration of vinblastine to the sciatic nerve decreases contractility of extensor digitorum longus muscle (EDL) following caffeine stimulation due to swelling and fragmentation of the nerve (3). The effect at the level of the nerve causes morphological changes to the muscle similar to denervation, uniforming the fiber type distribution, reducing the diameter of each fiber and the overall muscle's functional capacity (3, 174). In addition to the neurological insults that have a direct effect on muscle function and morphology, mitotic inhibitors are also known to have a direct effect on muscle tissue. Unfortunately, the literature on this topic is not well known. Whether an inability to transport energy (ATP/ADP) through the mitochondria concomitantly

with altered microtubule organization plays a role in the development of cardiotoxicity and muscle weakness has yet to be explored.

2.4.5.1 Human studies utilizing microtubule targeted chemotherapies

A limiting factor in human cancer research is the inability to delineate the contribution of adverse effects from the tumor and the chemotherapy delivered. Correlations can be made based on treatment regime and development of side effects to attempt to elucidate their origins. 58% of women diagnosed with metastatic breast cancer receiving first line taxane-based chemotherapy developed sarcopenia during their treatment regime (144). In addition, 5 hours following a single dose of chemotherapy containing vinblastine, a 32-year old male with no prior cardiac risk factors suffered an acute myocardial infraction (49). Perhaps, these cardiac and skeletal muscle decrements may be due to an impairment in the ability of the muscle to maintain or regulate ATP/ADP diffusion which is critical for cell survival as mentioned above. Currently, a mechanism explaining these reported side effects is unknown. In the absence of cancer, endogenous manipulation of cardiac microtubule architecture through the release of macrophage migration inhibitory factor (MIF) induced mitochondrial dysfunction measured by reduced respiratory capacity while also reducing cardiac contractility (110). This study suggests that it is not just the cytotoxic effect of chemotherapy that contributes to cardiac and skeletal muscle dysfunction, but the disorganized microtubules as well.

2.5.4.2 Rodent studies utilizing microtubule targeted chemotherapies

Rodent studies allow researchers to delve deeper into research allowing the isolation of the effects of tumors from the chemotherapy administered. Indeed, this also allows the independent isolation of the effect of microtubule disorganization (using microtubule targeted chemotherapies) without the systemic effects of a tumor present. Historically, the use of mitotic

inhibitors was known to induce peripheral neuropathy, believed to be the cause of any myopathy seen. Konish and colleagues (1984) revealed the appearance of basophilic granular deposits in combination with degenerating muscle fibers prior to the development of peripheral neuropathy suggesting a direct cytotoxic effect to the muscle (71, 174). Other cellular metabolic impairments as a result of microtubule stabilization or destabilization is currently unexplored in skeletal muscle. In ventricular cardiomyocytes, contractile amplitude and calcium transients were significantly reduced following a 4 hour incubation with 10μM taxol (50). Howarth and colleagues (1999) concluded that taxol caused an inhibition on sarcoplasmic reticulum calcium release. While this may be true, an unexplored aspect of the reported reduced contractile amplitude could also be due to an unmet energy demand. The addition of tubulin to isolated mitochondria reduced ADP stimulated respiration therefore limiting the production of ATP to fuel metabolic processes such as muscle contraction (127).

2.5.5 Is microtubule disruption and mitochondrial dysfunction associated with muscle dysfunction?

Currently there is a gap in the literature where microtubule targeted compounds appear to induce ROS, stimulate mitochondrial dysfunction and apoptosis through unknown mechanisms in cancer and non-cancer models. These impairments are linked with muscle weakness and impaired function with an unknown mechanism (Figure 2-5). Alternatively, a new model of mitochondrial bioenergetic impairment has been proposed whereby the cytoskeleton – more specifically, microtubules – a functional unit of muscle – may regulate mitochondrial bioenergetics, the organelle largely responsible for regulating cell death or survival. This thesis has been describing the tubulin-VDAC interaction as a novel mechanism but, as mentioned above, this model was first proposed in 1990 (131) and is now starting to catch the interest of researchers.

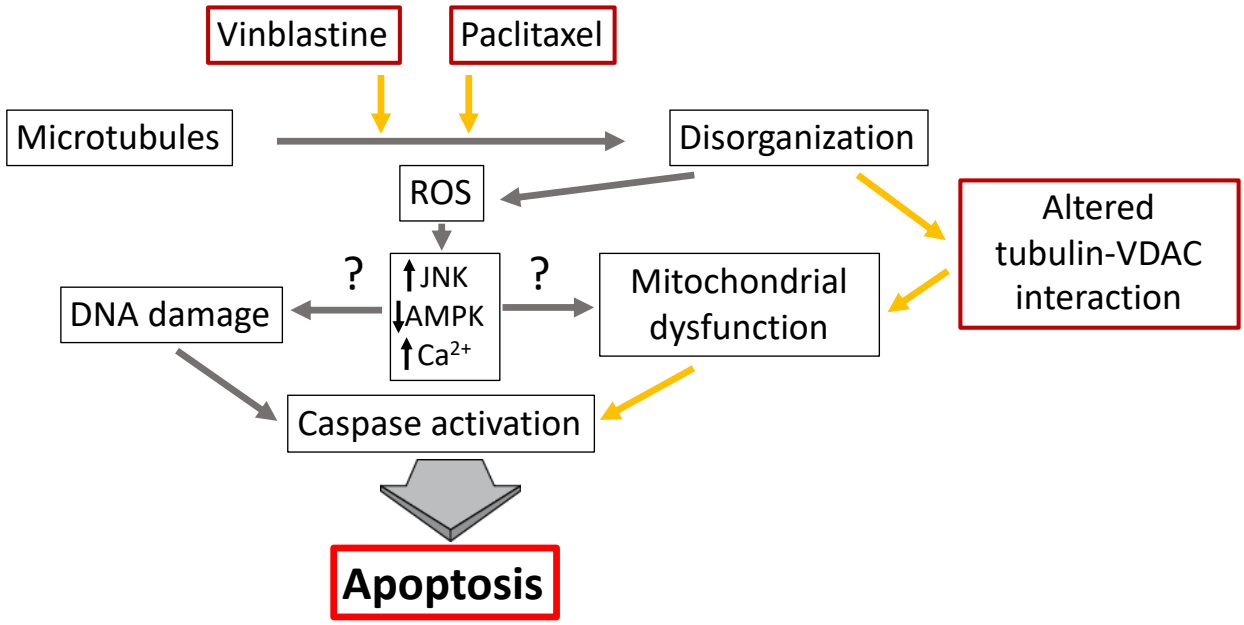

Figure 2-5. Activation of apoptosis in skeletal muscle by paclitaxel and vinblastine. Microtubule targeted chemotherapies paclitaxel and vinblastine are known to induce apoptosis in skeletal muscle with an unknown mechanism all resulting with mitochondrial dysfunction, cytochrome c oxidase release, caspase activation leading to apoptosis and cell death. Yellow arrows represent the pathway studied in this thesis. Schematic adapted from Chiu et al., 2012 (26).

2.5.6 Overview of Duchenne muscular dystrophy

Duchenne muscular dystrophy (DMD) is another muscle disorder with disorganized microtubules and mitochondrial dysfunction, known to exhibit sever muscle weakness and dysfunction. Duchenne muscular dystrophy (DMD) is an X-linked disease effecting 1-3600 males (18, 19). This disease is characterized by weak proximal muscles with early phenotypical onset (~5 years old) where the first distinguishable signs is through Gowers' manoeuver used by children to get into a standing position (19). Significant decrements in muscle strength ensues as these males age resulting in the need of ambulatory and respiratory assistance by young adulthood. The average age of death is ~19 years old with the cause of death often due to respiratory failure or cardiac dysfunction (19).

DMD results from the partial or full loss of a single protein located in the sarcolemma of skeletal muscle named dystrophin (18). As one of the largest proteins in the body, dystrophin is responsible for anchoring intracellular structural components of the cell to the extracellular space. This provides structural integrity during muscle contraction keeping proteins and organelle in place. In the absence of dystrophin, each contraction or movement results in micro-tears along the sarcolemma, producing a low amount of force and causing host of metabolic insults resulting with increased intracellular calcium release and ROS production (5, 170). These intracellular impairments often result in muscle loss coupled with fat and fibrotic deposits (52). As DMD is a genetic disease, gene therapy appears to be the best route to developing a cure (120). In-lieu of a cure, therapeutic strategies aim to treat the side effects that result from the lack of dystrophin.

2.5.6.1 Microtubule disorganization in Duchene muscular dystrophy

Dystrophin is found bound to the sarcoglycan – dystroglycan complex embedded in the sarcolemma (Figure 2-5). Prins and colleagues (2009) were one of the first to suggest that dystrophin may bind to the cytoskeleton in a similar method to cytolinkers (111). Fluorescence microscopy revealed a highly disorganized pattern of α-tubulin in a mouse model of DMD, the mdx mouse (111). As mentioned above, α-tubulin is one of the building blocks in the formation of microtubules, responsible for maintaining structural integrity, organelle placement and protein transport. In addition to increased disorganization, both α- and β-tubulin protein content appeared to be increased in the mdx model without any changes in MAP proteins (111). In the absence of dystrophin, the nitric oxide pathway, calcium homeostasis and ROS production is perturbed (5). Microtubule contribution to these intracellular events is currently unknown.

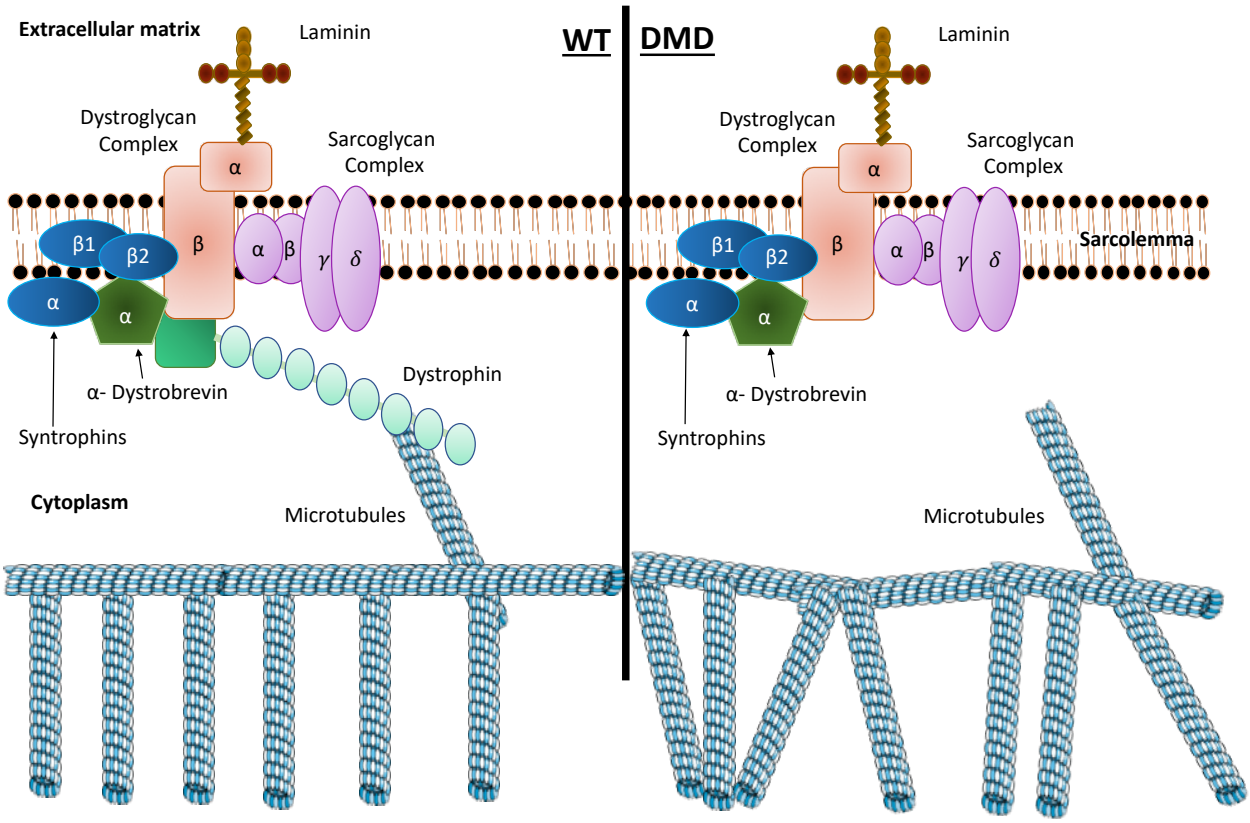

Figure 2-6. Representative schematic of microtubule disorganization in the absence of dystrophin in skeletal muscle. Connecting the extracellular space to the intracellular space is the dystroglycan-sarcoglycan complex where in WT muscles, dystrophin binds to α-dystrobrevin anchoring microtubules in place contributing to the overall structural integrity of the cell. In DMD muscle, dystrophin is absent, therefore, microtubules lack an anchor and become unstable and disorganized schematic adapted from Fairclough, Wood and Davies., 2013 (34).

2.5.6.2 Mitochondrial impairments in Duchene muscular dystrophy

Mitochondrial have become of particular interest in the DMD pathology as they are a major regulator of cell survival. One of the first comprehensive studies analyzing mitochondrial bioenergetics in permeabilized muscle fiber bundles (PmFB) from mdx mice determined a mitochondrial dysfunction as a result of this disease. These authors reported decreased maximal respiration, decreased H_2O_2 emission coupled with increased ROS scavenging when compared to wildtype controls (39).These tissues were also more susceptible to calcium induced cell death through induction of the mPTP (39). Of particular interest was the reduced H_2O_2 emission, as a muscle displaying constant regeneration with fat and fibrotic accumulation in addition to mitochondrial dysfunction, in theory, should have elevated H_2O_2 emission. Utilizing a more severe DMD mouse model – the D2.mdx – work from the Perry lab at York University has determined impaired H_2O_2 emission during impaired oxidative phosphorylation in cardiac, respiratory and skeletal muscles (51, 52). These mitochondrial bioenergetic impairments are strongly linked with the ability of ADP to be transported into the mitochondria to stimulate oxidative phosphorylation and produce ATP. Mitochondrial dysfunction is also associated with decrements in muscle function. D2.mdx mice display significantly reduced muscle strength measured through cage hang time, grip strength and hind-limb force production in addition to a decreased functional capacity measured through voluntary wheel running (52). A common factor linking whole muscle dysfunction and mitochondrial bioenergetic impairment is the

As microtubules are known to bind both mitochondria and the sarcolemma, the D2.mdx mouse model provides a novel model to further understand the tubulin-VDAC model. The disorganized microtubule architecture in the D2.mdx mouse sets up an endogenous model that does not introduce any cytotoxic compounds or external manipulation allowing the passive

observation of how the tubulin-VDAC model may result in mitochondrial and muscle functional impairments.

3 Objectives and hypothesis

3.1 Overview of thesis

The overall purpose of this thesis was to determine whether α-tubulin and βII-tubulin interact with VDAC2 in cardiac and skeletal muscles from rats and mice. This thesis explores pharmaceutical manipulated and genetic models of altered muscle microtubule organization to determine tubulin-VDAC interactions in muscle, and whether this alters ADP-stimulated respiration which is dependent in part on VDAC permeability.

3.2 Objective and hypothesis for study 1 (Chapter 4)

The current literature has identified tubulin as a novel regulator of VDAC permeability of ADP/ATP cycling, driving mitochondrial bioenergetics. To date, the direct measurement of tubulin interacting with VDAC has yet to be completed particularly in muscle. In addition, it remains unknown whether perturbations to the microtubule architecture alters this interaction and in doing so, alters ADP-dependent mitochondrial bioenergetics. The purpose of study 1 was to determine whether α-tubulin and βII-tubulin interact with VDAC2 in EDL single fibers. We then aimed to determine whether this interaction is altered following microtubule stabilization/destabilization following separate *in-vitro* paclitaxel and vinblastine incubations as an approach to alter microtubule organization in muscle. Lastly, we aimed to determine which ADP-dependent bioenergetic functions are impaired following incubations with these microtubule targeted compounds.

Hypothesis

1) In untreated EDL muscles, both α-tubulin and βII-tubulin will interact with VDAC2 on the mitochondrial outer membrane.

2) *In-vitro* incubations with paclitaxel will cause an increase in microtubule network while vinblastine incubations will cause a decrease in microtubule network.
3) Treatment of muscle fiber bundles with paclitaxel increases α-tubulin and βII-tubulin interaction with VDAC2. This increased interaction will limit the ability of ADP to diffuse through VDAC, impairing ADP-stimulated respiration and attenuation of H_2O_2 emission.
4) Treatment of muscle fiber bundles with vinblastine will decrease α-tubulin and βII-tubulin interaction with VDAC2. This decreased interaction will enhance the diffusion of ADP through VDAC, increasing ADP-stimulated respiration and increasing the sensitivity of ADP to attenuate H_2O_2 emission.
5) As VDAC is speculated to be a central component to the mitochondrial permeability transition pore (mPTP), paclitaxel and vinblastine treatment will alter calcium retention capacity, increasing the cell's susceptibility to apoptosis induced death.

3.3 Objective and hypothesis for study 2 (Chapter 5)

Cardiotoxicity remains to be one of the largest contributors to reduced quality of life in individuals receiving microtubule targeted chemotherapies. Cardiac mitochondrial dysfunction is believed to play a role in the development of this pathology but an exact mechanism remains unknown. The main objective of study 2 was to explore the contribution of the tubulin-VDAC interaction to the development of mitochondrial dysfunction through *in-vitro* and *in-vivo* methodologies. First, we aimed to determine the extent of mitochondrial bioenergetic impairments caused by 2-days of *in-vivo* paclitaxel and vinblastine injections. To determine whether the α-tubulin and βII-tubulin interaction is involved in bioenergetic impairments

observed *in-vivo*, *in-vitro* incubations experiments were utilized to determine protein-protein interactions and then related to mitochondrial bioenergetics. Lastly, to determine whether findings in cardiac tissue are similar to other oxidative tissue, the soleus PmFB was incubated *in-vitro* with both paclitaxel and vinblastine to determine whether the changes in mitochondrial bioenergetics were similar to cardiac tissue.

Hypotheses:

1) *In-vivo* injections with paclitaxel and vinblastine over 2-days in Wistar rats will alter ADP-dependent mitochondrial bioenergetics in a creatine dependent and independent manner. In addition, these cytotoxic drugs will increase the cells susceptibility to death through altered calcium retention capacity and activation of apoptosis through caspases activation.
2) Muscle fiber bundles incubated with paclitaxel will limit ADP-stimulated respiration and ADP attenuation of H_2O_2 in response to an increased α-tubulin and βII-tubulin interaction with VDAC2. Muscle fiber bundles incubated with vinblastine will increase ADP-stimulated respiration and attenuation of H_2O_2 emission in response to a decreased α-tubulin and βII-tubulin interaction with VDAC2
3) As VDAC is a central component of the mPTP, paclitaxel will decrease while vinblastine will increase calcium retention capacity altering the cells susceptibility to apoptosis measured through caspase activation.
4) Soleus muscle fiber bundles incubated with paclitaxel will decrease while vinblastine increases ADP-stimulated bioenergetics. Similarly, paclitaxel and vinblastine will decrease and increase calcium retention capacity respectively, altering the cells susceptibility to apoptosis.

3.4 Objective and hypothesis for study 3 (Chapter 6)

Muscle weakness is a common side effect reported in individuals with cancer. The contribution of the tumor or chemotherapy in the development of muscle weakness is unclear. Following 2-days of *in-vivo* treatment in Wistar rats, we aim to determine voluntary and in-voluntary muscle function capacity as a result of paclitaxel and vinblastine injections. Mitochondrial bioenergetic assessments were then completed to determine whether muscle functional decrements were associated with altered mitochondrial function. To uncover whether the α-tubulin and βII-tubulin interaction with VDAC2 was involved in the mitochondrial dysfunction observed, protein-protein interaction analysis was also completed.

Hypotheses:

1) Following 2-days of both paclitaxel and vinblastine injections, Wistar rats will have reduced voluntary running capacity, grip strength and hind-limb force production.
2) Soleus and white gastrocnemius muscles will exhibit ADP-dependent mitochondrial bioenergetic changes in a creatine dependent and independent manner.
3) ADP-dependent bioenergetic changes will be related to increased and decreased α-tubulin and βII-tubulin interaction with VDAC2 in response to paclitaxel and vinblastine injections respectively.
4) Both paclitaxel and vinblastine will increase the cells susceptibility to apoptosis induced death through altered calcium retention capacity and caspase activation.

3.5 Objective and hypothesis for study 4 (Chapter 7)

An underlying result of Duchenne muscular dystrophy is a disorganized microtubule architecture contributing to whole cell impairments seen with this disease. Previously, our lab uncovered reduced muscle functional capacity and mitochondrial bioenergetic impairments in

the rodent model of Duchenne muscular dystrophy. The objective of this study was to utilize the rodent model of Duchenne muscular dystrophy – a genetic model of altered microtubule organization – to determine whether the α-tubulin-VDAC2 interaction contributes to bioenergetic impairments observed with this disease.

Hypotheses:

1) Microtubule organization will be significantly disorganized in the D2.*mdx* mouse model of Duchenne muscular dystrophy.
2) Disorganized microtubules will result in an altered α-tubulin-VDAC2 interaction in D2.*mdx* mice when compared to wildtype.
3) Disorganized microtubules in combination with an increased α-tubulin-VDAC2 interaction contributes to ADP-dependent mitochondrial bioenergetic impairments found in the D2.*mdx* mouse when compared to wildtype.

3.6 Methodological considerations: The initial design for the above-mentioned studies intended to progress from pharmacological manipulations of microtubules using *in-vitro* and *in-vivo* approaches to a genetic model of disorganized microtubule architecture. The *in-vitro* model analyzed EDL, cardiac, and soleus muscles together to determine changes in tubulin-VDAC interaction with microtubule manipulation across an oxidative spectrum of muscles. We then aimed to continue with the same tissues to an *in-vivo* model to determine whether the observations *in-vitro* were also observed *in-vivo* and in relation to skeletal muscle function. The *in-vivo* study posed some limitation during the selection of tissues to harvest; one leg of tissue would not be usable as it would be utilized for *in-vivo* hind-limb force analyses. This would then leave only one EDL muscle to be divided between mitochondrial bioenergetics (fresh tissue required), embedded sections, glutathione measures (not included), and frozen assays. The resolution was then to select a larger glycolytic tissue capable of meeting all experimental needs, which led to our choice of the white gastrocnemius. During the design of the genetic model (D2.*mdx*) we returned to the EDL muscle given both limbs were available for mitochondrial and imaging analyses.

3.7 Additional Scientific Contributions

The work presented below comprises the contributions made to various studies throughout my PhD not included in this thesis.

Co-First Author Published

1. Hughes MC*., **Ramos SV***., Turnbull PC., Edgett BA., Huber JS., Polidovitch N., Schlattner U., Backx PH., Simpson JA., and Perry CGR. (2019) Impairments in left ventricular mitochondrial bioenergetics precede overt cardiac dysfunction and remodelling in Duchene muscular dystrophy. *Journal of Physiology*, (*In press*) (* denotes equal contributions)

2. Hughes MC*., **Ramos SV***., Turnbull PC., Rebalka IA., Cao A., Monaco CMF., Varah NE., Edgett BA., Huber JS., Tadi P., Schlattner U., Simpson JA., Hawke TJ., and Perry CGR. (2019) Mitochondrial H2O2 emission during impaired oxidative phosphorylation is associated with early myopathy in Duchenne muscular dystrophy. *The Journal of Cachexia, Sarcopenia and Muscle (JCSM*) (*In press*) (* denotes equal contributions)

Co-Author Published

1. Rudnicki M., Abdifarkosh G., Nwadozi E., **Ramos SV**., Makki A., Sepa-Kishi DM., Ceddia RB., Perry CGR., Roudier E., and Haas TL. (2018) Endothelial-specific FoxO1 depletion prevents obesity-related disorders by increasing vascular metabolism and growth. *eLife,* 4;7. pii e39780

2. Song E., **Ramos SV**., Huang X., Liu Y., Botta A., Sung HK., Turnbull PC., Wheeler MB., Berger T., Wilson DJ., Perry CGR., Mak TW., and Sweeney G. (2017). Holo-lipocalin-2-derived siderophores increase mitochondrial ROS and impair oxidative phosphorylation in rat cardiomyocytes. *Proceedings of the National Academy of Sciences (PNAS),* 115(7):1576-1581

3. Monaco CMF., Hughes MC., **Ramos SV**., Varah NE., Lamberz., Rahman FA., McGlory C., Tarnopolsky MA., Krause MP., Laham R., Hawke TJ., and Perry CGR. (2018). Altered mitochondrial bioenergetics and ultrastructure in skeletal muscle of young adults with type 1 diabetes. *Diabetologia*, 61(6):1411-1423

4. MacPherson REK., Dragos SM., **Ramos SV**., Sutton C., Frendo-Cumbo S., Castellani L., Watt MJ., Perry CGR., Mutch DM., and Wright DC. (2016). Reduced ATGL-mediated lipolysis attenuates beta-adrenergic-induced AMPK signaling, but not the induction of PKA-targeted genes, in adipocytes and adipose tissue. *American Journal of Physiology, Cell Physiology*, 311:C269-C276

5. Hughes MC., **Ramos SV**., Turnbull PC., Nejatbakhsh A., Beachler BL., Tahmasebi H., Laham R., Gurd BJ., Quadrilatero J., Kane DA., and Perry CGR. (2015). Mitochondrial

bioenergetics and fiber type assessments in microbiopsy vs. Bergstrom percutaneous sampling of human skeletal muscle. *Fontiers in Physiology,* 6:360

Chapter 4

Altered skeletal muscle microtubule-mitochondrial VDAC2 binding is related to bioenergetic impairments after paclitaxel but not vinblastine chemotherapies.

This chapter is an original published article in the *American Journal of Physiology*; Cell, Rapid Reports. It is included in this thesis in the published format.

Assay development prior to initiation of experiments

- Optimization of mitochondrial respiration and H_2O_2 kinetics following the incubation of various microtubule targeted compounds
- Single extensor digitorum longs (EDL) fiber isolation and fixation
- Immunohistochemical staining of EDL single fibers
- Optimization and protocol development of the proximity ligation assay

Author contributions: Initial study design was completed by Christopher GR Perry (CGRP), Meghan C Hughes (MCH) and the previous undergraduate thesis students. Tissue harvest and experimental data collection for this and subsequent chapters were completed by Sofhia V Ramos (SVR) and MCH because mitochondrial bioenergetic assays require the use of fresh tissues and therefore required the presence of two people to complete assays in a timely manner. SVR analyzed data, SVR, MCH and CGRP interpreted results, SVR and CGRP, prepared figures and drafted manuscript. All authors edited, revised and approved final version of manuscript.

Altered skeletal muscle microtubule-mitochondrial VDAC2 binding is related to bioenergetic impairments after paclitaxel but not vinblastine chemotherapies

Authors: Sofhia V. Ramos*, Meghan C. Hughes*, Christopher G.R. Perry
School of Kinesiology and Health Science, Muscle Health Research Center, York University, 4700 Keele Street, Toronto, ON, Canada, M3J 1P3
*Represents equal contributions

List of abbreviations

VDAC – Voltage dependent anion channel

ADP – Adenosine diphosphate

ATP- Adenosine triphosphate

PmFB – Permeabilized fiber bundles

mPTP- Mitochondrial permeability transition pore

PDC – Pyruvate dehydrogenase complex

CRC – Calcium retention capacity

DMSO – Dimethyl sulfoxide

Running Head: Microtubule stability and mitochondrial bioenergetics

Abstract

Microtubule-targeting chemotherapies are linked to impaired cellular metabolism which may contribute to skeletal muscle dysfunction. However, the mechanisms by which metabolic homeostasis is perturbed remains unknown. Tubulin, the fundamental unit of microtubules, has been implicated in the regulation of mitochondrial-cytosolic ADP/ATP exchange through its interaction with the outer membrane voltage-dependent anion channel (VDAC). Based on this model, we predicted that disrupting microtubule architecture with the stabilizer paclitaxel and destabilizer vinblastine would impair skeletal muscle mitochondrial bioenergetics. Here we provide *in-vitro* evidence of a direct interaction between both α-tubulin and βII-tubulin with VDAC2 in un-treated single extensor digitorum longus fibres. Paclitaxel increased both α- and βII-tubulin-VDAC2 interactions whereas vinblastine had no effect. Utilizing a permeabilized muscle fiber bundle preparation that retains the cytoskeleton, paclitaxel treatment impaired the ability of ADP to attenuate H_2O_2 emission, resulting in greater H_2O_2 emission kinetics. Despite no effect on tubulin-VDAC2 binding, vinblastine still altered mitochondrial bioenergetics through a surprising increase in ADP-stimulated respiration while also impairing ADP-suppression of H_2O_2 and increasing mitochondrial susceptibility to calcium-induced formation of the pro-apoptotic permeability transition pore. Collectively, these results demonstrate that altering microtubule architecture with chemotherapeutics disrupts mitochondrial bioenergetics in EDL skeletal muscle. Specifically, microtubule stabilization increases H_2O_2 emission by impairing ADP sensitivity in association with greater tubulin-VDAC binding. In contrast, decreasing microtubule abundance triggers a broad impairment of ADP's governance of respiration and H_2O_2 emission as well as calcium retention capacity albeit through an unknown mechanism.

Keywords: microtubule, mitochondria, chemotherapy, paclitaxel, vinblastine, fatigue

Introduction

Two common classes of chemotherapeutics are the microtubule-targeting taxanes (eg. paclitaxel, or taxol) and vinka alkaloids (eg. vinblastine) which are used as treatments for solid-state tumors in multiple cancers. Many patients receiving these types of chemotherapies report symptoms of fatigue (152), and tumor-free rat models injected with these compounds show severe hind-limb muscle weakness and impaired cardiac contraction (50, 71). This weakness has been associated with the development of peripheral neuropathies induced by chemotherapies, where paclitaxel and vinblastine alter neuronal microtubules causing axonal dysfunctions and transmission impairments (37, 64). These peripheral nerve dysfunctions have been associated with marked mitochondrial respiratory impairments leading to substantial morphological changes to skeletal muscle and cellular metabolic stress (37, 47, 71). However, the degree to which this also occurs in skeletal muscle fibres remains unknown. Likewise, the mechanism by which these drugs impair oxidative phosphorylation is uncertain as is their influence on mitochondrial reactive oxygen species emission and calcium-induced permeability transition pore (mPTP) formation. Given all three bioenergetic functions are critical determinants of cell fate (97), understanding the relationship between altered microtubule dynamics and mitochondrial bioenergetics may provide insight into the mechanism by which these compounds disturb cellular metabolism in muscle.

Both paclitaxel and vinblastine disrupt the normal dynamics of microtubules leading to cell death following mitotic arrest in tumors (23). An emerging model has proposed that microtubules regulate mitochondrial bioenergetics in muscle through direct binding of tubulin to the ADP/ATP exchanger voltage dependent anion channel (VDAC) on the outer mitochondrial membrane (Figure 1A) (42). The available literature suggests α- and β-tubulin likely binds

VDAC in muscle which may impede ADP import, thereby implicating microtubules as regulators of ADP-dependent mitochondrial bioenergetics (126, 127, 161). As the model posits that any change in tubulin-VDAC binding would alter ADP's control of bioenergetics (Figure 1A), an extended prediction is that stressors that manipulate microtubule architecture may alter ADP-dependent bioenergetics. If true, this relationship may represent a novel mechanism by which microtubule-targeting chemotherapy disrupts cellular energy homeostasis in muscle.

The purpose of this study was to determine whether paclitaxel and vinblastine alter mitochondrial bioenergetics by manipulating tubulin-VDAC2 binding in skeletal muscle. VDAC2 is of particular interest as global gene knock down of VDAC1 (abundant on both sarcolemma and mitochondrial outer membranes) and VDAC3 (present on the mitochondrial outer membrane) isoforms permit proper embryonic and pup development whereas VDAC2 knock down resulted in embryonic death signifying its importance for survival (112). We employed a proximity ligation assay with 12-angstrom resolution (126, 161) to determine the extent of isoform-specific tubulin binding to VDAC2. We then determined the effect of these compounds on ADP-dependent bioenergetics, namely ADP-stimulated oxidative phosphorylation, ADP-attenuation of H_2O_2 emission as occurs through lowering membrane potential, as well as the propensity for mPTP formation as VDAC has been implicated in this process.

Materials and Methods

Animal Care

Male and female Wistar rats (180.9 ± 7.0g) bred at York University (Toronto, Ontario) but purchased at Charles River laboratories (Toronto, Ontario). Housing was maintained on a 12:12-h light dark cycle in pairs. Rats were fed standard rodent chow and had ad libitum access

to food and water. A total of 35 rats, ages 6-8 weeks, were used for the completion of bioenergetic (*n*=24) and immunohistochemical experiments (*n*=11). All procedures were in accordance to the Canadian Care Animal Committee and with approval from the York University Animal Care Committee (AUP 2016-19).

Preparation of permeabilized muscle fiber bundles (PmFB) and mitochondrial bioenergetic assays

The extensor digitorum longus (EDL) muscle was removed and immediately placed in BIOPS buffer on ice for further separation of fibers into intact bundles (2-4 mg wet weight) that were incubated at 4°C with either the microtubule stabilizer, paclitaxel (Tocris, 1097, Minneapolis, USA) at 23μM for 2hrs (96) or the microtubule destabilizer vinblastine (Sigma-Aldrich, V1377, Missouri, USA) at 3μM for 1hr (101). Control bundles were incubated in corresponding concentrations of the vehicle DMSO. Following incubations, bundles were permeabilized (PmFB) with saponin (75, 104) and washed for 15 minutes at 4°C. Bundles dedicated to H_2O_2 emission were permeabilized in the presence of 2,5-dinitrochlorobenzene (CDNB) to deplete glutathione and allow the detection of H_2O_2 emission (35). Respiration assays were completed using a high-resolution respirometer (Oroboros Instruments Corp., Innsbruck, Austria) at 37°C in MiRO5 respiration media supplemented with 20mM creatine (8, 136) and 5μM blebbistatin to prevent PmFB contraction (89, 106). Creatine was used to saturate mitochondrial creatine kinase to promote efficient cytosolic-mitochondrial exchange of creatine and phosphocreatine through VDAC, in addition to ADP/ATP, to optimize respiratory conditions (42).

Separate PmFB were used for fluorometric detection of H_2O_2 emission (QuantaMaster 40, HORIBA Scientific) with Amplex UltraRed as described previously (89). Briefly, PmFB

were placed into a quartz cuvette containing Amplex Ultra Red dissolved in Buffer Z. H_2O_2 emission was induced with the addition of 10mM pyruvate and 4mM malate (NADH, complex I) followed by a titration of ADP to determine the efficiency of attenuating H_2O_2 emission. Other PmFB were used to determine calcium retention capacity (CRC) utilizing EGTA coated cuvettes, loaded with 300μL of Buffer Y supplemented with 1μM calcium green-5N (Invitrogen), 2μM thapsigargin, 5mM 2-deoxyglucose, 2U/mL hexokinase, 20mM creatine, 5mM glutamate, 2mM malate, 5μM blebbistatin and 40μM EGTA. Briefly, Ca^{2+} uptake was initiated with 8nmol pulses of $CaCl_2$ with subsequent 4nmol pulses until mPTP opening was observed (QuantaMaster 80; HORIBA Scientific)(89).

Immunohistological experiments and image acquisition

EDL muscle was collagenase-treated, single fibers were isolated and then treated with 23μM paclitaxel, 3μM vinblastine or DMSO for 2hrs at room temperature. Following drug incubations fibers were washed, fixed, blocked and permeabilized in preparation for staining. Primary and secondary antibodies used were as follows; α-tubulin (1:1000, Sigma-Aldrich; T6199), β-II tubulin (1:250, Abcam; ab28036) (separate fibres), VDAC2 (1:250 santa cruz; 32059), Alexa Flour 488 (Invitrogen/Thermo-Fisher Scientific, A21121) and Alexa Flour 555 (Invitrogen/Thermo-Fisher Scientific, AS1431). The proximity ligation procedures were completed as previously done (63, 126). Briefly, fibers containing primary antibodies were incubated with oligonucleotide secondary probes and then subsequently with detection reagents allowing the quantification at a specific wavelength. All fibers were coated with mounting media and secured with a cover slip. Minimal background signal during the proximity ligation assay was verified by incubating fibres with the probes, ligase and polymerase using each antibody

above in isolation (Figure 1B). Control experiments confirmed the specificity of the proximity ligation assay used to detect tubulin-VDAC2 interactions (Figure 1B).

Images were acquired using a Zeiss laser scanning confocal microscope 700 (Carl Zeiss, Thornwood, NY). Images were collected with a 40X oil-immersion lens with the pin hole adjusted to 1AU capturing 3 fields of view per sample with 8-12 stacks and a z-step of 0.23 μm. Image quantitation was completed using Imaris image quantifying software (Bitplane, Zurich, Switzerland) using the spot tool to identify protein-protein interactions.

Analysis and statistics

Results are reported as mean ± SEM with significance accepted at $p< 0.05$. PmFB were randomized into groups and all analyses were completed in an un-blinded fashion. Outliers were omitted in accordance with the ROUT test. The D'Agostino–Pearson omnibus or Shapiro-Wilks normality test was first performed to determine whether data resembled a Gaussian distribution. Given all data passed normality, differences between the means were then tested (GraphPad Prism 7, La Jolla, CA) by one-way ANOVA for proximity ligation assays, two-way ANOVA for ADP-stimulated respiration and attenuation of H_2O_2 emission followed by Fisher's least squares difference post-hoc analyses when a significant *F* ratio was obtained. A student's un-paired t-test was used to test differences in CRC and all other H_2O_2 emission data in absence of ADP.

Results

Paclitaxel increased both α-tubulin-VDAC2 (p=0.001) and β-II-tubulin-VDAC2 interactions (p=0.0001) (Figure 1B, C, D) which appeared to be associated with altered organization of α-tubulin as has been shown previously (65) but not βII-tubulin (Figure 2). Paclitaxel α- (p=0.0002) and βII-tubulin-VDAC2 (p=0.002) interaction was also significantly higher when comparing paclitaxel and vinblastine. Vinblastine had no effect on either isoform's

interaction with VDAC2 (Figure 1B, C, D) despite an apparent reduction in α-tubulin content (Figure 2).

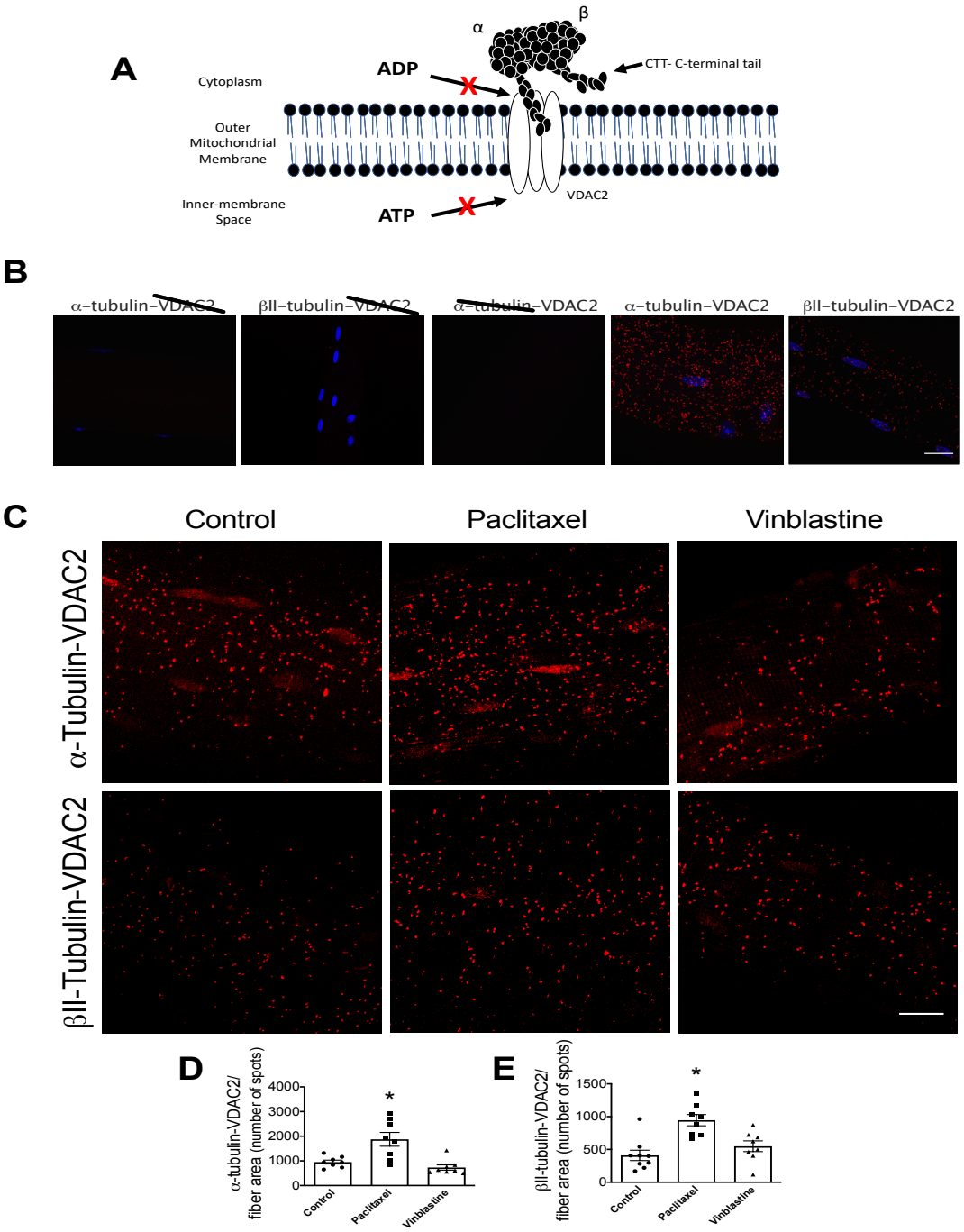

Figure 4-1. α-tubulin-VDAC2 interactions in EDL single fibers increase following Paclitaxel stabilization. A. Model of tubulin regulation of VDAC-dependent ADP/ATP exchange (adapted from (42)). Confocal microscopy images of single EDL **B.** Control experiments in the presence of either α-tubulin, βII-tubulin or VDAC2 incubated alone or together (*n*=3) **C.** Proximity ligation assay representative images**. D.** Graphical depiction of α-tubulin-VDAC2 protein interaction, (*n*=8, **p*=0.001 vs control). **E.** Graphical depiction of βII-tubulin-VDAC2 interaction, (*n*=8-9, **p*=0.0001 vs control). Scale bar,16μm. Results are reported as means ± SEM.

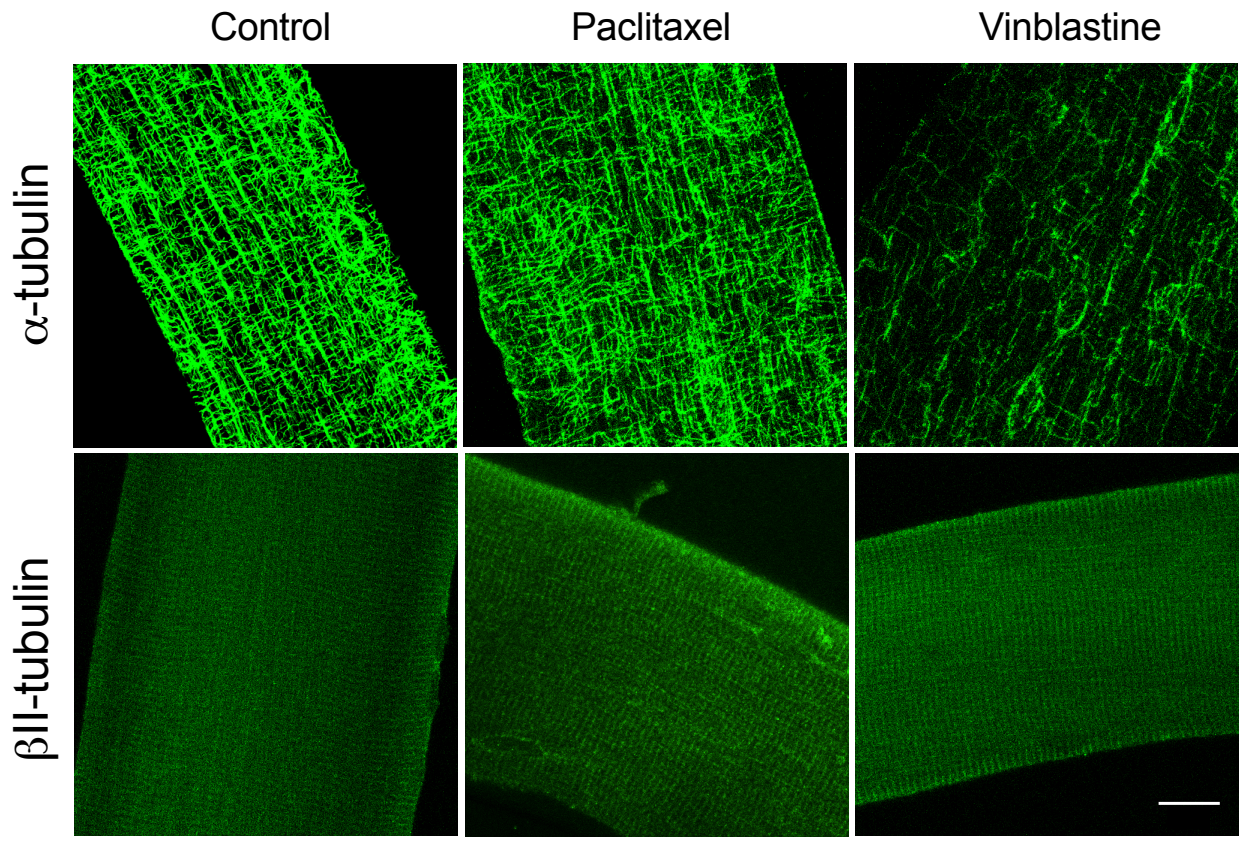

Figure 4-2. α-tubulin but not βII-tubulin organization is altered following microtubule-targeted chemotherapy. Confocal microscopy representative images of single EDL fibers stained with antibodies recognizing α-tubulin and βII-tubulin following either control (DMSO), paclitaxel or vinblastine treatment. Scale bar, 16μm.

We next determined the degree to which ADP-dependent mitochondrial bioenergetics were affected by either drug. After stimulating complex I-supported respiration with NADH (generated by pyruvate and malate), subsequent titrations of ADP were not affected by paclitaxel yet were surprisingly increased by vinblastine (Figure 3A, B). While neither drug affected H_2O_2 emission in the absence of ADP (Figure 3C, D), paclitaxel impaired the ability of ADP to attenuate H_2O_2 emission (Figure 3E, p=0.0006, main effect) consistent with greater interactions between VDAC2 and both β-II and α-tubulin. Vinblastine, while having no effect on tubulin-VDAC2 binding, also impaired ADP's attenuation of H_2O_2 (Figure 3F, p=0.002, main effect).

Similar impairments in the ability of ADP to attenuate H_2O_2 by both drugs were seen when supported by succinate (reverse electron flow to Complex I, data not shown). Pyruvate dehydrogenase complex-supported H_2O_2 was also assessed as a control given it is not regulated directly by ADP. No effect of either drug was observed (Figure 3G and H) suggesting that the drugs act specifically on ADP's ability to attenuate H_2O_2 as noted above.

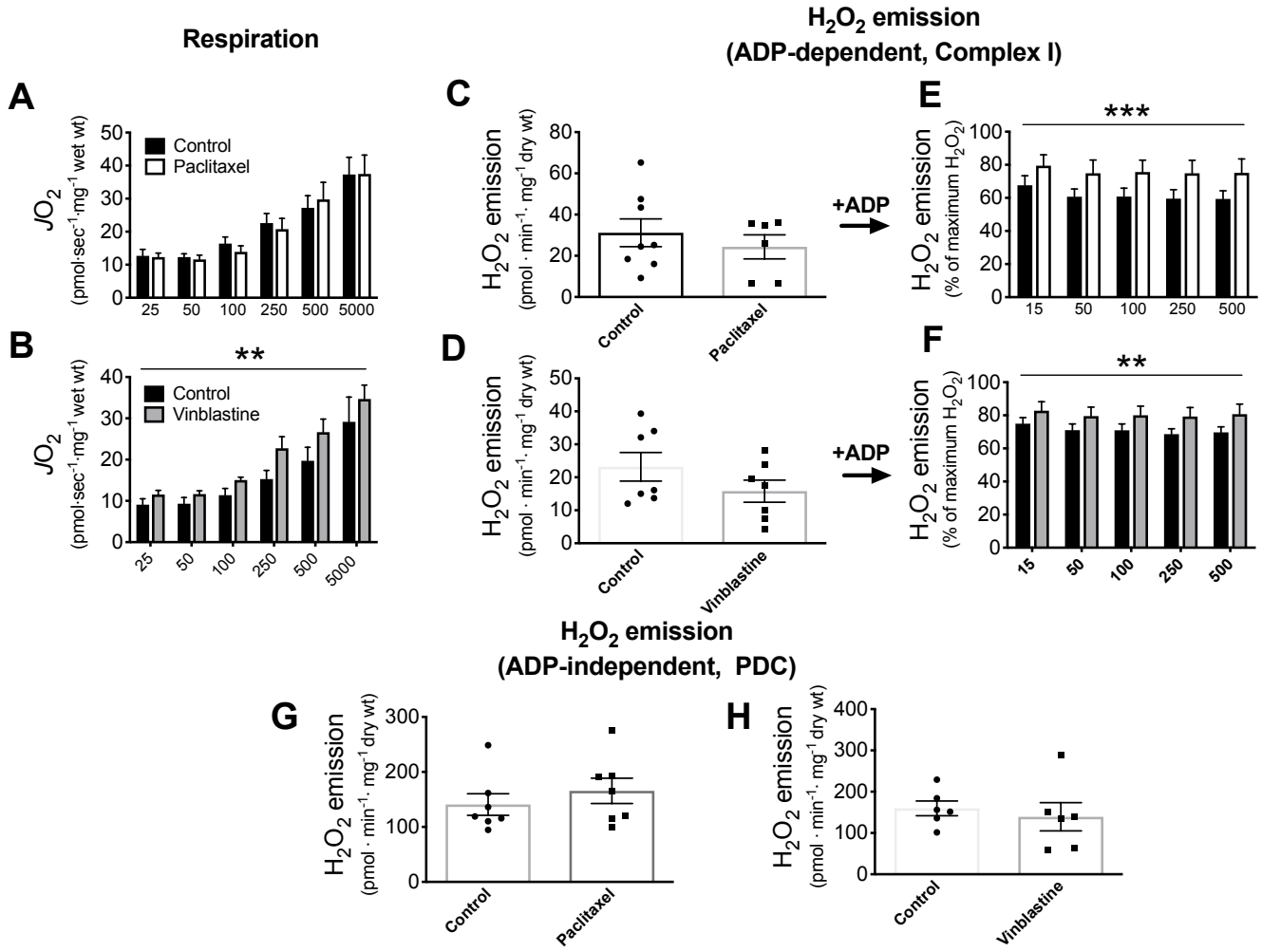

Figure 4-3. ADP-dependent mitochondrial bioenergetics is altered following microtubule-targeted chemotherapy incubations in EDL PmFB. Complex I-supported (NADH from 5mM pyruvate/4mM malate) State 3 (+ADP) respiration was tested following incubations with (*n*=6-8) **A.** paclitaxel and **B.** vinblastine. Complex I-supported (10mM pyruvate/4mM malate) H_2O_2 emission in the absence (*n*=6-8) **(C, D)** and presence of ADP **(E, F)** was determined following both paclitaxel and vinblastine incubations (*n*=6-8).

ADP-insensitive Pyruvate Dehydrogenase Complex (PDC)-supported (10mM pyruvate) H_2O_2 emission was tested with **G.** paclitaxel and **H.** vinblastine incubations (*n*=6-7). **p<0.01, ***p<0.001 vs control. Results are reported as mean ± SEM.

Given VDAC's potential role in the formation of the mPTP and mitochondrial induction of cell death (75), a calcium-titration 'stress' protocol was used to determine CRC as an index of the propensity for mPTP induction. Similar concentrations of calcium were required to open the mPTP following paclitaxel incubations (Figure 4A) while vinblastine demonstrated a reduced CRC suggesting a greater sensitivity to calcium-induced mPTP (Figure 4B, *p*=0.01).

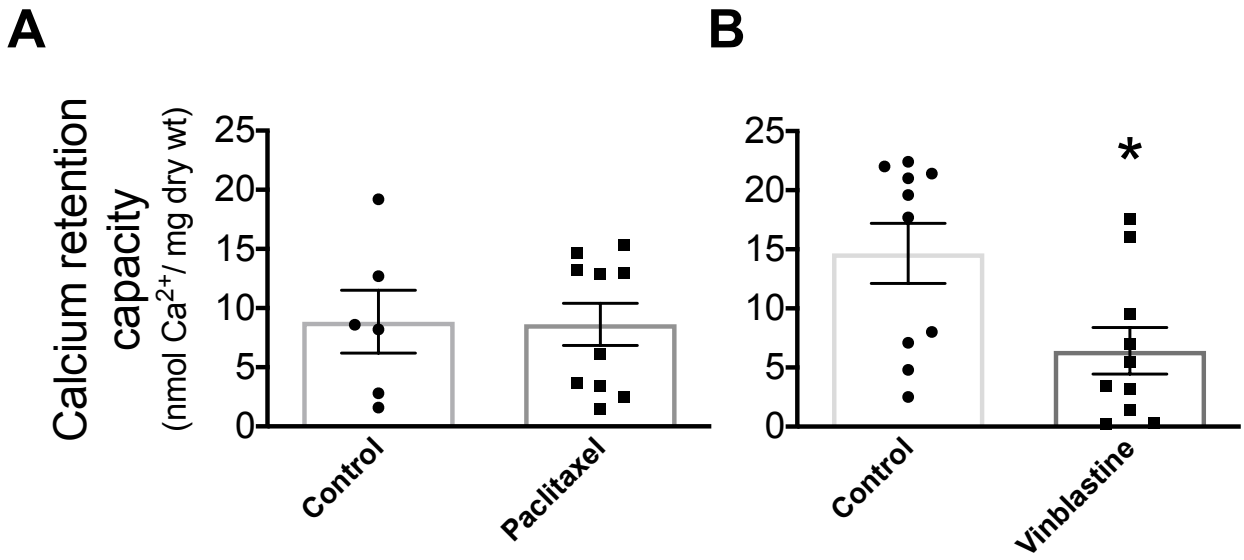

Figure 4-4. Calcium retention capacity is altered following vinblastine incubation in EDL PmFB. Mitochondrial calcium retention capacity following **A.** paclitaxel and **B**. vinblastine. *p<0.05 vs control, (*n*=6-10). Results are reported as mean ± SEM.

Discussion

Using a high-resolution proximity ligation assay, we demonstrate that both α- and βII-tubulin interact with VDAC2 in EDL muscle, confirming previous suggestions in skeletal muscle based on confocal fluorescent overlay approaches. This finding aligns with the proposed model that tubulin isoforms regulate ADP/ATP exchange through VDAC on the outer mitochondrial

membrane in skeletal muscle (161). We then treated muscles with the microtubule-stabilizer paclitaxel and destabilizer vinblastine to determine whether altering microtubule architecture changed tubulin-VDAC2 interactions and ADP-dependent mitochondrial bioenergetics. Here we show that paclitaxel increased α-tubulin-VDAC2 and βII-tubulin-VDAC2 interactions and impaired the ability of ADP to attenuate H_2O_2 emission, which supports the model. In contrast, vinblastine did not alter tubulin-VDAC2 interactions but still impaired ADP-dependent mitochondrial bioenergetics. These findings suggest that both cytotoxic drugs cause mitochondrial dysfunction but potentially through different mechanisms.

Several lines of evidence suggest that tubulin may impede ADP's control of mitochondrial bioenergetics by directly decreasing VDAC permeability. The organization of βII-tubulin in proximity to mitochondria in rat skeletal and cardiac muscle suggests its involvement in regulating mitochondrial bioenergetics (41) This interaction has also been explored in cancer cell lines where transmission electron microscopy experiments identified both α- and β-tubulin in close proximity with the mitochondria. Co-immunoprecipitation experiments have also identified α-tubulin and VDAC in mitochondrial isolations (20). In addition, trypsin removal of βII-tubulin increased ADP-stimulated respiration in cardiomyocytes while the addition of tubulin to isolated mitochondria decreased ADP-stimulated respiration, further supporting the role of tubulin in VDAC permeability regulation (127, 161). The present findings align with this model by demonstrating a direct interaction between VDAC2 and both α- and βII-tubulin in skeletal muscle, and that these interactions are increased by altering microtubule architecture with paclitaxel in conjunction with impaired ADP-control of H_2O_2 emission.

While paclitaxel increased tubulin-VDAC2 interactions and impaired ADP-attenuation of H_2O_2 emission, a similar impairment in ADP-stimulated respiration was not observed. This

finding does not align with the proposed model that tubulin regulates ADP's overall control of bioenergetics. The lack of effect of paclitaxel on ADP-stimulated respiration contrasts with evidence that the removal or addition of tubulin to permeabilized cardiomyocytes (40) and isolated brain mitochondria (126) increases and decreases ADP-stimulated respiration respectively. While the results challenge the model of tubulin's regulation of respiration, the differences between studies may be related to the examined tissues and cellular models or sample preparations (eg. cardiomyocytes, isolated brain mitochondria, cancer cell culture and permeabilized skeletal muscle fibres). A previous report in skeletal muscle demonstrated an inverse association between free/non-polymerized tubulin and mitochondrial sensitivity to ADP, suggesting free tubulin may regulate VDAC permeability to ADP, although the comparison was performed between muscles with differing ADP sensitivities rather than using an approach of manipulating free or polymerized tubulin. The present study suggests a refinement to the model in EDL whereby altering tubulin-VDAC2 binding in this muscle alters ADP-control of H_2O_2 emission specifically. The lack of effect on ADP-control of respiration is perplexing but may be due to slight changes in ADP permeability such that H_2O_2 emission responds with greater sensitivity than respiration, at least in muscle. In addition, it has been suggested that VDAC also facilitates the export of mitochondrial-derived phosphocreatine in addition to ADP/ATP cycling, but this is not fully established (42). Given creatine was present in the assays during respiration and H_2O_2 emission, it is possible that creatine/phosphocreatine cycling may also have been modulated by paclitaxel's effect on tubulin-VDAC2 and may serve as an area for future research. Finally, the lack of change in calcium-induced PTP in EDL with paclitaxel contrasts with previous work in permeabilized cardiomyocytes which reported increased propensity for mPTP formation (74). This may suggest that paclitaxel's effects on mPTP are fibre-type dependent.

Following vinblastine incubations, we reported a surprising increase in ADP-stimulated respiration, as well as an impairment of ADP suppression of H_2O_2 and increased susceptibility to apoptosis. However, there were no changes in tubulin-VDAC2 interactions which suggests off-target effects on mitochondrial bioenergetics. For example, vinblastine activates apoptosis through the c-Jun N-terminal protein pathway (JNK) as reported in human cervical carcinoma cells (70), and nocodazole – another microtubule destabilizer – triggers the release of cytochrome *c* oxidase through the formation of the mPTP (74). This is consistent with the reduced CRC seen in the present study whereby less calcium is required to trigger mPTP. An alternative mechanism to explore is the possibility that lower tubulin content following vinblastine treatment disrupts mitochondrial morphology by impairing tethering to microtubules through a Miro GTPase regulated docking system (74) which would occur independently of VDAC. It is also possible that vinblastine altered VDAC2 interactions with other isoforms of tubulin or tubulin interactions with mitochondrial VDAC1 or 3. These VDAC isoforms were not examined in the present study given VDAC1 is also on the sarcolemma and would be difficult to separate in the proximity ligation assay, whereas VDAC3 is less abundant than VDAC2 (85). Collectively, our findings suggest either the tubulin-VDAC model is more complex than previously proposed or vinblastine's effects on cellular stress responses linked to mitochondrial dysfunction are independent of tubulin-VDAC binding.

Conclusion

These findings demonstrate that microtubule-targeting chemotherapy impairs mitochondrial bioenergetics in EDL skeletal muscle. In the case of paclitaxel, we identified altered tubulin-VDAC2 interactions as a novel potential mechanism underlying this compound's effect on increasing H_2O_2 emission through impairing control by ADP. The effects of paclitaxel

also support the developing model that mitochondria are subject to regulation by cytoskeletal dynamics through microtubule influence on bioenergetic control by ADP, but the dissociation between ADP's control of respiration and H_2O_2 emission should be a focus for further investigation. Moreover, it appears that microtubule disruption by vinblastine is associated with impaired mitochondrial bioenergetics through mechanisms distinct from tubulin-VDAC interactions. Ultimately, these findings serve as a foundation for exploring the mechanism by which these chemotherapeutics contribute to muscle dysfunction and suggest microtubule dynamics may be a potential mechanism in this regard.

Author contributions: S.V.R., M.C.H., and C.G.R.P. contributed to conception and design of research; S.V.R. and M.C.H. performed experiments; S.V.R. analyzed data; S.V.R., M.C.H. and C.G.R.P. interpreted results; S.V.R. and C.G.R.P., prepared figures and drafted manuscript. S.V.R., M.C.H. and C.G.R.P. edited, revised and approved final version of manuscript.

Acknowledgements

We would thank Drs. Thomas Hawke and Donna D'Souza, McMaster University, for their initial guidance in single EDL fiber preparation.

Funding

This project was funded by the Natural Sciences and Engineering Research Council of Canada (436138-2013), James H. Cummings Foundation grant and a Canada Foundation for Innovation and Ontario Research Fund grant (32449) to C.G.R.P., S.V.R. received an Ontario Graduate Scholarship and M.C.H. received a NSERC CGS-PhD scholarship.

Supplemental figure – not included in published article

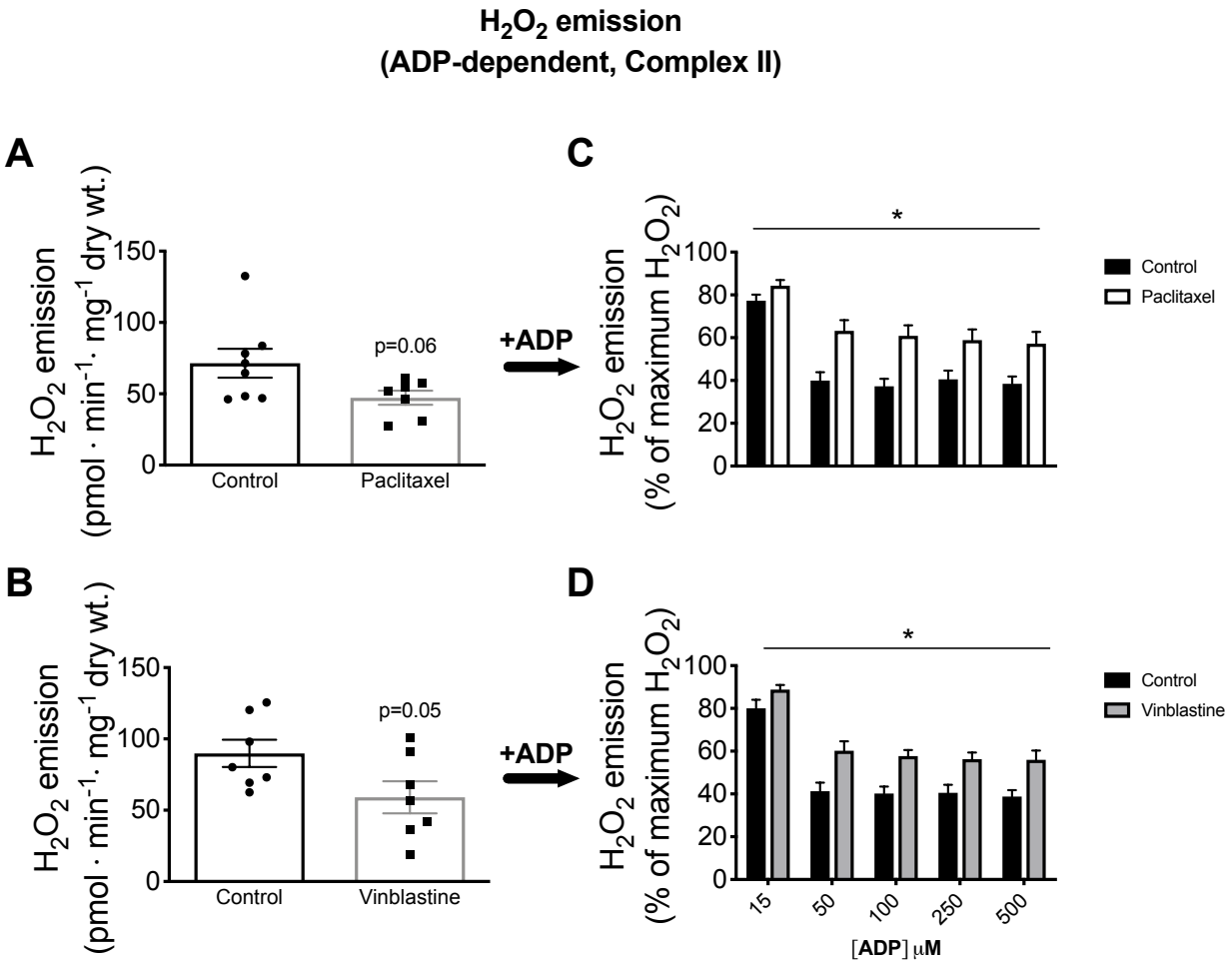

Supplemental figure 4-1. H_2O_2 emission and kinetics following microtubule-targeted chemotherapy incubations in EDL PmFB. Complex-II supported (FADH2 from 5mM succinate) H_2O_2 emission was tested in the absence of (A. and B.) and presence of (C. and D.) ADP following both paclitaxel and vinblastine incubations (n=7-8). *$p<0.05$ vs. control. Results are reported as mean ± SEM.

Chapter 5
Microtubule targeted chemotherapies impair mitochondrial ADP-sensitivity in rat myocardium

This chapter has been written in preparation for submission to the journal of *Biochimica et Biophysica Acta*. It is included in this thesis in the pre-submission format.

Assay development prior to initiation of experiments

- Optimization of mitochondrial respiration and H_2O_2 kinetics in cardiac tissue following the incubation of various microtubule targeted compounds
- Isolated cardiomyocyte immunohistochemical staining and optimization for proximity ligation assay

Author contributions: Initial study design was completed by Christopher GR Perry (CGRP), Meghan C Hughes (MCH) and the previous undergraduate thesis students. Tissue harvest and experimental data collection for this and subsequent chapters were completed by Sofhia V Ramos (SVR) and MCH because mitochondrial bioenergetic assays require the use of fresh tissues and therefore required the presence of two people to complete assays in a timely manner. ES harvested hearts and isolated cardiomyocytes used for imaging. SVR analyzed data, SVR, MCH and CGRP interpreted results, SVR and CGRP, prepared figures and drafted manuscript. All authors edited, revised and approved final version of manuscript.

Microtubule targeted chemotherapies impair mitochondrial ADP-sensitivity in rat myocardium.

Authors: Sofhia V. Ramos[a,c]., Meghan C. Hughes[a,c]., Erfei Song[b]., Trevor Teich[ac]., Gary Sweeney[b]., and Christopher G.R. Perry[a,c]

[a]School of Kinesiology and Health Science, [b]Department of Biology, [c]Muscle Health Research Center. York University, 4700 Keele Street, Toronto, ON, Canada, M3J 1P3

Abstract

Microtubule targeted chemotherapies have been known to induce mitochondrial dysfunction in muscle which may be linked to the development of cardiotoxicity reported in cancer patients. Unfortunately, mechanisms underlying mitochondrial dysfunctions have yet to be determined. An intriguing model presents the regulation of ADP permeability through an interaction between the monomeric component of microtubules, tubulin, and the voltage dependent anion channel (VDAC) in regulation of ADP permeability and therefore mitochondrial bioenergetic function. To explore this further, we aim to determine the effect of microtubule stabilization and destabilization on cardiac muscle mitochondrial bioenergetic function and its relation to the proposed tubulin-VDAC model utilizing *in-vivo* and *in-vitro* methods. Utilizing permeabilized muscle fiber bundle preparation, this work demonstrates impairments to ADP-depended respiration and attenuation of H_2O_2 emission in both *in-vivo* and *in-vitro* models' independent of a change in α- and βII-tubulin interaction *in-vitro*. These results may not be transferable to all oxidative tissues as only minor ADP-dependent mitochondrial bioenergetic impairments were observed following acute *in-vitro* treatment with microtubule targeted chemotherapies in soleus muscle. This work is the first to identify the onset of cardiac mitochondrial dysfunction in response to a 2-day treatment with microtubule targeted chemotherapies. While the tubulin-VDAC2 model was not fully supported, it does not discount the possibility of other tubulin and VDAC isoforms contributing to the mitochondrial dysfunctions observed.

Introduction

Microtubule targeted chemotherapies such as taxanes (eg. Paclitaxel) and vinka alkaloids (eg. Vinblastine) are commonly used therapies for treating breast, ovary and lung cancers (37, 119). These compounds prevent tumor cell growth by stabilizing or destabilizing microtubules, preventing spindle formation and further cell division. As chemotherapy is not cell specific, non-mitotic heart tissue is also exposed to the effects of microtubule stabilization or destabilization, losing its microtubule dynamics. Currently, there is a host of literature exploring the effect of microtubule targeted chemotherapy in the development of peripheral neuropathy but the effects on cardiac muscle and its contribution to cardiotoxicity remain largely unknown.

The mechanisms by which disorganized microtubules may contribute to cardiotoxicity with these chemotherapies remain incompletely characterized. The underlying role of microtubule dysregulation becomes more perplexing when considering that paclitaxel and vinblastine have also been linked to mitochondrial dysfunction in muscle (50, 71, 116). While microtubules serve diverse roles in cellular dynamics, the manner by which microtubule effects mitochondrial bioenergetics becomes an intriguing question as microtubules have been found to physically bind the outer mitochondrial membrane. This is mediated through an interaction between the voltage gated dependent anion channel (VDAC) and the dimeric component of microtubules, tubulin (40, 127). It has been speculated that tubulin directly mediates ADP permeability through its interaction with VDAC but it is currently unknown under what cellular conditions this interaction occurs.

The addition of tubulin to isolated mitochondria and removal of tubulin from cardiomyocytes by trypsin has revealed a decrease and increase and ADP stimulated respiration providing evidence that tubulin regulates ADP-dependent mitochondrial bioenergetics(40, 127). The

implications of this model are profound given ADP is required to drive oxidative phosphorylation (ie. ATP synthesis). In so doing, ADP attenuates membrane potential which decreases premature slip onto oxygen and subsequent reactive oxygen species generation emitted from mitochondria in the form of H_2O_2. Impairments in the ability of the mitochondria to produce or maintain adequate amounts of ATP has been linked to several diseases (39, 89, 149). As such, the possibility that microtubules may directly influence ADP import and ATP export from mitochondria positions this component of the cytoskeleton as a potential mediator of mitochondrial dysfunction in conditions of altered microtubule architecture. The degree to which such a microtubule-mitochondrial axis underlies metabolic dysfunction remains ill defined, particularly in muscle disorders. This model becomes particularly intriguing for models of cardiac dysfunction given much of the research on tubulin-VDAC regulation has been performed in cardiomyocytes (20, 127, 136, 161).

Limited work has been completed on elucidating the importance of microtubules in mitochondrial bioenergetic and functional regulation. Ventricular cardiomyocytes display reduced calcium transients and contractile amplitude in response to an acute taxol treatment (50). In addition, both microtubule stabilization and destabilization with paclitaxel and nocodozole respectively, have been shown to depolarize membrane potential and induced mitochondrial permeability transition pore (mPTP) formation, an indicator of the initiation of apoptosis (74). Central to these events is VDAC, where it is believed to play a central role in the maintenance of membrane potential and initiation of mPTP (10, 81, 128). Interestingly, microtubules also appear to play a pivotal role in these mitochondrial bioenergetic impairments as paclitaxel and nocodozole administration to isolated mitochondria did not change membrane potential, highlighting the importance of microtubules to mitochondrial bioenergetic function. What

remains unknown is whether the link between alterations in microtubule architecture and mitochondrial bioenergetic impairments lies within the proposed tubulin-VDAC model.

Microtubule stabilization increases the network density of microtubules while destabilization reduces it which may be impeding proper intracellular function (23, 65). In the heart, microtubule stabilization has been shown to limit contractile function which may lead to adverse cardiac events (65, 138, 159). Developing a better understanding of how the disorganization of microtubules alters the tubulin-VDAC interaction may provide further insight to understanding the cardio-toxic side effects seen with microtubule targeted chemotherapies.

The purpose of the current investigation is two-fold; first, we aim to determine the effects of paclitaxel and vinblastine chemotherapies administered *in-vivo* and *in-vitro* on cardiac muscle mitochondrial bioenergetics, specifically ADP-dependent respiration and attenuation of H_2O_2 emission as well as the cells susceptibility to death through the formation of the mPTP in cardiac muscle. We then explored whether such alterations in mitochondrial bioenergetics are related to altered tubulin-VDAC2 as previously proposed (40, 127). We hypothesized that microtubule stabilization will impair ADP-sensitivity through increased tubulin-VDAC2 interactions while microtubule destabilization enhances ADP-sensitivity through decreased tubulin-VDAC2 interactions. Through impaired ADP sensitivity, we also hypothesize that H_2O_2 emission and susceptibility to calcium-induced apoptosis will be impaired in response to both microtubule stabilizing and destabilizing drugs.

Methods

Laboratory animal care and handling

30 male Wistar rats, 4-6 weeks old (302.6 ± 7.3g) were purchased from Charles River Laboratories (Toronto, Ontario) and utilized for the completion of *in-vivo* experiments. 2

consecutive days prior to tissue harvest, 10 rats/group were randomly selected to receive either intravenous (tail vein) paclitaxel injections (1mg/kg body weight), subcutaneous (abdominal) vinblastine injections (1mg/kg body weight) or equal volumes of subcutaneous saline injections. For the completion of *in-vitro* experiments 36 male and female Wistar rats (30 rats utilized for mitochondrial bioenergetic analyses while 6 rats were utilized for cardiomyocyte isolations used for confocal microscopy described below) were bred at York University (Toronto, Ontario) but purchased at Charles River Laboratories (Toronto, Ontario) were used. These animals were utilized in conjunction with a previously published study that focused on extensor digitorum longus muscle (116). All experiments were performed at 6-8 weeks of age (184.3 ± 5.8 g). All animals were maintained on a 12:12-h light-dark cycle, fed standard rodent chow with *ad libitum* access to food and water. All procedures were in accordance to the Canadian Care Animal Committee and with approval from the York University Animal Care Committee (AUP 2016-19).

Preparation of permeabilized muscle fiber bundles (PmFB)

Rats were anesthetized with isoflurane at a rate of 5% and maintained at 3-5% for the duration of the tissue harvest. Following 2 days of injections, heart left ventricle was removed and immediately placed in ice cold BIOPS buffer containing (in mM): 50 MES Hydrate, 7.23 K_2EGTA, 2.77 CaK_2EGTA, 20 imidazole, 0.5 dithiothreitol, 20 taurine, 5.77 ATP, 15 PCr, and 6.56 $MgCl_2 \cdot 6\ H_2O$ (pH 7.1), in preparation for further dissection. Rats used for *in vitro* tissue treatments were sacrificed followed by removal of both heart left ventricle and soleus muscle. Using antimagnetic needle-tipped forceps under magnification (Zeiss 2000, Germany), tissues were trimmed of fat and connective tissue and separated into muscle bundles (1-3mg wet weight). Bundles allocated to *in-vitro* experiments were incubated with either microtubule

stabilizer paclitaxel (Torcris, 1097, Minneapolis, USA) at 23μM for 2hrs (96, 116) the microtubule destabilizer vinblastine (Sigma, V1377, Ontario, CA) at a 3μM for 1hr (101, 116) or corresponding concentrations of vehicle DMSO, all dissolved in BIOPS buffer. Following *in vitro* drug incubation or *in-vivo* treatments, muscle membranes were permeabilized with 40μg/ml saponin dissolved in BIOPS for 30 minutes at 4°C followed by 15 minutes of gentle shaking to wash out the cytosol to permit substrate diffusion to the mitochondria during experiments. Fibers were then washed with MIR05 buffer containing (in mM): 0.5 EGTA, 10 KH_2PO_4, 3 $MgCl_2 \cdot 6 H_2O$, 60 K-lactobionate, 20 Hepes, 20 Taurine, 110 sucrose and 1 mg/ml fatty acid free BSA (pH 7.1) for respiration experiments, buffer Z containing (in mM): 105 K-MES, 30 KCl, 10 KH_2PO_4, 5 $MgCl_2 \cdot 6 H_2O$, 1 EGTA and 5mg/ml BSA (pH 7.1) for H_2O_2 emission experiments, or buffer Y containing (in mM): 250 sucrose, 10 tris-HCl, 20 tris-base, 10 KH_2PO_4 and 0.5mg/mL BSA for calcium retention capacity experiments.

In-vivo and in-vitro mitochondrial bioenergetic assays

All mitochondrial bioenergetic assays were performed as described previously (52, 89, 116). A high-resolution respirometer (Oxygraph 2k, Oroboros Instruments Corp. Innsbruck, Austria) was used to determine oxygen consumption set to a temperature of 37°C and maintained at a constant stirring rate of 750rpm. *In-vivo* experiments were completed in 1) the presence of 20mM creatine to saturate mitochondrial creatine kinase (miCK) which stimulates the transport of high energy phosphates as phosphocreatine (PCr) through the outer mitochondrial membrane or 2) the absence of creatine to assess the contribution of passive ADP/ATP diffusion according to previous models (86, 140, 165, 166). All *in-vitro* experiments were completed in the presence of 20mM creatine. In both *in-vivo* and *in-vitro* conditions, respiration was stimulated with the addition of NADH from 5mM pyruvate/ 4mM malate followed by a titration of ADP to stimulate

state 3 respiration. Physiological (25μM), submaximal (500μM) and saturating (5000μM) ADP concentrations were used for *in-vivo* tissue experiments with the addition of 50μM, 100μM and 250μM ADP for the *in-vitro* tissue experiments to capture a wider range of physiological and submaximal ADP concentrations. 10mM glutamate was then added generate NADH and stimulate complex I-supported respiration in both *in-vivo* and *in-vitro* experiments. All experiments were completed with the addition of 10μM cytochrome c oxidase to ensure the integrity of the mitochondrial membrane was maintained during all experimental procedures. Experiments with <15% increase in respiration following addition of 10μM cytochrome c oxidase were accepted. Wet bundle weights were established prior to respiration experiments.

H_2O_2 emission experiments were completed using a high-resolution spectrofluorometer (QuantaMaster 40, HORIBA Scientific, Edision NJ, USA). During permeabilization, PmFB were co-incubated with 100μM CDNB to scavenge endogenous glutathione allowing the generation of H_2O_2 at the pyruvate dehydrogenase complex (35). Washed PmFB were placed into a quartz cuvette containing 1mL of Buffer Z with the addition of 10 μM Amplex Ultra Red, 0.5 U/ml horseradish peroxidase, 1 mM EGTA, 40 U/ml Cu/Zn-SOD1,5 μM BLEB and 20mM creatine or in the absence of creatine for *in-vivo* experiments. H_2O_2 emission was stimulated with the addition of 10mM pyruvate and 4mM malate followed by a titration of 25μM, 500μM and 5000μM ADP for *in-vivo* experiments and 15μM, 50μM, 100μM, 250μM and 500μM ADP for *in-vitro* experiments to drive oxidative phosphorylation thereby reducing H_2O_2 emission. Given the hypothesis focuses on the potential for tubulin to alter the influence of VDAC on ADP's control of bioenergetics, an ADP-independent H_2O_2 emission experiment was performed *in-vitro* by stimulating pyruvate dehydrogenase complex (PDC)-supported H_2O_2 emission by adding 10mM pyruvate, 4mM malate and 0.5μM rotenone to prevent complex I-induced H_2O_2 emission.

Susceptibility to calcium-induced apoptosis was measured through the formation of the mitochondrial permeability transition pore (mPTP). PmFB were placed into quartz cuvettes filled with buffer Y containing 1 μM Calcium Green-5N (Invitrogen), 2 μM thapsigargin, 5 mM 2-deoxyglucose, 2 U/mL hexokinase, 20mM creatine, 5 μM BLEB and 40 μM EGTA and placed into a high-resolution spectrofluorometer (QuantaMaster 80, HORIBA Scientific, Edision NJ, USA). Background fluorescence was determined with the addition of 5mM glutamate and 2mM malate. An initial 8 nmol pulse followed by subsequent 4 nmol pulses of $CaCl_2$ stimulates mitochondrial calcium uptake until the mPTP opens. Maximum fluorescence was established with the addition of two 1mM pulses of $CaCl_2$ (89, 116). Upon completion of experiments, PmFB were collected following both H_2O_2 emission and CRC experiments, lyophilized, and weighed for dry weights normalization of data. All bioenergetic experiments were conducted at 37°C with continuous stirring.

Western blotting and caspase activity assays

Frozen heart tissue collected from *in-vivo* injection rats were chipped and homogenized in 1.5ml tubes with an electric Teflon pestel submerged in homogenization buffer containing (mM): 40 Hepes, 120 NaCl, 1 EDTA, 10 $NaHP_2O_7 \cdot 10H_2O$ pyrophosphate, 10 β-glycerophosphate, 10 NaF and 0.3% CHAPS detergent (pH 7.1 adjusted using KOH). A BCA assay was used to determine protein concentration (Life Technologies, Carlsbad, CA, USA). Samples were prepared, ran through SDS-PAGE followed by a transfer onto a low-fluorescence polyvinylidene difluoride membrane. Following transfer, membranes were blocked with LI-COR Odyssey Blocking Buffer (LI-COR, Lincoln NE, USA) for 1 hour at room temperature prior to an over-night incubation with each respective primary antibody at 4°C. The following primary antibodies were used for the completion of Western blot experiments: electron transport chain

proteins (OXPHOS cocktail, ab110413, Abcam, Cambridge, UK, 1:250), VDAC2 (32059, Santa-Cruz, 1:1000), adenine nucleotide translocase 1 (ANT1) (ab180715, Abcam, 1:1000), mitochondrial creatine kinase (mtCK) (a generous gift from Dr. Uwe Schlattner, Grenoble, France, 1:1000), α-tubulin (T6199, Sigma-Aldrich, 1:1000) and β-II tubulin (ab28036, Abcam, 1:100). The next day, membranes were washed in TBST and incubated with the corresponding infrared fluorescent secondary antibody (LI-COR, Lincoln NE, USA) for 1 hour at room temperature. Membranes were imaged with an infrared imager (LI-COR CLx; LI-COR) and quantified with Image J software (ImageJ, http://imagej.nih.gov/ij/). Membranes were then stained for total protein using Amido Black total protein stain (A8181, Sigma, St Louis, MO, USA) for normalization.

Caspase 3, 8 and 9 activities were determined as described previously (32, 52). Briefly, heart tissue was chipped and homogenized in buffer containing (mM): 250 Sucrose, 50 Tris, 1 DTT, 1 EDTA, 5 $MgCl_2$ and 10% glycerol. Homogenates underwent a series of differential centrifugation to isolate the lysosome and proteasome fractions. The enzymatic activity of caspase 3, 8 and 9 were measured using the BioTek Cytation 3 fluorometric plate reader (BioTek, Winooski, VT, USA) with the following substrates: caspase 3, AC-DEVD-AMC (ALX-260-031-M001, Enzo Life Sciences, Farmingdale, NY, USA), caspase 8, AC-IETD-AMC (ALX-260-042-M001, Enzo Life Sciences, Farmingdale, NY, USA) and caspase 9, AC-LEHD-AMC (ALX-260-080-M001, Enzo Life Sciences, Farmingdale, NY, USA). Caspase activity was normalized to protein content measured through BCA assay (Life Technologies, Carlsbad, CA, USA).

In-vitro cardiomyocyte isolation and drug treatment

A separate cohort of rats (n=6) were sacrificed for cardiomyocyte isolation and immunohistochemical experiments utilizing previously published methods (108, 148). In brief, rats were first injected with heparin (100U/100g body weight) and then anesthetized by ketamine/xylaxine mixture 10 minutes later. The hearts were quickly excised and submerged in ice cold myocyte isolation B1 buffer containing (mM): 113 NaCl, 4.7 KCl, 0.6 KH_2PO_4, 0.6 Na_2HPO_4, 1.2 $MgSO_4 \bullet 7H_2O$, 10 Hepes, 4.6 $NaHCO_3$, 5.5 glucose, 10 2,3-butanedione monoxime and 30 taurine to cease the heart from pumping. The cannulated heart (controlled within 2 minutes after isolation) was perfused with oxygenated B1 for 6 minutes and subsequently perfused with B1 supplemented with Liberase Research Grade (Roche) at 0.2g/mL at 37°C for up to 6 minutes. The development of a pale coloring and softer texture indicated that the left ventricle was ready to be isolated followed by a rinse with B1 buffer twice. Left ventricle was quickly minced into small pieces in stopping buffer (B1 supplemented with 0.02g/mL BSA and 200 μM $CaCl_2$) at 37°C for 10 minutes with pipetting every 2 minutes. Following filtration of the cell suspension through a 200μM cell strainer, cardiomyocytes were collected by centrifugation for 1 minute at 42 x g. Once isolated cardiomyocytes were adhered to laminin (10μg/ml, Invitrogen) coated coverslips for 1 hour in M199 medium (Gibco Life technologies), supplemented with 100mg/L L-glutamine, 25mM Hepes, 50U/L penicillin-streptomycin (P/S), Hanks' salt, 0.02% BSA and 50mM 2.3-butanedione monoxime. After adherence, cardiomyocytes were incubated with either paclitaxel, vinblastine or control (DMSO) at the concentrations and volumes listed above for 2hrs in an incubator. Following drug incubations fibers were washed 3 times with PBS^{++} and subsequently fixed with neutral formalin for 10 minutes at room temperature followed by 3x5min washes with PBS^{++} (148) for further processing.

Proximity ligation assay

The proximity ligation assay was used to determine protein-protein interactions between α-tubulin-VDAC2 and βII-tubulin-VDAC2. Isolated cardiomyocytes adhered to a coverslip were permeabilized with 0.1% triton X100 for 15min followed by blocking for 1hr in 5% BSA PBS^{++}. Cells were co-stained with α-tubulin (1:1000 sigma; T6199) or βII tubulin (1:250 Abcam; ab28036) for 4hrs at room temperature followed by VDAC2 (1:250 Santa Cruz; 32059) overnight at 4°C. Following primary antibody incubations, cardiomyocytes were washed and incubated with Duolink® in-situ PLA anti-goat minus (sigma; DUO92006) and anti-mouse plus (DUO92001) probes for 1hour at 37°C. Cardiomyocytes were then washed and incubated with the Duolink® in-situ detection reagents red (sigma; DUO92008) to allow for the detection of each protein-protein interaction. Negative control experiments have been completed and published to determine the antibody specificity of the assay (116). Coverslips were coated with mounting media and carefully placed on a microscope slide.

Image capture and quantitation

Images were acquired using a Zeiss laser scanning confocal microscope 700 (Carl Zeiss, Thornwood, NY). Control experiments completed to determine the specificity of the proximity ligation assay were completed in previously published manuscript (116). Images were captured with a 40X oil objective with the pin hole was adjusted to 1AU capturing 8-12 stacks with a z-step of 0.23 μm. Image quantitation was completed using Imaris image quantifying software (Bitplane, Zurich, Switzerland) where images were reconstructed into 3D allowing the use of the spot tool to identify protein-protein interaction yielding the number of spots per image.

Analysis and statistics

Results are reported as mean ± SEM with significance accepted at $P< 0.05$. Outliers were omitted in accordance with the ROUT test, and the D'Agostino-Pearson omnibus or Shapiro-Wilks normality test was performed to determine whether the data followed a normal distribution. As all data passed normality, a one-way ANOVA was completed for proximity ligation assays and complex I and II stimulated respiration. A two-way ANOVA was completed for ADP-stimulated respiration and ADP-attenuation of H_2O_2 emission followed by Fisher's least squares difference post-hoc analysis when a significant F ratio was obtained. To test differences in CRC, caspase activity and protein densitometry and other H_2O_2 emission data in the absence of ADP, a student's un-paired t-test was used. All analysis was completed using Prism 8 (GraphPad Prism 8, La Jolla, CA).

Results

Regulation of ADP kinetics is impaired following 2 days of paclitaxel and vinblastine injections

In the presence of 20mM creatine, ADP-stimulated respiration (p=0.56, Figure 5-1A) and further isolation of complex I with the addition of glutamate (p=0.63, Supplemental figure 5-1A) were unchanged when compared to saline. In the absence of creatine, ADP-stimulated respiration was significantly reduced compared to saline (main effect, p=0.01, Figure 5-1D) and was further impaired during the addition of glutamate to further isolate complex I (p=0.003 vs saline and p=0.03 vs. paclitaxel, Supplemental figure 5-1D). Pyruvate/malate-stimulated H_2O_2 emission (p=0.13, Figure 1B) and ADP-attenuation of H_2O_2 emission (p=0.08, Figure 5-1C) in the presence of 20mM creatine were similar to saline. In the absence of creatine, pyruvate/malate stimulated H_2O_2 emission was unchanged compared to control (p=0.55, Figure 5-1E) while ADP-attenuation of H_2O_2 emission was significantly higher following both paclitaxel and

vinblastine injections when compared to saline (main effect, p=0.003, Figure 5-1F). These bioenergetic impairments were independent of any change in protein content of mitochondria measured by the complexes of the electron transport chain (p=0.88), VDAC2 (p=0.85), ANT (p=0.41), mtCK (p=0.20), α-tubulin (p=0.50), and βII-tubulin (p=0.58) (Supplemental Figure 5-3A-G). Calcium retention capacity, used to determine the propensity for mPTP opening, was not altered following both *in-vivo* injections (p=0.71) and *in-vitro* incubations with paclitaxel (p=0.84) and vinblastine (p=0.65) (Supplemental Figure 5-4A-B). Furthermore, caspase activation was not evident as caspase 3 (p=0.79), caspase 8 (p=0.60) and caspase 9 (p=0.31) activity were similar between groups (Supplemental Figure 5-4D-F).

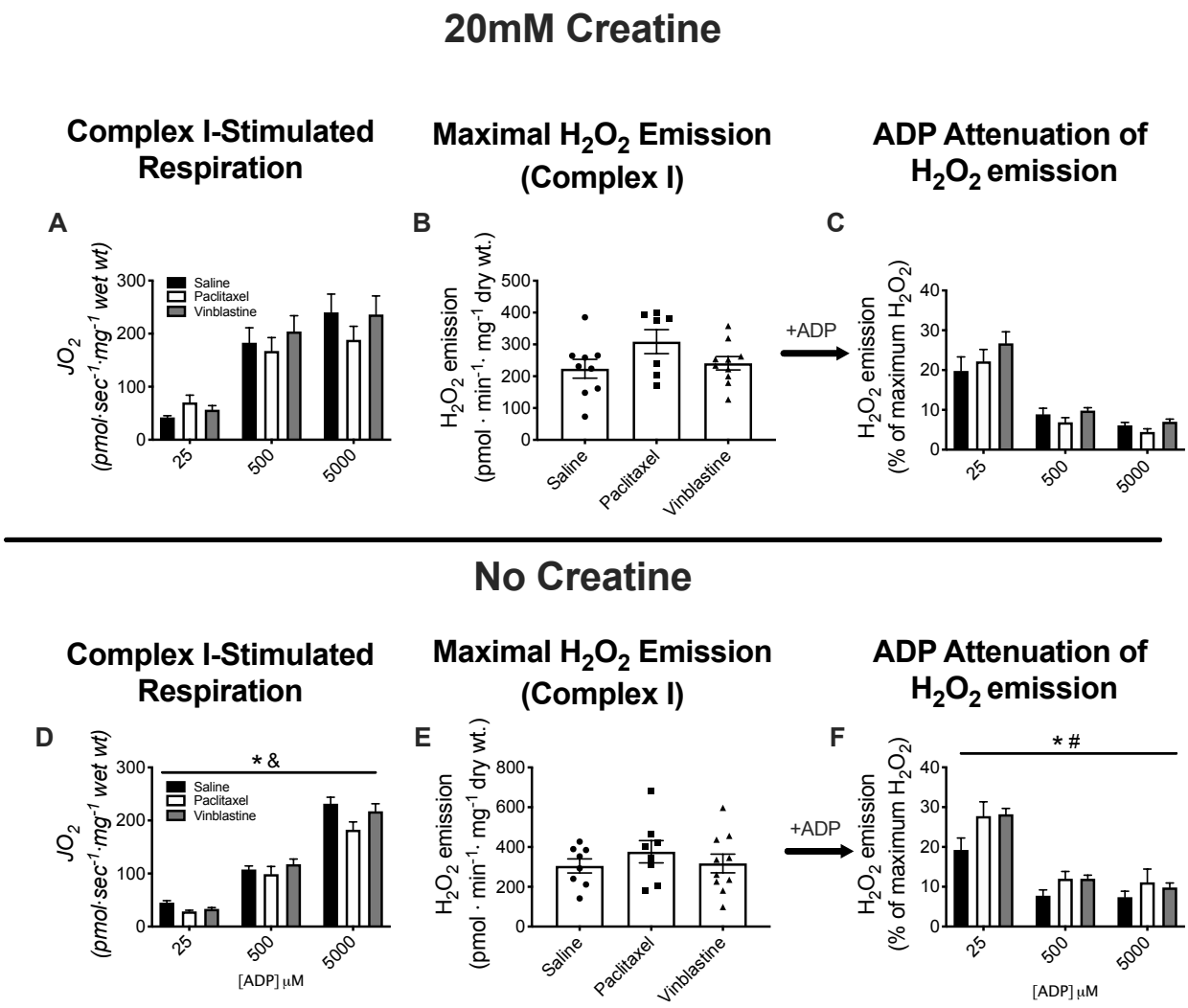

Figure 5-1. Mitochondrial bioenergetics in left ventricle PmFB following a two-day in-vivo treatment with either paclitaxel or vinblastine. State 3 respiration supported by complex I (NADH from pyruvate/malate) (n=8-10) in the **A.** presence and **D.** absence of creatine. Complex I-stimulated H_2O_2 emission (n=7-10) in the **B.** presence and **E.** absence of creatine followed by an ADP titration (n=7-10) in the **C.** presence and **F.** absence of creatine. Results are reported as mean ± SEM. (*p≤0.05 saline vs. paclitaxel, #p<0.05 saline vs. vinblastine, &p<0.05 paclitaxel vs. vinblastine).

Acute in-vitro incubations with paclitaxel and vinblastine impair mitochondrial ADP-dependent kinetics and reduces H_2O_2 emission

All in-vitro experiments were completed in the presence of 20mM creatine. PmFB treated with paclitaxel and vinblastine both displayed a main effect for reduced ADP-stimulated

respiration (paclitaxel; p=0.001, Figure 5-2A), (vinblastine; p=0.001, Figure 5-2D). Further stimulation of complex I with glutamate trended lower when compared to control (p=0.06, Supplemental figure 5-2A) following paclitaxel incubations with no differences following vinblastine incubations (p=0.24, Supplemental figure 5-2B). Pyruvate/malate stimulated H_2O_2 emission trended to be lower following paclitaxel incubation (p=0.08, Figure 5-2B) and was significantly lower following vinblastine incubations (p=0.002, Figure 5-2E). The ability of ADP to drive oxidative phosphorylation and reduce H_2O_2 emission was also significantly impaired following both paclitaxel (main effect; p=0.0001, Figure 5-2C) and vinblastine (main effect, p=0.0001, Figure 5-2F) incubations. Pyruvate/malate stimulated H_2O_2 emission at complex I are both modulated by the presence of ADP. To determine whether these microtubule targeted chemotherapies target the mitochondria in a non-ADP dependent manner we also explored the emission potential of the pyruvate dehydrogenase complex (PDC). Here we uncovered no differences following paclitaxel incubation (p=0.59, Supplemental figure 5-2A), but significantly decreased H_2O_2 emission following vinblastine incubation (p=0.003, Supplemental figure 5-2B).

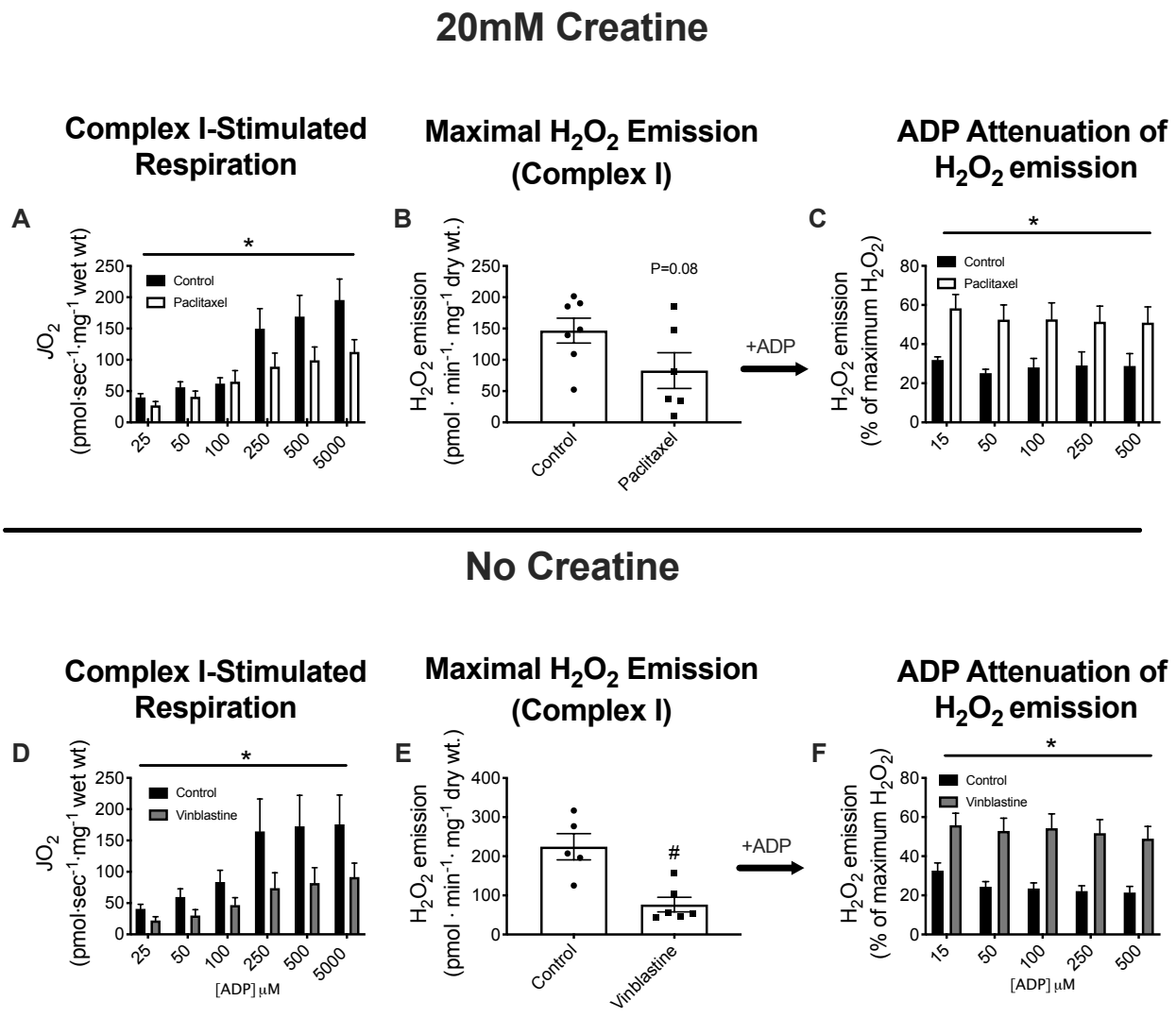

Figure 5-2. Mitochondrial bioenergetics in heart left ventricle PmFB following in-vitro incubations in the presence of 20mM creatine. State 3 respiration supported by complex I (NADH from pyruvate/malate) following **A.** paclitaxel (n=8) and **D.** vinblastine (n=6-7) Incubations. Complex I-stimulated H_2O_2 emission following **B.** paclitaxel (n=6-7) and **E.** vinblastine (n=5-6) incubations, followed by an ADP titration **C.** paclitaxel (n=6-8) and **F.** vinblastine (n=5-6). Results are reported as mean ± SEM. (*p≤0.01 vs. control, #p<0.05 vs. control).

Impairments in ADP kinetics are independent of tubulin-VDAC interaction

Acute paclitaxel and vinblastine incubations on isolated cardiomyocytes had no effect on α-tubulin- (p=0.44, Figure 5-3B) and βII-tubulin-VDAC2 (p=0.90, Figure 5-3C) interaction with VDAC2.

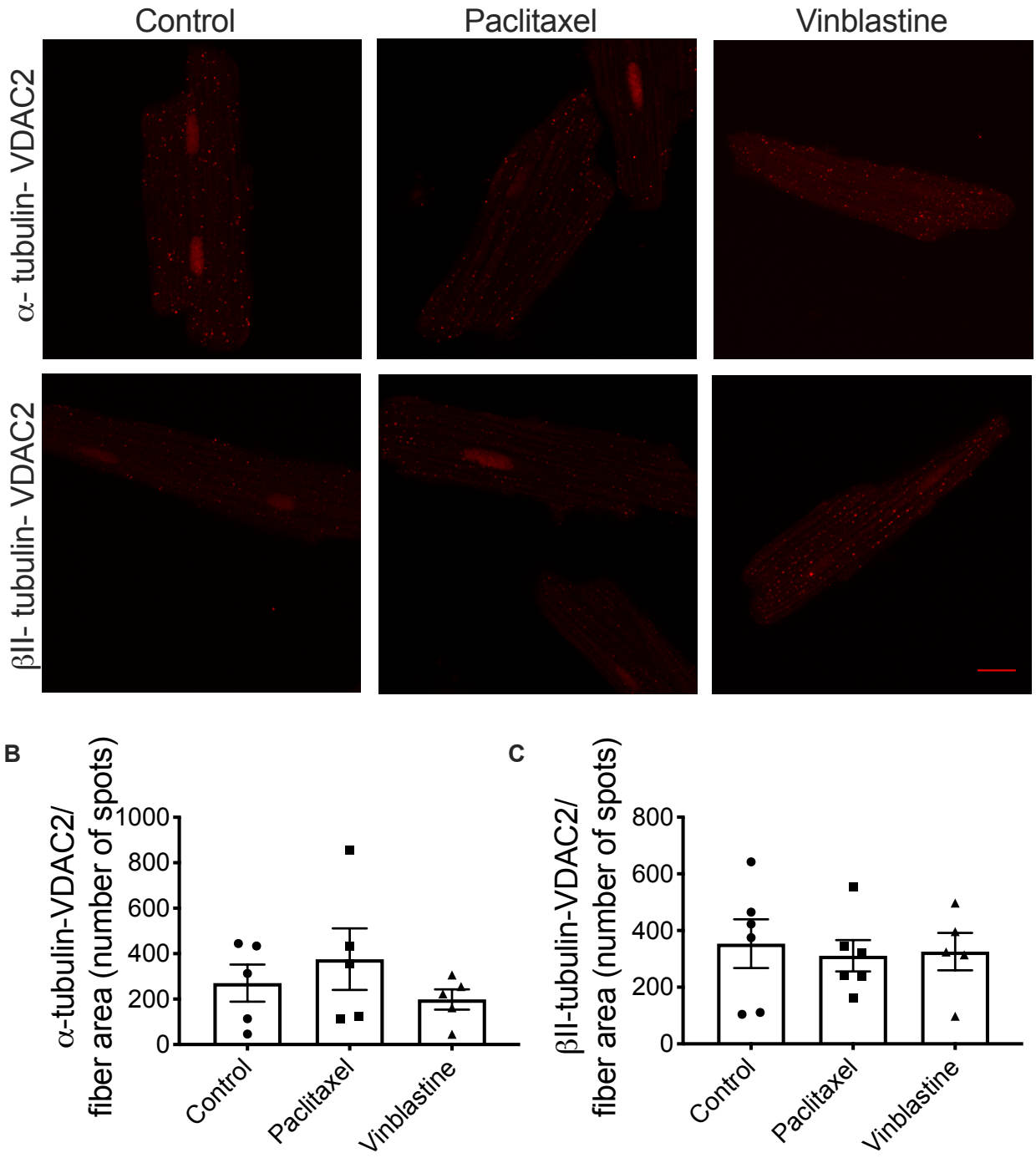

Figure 5-3. Tubulin-VDAC2 interaction in left ventricle isolated cardiomyocytes. A. Representative confocal image of α- and βII-tubulin-VDAC2 interaction following paclitaxel and vinblastine incubations. Graphical depiction of **B.** α-tubulin-VDAC2 interaction (n=5) and **C.** βII-tubulin-VDAC2 interaction (n=5-6). Results are expressed as mean ± SEM.

ADP specific impairments from microtubule targeted chemotherapies may not be specific to all highly-oxidative tissues

To determine whether the mitochondrial bioenergetic impairments found in cardiac tissue was determined by the tissue's oxidative capacity, the soleus muscle was also acutely treated with both paclitaxel and vinblastine *in-vitro* with all bioenergetic assays completed in the presence of 20mM creatine. ADP-stimulated respiration was similar to control following paclitaxel incubations (p=0.24, Figure 5-4A) while following vinblastine incubations, respiration was significantly reduced (main effect; p=0.02, Figure 5-4B). Pyruvate/malate stimulated H_2O_2 emission and attenuation by ADP was unaltered following both paclitaxel (H_2O_2 emission; p=0.15, ADP kinetics; p=0.99, Figure 5-4C and E) and vinblastine (H_2O_2 emission; p=0.84, ADP kinetics, p=0.98, Figure 5-4D and F) incubations when compared to control. Lastly, calcium retention capacity was lower, but not significant compared to control following paclitaxel (p=0.08, Figure 4G) and vinblastine (p=0.09, Figure 5-4H) incubations.

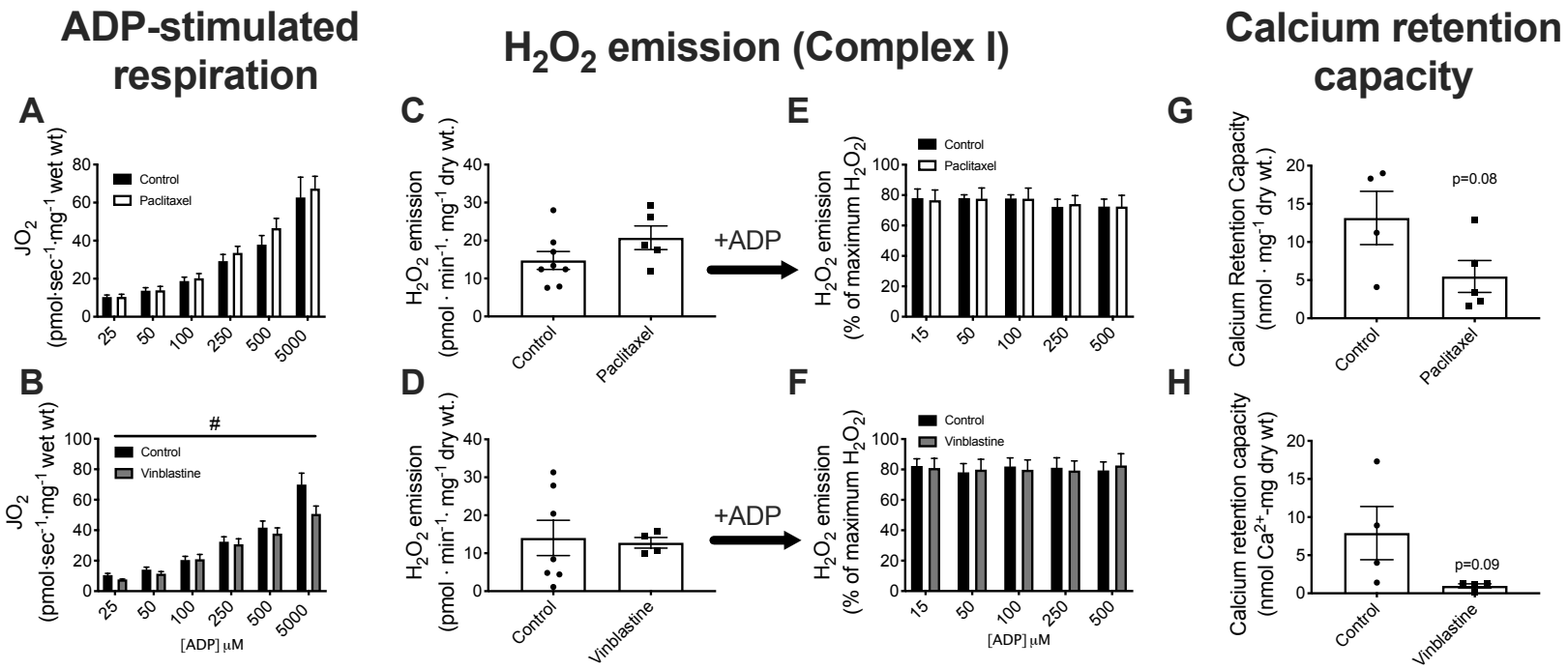

Figure 5-4. Mitochondrial bioenergetics in soleus PmFB following in-vitro incubations in the presence of 20mM creatine. State 3 respiration supported by complex I (NADH from pyruvate/malate) following **A.** paclitaxel (n=7-8) and **B.** vinblastine (n=7-8) incubations. Complex I-stimulated H_2O_2 emission following **C.** paclitaxel (n=5-8) and **D.** vinblastine (n=4-7) followed by an ADP titration **E.** paclitaxel (n=6-8) and **F.** vinblastine (n=7). Calcium retention capacity following **G.** paclitaxel (n=4-5) and **H.** vinblastine (n=4) incubations. Results are reported as mean ± SEM. (#p<0.05 vs. control).

Discussion

The mechanisms underlying cardiotoxicity following chemotherapy remain poorly understood. Using *in-vivo* treatments, the present investigation revealed mitochondrial bioenergetic impairments in cardiac tissue in response to two microtubule targeted chemotherapies, paclitaxel and vinblastine. To further elucidate a mechanism, *in-vitro* methodologies were employed identifying mitochondrial bioenergetic impairments under both conditions independent of any change in mitochondrial associated protein content and tubulin-VDAC2 interactions. These impairments are specific to cardiac tissue because when completed in the highly oxidative soleus skeletal muscle PmFB, the majority of the ADP-dependent mitochondrial impairments in cardiac tissue were absent. These findings suggest that microtubule targeted chemotherapies may have a direct effect on the mitochondria, limiting the ability of ADP to produce energy and attenuate H_2O_2 emission.

Short term in-vivo microtubule targeted chemotherapy impairs ADP-dependent mitochondrial bioenergetics through creatine independent pathways

To adequately capture mitochondrial bioenergetic function *in-vitro*, we have attempted to mimic *in-vivo* conditions by maintaining the cells ultrastructure with PmFB, supplementing our respiration and H_2O_2 media with the necessary metabolites and maintaining adequate O_2 concentrations (104). This allows for further manipulation of the system to obtain even more information; in this scenario, it allowed for further examination of ADP transport through the mitochondria. Cytosolic-mitochondrial exchange of ADP/ATP occurs in part through passive diffusion of ADP and ATP via VDAC and the adenine nucleotide translocator (ANT) on the outer and inner mitochondrial membranes respectively. This process is thought to represent 20% of the total energy transport that occurs in the mitochondria (4, 133). Another mechanism to

exchange ADP and ATP through the mitochondrial membranes is facilitated through the transport of high energy phosphates donated from PCr, and transferred to ADP and ATP (133, 165). This is facilitated through cytosolic and mitochondrial creatine kinase (cCK and miCK, respectively) providing a faster route for energy exchange contributing to 80% of the energy exchange that occurs through the mitochondrial membrane (4, 44, 75, 165, 167). These methodologies allow us to create a creatine dependent (utilizing cCK and miCK) condition with the addition of 20mM creatine into our respiration and H_2O_2 media saturating cCK and miCK and creatine independent (passive diffusion) conditions with the absence of creatine. With this, we can further extrapolate the contribution of each energy exchange system following microtubule stabilization or destabilization.

In the current study, under *in-vivo* conditions impairments in ADP kinetics were found only in the no creatine condition. Reduced ADP-stimulated respiration and an inability of ADP to attenuate H_2O_2 emission following both microtubule stabilization and destabilization were also observed. It was very peculiar that only one energy transport pathway was impaired following the injection of cytotoxic drugs, while also being the less dominate and inefficient pathway. There is a vast amount of literature outlining the importance of creatine and miCK for the adequate supply of energy to the cell which may also be the reason why we impairments in the creatine independent pathway was observed. Perhaps the cell is attempting to preserve its more efficient pathway by "sacrificing" its inefficient pathway. In addition, paclitaxel and vinblastine *in-vivo* injections were completed daily over 2 days which may not be enough time to elicit the extreme morphological and pathophysiological changes seen previously (23, 50). In addition, the current report may be only capturing the initial bioenergetic impairments that occur with microtubule manipulation. Although Gilliam and colleagues (2013) discovered whole body

deficits coupled with impaired mitochondrial bioenergetics at 24-72 hours following a single injection of doxorubicin in rats (38), the mechanism remains unknown given this compound is thought to target nuclear processes. In this current report, paclitaxel and vinblastine specifically target microtubules which may require more time for its molecular mechanism to ensue, especially in a non-mitotic cell.

Acute in-vivo microtubule targeted chemotherapy incubations impair mitochondrial bioenergetics

In-vitro incubation of cardiac tissue with paclitaxel and nocodazole, a microtubule destabilizer – similar to vinblastine-, has been previously shown to depolarize mitochondrial membrane potential and open the mitochondrial permeability transition pore (mPTP), which is believed to be responsible for the release of cytochrome c oxidase, activating pro-apoptotic pathways (74, 128). These authors have concluded that disrupting the microtubule organization in cardiac tissue alters mitochondrial function, but the regulation of ADP transport was not investigated. In addition, cardiomyocytes treated with trypsin in an attempt to remove βII-tubulin resulted with increased respiratory capacity indicating that the removal of βII-tubulin relieved its inhibition on VDAC increasing the permeability of ADP (40). Similarly, the addition of tubulin to isolated mitochondria decreased respiration suggesting that tubulin limited ADP diffusion through VDAC (127). These and other studies (42, 136, 145, 161) strongly suggest that microtubules, specifically tubulin, may be involved in the regulation of ADP permeability through VDAC. More recently, our laboratory revealed a direct interaction between α- and βII-tubulin and VDAC2 in single extensor digitorum longus muscles (EDL) which was linked to impaired ADP kinetics. To further deduce the mechanism underlying the bioenergetic impairments seen *in-vivo*, we completed bioenergetic assays using an *in-vitro* model, acutely

incubating heart tissue with paclitaxel and separately vinblastine to observe the bioenergetic changes that may be occurring. Here we also observed similar impairments in ADP-dependent respiration and attenuation of H_2O_2 emission with both paclitaxel and vinblastine incubations. To determine whether these impairments were mediated by a change in tubulin-VDAC interaction we used employed the proximity ligation assay capable of detecting protein-protein interactions (<30nm resolution) in isolated cardiomyocytes following incubations with paclitaxel and vinblastine. There was no change in both α- and βII-tubulin-VDAC2 interaction, suggesting that an alternate mechanism may be at play.

As mentioned above, there is a strong line of evidence suggesting that the tubulin-VDAC interaction governs the permeability of ADP through VDAC and therefore regulates mitochondrial respiratory capacity (40, 127, 161). Although the current study did not see a change in tubulin-VDAC interaction, tubulin binding to VDAC may still play an important physiological role when bound to VDAC. Perhaps in cardiomyocytes, a change in number of tubulin-VDAC2 binding may not be indicative of any small morphological changes that may be occurring with microtubule stabilization and destabilization undetectable with confocal microscopy. VDAC2 is the essential isoform required to sustain life (25), but this does not discount the contribution that other VDAC and tubulin isoforms may have. Specifically, each tissue, whether it be smooth, cardiac or skeletal muscle, may express different quantities of different tubulin isoforms which has been previously shown to be a contributing factor when analyzing tubulin-VDAC interactions (126). Further work is needed to distinguish the potential for various tubulin and VDAC isoform interactions and its contribution to mitochondrial bioenergetics.

Bioenergetic responses to microtubule targeted chemotherapy may be tissue specific

Cardiac and skeletal muscles fibers are non-mitotic but may still be susceptible to the effects of microtubule stabilization and destabilization given the important role of this cytoskeletal component in a variety of cell functions. Several similarities exist between cardiac and the soleus muscles; 1) they are both highly oxidative tissues reliant on stored fuels, specifically fat, to generate energy, 2) they both have a high mitochondria content necessary to generate large amounts of energy and lastly 3) although cardiac muscle contraction is an involuntary occurrence that does not stop, the soleus muscle is a postural muscle that is constantly activated making it unique and resilient, similarly to cardiac muscle. Due to these reasons, this report explored whether the same bioenergetic impairments were present in soleus muscle following an acute *in-vitro* incubation with paclitaxel and vinblastine. Surprisingly, the majority of ADP dependent bioenergetic impairments seen in cardiac muscle was absent in soleus. Vinblastine had specific effects on respiration whereby respiration was significantly reduced while there were no differences in attenuation of H_2O_2 emission compared to control. In addition, calcium retention capacity was lower in the soleus while *in-vivo* and *in-vitro* microtubule disorganization had no effect in cardiac muscle. These data suggest that although these two tissues have some similarities, the bioenergetic impairments that ensue in response to microtubule disorganization may be mediated through different pathways that requires further investigation

Conclusion

In summary, impairments to ADP stimulated respiration and attenuation of H_2O_2 were identified in both *in-vivo* and *in-vitro* models, in a creatine independent manner following paclitaxel administration independent of any change in α- and βII-tubulin-VDAC2 interaction. These finding are not ubiquitous for all oxidative tissues as soleus muscles incubated with both

paclitaxel and vinblastine in-vitro did not display all ADP-dependent bioenergetic impairments but rather a reduced calcium retention capacity suggesting an increased susceptibility to apoptosis. Further work exploring the various tubulin and VDAC isoforms and interactions may reveal whether another combination regulates ADP-dependent mitochondrial bioenergetics in various muscle tissues. Nonetheless, the present work is the first to identify that only 2 days of *in-vivo* treatment with paclitaxel induces cardiac mitochondrial dysfunction. The more potent effects seen of both paclitaxel and vinblastine during *in-vitro* treatments might suggest that more concentrated tissue uptake renders both compounds as mito-toxic in cardiac tissue.

Supplemental figures – to be included in journal submission

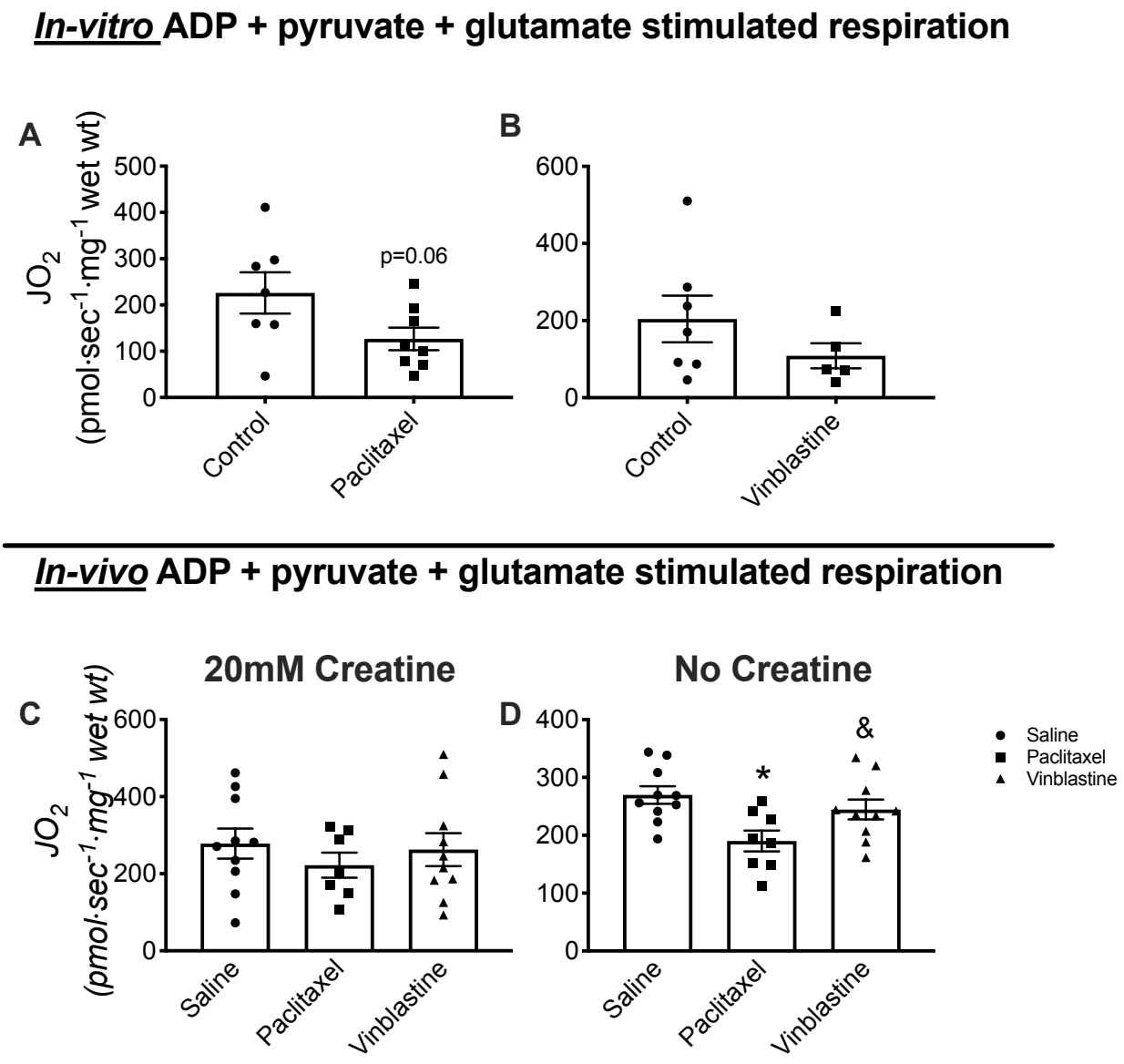

Supplemental figure 5-1. Complex I- stimulated respiration in left ventricle PmFB following a two-day in-vivo treatment with either paclitaxel or vinblastine. State 3 respiration supported by complex I (NADH from pyruvate/malate + glutamate) following **A.** paclitaxel and **B.** vinblastine incubations (n=7-10). State 3 respiration supported by complex I (NADH from pyruvate/malate + glutamate) in the **C.** presence and **D.** absence of creatine (n=7-10). Results are reported as mean ± SEM. (*p≤0.05 saline vs. paclitaxel, &p<0.05 paclitaxel vs. vinblastine

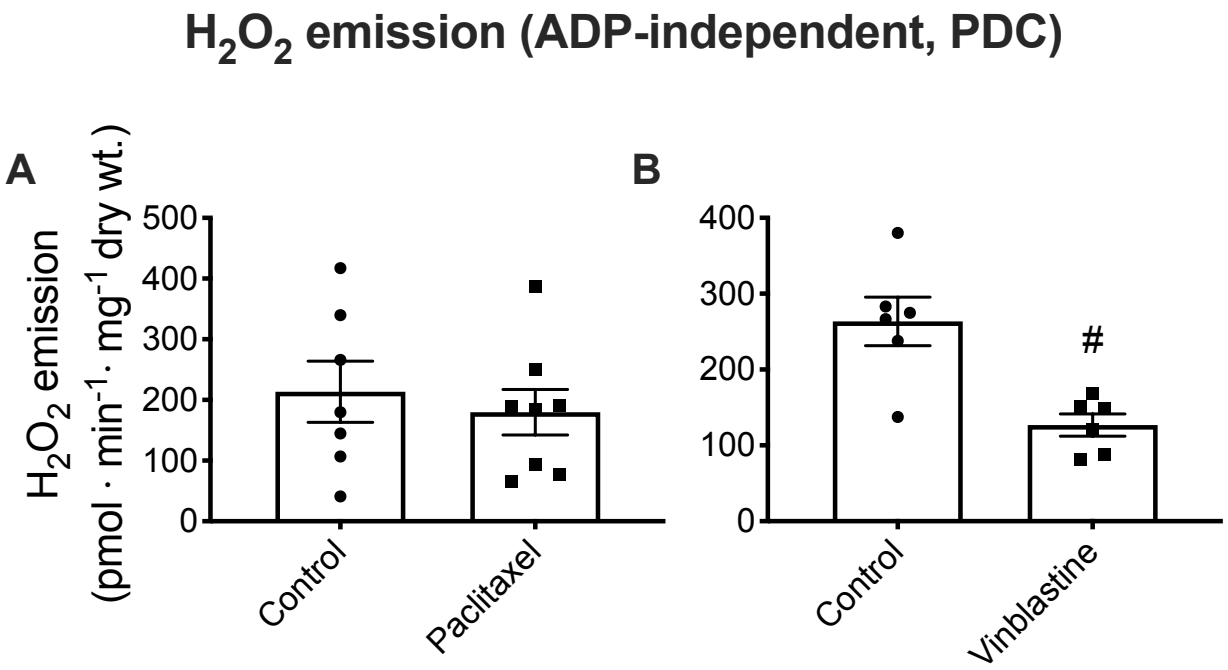

Supplemental Figure 5-2. Pyruvate dehydrogenase complex (PDC) H2O2 emission from heart left ventricle PmFB. H_2O_2 emission from pyruvate dehydrogenase complex (ADP-independent) was tested following **A.** paclitaxel (n=7-8) and **B.** vinblastine (n=6) incubations. Results are reported as mean ± SEM. (#p<0.05 vs. control).

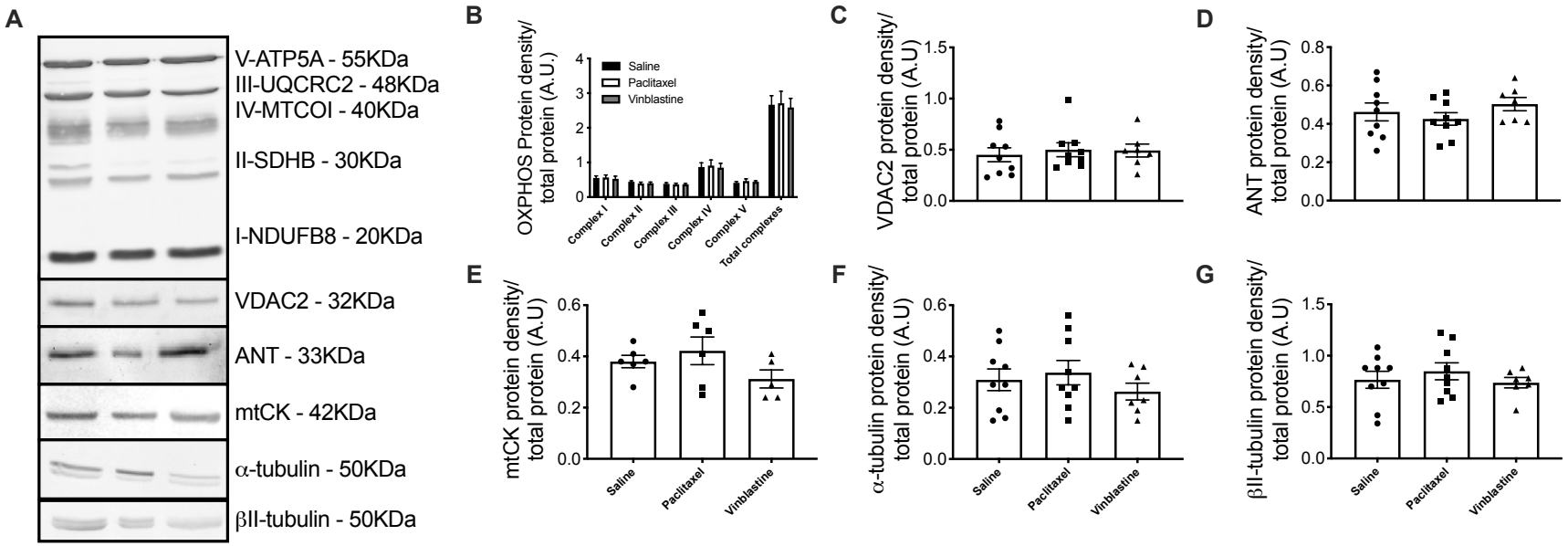

Supplemental figure 5-3. A. Representative Western blot of mitochondrial and microtubule proteins. B. Integrative densitometry of the proteins of the electron transport chain (complex I-V) (n=5-6), **C.** voltage dependent anion channel (VDAC) 2 (n=7-9), **D.** Adenine nucleotide translocase (ANT)1 (n=7-9), **E.** mitochondrial creatine kinase (mtCK) (n=5-6), **F.** α-tubulin (n=7-9), and **G.** βII-tubulin (n=7-9). Results are reported as mean ± SEM.

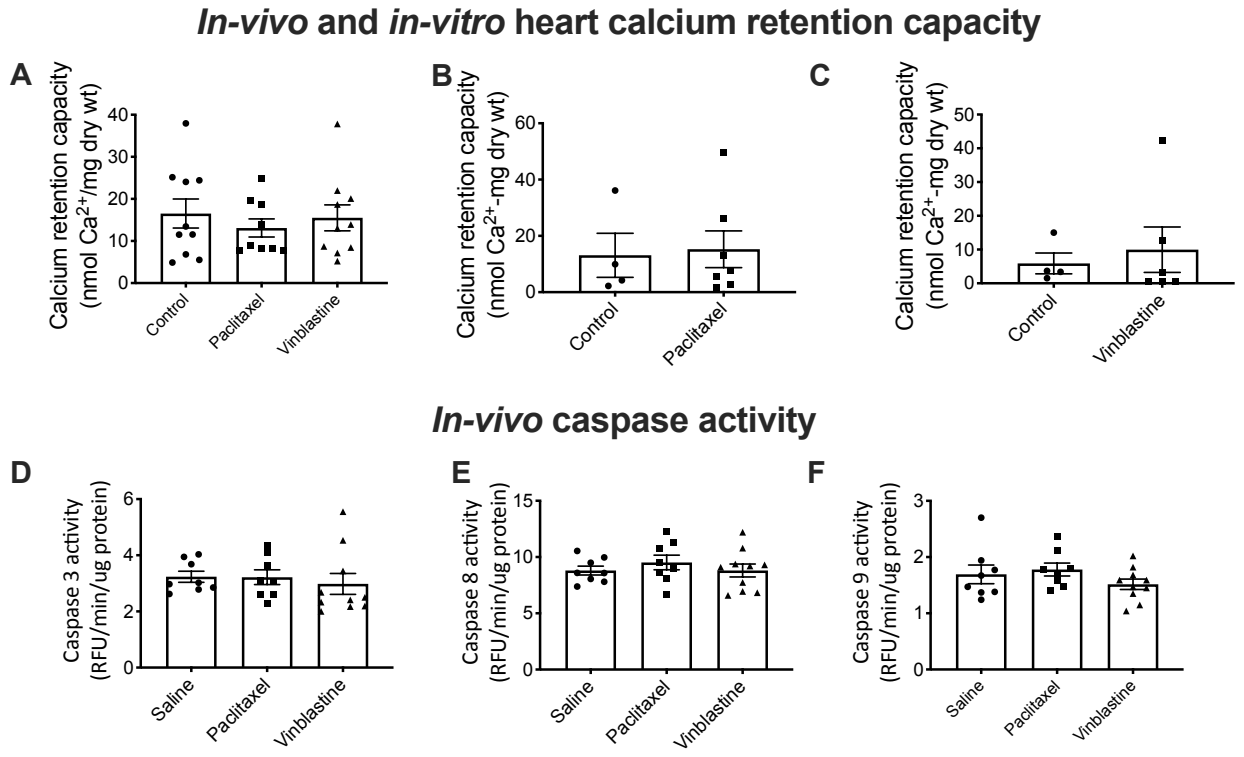

Supplemental figure 5-4. Measurements of susceptibility to apoptosis induce cell death in heart left ventricle tissue. Calcium retention capacity following **A.** in-vivo saline, paclitaxel and vinblastine injections (n=9-10), **B.** in-vitro paclitaxel (n=4-7) and **C.** vinblastine (n=4-6) incubations. **D.** Caspase 3 (n=8-10), **E.** caspase 8 (n=8-10) and **F.** caspase 9 (n=8-10) activity following in-vivo saline, paclitaxel and vinblastine injections.

Chapter 6

Divergent muscle function and mitochondrial bioenergetic responses to microtubule targeted chemotherapy in oxidative and glycolytic skeletal muscles

Sofhia V. Ramos., Meghan C. Hughes, Trevor Teich., Patrick C Turnbull and Christopher G.R. Perry
Muscle Health Research Center, School of Kinesiology and Health Science, York University, 4700 Keele Street, Toronto, ON, Canada M3J 1P3

This chapter is in preparation for submission. A journal has yet to be confirmed.

Experimental development prior to initiation of experiments

- Whole body in-vivo muscle functional tests: voluntary running and grip strength
- In-vivo muscle force analysis
- Frozen tissue embedding, sectioning and staining
- Re-optimization of proximity ligation assays for sectioned muscle

Author contributions: Initial study design and experimental protocols developed by SVR and CGRP. SVR, MCH and CGRP contributed to the conception and design of this study. SVR, TT MCH and PCT performed experiments. SVR analyzed data. SVR and CGRP interpreted results. SVR., and CGRP drafted manuscripts and prepared figures.

Abstract

Microtubule targeted chemotherapies have been implicated in the development of muscle weakness. These drugs target and kill mitotic cancer cells through the prevention of mitotic spindle formation, preventing cell division thereby killing tumor cells. This, unfortunately, also alters the microtubule arrangement in skeletal muscle and may contribute to muscle weakness seen with chemotherapy treatment. Emerging evidence suggests that the monomeric subunit of microtubules, tubulin, bind and regulate the permeability of ADP/ATP in the mitochondria through an interaction with the voltage gated dependent anion channel (VDAC). To further test this model, we determined the effect of 2-days of injecting microtubule stabilizing (paclitaxel) and destabilizing (vinblastine) chemotherapies on mitochondrial bioenergetics in relation to the tubulin-VDAC model and whole muscle function in soleus and white gastrocnemius (WG) muscles. Whole body and muscle functional analysis revealed decreased voluntary running following vinblastine injections and a surprising increase in torque frequency following paclitaxel injections. These changes in muscle function were related to increased βII-tubulin-VDAC2 interaction only following microtubule stabilization with paclitaxel in embedded soleus muscle. However, ADP-dependent respiration and H_2O_2 emission were unaltered, suggesting the changes in tubulin-VDAC interaction and muscle function were independent of mitochondrial bioenergetic responses to these compounds. In contrast, WG displayed decreased respiration and H_2O_2 kinetics in response to paclitaxel treatment suggesting that these microtubule targeted compounds affect oxidative and glycolytic tissues differently. These results suggest that altering mitochondrial bioenergetic responses to altered microtubule architecture may not be linked solely through the previously proposed tubulin-VDAC model, and that microtubule-targeting chemotherapies may affect muscle mitochondria through alternative mechanisms.

Introduction

The mechanisms by which chemotherapies cause muscle weakness remain poorly understood. As there are many forms of chemotherapies, it stands that each type may trigger unique mechanisms of muscle dysfunction. One type of chemotherapy known as mitotic inhibitors can either stabilize microtubules, locking them in a polymerized state or destabilize microtubules by preventing polymerization; this in turn, prevents the tumor cell from dividing and ultimately lead to cell death (23, 130). While these chemotherapies are effective at slowing or killing cancer cells, they also target other cells in the body such as skeletal muscle.

Individuals receiving chemotherapy endure a series of side-effects including mouth sores, nausea, vomiting, diarrhea, sleeplessness, and peripheral neuropathies (37, 119, 129, 171). Of particular interest is the muscle weakness that patients experience. Research on male and female cancer patients reported that muscle mass is directly related to strength and fatigue during treatment (67). This is coupled with reduced muscle size measured through DEXA and reductions in single fiber cross sectional area (157). Cellular analysis of a single dose of vinblastine resulted a host of morphological changes to gastrocnemius and soleus muscles including de-arranged intermyofibular networks and deposits of vacuoles and concentric laminar structures, all without any changes to the peripheral nerve in a rodent model (71). The effect that these morphological changes – in response to chemotherapy treatment – have on muscle intracellular function is currently unknown. It seems possible that an altered microtubule ~~intracellular~~ morphology may be a contributing factor towards the development of altered muscle function as shown as by increased muscle stiffness following microtubule stabilization in flexor digitorum brevis (FDB) muscles (65).

More recently, work presented by three labs, Saks and colleagues (136), Rostovsteva and colleagues (127) and Carre and colleagues (20), have suggested a novel model whereby microtubules regulate ADP permeability into the mitochondrial through an interaction with the voltage dependent anion channel (VDAC) on the outer mitochondrial membrane (136). Specifically, the monomeric component of microtubules known as tubulin, is believed to physically insert its C-terminal tail into the VDAC channel preventing the diffusion of ADP/ATP. The current understanding of this model has been primarily driven by studies utilizing reconstructed planar lipid membranes in bedded with VDAC where the addition of tubulin, changes to mitochondrial membrane lipid composition, phosphorylation and detyrosination of tubulin can alter this interaction (125, 127, 145, 146). Studies in permeabilized muscle fiber bundles – where microtubule organization remains in-tact – reveal increased ADP-dependent respiration with the removal of βII-tubulin from cardiomyocytes and decreased respiration with the addition of tubulin to isolated mitochondria (40, 127). Together, these studies support the model of tubulin regulation of VDAC permeability. Unfortunately, these studies are inconsistent in reporting tubulin and VDAC isoforms, in addition to mirroring *in-vivo* conditions.

Previous work from our laboratory has identified a direct protein-protein interaction between both α- and βII-tubulin and VDAC2 in EDL muscle (116). When reviewing the current literature these two tubulin isoforms appeared to be the most relevant to skeletal muscles while knockout studies of VDAC2 result in embryonic death highlighting its important contribution to sustaining energy and survival (25, 85) influencing the decision to explore these isoforms. Perturbing the microtubule architecture with microtubule targeted chemotherapy paclitaxel increased the amount of α- and βII-tubulin-VDAC2 interaction while impairing H_2O_2 kinetics

(115). What remains unknown is whether *in-vivo* administration of microtubule targeted chemotherapies also impair ADP-dependent mitochondrial bioenergetics in a tubulin-VDAC dependent manner, which may then be related to muscle weakness commonly seen with chemotherapy treatments.

The purpose of this investigation was to determine whether short-term treatments with microtubule stabilizer, paclitaxel, and destabilizer, vinblastine, cause mitochondrial dysfunction in relation to altered tubulin-VDAC interactions, and whether this relationship was associated with muscle weakness. We hypothesize that microtubule targeted chemotherapy will cause muscle weakness, related to impaired mitochondrial bioenergetics, linked to increased α- and βII-tubulin-VDAC2 interaction following paclitaxel treatment vs decreased interactions following vinblastine.

Methods

Animal Handling

30 male Wistar rats (6-8 weeks old) ordered from Charles Rivers Laboratory (Toronto, Ontario, CA) were used for the completion of this project. Rats were housed in pairs and acclimatized for 5 days prior to the initiation of experiments where they were then singly housed with a running wheel. Housing was maintained on a 12:12 light-dark cycle with ad-libitum access to food and water. All procedures were approved and in accordance with Canadian Care Animal Committee and the York University Animal Care Committee (AUP; 2016-19).

Muscle function

Voluntary wheel running

Following acclimatization rats were randomly selected into either saline, paclitaxel or vinblastine injection groups. Voluntary wheel running was recorded daily for 5 days prior to initiation and during injection days to determine activity before and following microtubule targeted chemotherapy treatment. Each rat was place in a specialized cage with 24-hour access to a running wheel (Harvard Apparatus) where running distance was recorded at the same time each day. Each wheel contained a magnet and a sensor which was connected to an electric counter. Revolutions were recorded and multiplied by the known distance of the wheel (108cm) to obtain distance traveled. Once the distance was recorded, the electronic counter was reset to 0. Voluntary running log was maintained before and during microtubule targeted chemotherapy injections.

Fore-limb grip strength

On the last day of pre-injection voluntary running, grip strength was measured using a force transducer (Mark 10 Digital Force Guage, Copiague, NY) with an attached metal grid

secured to the edge of a table. Held by the tail, rats were brought to the grid, allowing their front paws to grip while being lightly pulled away until their grasp was broken. Rats repeated 3 reps of grip pulls recording the maximum peak tension of the 3 trials (88). Data was omitted from non-compliant rats. Fore-limb grip strength was measured the day before and after 2-days of microtubule targeted chemotherapy injections.

In-vivo hind-limb force production

1-day prior to and following 2-days of saline, paclitaxel or vinblastine injections, *in-vivo* plantar flexor muscle torque was measured. Rats were anesthetized with isoflurane (5%) and maintained at 3-4% for the duration of the experiment. Rats were placed on a heated platform (37°C) where the fur from the left hind limb was shaved off with rodent clippers and the entire hind limb was sterilized with 3 washes of iodine. The left paw was secured to an Aurora scientific 305C-FP foot plate attached to the shaft of a servomotor. The left knee was raised to a 90° angle and clamped in place limiting any upper-limb movement. Percutaneous needle electrodes were sterilized and optimally placed under the skin applying electrical stimulus using an Aurora Scientific 701C electrical stimulator. Amperage, needle placement and muscle length was optimized with a series of twitch contractions. Maximum torque was derived from a series of isometric contractions at various stimulation frequencies (25-250Hz) (150). Plantar flexor muscle torque was determined the day prior to initiation of microtubule targeted chemotherapy injections and on the day of tissue harvest.

Administration of microtubule targeted chemotherapy and tissue harvest

Following acclimatization rats were randomly selected into either saline, paclitaxel or vinblastine injection groups. Rats received a dose of 1mg/kg body weight and equal volumes of saline for controls based on previous literature and recommendations from the university

veterinarian (14, 55, 101). Saline and vinblastine treated rats received intraperitoneal injections while paclitaxel treated rats received intravenous injections as paclitaxel has been shown to cause atrophy and lesions at injection sites (14, 55). Rats received their respective injections at the same time for two consecutive days. The day after injections, rats were anesthetized with isoflurane where the white gastrocnemius (WG) plantaris, soleus, extensor digitorum longus (EDL), tibalis anterior, diaphragm and heart muscles were removed and prepared for subsequent experiments. The soleus and WG muscles were removed, placed on ice and quickly divided for bioenergetic experiments, OCT embedding and snap frozen for frozen assays.

Mitochondrial bioenergetic assays

Preparation of permeabilized muscle fiber bundles (PmFB)

Soleus and WG muscles allocated for mitochondrial bioenergetic experiments were trimmed of fat and connective tissue and submerged into ice cold BIOPS buffer containing (mM): 50 MES, 7.23 K_2EGTA, 2.77 CaK_2EGTA, 20 Imidazole, 0.5 Dithiothreitol (DTT), 20 Taurine, 5.77 ATP, 15 phosphocreatine and 6.56 $MgCl_2 \bullet 6H_2O$ (pH 7.1) (51, 75, 89, 104). Muscle fiber bundles (1-3mg wet weight) were prepared in 16mm dishes filled with BIOPS buffer using antimagnetic needle tipped forceps under magnification (Zeiss, 2000, Germany) maintained at 4°C. Bundles were then placed in centrifuge tubes containing 40ug/ml saponin dissolved in BIOPS buffer to selectively permeabilize the cholesterol rich sarcolemma, washing the cytosol, allowing substrates to enter the cell and stimulate the mitochondria. Fibers allocated for pyruvate stimulated H_2O_2 emission were permeabilized in the presence of 100μM 2,4-dinitrochlorobenzene (CDNB), depleting endogenous glutathione allowing the generation of H_2O_2 from complex I of the electron transport chain (35, 51). Permeabilized muscle fiber bundles (PmFB) allocated for respiration experiments were washed with MIR05 buffer

containing (mM): 0.5 EGTA, 10 KH_2PO_4, 3 $MgCL_2$•6 H_2O, 60 K-lactobionate, 20 hepes, 20 taurine, 110 sucrose and 1 mg/ml fatty acid free BSA (pH 7.1), and PmFB allocated for H2O2 emission experiments were washed with Buffer Z containing (mM): 105 K-MES, 30 KCl, 10 K_2PO_4, 5 $MgCl_2$•6 H_2O, 1 EGTA and 5 mg/ml BSA (pH 7.1) for 15 minutes at 4°C. PmFB allocated for calcium retention capacity assays were washed for 10 minutes in Buffer Y containing (mM): 250 sucrose, 10 tris-HCl, 20 tris Base, 10 KH_2PO_4, and 0.5mg/ml BSA followed by another 10 minutes with 10μM blebbistatin dissolved in Buffer Y at 4°C. Wet weights were obtained for PmFB selected for respiration experiments while PmFB selected for H_2O_2 and calcium retention capacity were removed from the cuvette, dried and lyophilized to obtain dry weight for normalization.

Mitochondrial respiration

PmFB were placed into a high-resolution respirometer, Oroboros Oxygraph-2k (Oroboros Instruments, Corp. Innsbruck, Austria) containing 2mls of either MIR05 buffer with or without 20mM creatine to maximally stimulated mitochondrial creatine kinase (8, 44, 136), maintained at 37°C with a stir speed of 750rpm. All experiments began with a starting [O_2] of ~350μM, and were completed before the chamber reached 150μM [O_2]. State 3 respiration was achieved with the addition of 5mM pyruvate and 4mM malate to stimulate complex I through NADH, followed by a titration of ADP at physiological (25μM), submaximal (300μM and 500μM) and maximal (5mM and 10mM) [ADP] in soleus PmFB and physiological (25μM), submaximal (500μM) and maximal (5mM) [ADP] in the WG PmFB (75, 116). Complex I and II were further isolated with the addition of 5mM glutamate and 20mM Succinate respectively. Mitochondrial membrane integrity was determined with the addition of 10μM cytochrome c oxidase with all responses maintained below 15%.

H_2O_2 emission

PmFB were submerged into 1ml of buffer Z containing 10μM Amplex UltraRed, 0.5U/ml horse radish peroxidase, 40U/ml Cu/Zn-SOD1 and 5μM BLEB in a quartz cuvette maintained at 37°C with constant stirring. H_2O_2 emission was detected fluorometrically (QuantaMaster 40, HORIBA Scientific, Edison, NJ, USA) with the addition of 10mM pyruvate and 4mM malate. To determine the ability of ADP to reduce H_2O_2 emission by driving ATP production, a titration of ADP was added at physiological (25μM), submaximal (500μM) and maximal (5mM) [ADP] for both soleus and WG PmFB.

Calcium retention capacity

To determine the cells susceptibility to induce mitochondrial permeability transition pore (mPTP) opening, PmFB were placed into quartz cuvettes containing 300μL of buffer Y containing 1 μM Calcium Green-5N (Invitrogen), 2 μM tharpsigargin, 5 mM 2-deoxyglucose, 2 U/mL hexokinase, 20mM creatine, 5 μM BLEB and 40 μM EGTA, placed in a high-resolution fluorometer (QuantaMaster 80, HORIBA Scientific, Edison, NJ, USA). Background fluorescence was obtained with the addition of 5mM glutamate and 2mM malate followed by an initial 8nm $CaCl_2$ pulse with subsequent 4nm $CaCl_2$ pulses until mPTP opening was evident. Maximum florescence was achieved following the addition of two 0.5mM pulses of $CaCl_2$ saturating the fluorophore.

Immunohistochemistry

Soleus muscle allocated for histology was cleaned and cut of fat and connective tissue on ice and placed in O.C.T embedding compound (Tissue Tek) so that fibers lay longitudinally to obtain muscle cross-sections. Embedded soleus muscle was then submerged into liquid nitrogen cooled 2-methlybutane and stored at -80°C. Prior to slicing the muscle sections, frozen

embedded soleus muscle was brought up to and maintained between -19°C - 21°C. Soleus muscle was sliced in triplicate 10μm thick slices/slide on three separate slides. Slides containing muscle sections were stored at -20°C.

Soleus muscle sections were fixed with 4% paraformaldehyde and permeabilized with 0.5% triton-X100 dissolved in PBS followed by blocking for 1 hour with 5% BSA dissolved in PBS at room temperature. Primary antibodies for α-tubulin (Sigma-Aldrich; T6199; 1:1000) and βII-tubulin (Abcam: ab28036; 1:250) were incubated on separate slides for 4 hours at room temperature followed by an overnight incubation on all slides with voltage dependent anion channel (VDAC) 2 primary antibody (Santa-Cruz; 32059, 1:250) at 4°C. The following day muscle sections were prepared for the proximity ligation assay as described previously with a few modifications (15, 116). Briefly, sections were washed with the buffer provided in the assay kit and incubated with probes matching the primary antibodies for 1.5 hours followed incubations with detection reagents red (Sigma-Aldrrich; DUO92008). Muscle sections were coated with 5μL of mounting medium and sealed with a coverslip.

Image acquisition

Confocal microscopy images were acquired using a Zeiss laser scanning confocal microscope 700 (Carl Zeiss, Thornwood, NY). Images were captured using a 40x oil objective with the pin hole adjusted to 1AU with a z-step of 0.23μm capturing 10-15 slices. Three separate images per muscle section per slide were imaged. Analysis was completed using Imaris image quantifying software (Bitplane, Zurich, Switzerland) where images were reconstructed into 3D and using the spot tool, each individual spot (protein-protein interaction) was counted yielding number of spots.

Western blotting and caspase activity assay

Western blot procedures were completed as described previously (51, 176). Briefly, frozen soleus and WG muscles were chipped and homogenized. Protein content was determined using a BCA protein assay kit (Life Technologies, Carlsbad, CA, USA). Samples were prepared and proteins were separated on a 12% gel followed by a transfer onto a low-fluorescence polyvinylidene difluoride membrane. Following blocking, membranes were incubated overnight at 4°C with the following primary antibodies: electron transport chain proteins (OXPHOS cocktail, ab110413, Abcam, Cambridge, UK, 1:250), VDAC2 (32059, Santa-Cruz, 1:1000), adenine nucleotide translocase 1 (ANT1) (ab180715, Abcam, 1:1000), mitochondrial creatine kinase (mtCK) (a generous gift from Dr. Uwe Schlattner, Grenoble, France, 1:1000), α-tubulin (T6199, Sigma-Aldrich, 1:1000) and β-II tubulin (ab28036, Abcam, 1:100). The following day membranes were washed and incubated with their corresponding infrared fluorescent secondary antibody (LI-COR, Lincoln NE, USA), imaged with a LI-COR infrared imager and analyzed with ImageJ software (ImageJ, http://imagej.nih.gov/ij/).

Mitochondrial derived caspases 3 and 9, and cytosolic caspase 8 was determined as described previously (32, 52). Proteosomal fractions were isolated from soleus and WG homogenates to determine the enzymatic activity of caspase 3 AC-DEVD-AMC (ALX-260-031-M001, Enzo Life Sciences, Farmingdale, NY, USA), caspase 8, AC-IETD-AMC (ALX-260-042-M001, Enzo Life Sciences, Farmingdale, NY, USA) and caspase 9, AC-LEHD-AMC (ALX-260-080-M001, Enzo Life Sciences, Farmingdale, NY, USA). Caspase activity was normalized to protein content.

Analysis and Statistics

Outliers were omitted with the ROUT test and normal distribution was tested with the D'Agostino-Pearson omnibus or Sharpiro-Wilks test. A one-way ANOVA was completed for

H_2O_2 emission in the absence of ADP, proximity ligation assay analysis, calcium retention capacity, caspase activity assays and all Western blot analysis except for the proteins of the electron transport chain (OXPHOS). A two-way ANOVA was completed for ADP-stimulated respiration, ADP attenuation of H_2O_2 emission and the Western blot for the proteins of the electron transport chain (OXPHOS). The Fisher's least squares difference post-hoc analysis was completed when a significant F ratio was obtained. All data analysis was completed using Prism 8 (Graphpad prism 8, La Jolla, CA) and results are reported as mean ± SEM with significance accepted at $P<0.05$.

Results

Whole body effects of paclitaxel and vinblastine injections

Body weight did not change following 2 days of either control (saline), paclitaxel, or vinblastine injections (Table 1). To determine whether microtubule stabilization with paclitaxel or destabilization with vinblastine would have muscle specific changes, each muscle was carefully harvested and weighed before processing. We found significantly higher in diaphragm muscle weight following paclitaxel injections (saline; 0.44 ± 0.06g vs. paclitaxel; 0.60 ± 0.03g, p=0.02, Table 1) and significantly lower weight following vinblastine injections in the gastrocnemius (saline; 1.55 ± 0.07g vs. vinblastine; 1.33 ± 0.11g p=0.0004 and vs. paclitaxel; 1.57 ± 0.06g, p=0.0002) and heart muscles (saline; 1.09 ± 0.05g vs. vinblastine; 0.95 ± 0.03g, p=0.02 and vs. paclitaxel; 1.11 ± 0.05g, p=0.009, Table 1).

Table 6-1. Body and tissue weights before and after 2-days microtubule targeted chemotherapy injection. Results are expressed as means ± SEM. $p<0.05 vs. saline, #p<0.05 vs. paclitaxel and &p<0.05 vs. vinblastine

	Saline	Paclitaxel	Vinblastine
Body Weight (g)			
Pre – injection	301.1 ± 14.1	308.8 ± 14.5	305.0 ± 11.3
Post – injection	305.0 ± 13.7	306.4 ± 14.1	296.7 ± 12.0
Tissue Weight (g)			
Soleus	0.17 ± 0.01	0.16 ± 0.01	0.14 ± 0.01
Plantaris	0.27 ± 0.02	0.26 ± 0.02	0.24 ± 0.02
Gastrocnemius	1.55 ± 0.07	1.57 ± 0.06	1.33 ± 0.11$^{\$\#}$
Tibalis Anterior (TA)	0.60 ± 0.04	0.58 ± 0.03	0.53 ± 0.03
Extensor digitorum longus (EDL)	0.15 ± 0.01	0.14 ± 0.01	0.14 ± 0.01
Diaphragm	0.44 ± 0.06	0.60 ± 0.03$^{\$}$	0.49 ± 0.04
Heart	1.09 ± 0.05	1.11 ± 0.05	0.95 ± 0.03$^{\$\#}$

Rats were randomly placed into either saline, paclitaxel or vinblastine groups in an un-blinded manner. Following saline injections there were no significant differences in voluntary running distance (pre- 3.13 ± 0.61, post- 2.25 ± 0.45 km, p=0.13, Figure 6-1 A). Interestingly, following both paclitaxel (pre- 4.87 ± 0.58, post- 2.16 ± 0.42 km, p=0.0004, Figure 6-1 B) and vinblastine (pre- 4.88 ± 1.21, post- 0.7 ± 0.36 km, p=0.0001 Figure 6-1 C) injections, there was a significant decrease in voluntary running distance. Whole body strength was asses through fore-limb grip strength with no differences following saline injections (pre-15.93 ± 1.56, post-16.51 ± 2.02, p=0.40, Figure 6-1 D). Following paclitaxel injections there was a significant decrease in forelimb force production (pre- 15.26 ± 1.22, post- 11.89 ± 1.02, p=0.02, Figure 6-1 E). Lastly, following vinblastine injections there were no differences in forelimb grip strength (pre- 15.98 ± 1.61, post- 13.42 ± 1.67, p=0.14, Figure 6-1 F).

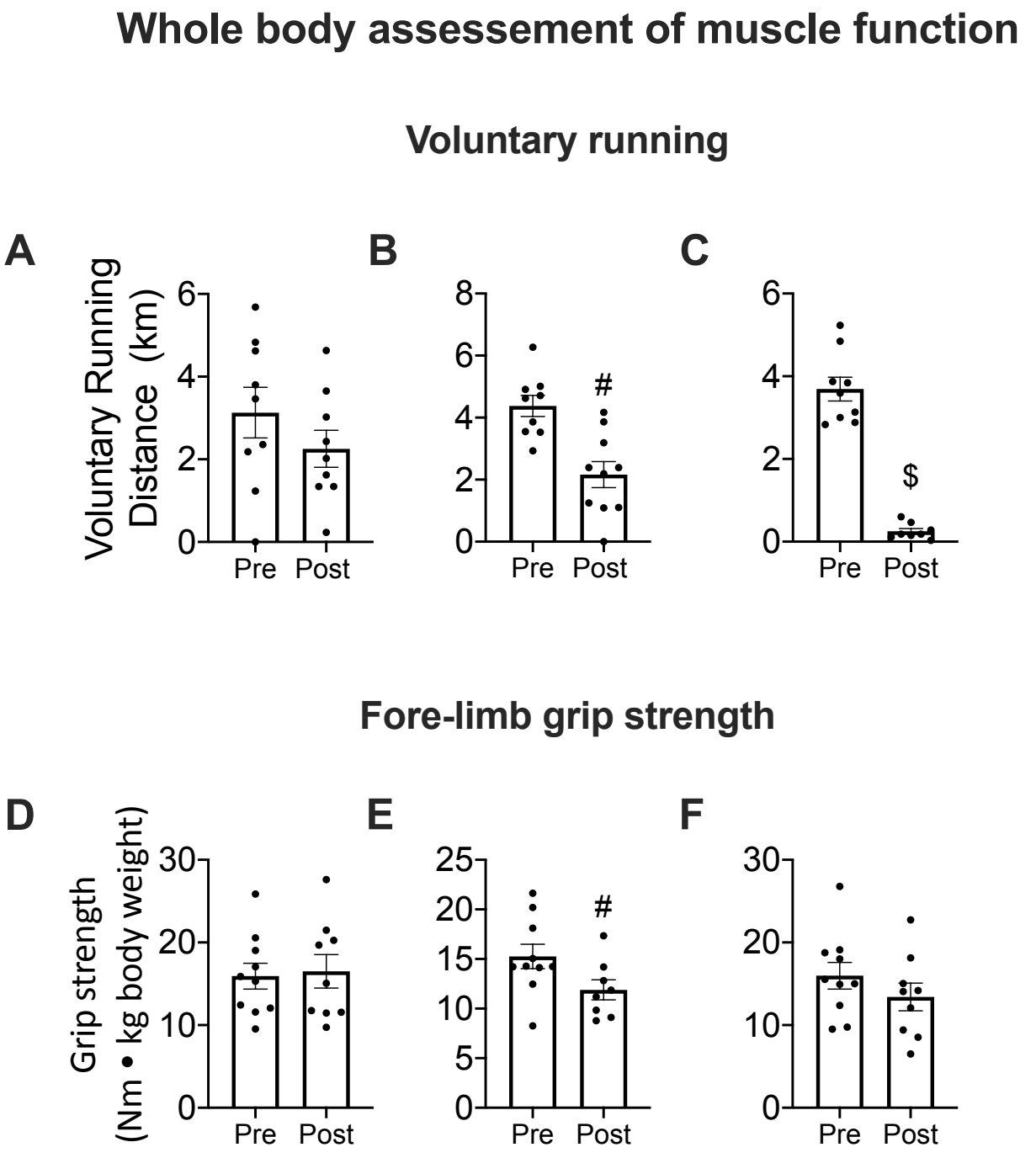

Figure 6-1. Whole body assessments of muscle function. 5-Day voluntary cage wheel running distance (n=10 measured over 5 days) measured pre- and post- **A.** saline, **B.** paclitaxel and **C.** vinblastine injections. Maximal forelimb grip strength measured pre- and post- **D.** saline **E.** paclitaxel and **F.** Vinblastine injections (n=10). Results are represented as means ± SEM. #p<0.05 saline vs. paclitaxel, $p<0.05 saline vs. vinblastine and &p<0.05 paclitaxel vs. vinblastine.

In-vivo hind-limb muscle force was tested to determine whether altering microtubule organization would affect the muscles ability to generate force. Percutaneous needle electrodes stimulated plantar flexion at the ankle generating a torque reported as (nM/mg body weight). Following 2-days of saline ($p=0.27$), paclitaxel ($p=0.55$) and vinblastine ($p=0.51$) injection there were no differences in maximum torque (Figure 6-1A, D and G). Following paclitaxel injections, torque frequency was significantly increased compared to pre-injection frequencies (main effect, $p=0.01$, Figure 6-1E) whereas vinblastine injected rats resulted with a lower torque frequency curve following injections ($p=0.056$) (Figure 6-1H) with no differences in saline injected rats ($p=0.12$, Figure 6-1B).

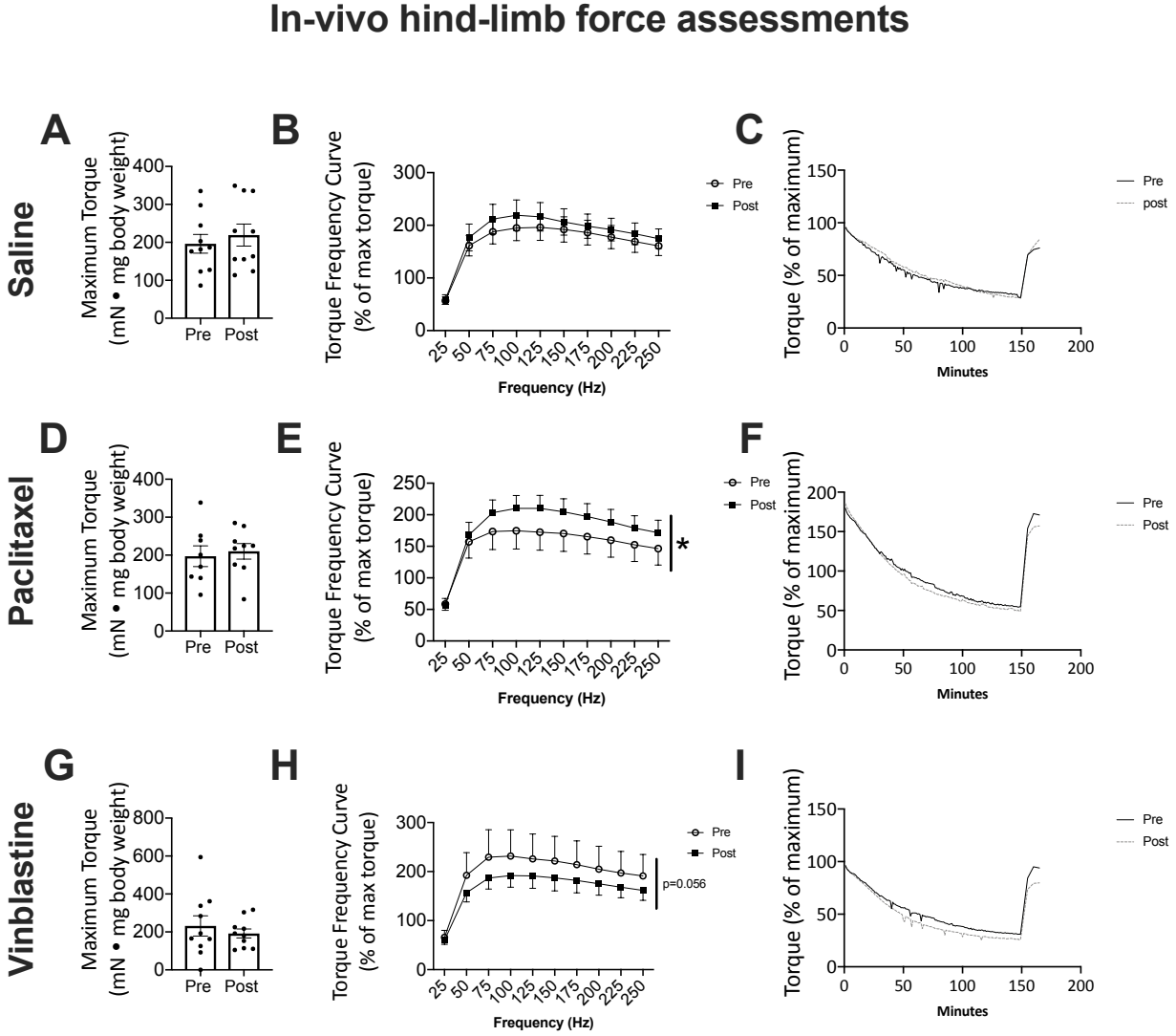

Figure 6-2. Functional and in-vivo assessment of activity and muscle strength. *In-vivo* hind-limb maximal torque and torque frequency prior to and following 2 days of saline (n=10) (**A – C**), paclitaxel (n=9-10) (**D – F**) and vinblastine (n=10) (**G – I**) injections. Results are represented as means ± SEM. *p<0.05, #p<0.05 saline vs. paclitaxel, $p<0.05 saline vs. vinblastine and &p<0.05 paclitaxel vs. vinblastine.

Mitochondrial bioenergetic impairments may be associated with changes in tubulin-VDAC interaction in soleus muscles

Our laboratory has previously shown an altered microtubule organization in response to both paclitaxel and vinblastine in-vitro incubations (116). A proximity ligation assay was used to determine whether 2-days of paclitaxel or vinblastine injections alters the tubulin-VDAC interaction where we found no changes in α-tubulin-VDAC2 interaction ($p=0.06$) while paclitaxel significantly increased βII-tubulin-VDAC2 interaction (saline vs. paclitaxel; $p=0.004$ and vs. vinblastine; $p=0.009$, Figure 6-3B and C).

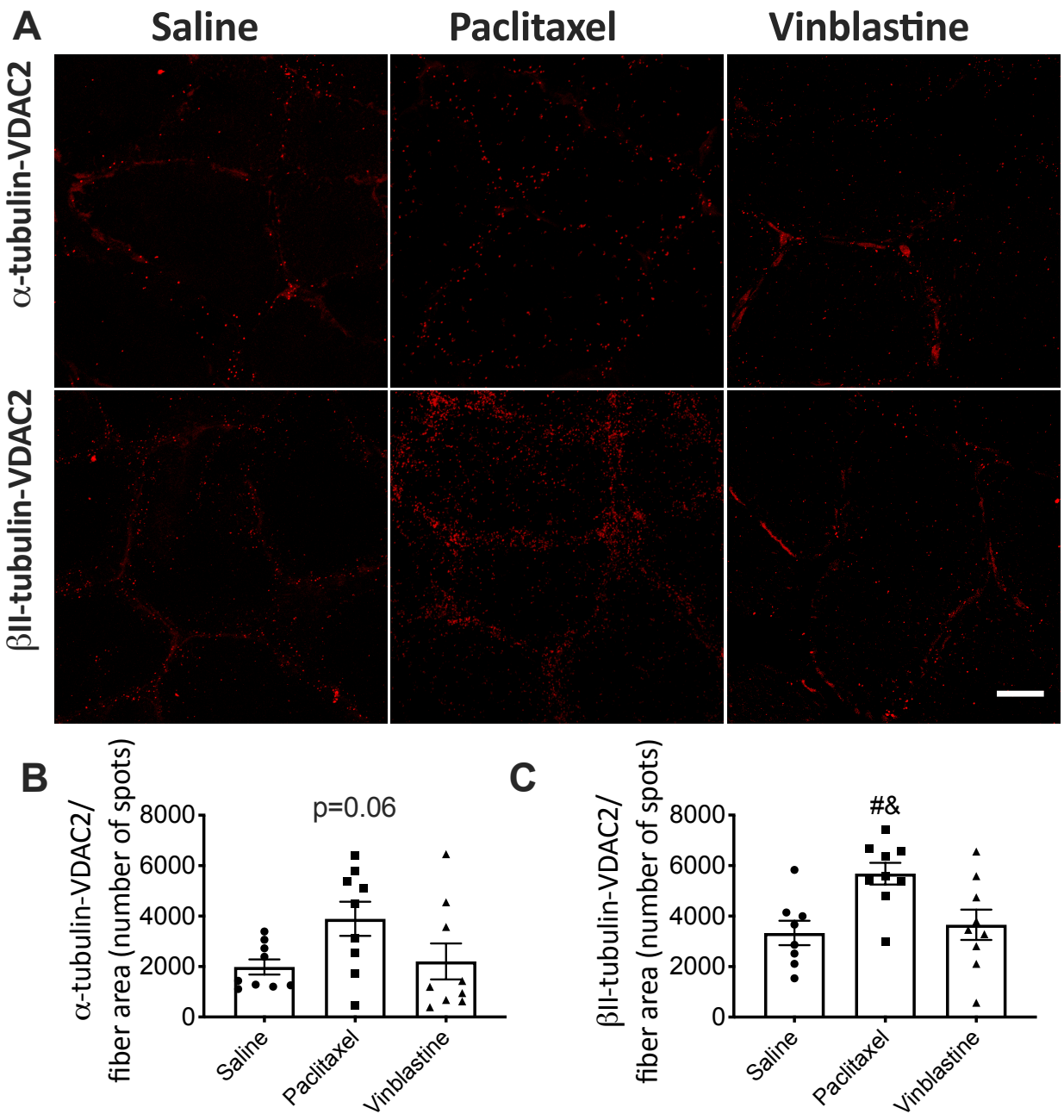

Figure 6-3. Protein-protein interaction between tubulin-VDAC2 in soleus muscle. A. Representative images of α-tubulin-VDAC2 and βII-tubulin-VDAC2 interaction in soleus muscle sections following 2-days of saline, paclitaxel or vinblastine in-vivo injections. Graphical depiction of **B.** α-tubulin-VDAC2 (n=9) and **C.** βII-tubulin-VDAC2 (n=8-9) interactions following 2-days of saline, paclitaxel or vinblastine injections. Results are represented as means ± SEM. #p<0.05 saline vs. paclitaxel and &p<0.05 paclitaxel vs. vinblastine. Scale bar, 20μm.

Complex I-stimulated respiration in the presence of 20mM creatine was similar at all [ADP] between saline, paclitaxel and vinblastine injected rats ($p=0.58$, Figure 6-4A). Similarly, there were no differences in maximal complex I-stimulated H_2O_2 emission between groups ($p=0.92$, Figure 6-4B) with a main effect found following vinblastine injections resulting with a decreased ability of ADP to attenuate H_2O_2 emission (+10 to 51%, $p=0.009$, Figure 6-4C). In the absence of creatine, a main effect was found for complex I-stimulated respiration where both paclitaxel (+4 to 37%, $p=0.001$) and vinblastine (+2 to 41%, $p=0.03$) injections increased respiration compared to saline treatment (Figure 6-4D). Both paclitaxel and vinblastine yielded divergent responses in H_2O_2 emission in the absence of creatine with paclitaxel increasing (+53%, $p=0.06$) and vinblastine significantly decreasing (-34%, $p=0.01$) H_2O_2 emission following 2-days of injections (Figure 6-4E). A main effect was uncovered displaying impaired ADP sensitivity following vinblastine injections compared to saline (+50-56%, $p<0.0001$) and paclitaxel (+18-54%, $p=0.006$) injections (Figure 6-4F).

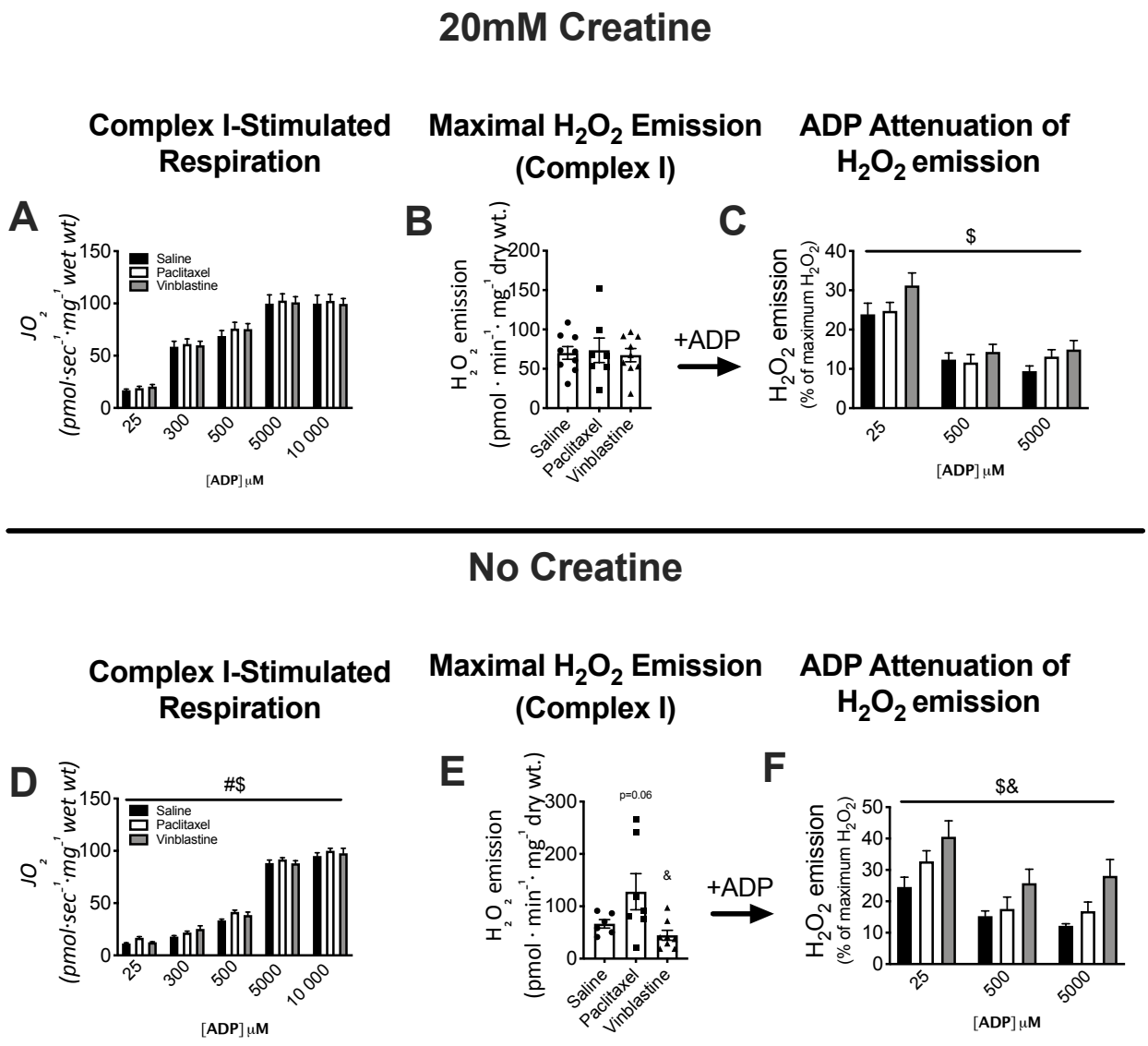

Figure 6-4. Soleus PmFB mitochondrial bioenergetics. In the presence of 20mM creatine; **A.** Complex I-supported respiration stimulated with pyruvate (5mM) and malate (4mM) at physiological (25μM) submaximal (300 and 500μM) and maximal (5mM and 10mM) ADP concentrations (n=8-10). **B**. Complex I-stimulated H_2O_2 emission stimulated in the presence of pyruvate (10mM) and malate (4mM) (n=7-10) **C.** H_2O_2 emission at a given ADP concentration expressed as a percent of maximal H_2O_2 emission. In the absence of creatine; **D.** Complex I-supported respiration stimulated with pyruvate (5mM) and malate (4mM) at physiological (25μM) submaximal (300 and 500μM) and maximal (5mM and 10mM) ADP concentrations (n=8-10). **E.** Complex I-stimulated H_2O_2 emission stimulated in the presence of pyruvate (10mM) and malate (4mM) (n=8-10) **F.** H_2O_2 emission at a given ADP concentration expressed as a percent of maximal H_2O_2 emission. Results are represented as means ± SEM. #p<0.05 saline vs. paclitaxel, $p<0.05 saline vs. vinblastine and &p<0.05 paclitaxel vs. vinblastine.

Paclitaxel injections impairs the ability of ADP to attenuate H_2O_2 emission in WG muscle

In the presence of 20mM creatine, complex I-stimulated respiration (p=0.92, Figure 6-5A) and maximal H_2O_2 emission (p=0.19, Figure 5-6B) was similar between saline, paclitaxel and vinblastine injected groups. No change was observed in ADP sensitivity between groups (p=0.27, Figure 6-5C). In the absence of creatine, a main effect was observed for reduced complex I-stimulated respiration following paclitaxel injections compared to both saline (-12 to -31%, p=0.02) and vinblastine (-20 to -34%, p=0.001) injection groups (Figure 6-5D). Maximal H_2O_2 emission (p=0.21, Figure 6-5E), and ADP sensitivity (p=0.83, Figure 6-5F) was similar between saline paclitaxel and vinblastine injection groups.

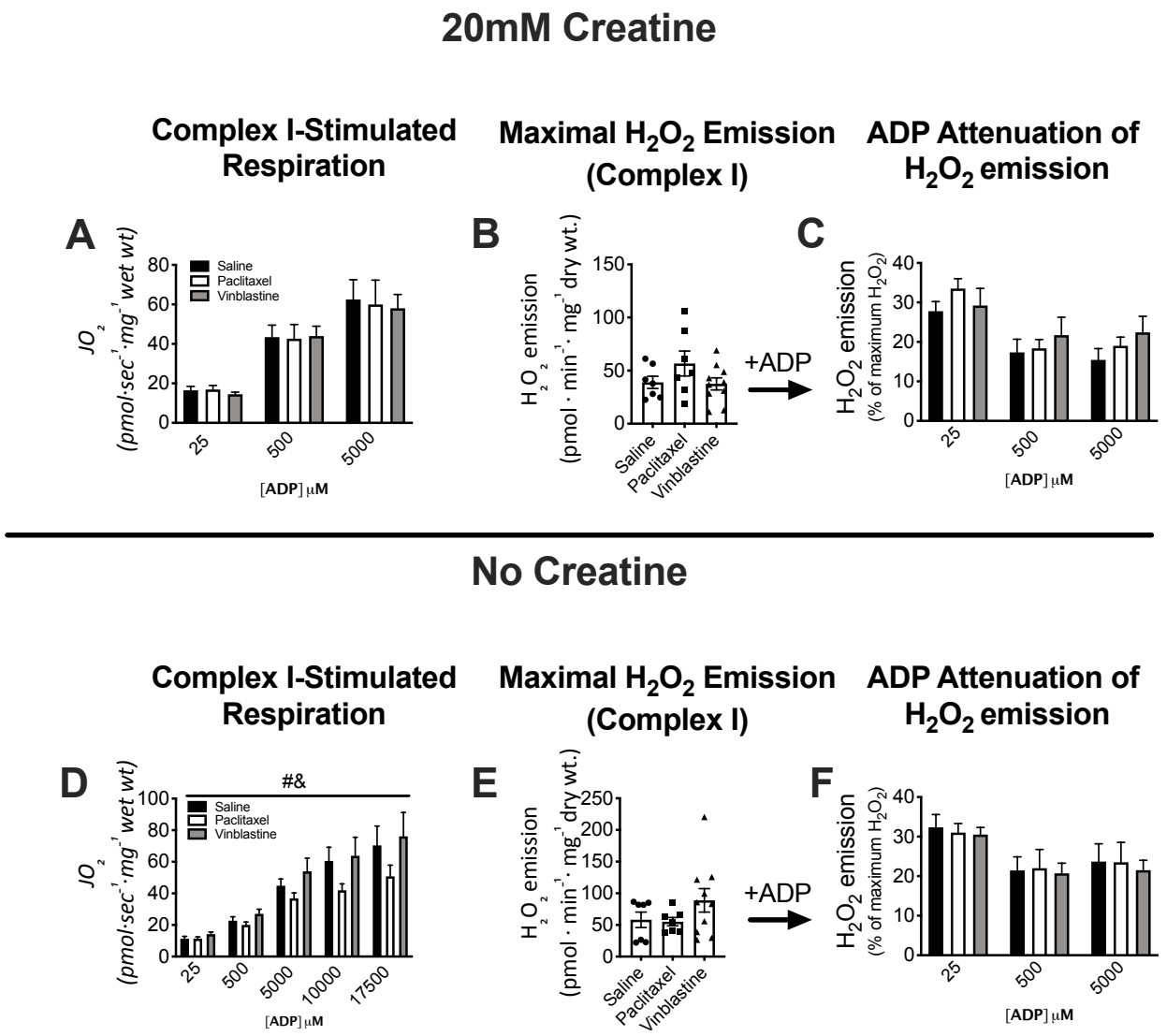

Figure 6-5. White gastrocnemius PmFB mitochondrial bioenergetics. In the presence of 20mM creatine; **A.** Complex I-supported respiration stimulated with pyruvate (5mM) and malate (4mM) at physiological (25μM) submaximal (500μM) and maximal (5mM and 10mM) ADP concentrations (n=8-10). **B**. Complex I-stimulated H_2O_2 emission stimulated in the presence of pyruvate (10mM) and malate (4mM) (n=7-10) **C.** H_2O_2 emission at a given ADP concentration expressed as a percent of maximal H_2O_2 emission (n=8-10). In the absence of creatine; **D.** Complex I-supported respiration stimulated with pyruvate (5mM) and malate (4mM) at physiological (25μM) submaximal (500μM) and maximal (5mM, 10mM and 17.5mM) ADP concentrations (n=9-10). **E.** Complex I-stimulated H_2O_2 emission stimulated in the presence of pyruvate (10mM) and malate (4mM) (n=8-10) **F.** H_2O_2 emission at a given ADP concentration expressed as a percent of maximal H_2O_2 emission. Results are represented as means ± SEM. #p<0.05 saline vs. paclitaxel, and &p<0.05 paclitaxel vs. vinblastine.

Decreased susceptibility to apoptotic cell death in WG muscle following vinblastine injections with divergent responses in soleus muscle.

The susceptibility of the mitochondrial permeability transition pore formation was tested through the calcium retention capacity assay yielding significantly increased ability to retain calcium following vinblastine injections (+144%, p=0.01) compared to control and paclitaxel (Figure 6-6D). In addition, this increase is associated with decreased mitochondrial activated caspase 3 (-26% vs. saline, p=0.02 and -24% vs. paclitaxel, p=0.03, Figure 6-6E), and caspase 9 (-31% vs. saline, p=0.01 and -35% vs. paclitaxel, p=0.002, Figure 6-6G) compared to both saline and paclitaxel treated groups. Similarly, caspase 8 activity was significantly decreased following vinblastine injections when compared to both saline and paclitaxel treatment groups (-34% vs. saline, p=0.005 and -25% vs. paclitaxel, p=0.04, Figure 6-6F).

Calcium retention capacity in soleus muscle was significantly increased following both paclitaxel (+90%, p=0.01) and vinblastine (+79%, p=0.03) injections when compared to the saline treated group (Figure 6-6A). Interestingly, paclitaxel elicited an increase in caspase 3 activity (+29%, p=0.01) while vinblastine trended to increase as well (p=0.06, Figure 6-6B). No change in caspase 8 activity was observed following both paclitaxel and vinblastine treatment (p=0.13, Figure 6-6C).

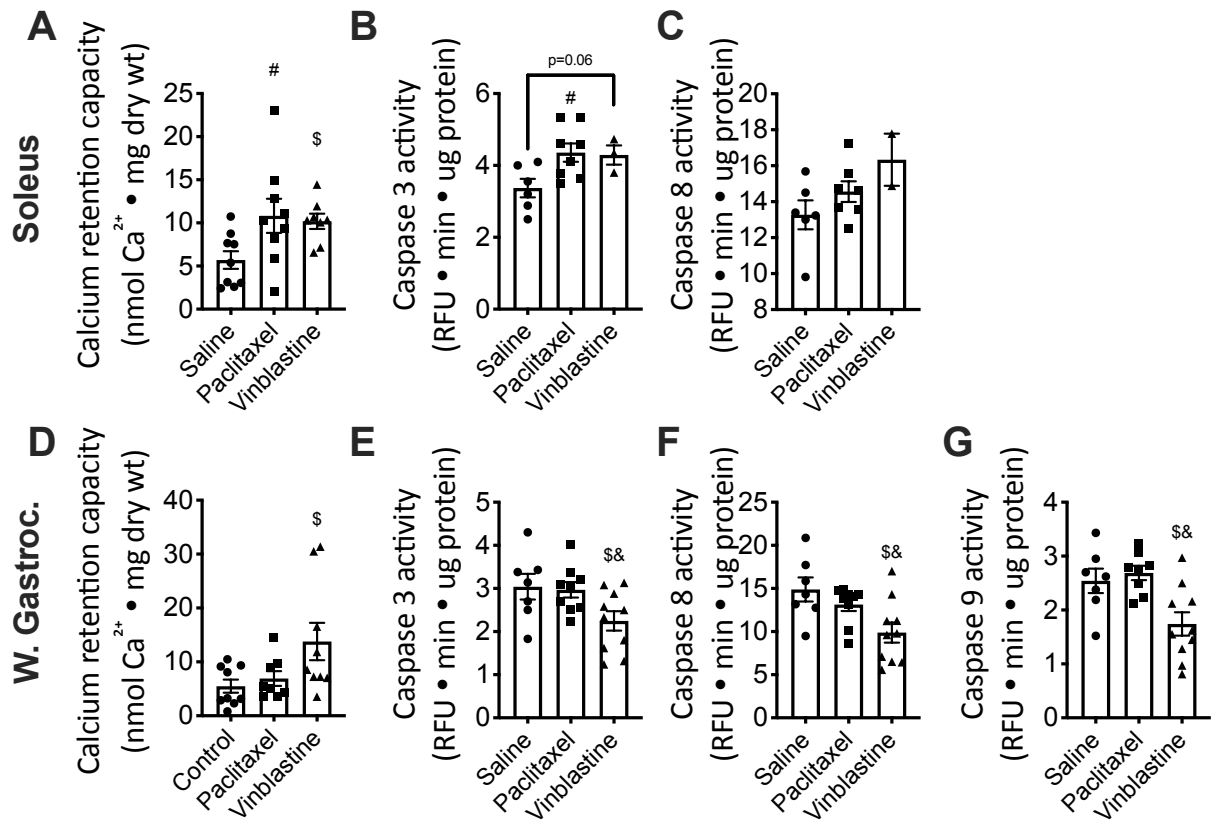

Figure 6-6. Measures of susceptibility to cell death. A. Calcium retention capacity (n=9) **B.** caspase 3 (n=3-8) and **C.** caspase 8 (n=2-7) activity in soleus muscles following 2-days of saline, paclitaxel or vinblastine injections. **D.** Calcium retention capacity (n=8-9), **E.** caspase 3 (n=7-10), **F.** caspase 8 (n=7=10) and **G.** caspase 9 (n=7-10) activity in white gastrocnemius. Muscles following 2-days of saline, paclitaxel or vinblastine injections. Results are represented as means ± SEM. #p<0.05 saline vs. paclitaxel, $p<0.05 saline vs. vinblastine and &p<0.05 paclitaxel vs. vinblastine.

Mitochondrial bioenergetic responses to acute non-specific hind-limb muscle contraction

The hind-limb *in-vivo* stimulation protocol provided a preliminary opportunity to determine the effects of contraction on mitochondrial bioenergetics following paclitaxel and vinblastine treatment. As shown in supplemental figure 6-1, contraction following paclitaxel treatment increased ADP-stimulated respiration in the presence (+9 to24%, p=0.001) and absence (+9 to +29%, p=0.01) of creatine while impairing ADP attenuation of H_2O_2 emission (+69 to 133%, p=0.0002) in the absence of creatine in soleus muscles. In addition, vinblastine treatment also displayed impaired ADP attenuation of H_2O_2 emission in the absence of creatine (+98 to 157%, p<0.0001) following acute non-specific hind-limb contraction in soleus PmFBs. In the WG muscle, paclitaxel and vinblastine did not alter ADP-stimulated respiration in the presence or absence of creatine. In the presence of creatine, paclitaxel significantly increased the ability of ADP to attenuate H_2O_2 emission (-23 to -33%, p=0.04) with no effect in the absence of creatine. Vinblastine treatment following acute non-specific muscle contracted decreased the ability of ADP to attenuate H_2O_2 emission when compared to paclitaxel (-16 to -24%, p=0.008). Lastly, implementation of this stimulation protocol had no effect on calcium retention capacity following paclitaxel (p=0.14) and vinblastine (p=0.64) treatment (Supplemental figure 6-3).

Discussion and conclusions

In this report, we have demonstrated that 2-days of *in-vivo* microtubule targeted chemotherapies produced divergent drug effects on both oxidative soleus and glycolytic WG muscles. Vinblastine, a microtubule destabilizer, significantly lowers voluntary running capacity while also reducing the amount of force produced from the hind-limb muscles. Paclitaxel, a microtubule stabilizer significantly increases *in-vivo* hind-limb muscle force production without altering whole body strength or voluntary running capacity. These functional measures are

associated with altered mitochondrial bioenergetics in oxidative soleus and glycolytic WG, in response to microtubule manipulation. In the soleus, we found that vinblastine impairs ADP sensitivity in a creatine dependent and independent manner, regardless of no change in the tubulin-VDAC2 interaction. Interestingly, paclitaxel did not appear to have a damaging effect in the soleus but instead increased ADP-stimulated respiration, in a creatine independent manner. In addition, there were trends for increased maximal H_2O_2 emission despite no effect on ADP sensitivity/ability to attenuate H_2O_2. To further understand how microtubule manipulation may be effecting different muscle fiber types we also looked at the WG muscle. We found no changes in respiration or H_2O_2 emission following vinblastine treatment. Following paclitaxel treatment, we uncovered increased submaximal H_2O_2 emission in the presence of creatine and reduced ADP-stimulated respiration in the absence of creatine. This work has uncovered the effect of microtubule targeted chemotherapy in a non-mitotic cell type where bioenergetic impairments may be related to muscle weakness commonly seen during and following chemotherapy.

Paclitaxel increases both α- and βII-tubulin – VDAC interaction without impairing mitochondrial bioenergetics

The literature strongly suggests that ADP/ATP flux regulation is mediated through an interaction between tubulin and VDAC on the outer mitochondrial membrane. In reconstructed plannar phospholipid membranes, nano-molar concentration of dimeric tubulin is sufficient enough to elicit VDAC closure (127). The mitochondrial lipid membrane composition is also involved in the tubulin – VDAC interaction as membranes of giant unilamellar vesicles enriched with dioleoyphosphatidylethanolamine (DOPE) increases the affinity of tubulin binding with VDAC (125). Phosphorylation of VDAC by glycogen synthase kinase-3β and protein kinase A (146) significantly increases tubulin binding to VDAC while detyrosination of an α-tubulin tail also promotes VDAC binding (145). There appears to be so many conditions that promote

tubulin-VDAC binding which presents a level of difficultly when trying to understand the contribution of this interaction to muscle energy exchange. We have previously shown, in an *in-vitro* model, that stabilization of microtubules with paclitaxel promotes both α- and βII-tubulin interaction with VDAC2 limiting the ability of ADP to attenuate H_2O_2 emission in the extensor digitorum longus muscle (116). In the current report, we aimed to determine whether this interaction would increase with *in-vivo* administration of paclitaxel and to what extent would this effect skeletal muscle function. Although we report an increased interaction of βII-tubulin-VDAC, this did not result in detrimental effects to mitochondrial bioenergetics in the soleus muscle. In fact, we report a main effect for increased oxygen consumption during creatine independent ADP-stimulated respiration in soleus muscles. Microtubule density is known to differ amongst different fiber types which may elicit different effects in different tissues (16). This data suggest that the tubulin-VDAC model may be dependent on the fiber type of the muscle.

In another highly oxidative tissue, unpublished work from our lab revealed creatine independent mitochondrial bioenergetic impairments in cardiac muscle following *in-vivo* injections of paclitaxel (unpublished). Further investigation through *in-vitro* paclitaxel incubations uncovered impaired oxygen consumption and an inability of ADP to reduce H_2O_2 emission. Interestingly, these *in-vivo* and *in-vitro* cardiac mitochondrial bioenergetic impairments were present without any change in both α- and βII-tubulin – VDAC2 interaction (unpublished). Similarly to the present manuscript, *in-vitro* incubations of paclitaxel in the soleus muscle did not alter ADP-dependent bioenergetics which – comparing the oxidative heart and soleus – would suggest that 1) the exploration of other tubulin and VDAC isoforms need to be

examined for protein-protein interactions (126) and 2) paclitaxel may be impairing mitochondrial and muscle function through an alternative mechanism in different tissue types.

As VDAC is involved in the formation of the mPTP, we also explored whether calcium induced apoptosis was increased following paclitaxel injections. Surprisingly we found an increased calcium retention capacity in both soleus and WG in response to vinblastine which suggests that a given calcium stress is less able to induce mitochondrial permeability transition pore formation – a key event that permits pro-apoptotic stimuli to exit the mitochondria and trigger apoptosis. Indeed, in WG this greater calcium retention capacity was associated with less mitochondrial-linked caspase 3 activation suggesting calcium stress was inducing less apoptosis after vinblastine treatment. While speculative, this is not necessarily a positive outcome as vinblastine may prevent normal muscle turnover – a possibility that is consistent with reduced hind-limb torque. However, in soleus both paclitaxel and vinblastine increased calcium retention capacity and caspase 3 activities while βII tubulin-VDAC2 interactions were increased only following paclitaxel treatment, suggesting that the tubulin-VDAC model may not be the only mechanism triggering apoptosis in this oxidative muscle.

Boudriau and colleagues (1993) determined that oxidative muscles contain 1.7-fold higher α-tubulin content compared to glycolytic muscles (16). In addition, confocal microscopy analyzing the distribution of βII-tubulin and VDAC revealed a close proximity between these two proteins in WG (161) which sparked our interested in exploring the effect of altering microtubule organization in a glycolytic tissue. Surprisingly, we uncovered increased submaximal H_2O_2 emission with no impairments to ADP sensitivity in the presence of creatine. In addition, paclitaxel significantly reduced ADP-stimulated respiration when compared to the saline treated group in the absence of creatine. Drawing on the assumption that glycolytic

muscles would respond similarly, this decline in respiration may be due to an increased α- and βII-tubulin – VDAC2 interaction seen in the EDL muscle (116) limiting the ability of ADP to diffuse through the mitochondria. A limitation to the current manuscript was the inability to measure the α- and βII-tubulin – VDAC2 interaction in the WG but we can speculate that following paclitaxel injection this interaction would increase similarly to the glycolytic EDL due to the similarities in fiber type composition (33, 116). Similarly to the EDL, we report no changes in susceptibility to cell death through calcium and caspase activation.

Vinblastine impairs soleus mitochondrial ADP-dependent mitochondrial bioenergetics independent of the tubulin – VDAC2 interaction

Destabilization of microtubules with the use of vinblastine has been previously shown to have debilitating side effects in rodent models. Konishi and colleagues (1984) report significant morphological changes to the skeletal muscle which was linked to impaired functional capacity (71). In addition, a microtubule destabilizing compound very similar to vinblastine named nocodozole has been shown to induce the mPTP, signaling the initiation of apoptosis in cardiomyocytes with *in-vitro* (10μM) conditions (74). Unfortunately, there is not much literature to draw on to further our understanding of how microtubule destabilization with vinblastine effects skeletal muscle mitochondrial bioenergetics, highlighting the importance of this work. In the presence of creatine we uncovered impaired ADP sensitivity regardless of changes in maximal and submaximal H_2O_2 emission. This was further exacerbated in the absence of creatine where vinblastine significantly reduced ADP-stimulated respiration, maximal H_2O_2 emission and ADP sensitivity. These effects were seen with no changes in the α- and βII-tubulin – VDAC2 interaction. Drawing from a study completed by Gilliam and colleagues (2013), where maximal H_2O_2 emission at 2, 24, and 72 hours following a single dose of doxorubicin chemotherapy was measured yielding decreased H_2O_2 emission over time. Similarly, a panel of microtubule targeted

compounds have been shown to increase OXPHOS gene expression by activating PGC-1α while decreasing ROS emission through upregulation of MnSOD in C_2C_{12} cells (164). These two studies and the findings of the current report suggest that changes in ADP/ATP flux and ROS emission may be transient and depend on the time and dose of vinblastine administration.

Vinblastine treatment had no effect on ADP-dependent mitochondrial bioenergetics or maximal H_2O_2 production in the WG muscle. This may be explained by the reduced number of microtubules in a more glycolytic tissue potentially rendering further depolymerisation insignificant (16) when compared to the effect of paclitaxel on microtubules. Although there were no bioenergetic impairments in response to paclitaxel, we observed a significant decrease in whole gastrocnemius muscle weight which is coupled with significantly reduced voluntary running distance and a trend for a reduced torque frequency following vinblastine treatment. The functional and microscopy data gathered here would suggest that vinblastine may be effecting the muscle through an alternate pathway.

The mechanisms of cell death from microtubule targeted chemotherapies in cancer cells is well known (94, 102, 117, 137, 168). Vinblastine is known to induce cell cycle arrest and activation of c-Jun-N-terminal protein pathway, contributing to the initiation of apoptosis through the activation of caspase 3 (69, 137). In-vitro incubations with vinblastine in EDL PmFB show a reduced capacity for calcium retention suggesting an increased susceptibility to apoptosis (116). Interestingly, following *in-vivo* injections, it appears that vinblastine is inhibiting the induction of apoptosis through an increased calcium retention capacity and reduced activity of caspases 3, 8 and 9. This is particularly confusing as we expected glycolytic tissues to respond similarly to vinblastine. These data suggest that the route of vinblastine administration may play a role in its activity.

In conclusion, these results suggest that short-term treatments with microtubule targeted chemotherapies alter mitochondrial bioenergetics but do not fully support the tubulin-VDAC model of mitochondrial bioenergetic regulation. Surprisingly, microtubule stabilization increased while destabilization decreased force production but may be occurring independently of bioenergetic impairments resulting from an altered tubulin-VDAC interaction. Overall, the current model of tubulin regulation of VDAC permeability may be more complex than initially proposed (127, 136). Further work is needed to completely elucidate the contribution of the tubulin-VDAC interaction in mediating these mitochondrial and muscle impairments, as well as alternative mechanisms by which these compounds alter mitochondrial bioenergetics.

Acknowledgements: We would like to thank Drs. Michael Riddell and Emily Dunford for the use of their laboratory's rat running wheels and guidance throughout this project. We would also like to thank Dr. Rolando Ceddia for providing access and space in his laboratory to house our 3-in-1 whole animal muscle force testing system.

Funding: This project was funded by the Natural Sciences and Engineering Research Council of Canada (436138-2013), James H. Cummings Foundation grant and a Canada Foundation for Innovation and Ontario Research Fund grant (32449) to CGRP, SVR received the Queen Elizabeth II Graduate Scholarship, PCT and MCH received a NSERC CGS-PhD scholarship

Supplemental Figures

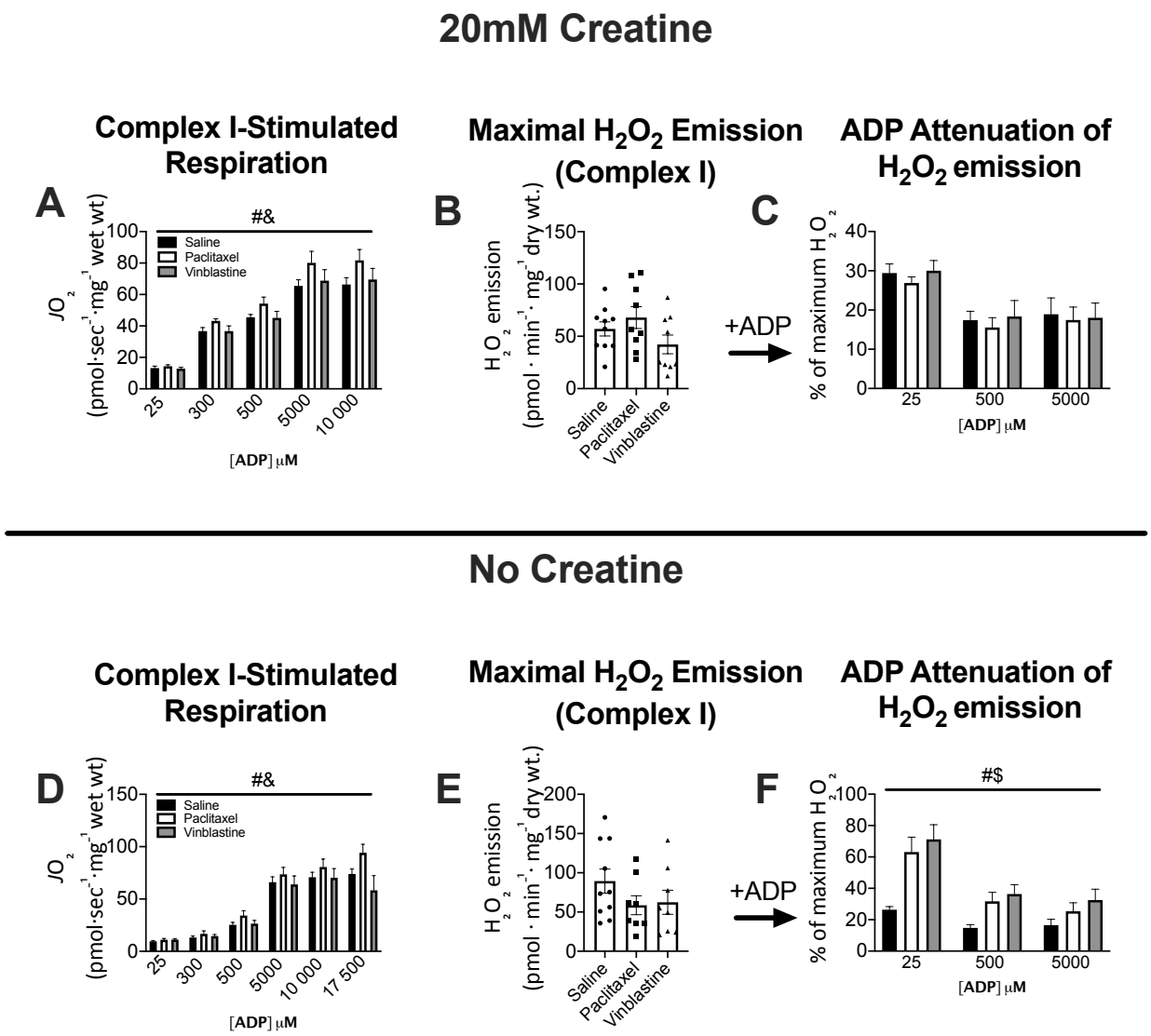

Supplemental figure 6-1. Soleus PmFB mitochondrial bioenergetics following in-vivo muscle contraction. In the presence of 20mM creatine; **A.** Complex I-supported respiration stimulated with pyruvate (5mM) and malate (4mM) at physiological (25μM) submaximal (300 and 500μM) and maximal (5mM and 10mM) ADP concentrations (n=9-10). **B**. Complex I-stimulated H_2O_2 emission stimulated in the presence of pyruvate (10mM) and malate (4mM) (n=9-10) **C.** H_2O_2 emission at a given ADP concentration expressed as a percent of maximal H_2O_2 emission. In the absence of creatine; **D.** Complex I-supported respiration stimulated with pyruvate (5mM) and malate (4mM) at physiological (25μM) submaximal (300 and 500μM) and maximal (5mM and 10mM) ADP concentrations (n=9-10). **E.** Complex I-stimulated H_2O_2 emission stimulated in the presence of pyruvate (10mM) and malate (4mM) (n=8-10) **F.** H_2O_2 emission at a given ADP concentration expressed as a percent of maximal H_2O_2 emission. Results are represented as means ± SEM. #p<0.05 saline vs. paclitaxel, $p<0.05 saline vs. vinblastine and &p<0.05 paclitaxel vs. vinblastine.

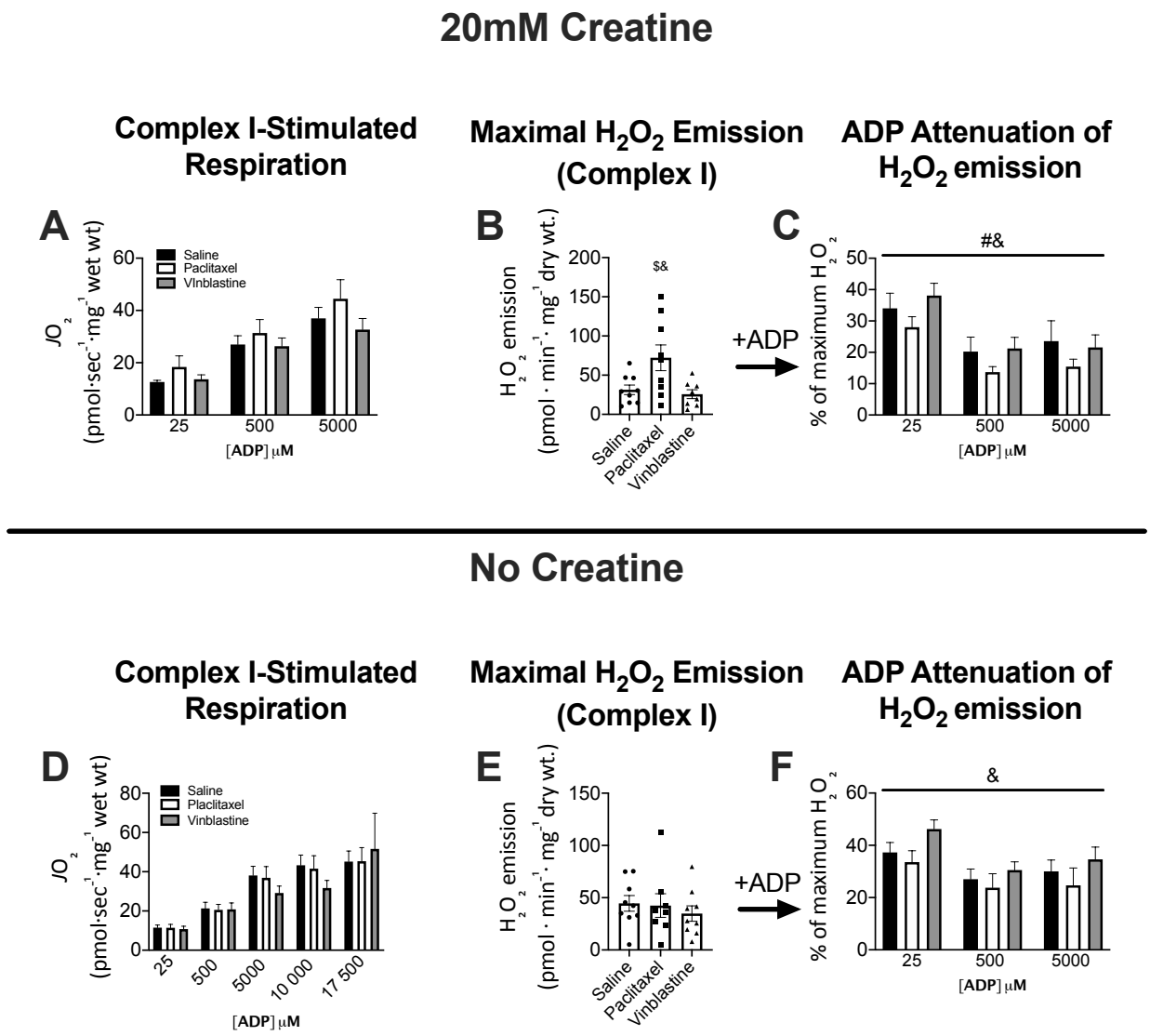

Supplemental figure 6-2. White gastrocnemius. PmFB mitochondrial bioenergetics following in-vivo muscle contraction. In the presence of 20mM creatine; **A.** Complex I-supported respiration stimulated with pyruvate (5mM) and malate (4mM) at physiological (25μM) submaximal (300 and 500μM) and maximal (5mM and 10mM) ADP concentrations (n=9-10). **B**. Complex I-stimulated H_2O_2 emission stimulated in the presence of pyruvate (10mM) and malate (4mM) (n=9) **C.** H_2O_2 emission at a given ADP concentration expressed as a percent of maximal H_2O_2 emission. In the absence of creatine; **D.** Complex I-supported respiration stimulated with pyruvate (5mM) and malate (4mM) at physiological (25μM) submaximal (300 and 500μM) and maximal (5mM and 10mM) ADP concentrations (n=8-10). **E.** Complex I-stimulated H_2O_2 emission stimulated in the presence of pyruvate (10mM) and malate (4mM) (n=8-9) **F.** H_2O_2 emission at a given ADP concentration expressed as a percent of maximal H_2O_2 emission. Results are represented as means ± SEM. #$p<0.05$ saline vs. paclitaxel, \$$p<0.05$ saline vs. vinblastine and &$p<0.05$ paclitaxel vs. vinblastine.

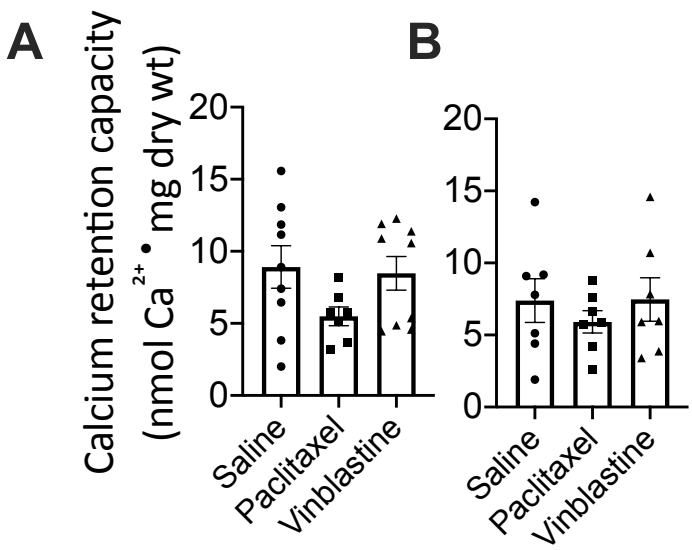

Supplemental figure 6-3. Calcium retention capacity following in-vivo contraction. A. Soleus and **B.** white gastrocnemius calcium retention capacity following 2-days of saline, paclitaxel or vinblastine injections and in-vivo muscle contractions. Results are expressed as means ± SEM.

Chapter 7

Mitochondrial bioenergetic dysfunction in Duchenne muscular dystrophy is associated with microtubule disorganization in skeletal muscle

This chapter is currently under first round of revisions in *PLOS one* PONE-D-19-09897. It is included in this thesis in the submitted format.

Author contributions: SVR and MCH designed the study and collected data. SVR, analyzed data and drafted manuscript. SVR, MCH and CGRP approved and finalized submitted version.

Mitochondrial bioenergetic dysfunction in Duchenne muscular dystrophy is associated with microtubule disorganization in skeletal muscle

Authors: Sofhia V. Ramos[*], Meghan C. Hughes[*], Catherine A. Bellissimo, Christopher G. R. Perry
[*]Denotes equal contributions

Affiliations: School of Kinesiology and Health Sciences, Muscle Health Research Center, York University, 4700 Keele Street, Toronto, ON, Canada, M3J 1P3

Short title: Mitochondrial bioenergetic dysfunction in Duchenne muscular dystrophy

Abstract

In Duchenne muscular dystrophy, a lack of dystrophin leads to extensive muscle weakness and atrophy that is linked to cellular metabolic dysfunction and oxidative stress. This dystrophinopathy results in a loss of tethering between microtubules and the sarcolemma. Microtubules are also believed to regulate mitochondrial bioenergetics potentially by binding the outer mitochondrial membrane voltage dependent anion channel (VDAC) and influencing permeability to ADP/ATP cycling. The objective of this investigation was to determine if a lack of dystrophin causes microtubule disorganization concurrent with mitochondrial dysfunction in skeletal muscle, and whether this relationship is linked to altered binding of tubulin to VDAC. In extensor digitorum longus (EDL) muscle from 4-week old D2.*mdx* mice, microtubule disorganization was observed when probing for α-tubulin. This cytoskeletal disorder was associated with a reduced ability of ADP to attenuate H_2O_2 emission during impaired oxidative phosphorylation relative to wildtype controls. However, this was not associated with altered α-tubulin-VDAC2 interactions. These findings reveal that microtubule disorganization in dystrophin-deficient EDL is associated with impaired ADP control of mitochondrial bioenergetics, and suggests that mechanisms alternative to α-tubulin's regulation of VDAC2 should be examined to understand how cytoskeletal disruption in the absence of dystrophin may cause metabolic dysfunctions in skeletal muscle.

Key Words: Duchenne muscular dystrophy, mitochondrial dysfunction, VDAC, tubulin, cytoskeleton, skeletal muscle

Introduction

In Duchenne muscular dystrophy (DMD), mutations in the X-linked gene dystrophin leads to progressive weakness in locomotor muscles. Occurring in 1:3500-5000 males, the absence of this cytoskeletal-sarcolemmal linker protein results in a compromised cell membrane that becomes damaged after contraction (5, 18). While persistent calcium influx has been linked to repeated cycles of fibre degeneration and regeneration (18), the loss of dystrophin has also been shown to cause disorganization of microtubules, specifically measured as α-tubulin, in extensor digitorum longus (EDL) muscle in C57Bl/10*mdx* mice, given dystrophin is a microtubule anchor (13, 111). However, the manner by which this altered microtubule network contributes to metabolic dysfunction remains unclear.

Mitochondrial dysfunctions have also been identified in skeletal muscle, diaphragm and heart from mouse models of Duchenne muscular dystrophy (39, 53, 107, 154, 170). A specific impairment in the ability of ADP to attenuate mitochondrial H_2O_2 emission during impaired oxidative phosphorylation was identified in multiple muscles at 4 weeks of age in D2.*mdx* mice (52) The cause for this mitochondrial dysfunction was not identified, although multiple stressors inherent in the disease could be contributors. One possibility may be that mitochondrial dysfunctions arise from a disorganized cytoskeletal network that was reported previously in the C57Bl/10.*mdx* model (13, 111). Specifically, as mitochondria are known to bind to tubulin, a component of microtubules (20, 115, 127, 145), it is possible that altering microtubule architecture may influence mitochondrial bioenergetics. Indeed, we have previously shown that inducing microtubule disorganization in EDL with microtubule-stabilizing and destabilizing compounds alters ADP's control of mitochondrial bioenergetics (116). As such, it seems plausible that the disorganized microtubule network in EDL from C57Bl/10.*mdx* mice (111) are

related to mitochondrial dysfunctions observed in other muscles (39, 53, 154, 170). However, this relationship has not been definitively demonstrated within the same muscle of the same mouse model, nor has a potential mechanism been explored for how microtubules may alter mitochondrial function in this disorder.

The first objective of the present study was to determine if disorganized microtubules are associated with a loss of ADP's central control of mitochondrial bioenergetics in EDL muscle of D2.*mdx* mice. We have previously used this mouse model to explore mitochondrial dysfunction in other muscles but it has yet to be examined for microtubule disorganization (53). The second objective was to explore whether this potential relationship was related to altered tubulin-VDAC binding stemming from disorganized microtubules. Specific attention was given to α-tubulin considering it binds various isotypes of β-tubulin as an α/β heterodimer with the CTT tail of both components having affinity for VDAC (40, 126, 127, 161). VDAC2 was selected given 1) its deficiency results in embryonic death thereby demonstrating its importance (112), 2) it has been proposed that VDAC2 may uniquely regulate the more efficient creatine-dependent phosphate shuttling mechanism (4, 7, 86, 165) and 3) because we have previously shown that tubulin-VDAC2 interactions are changed when microtubule organization is altered by paclitaxel (115). The results demonstrate a relationship between microtubule disorganization and impaired ADP control of H_2O_2 emission during oxidative phosphorylation. Contrary to the hypothesis, this dysfunction was not associated with altered α-tubulin-VDAC2 binding as detected by a proximity ligation approach (<30nm resolution) (82). These findings highlight the association between microtubule networks and mitochondrial dysfunction in DMD suggesting an important role of cytoskeletal architecture in mediating metabolic dysfunction in this disease. The results

also challenge the model of tubulin regulation of VDAC permeability to ADP, although alternative mechanisms for future investigation are discussed.

Materials and Methods

Animal Care

Briefly, male 4-week old D2.*mdx* mice (29) were used from a colony at York University originally established with breeding pairs from Jackson Laboratories (Bar Harbor, United States). Due to breeding issues, separate male wildtype (WT) DBA/2J mice were purchased from Jackson Laboratories and were acclimated for 72 hours before experiments were performed. All experiments and procedures were approved by the Animal Care Committee at York University (AUP approval number; 2016-18). Other muscles from these mice were used for separate manuscripts in preparation at the time of this submission.

Preparation of permeabilized muscle fibre bundles (PmFB)

All experimental procedures were completed as reported previously (104, 115). Mice were anesthetized with isoflurane and maintained at a 3-5% flow rate for the duration of the tissue harvest. EDL muscles were removed and quickly placed in BIOPS buffer containing (mM): 50 MES, 7.23 K_2EGTA, 2.77 CaK_2EGTA, 20 Imidazole, 0.5 Dithiothreitol (DTT), 20 Taurine, 5.77 ATP, 15 phosphocreatine and 6.56 $MgCl_2 \bullet 6H_2O$ (pH 7.1) (53, 76, 104, 115, 156) on ice. Tissue was trimmed of fat and connective tissue in BIOPS buffer maintained at 4°C and separated using antimagnetic needle-tipped forceps under magnification (Zeiss 2000, Germany). Each 1-3 mg bundle was permeabilized with 40μg/ml saponin in BIOPS for 30 min. PmFB allocated for pyruvate-induced H_2O_2 emission were permeabilized in the presence of 35μM 2,4-dinitrochlorobenzene (CDNB) to remove endogenous glutathione and permit detection of H_2O_2 emission supported by the pyruvate dehydrogenase complex (36). Once permeabilized, PmFB

were washed for 15 min at 4°C in MiRO5 buffer containing (mM): 0.5 EGTA, 10 KH_2PO_4, 3 $MgCL_2$•6 H_2O, 60 K-lactobionate, 20 hepes, 20 taurine, 110 sucrose and 1 mg/ml fatty acid free BSA (pH 7.1) for respiration experiments, buffer Z containing (mM): 105 K-MES, 30 KCl, 10 K_2PO_4, 5 $MgCl_2$•6 H_2O, 1 EGTA and 5 mg/ml BSA (pH 7.1) for H_2O_2 emission assays and buffer Y containing (mM): 250 sucrose, 10 tris-HCl, 20 tris Base, 10 KH_2PO_4, and 0.5mg/ml BSA for 10 min and then again in buffer Y with 10μM blebbistatin to determine calcium retention capacity. All wash steps were completed at 4°C.

Bioenergetic assays

PmFB were placed into a high-resolution respirometer (Oroboros Instruments, Corp. Innsbruck, Austria) with two different buffer conditions designed to model *in-vivo* metabolic control conditions; in the presence of 20mM creatine to promote cytoplasmic-mitochondrial cycling of creatine/phosphocreatine ("phosphate shuttling") through mitochondrial creatine kinase (mtCK) in the inner membrane space (4, 86, 156) and in the absence of creatine to promote ADP/ATP cycling. Approximately 350μM of O_2 was added to each chamber with each experiment completed before reaching 150μM O_2. Other technical details of respirometer settings and conditions are described previously (53, 75, 89, 104, 115, 156). Experiments were performed in the presence of 5μM blebbistatin to prevent ADP-induced muscle contraction (53, 104, 105) and normalized to wet weight. State 3 respiration was supported by 5mM pyruvate + 2mM malate (NADH, complex I) followed by ADP titrations at 25, 100, 500 and 5000μM ADP. 10μM cytochrome c was added to test for intactness of the outer mitochondrial membrane, with all responses exhibiting <15% increase in respiration. 20mM succinate ($FADH_2$) was then added for complex II-supported respiration.

PmFB were placed into a quartz cuvette containing 1ml of Buffer Z containing 10μM Amplex UltraRed, 0.5U/ml horse radish peroxidase, 40U/ml Cu/Zn-SOD1 and 5μM BLEB to measure H_2O_2 emission. Experiments were completed fluorometrically (QuantaMaster 40, HORIBA Scientific, Edison, NJ, USA) with continuous stirring and maintained at 37°C. Pyruvate (10mM)/malate (4mM) were used to stimulate H_2O_2 emission at complex I (NADH) followed by ADP titrations at 25, 100 and 500μM ADP to attenuate H_2O_2 emission during oxidative phosphorylation. Upon completion, bundles were blotted dry and lyophilized to obtain a dry weight for normalization as previously described (53, 89, 115).

Calcium retention capacity (CRC) was performed fluorometrically (QuantaMaster 80, HORIBA Scientific, Edison, NJ, USA) with a separate batch of PmFB as previously described (6, 35, 53) with the addition of 5mM ADP to mimic physiological conditions. PmFB were placed into a quartz cuvette containing Calcium Green-5N (Invitrogen) dissolved in Buffer Y (35) where an initial 8nm $CaCl_2$ pulse was added followed by 4nm $CaCl_2$ pulses until mitochondrial permeability transition pore opening was evident. Two 0.5mM pulses of $CaCl_2$ were then added to establish maximum fluorescence by saturating the fluorophore. Similarly to H_2O_2 bundles, PmFB were lyophilized to obtain dry weights for normalization.

Single fibre isolation, immunofluorescent staining and proximity ligation assay

A separate set of D2.*mdx* and control DBJ/2J mice (*n*=8-10) were used for immunofluorescent experiments as described previously (115). Briefly, EDL single fibres were isolated with 0.2% collagenase type 4 (Worthington, LLS004188, Lakewood, NJ) for 70 min (maintained at 37°C) and triturated until viable single fibres were released. Fibres were fixed with 4% paraformaldehyde for 10 min, permeabilized with 0.01% triton-X100 for 10 min and then blocked with 5% BSA PBS^{++} for 60 min, all at room temperature. Samples were then

incubated with α-tubulin (1:1000 Sigma, T6199) for 4 hours at room temperature followed by VDAC2 overnight at 4°C (1:250, Santa Cruz, 32059). Half of the fibres were used for detection of α-tubulin following incubation with the secondary antibody Alexa Flour 488 (Invitrogen, A21121).

The remaining fibres retained following primary antibody incubations were used for determination of protein-protein interaction by proximity ligation assay. Fibres were probed according to manufacturer's instructions with some modifications described previously (115). Briefly, proximity ligation assay anti-goat minus (Sigma, DUO92001) and anti-mouse plus (Sigma, DUO92006) probes were used to detect primary antibodies used above. Single fibres were incubated with anti-goat minus and anti-mouse plus probes (1:5 dilution) for 1 hour prior to a treatment with the detection reagents red (Sigma, DUO92008) consisting of a 30 min incubation with the provided ligase to splice the oligonucleotide ends of the probes together, and a 1 hour 40 min incubation with the provided polymerase to read and amplify the signal on the resulting DNA strand. All incubations were completed at 37$^{°C}$. Fibres were coated in anti-fade mounting medium and covered with a coverslip.

Image capture and quantitation

A Zeiss laser scanning confocal microscope 700 (Carl Zeiss) was used to acquire images with a 63X oil immersion objective with the pin hole set to 1AU capturing 8-10 stacks with a z-step of 0.32 μm at 3 different points along the fibre. To detect α-tubulin on immunohistochemically stained samples, fibres were excited at 488nm for α-tubulin. Samples were excited at 594nm to capture α-tubulin-VDAC2 interactions. Images were analyzed using Imaris image quantifying software (Bitplane).

Western blotting

Western blotting procedures were completed as previously reported (51, 53) using rodent OXPHOS Cocktail, ab110411, Abcam, Cambridge, UK, 1:250 dilution), VDAC2 (Santa-Cruz, 32059, Dallas, TX, 1:1000 dilution) and adenine nucleotide translocase 1 (ANT1, ab180715, Abcam, 1:1000 dilution) antibodies.

Statistics

The ROUT test was used to omit outliers followed by the D'Agostino-Pearson omnibus normality test to verify that all data followed a normal distribution. Statistical differences were assessed by two-way ANOVA for ADP-stimulated respiration and attenuation of H_2O_2 emission followed by Bonferroni multiple comparison post-hoc analysis when appropriate. Differences in glutamate and succinate stimulated respiration, H_2O_2 emission in the absence of ADP and CRC were determined through a student's un-paired t-test (GraphPad Prism 7, La Jolla, CA). Results are reported as mean ± SEM with significance accepted at $p< 0.05$.

Results

Altered microtubule organization is associated with impaired ADP-control of bioenergetics in D2.mdx mice

Confocal microscopy confirmed the disorganization of microtubule architecture in EDL from D2.*mdx* compared to WT as was reported previously in C57.Bl/10*mdx* (Figure 7-1)(13, 111). As microtubules have been proposed to regulate ADP permeability through VDAC, we next determined the ability of ADP to stimulate respiration and lower H_2O_2 emission during oxidative phosphorylation. In the presence of creatine-supported phosphate shuttling (4, 43, 86, 165) complex I-supported respiration (NADH from pyruvate) was impaired in D2.*mdx* vs WT at 500μM (-43%, p=0.0008) and 5mM ADP (-38%, p<0.0001) with a main effect observed across groups (p<0.0001) (Figure 7-2A), as was combined complex I and II (additional $FADH_2$ from

succinate) (p=0.0002) (Figure 2B). Similar results were obtained in the absence of creatine in the media – a condition that promotes ADP/ATP cycling without the more efficient mitochondrial creatine kinase-dependent phosphate shuttling (4, 42, 86, 165) - for complex I-supported respiration at 5mM (-31%, p<0.0001) and 30mM ADP (-30% p<0.0001) with a main effect observed across groups (p<0.0001) (Supplemental figure 7-1A) in addition to combined complex I and II respiration (-48%, p=0.001) (Supplemental Figure 7-1B).

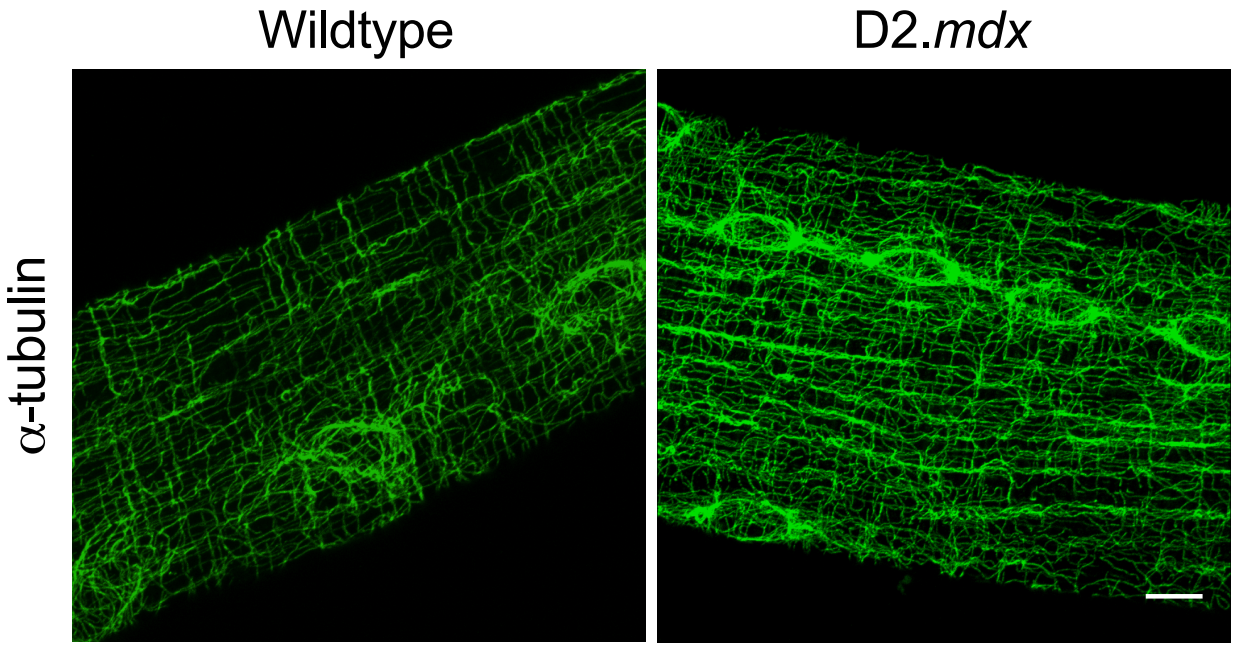

Figure 7-1. Microtubule organization. Confocal microscopy of α-tubulin-stained single EDL fibres from WT and D2.*mdx* mice (n=5-8). Scale bar, 10μm.

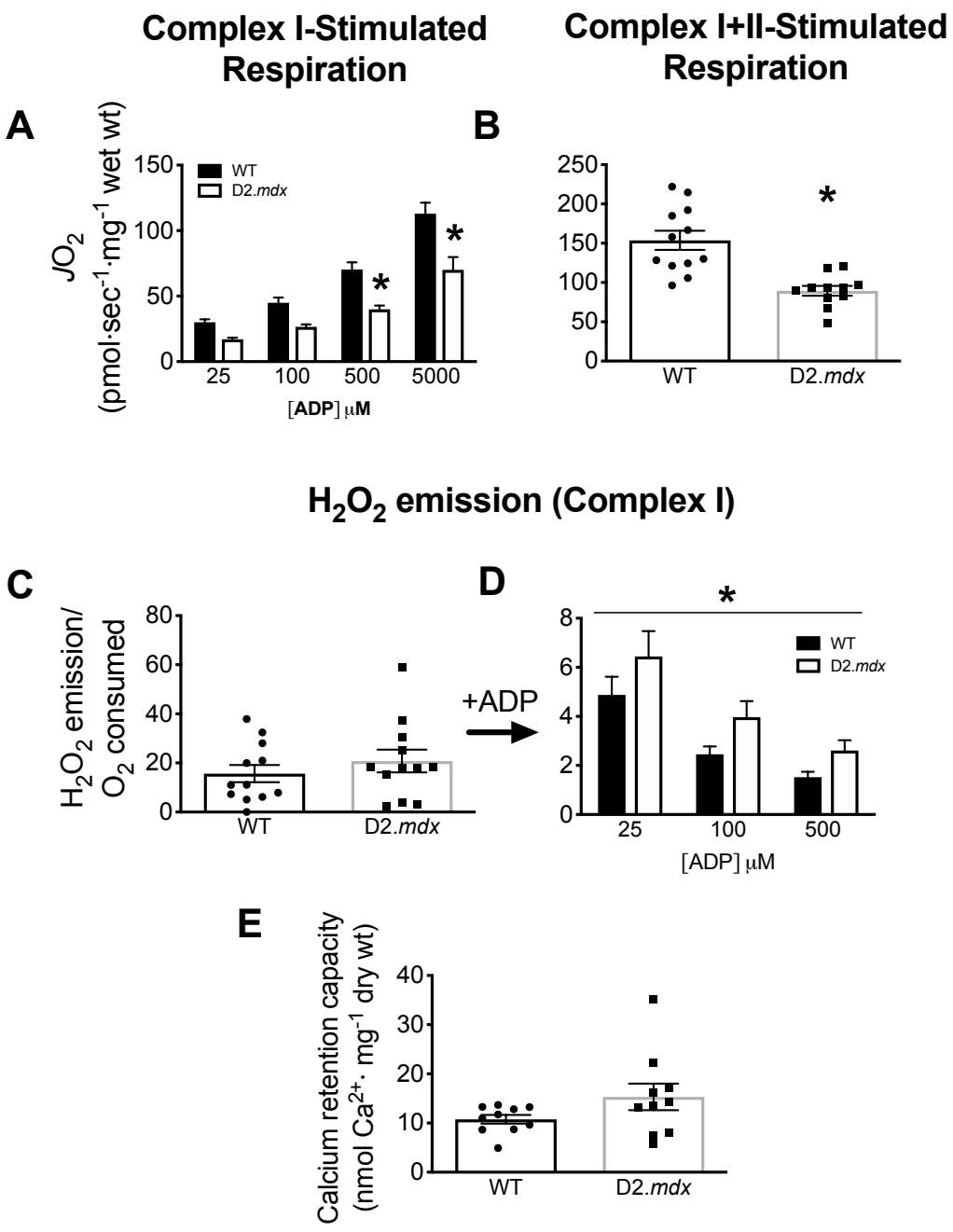

Figure7-2. Mitochondrial bioenergetics in EDL PmFB. ADP-stimulated respiration was initially supported by complex I (NADH from 5mM pyruvate/4mM malate) in the presence of creatine (*n*=12) **(A)** followed by complex II ($FADH_2$ from 20mM succinate) (*n*=11-12) **(B)**. H_2O_2 emission was stimulated at complex I (NADH from 10mM pyruvate/4mM malate) in the presence of creatine (*n*=12) **(C)** followed by an ADP titration (*n*=11-12) **(D)**. Calcium retention capacity (*n*=10) **(E)**. Results are reported as mean ± SEM, (**p*<0.05).

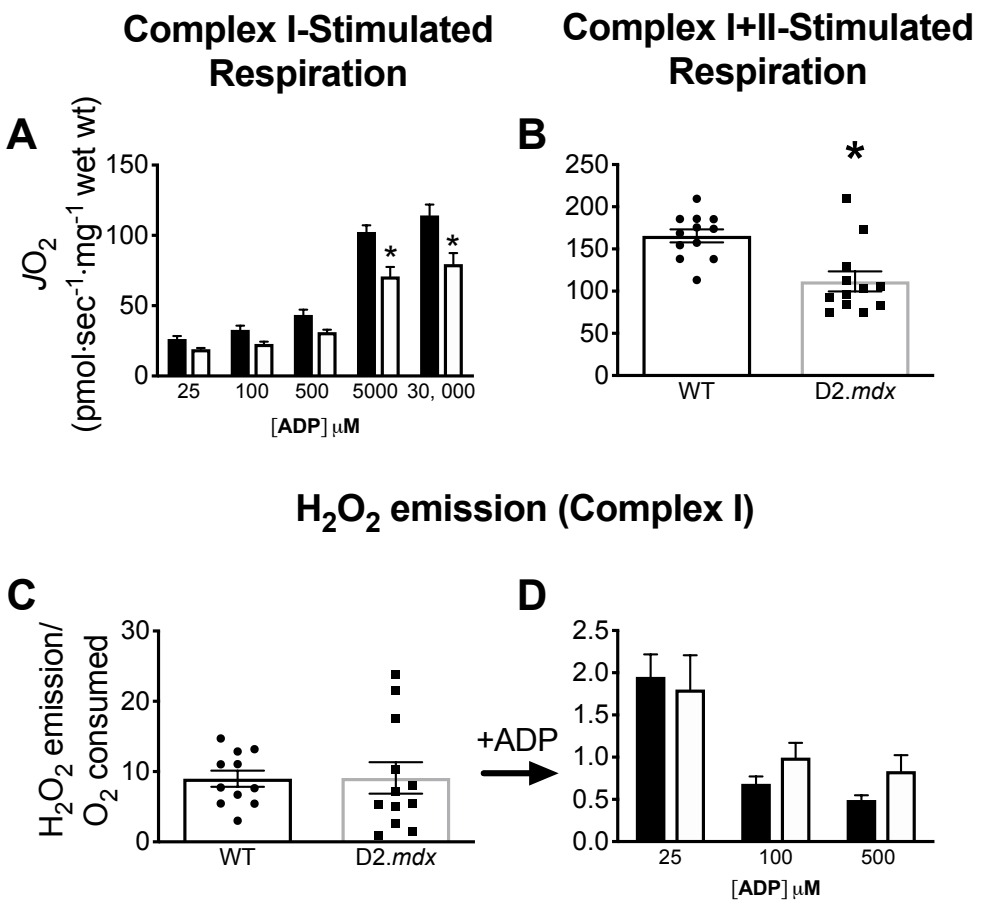

Supplemental figure 7-1. Mitochondrial bioenergetics in the absence of creatine in EDL PmFB. ADP-stimulated respiration supported by complex I (NADH from 5mM pyruvate/4mM malate) (*n*=12) **(A)** followed by complex II ($FADH_2$ from 20mM succinate) (*n*=12) **(B)**. H_2O_2 emission was stimulated at complex I (NADH from 10mM pyruvate/4mM malate) (*n*=11-12) **(C)** followed by an ADP titration (*n*=12) **(D)**. Results are reported as mean ± SEM, (**p*<0.05).

Maximal H_2O_2 emission during State II/uncoupled respiration (no ADP) was similar between D2.*mdx* and WT in the presence (*p*=0.39) (Figure 7-2C) and absence of creatine (*p*=0.97) (Supplemental figure 7-1C). The ability of ADP to attenuate H_2O_2 emission during oxidative phosphorylation was impaired (main effect, *p*<0.0001) (Figure 7-2D). This impairment in ADP was not observed in the absence of creatine in the media (Supplemental figure 7-1D).

These findings demonstrate a specific impairment in the ability of creatine to improve ADP's control of bioenergetics as reported previously in dystrophin-deficient muscle (51, 53).

We next employed a calcium retention capacity assay to determine whether dystrophic muscle is more susceptible to mPTP formation (which is believed to involve VDAC) (128). However, no differences were observed between WT and D2.*mdx* EDL (p=0.13) (Figure 7-2E).

Reduced ANT1 protein content, but not α-tubulin-VDAC2 interactions, may contribute to mitochondrial ADP-impairments in D2.mdx mice

A proximity ligation assay was used to determine whether α-tubulin-VDAC2 interactions were different between D2.*mdx* and WT (115, 127, 136). However, similar protein-protein interactions were found in D2.*mdx* and WT mice (p=0.83) (Figure 7-3). No changes were observed in specific subunits of complexes I (p=0.54), II (p=0.12), III (p=0.70), IV (p=0.50) or V (p=0.48) nor their sum (p=0.45) (Figure 4A). VDAC2 (p=0.10) (Figure 7-4B) protein content was similar between WT and D2.*mdx* while the inner mitochondrial membrane transport protein adenine nucleotide translocase 1 (ANT1) was significantly reduced in D2.*mdx* compared to WT (-27%, p=0.03) (Figure 7-4C).

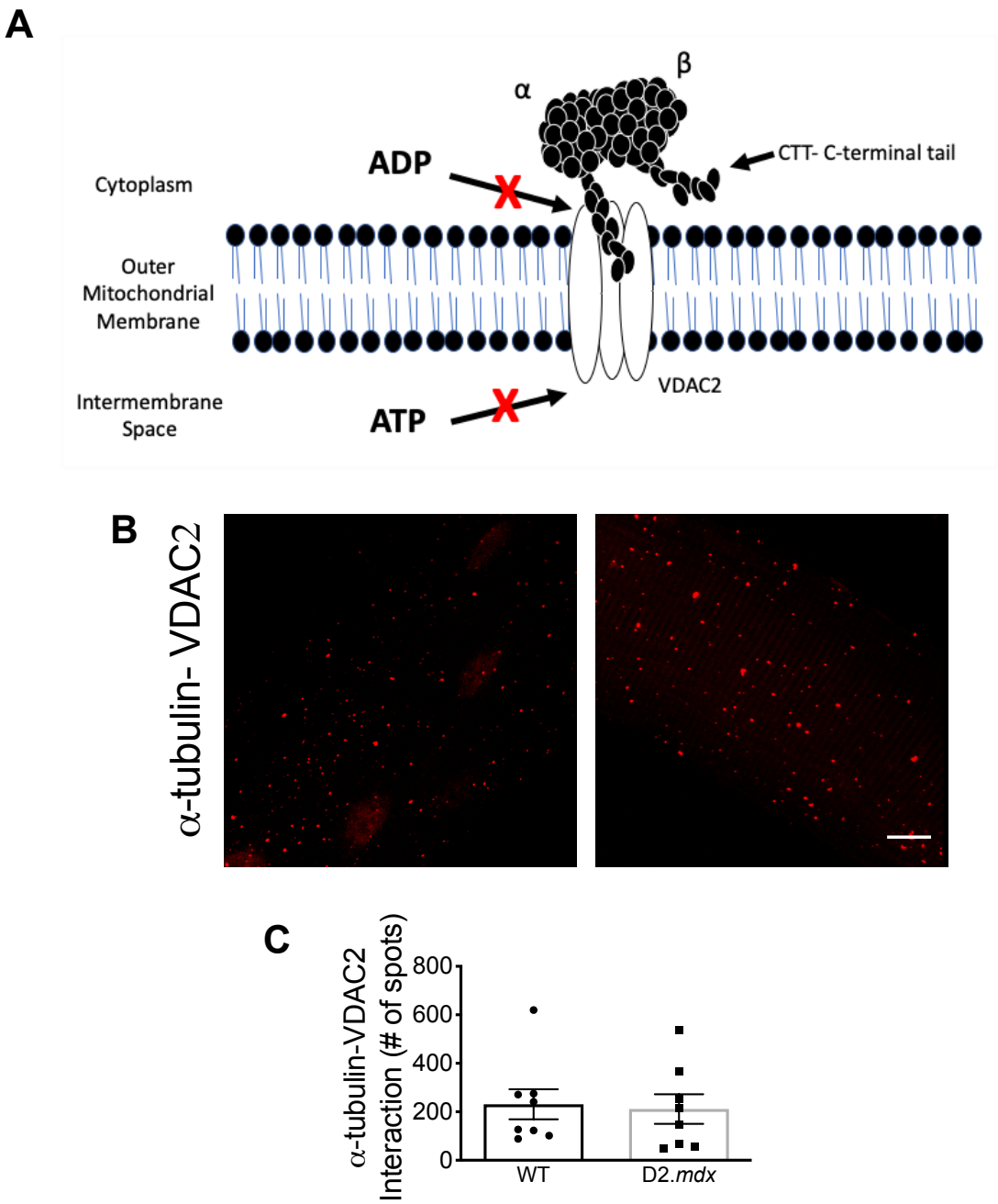

Figure 7-3. α-tubulin – VDAC2 interactions in single EDL fibres. Schematic representing the model of α-tubulin-VDAC2 interaction **(A)**. Confocal microscopy images **(B)** and graphical depiction of the proximity ligation assay of α-tubulin-VDAC2 (*n*=8) **(C)**. Scale bar, 10μm. Results are reported as mean ± SEM.

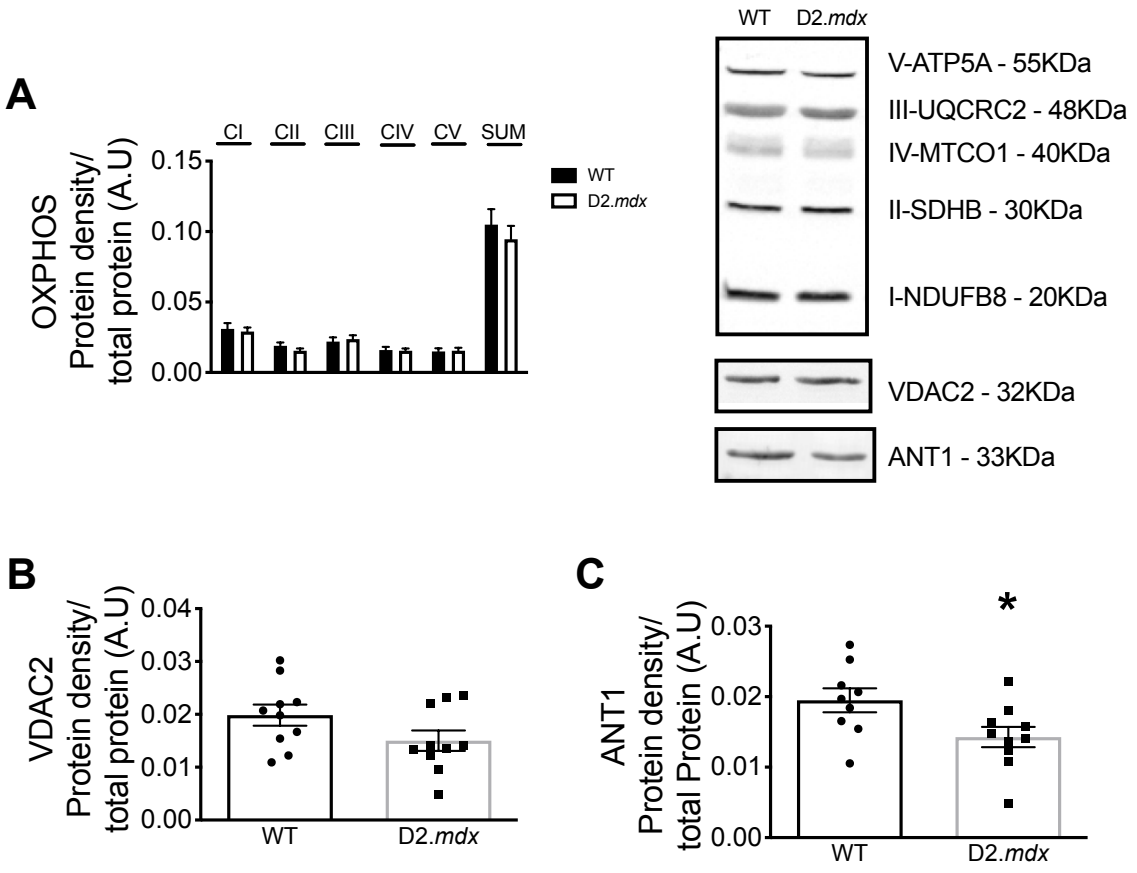

Figure 7-4. Protein content of mitochondrial proteins. Integrated densitometry for subunits of electron transport chain complexes I-V (OXPHOS; *n*=10-11), **(A)** VDAC2 (*n*=10) **(B)** and ANT1 (*n*=9-10) **(C)** with representative blots. Results are reported as mean ± SEM, (**p*<0.05).

Discussion

In D2.*mdx* mice, we demonstrate that microtubule disorganization in EDL muscle is associated with a reduced ability of ADP to stimulate mitochondrial oxidative phosphorylation and attenuate H_2O_2 emission. However, contrary to the hypothesis, there were no differences in the degree of α-tubulin-VDAC2 interactions assessed by proximity ligation assay. These findings demonstrate that microtubule disorganization and mitochondrial dysfunction occur concurrently in dystrophin-deficient muscle, but that the tubulin-VDAC model of bioenergetic

control may not represent a causal link between these two phenomena leaving the possibility that other mechanisms may exist.

Model of tubulin regulation of VDAC permeability

Impaired mitochondrial bioenergetics is thought to contribute to muscle weakness in Duchenne muscular dystrophy (39, 51, 53). However, the specific link between dystrophin deficiency and mitochondrial dysfunction has not been fully resolved. While Ca^{2+} stress has been proposed as a primary cause of swollen mitochondria and impaired oxidative phosphorylation in *mdx* mice (170), separate observations of altered microtubule networks (13, 66, 111) were also linked to disrupted cytosolic NADPH oxidase-induced ROS and Ca^{2+} signaling (66). An intriguing possibility of a mitochondrial link to microtubule disorganization emerges when considering the separate discoveries that tubulin components of microtubules can directly bind to VDAC on the outer mitochondrial membrane and decrease its permeability to ADP/ATP cycling (4, 42, 124, 126, 127). Considering that pharmacological alterations of microtubule networks changes tubulin-VDAC interactions and ADP-dependent bioenergetics (115), it seems plausible that the distinct observations of disorganized microtubules and mitochondrial dysfunctions in D2.*mdx* muscle may be due to altered microtubule-VDAC interactions. Such an observation would implicate microtubule disorganization in D2.*mdx* mice as a modulator of mitochondrial dysfunction in addition to the cytosolic stressors noted previously (66).

However, the present findings demonstrate no differences in the degree of α-tubulin-VDAC2 interactions despite the association between microtubule disorganization and mitochondrial dysfunction. Nevertheless, this observation does not rule out the possibility of other tubulin-VDAC interaction combinations. For example, while the CTT tail of α-tubulin has been shown to block the pore of VDAC, there is a greater affinity of the CTT tail on certain β

isotypes, particularly βIII and VDAC1 (126). In addition, it has been suggested that free βII tubulin binds VDAC in muscle – independent of heterodimeric tubulin – such that this free pool may be a distinct regulator of ADP/ATP cycling through VDAC (161). Lastly, the affinity of tubulin binding can be modulated through post translational modifications (145) such as phosphorylation (146) or altered mitochondrial membrane lipid composition (125) which highlights the complexity of the potential regulation of this pathway. The present findings warrant additional investigation into these alternative possibilities of how microtubule network dynamics may change the regulation of ADP-control of bioenergetics through VDAC.

This study does not rule out the possibility that VDAC1 or VDAC3 are differentially affected by disorganized microtubule networks in D2.*mdx* muscle. However, it has been suggested that only VDAC2 regulates the effect of creatine on respiration through phosphate shuttling (7), as assessed in the present study, possibly by being functionally linked to mitochondrial creatine kinase as well as tubulin in a super-complex (42). The lethality of VDAC2 knockout mice also suggests its importance in regulating mitochondrial bioenergetics (112). Nevertheless, the lack of change in α-tubulin-VDAC2 in the present investigation warrants further study of VDAC1 and 3 interactions with tubulin isotypes in *mdx* muscle given their influence on respiration, particularly in the absence of creatine(112).

Lastly, an additional relationship was found between reduced ANT1 content and impaired ADP-dependent mitochondrial bioenergetics. As ANT1 is found on the inner mitochondrial membrane, it is not thought to bind tubulin directly but may still be part of a larger complex with mitochondrial creatine kinase and VDAC (4). Reduced ANT1 may be a distinct contributor to impaired ADP-control of bioenergetics in EDL muscle similar to the reductions

previously reported in white gastrocnemius and quadriceps in D2.*mdx* mice at the same age of 4 weeks (51, 53).

In conclusion, the present investigation demonstrates that microtubule disorganization is associated with mitochondrial dysfunction within the same muscle of dystrophin-deficient mice, but this may not be mediated by altered α-tubulin-VDAC2 interactions. Additional research is warranted given the proposed model of tubulin-VDAC regulation of bioenergetics is complex and captures the role of phosphate exchange in the form of creatine-dependent phosphate shuttling through mitochondrial creatine kinase as well as creatine-independent ADP/ATP cycling, both of which may depend on the specific VDAC isoform interacting with specific tubulin isotypes. The association between microtubule organization and mitochondrial dysfunction reported herein serves as a foundation for extensive exploration between these various combinations to determine if microtubules truly 'link' dystrophin deficiency to mitochondrial bioenergetics.

Acknowledgements

None.

Author Contributions

All authors designed the study and collected data. S.V.R., M.C.H. and C.G.R.P. analyzed data and drafted manuscript. All authors approved the final version.

Funding Sources

This work was funded by the National Science and Engineering Research Council of Canada (NSERC #436138-2013) and an Early Researcher Award from the Ministry of Research, Innovation and Science. Infrastructure was supported by the Canada Foundation for Innovation,

the Ontario Research Fund and the James H. Cummings Foundation. S.V.R. and C.A.B. were supported by an Ontario Graduate Scholarship. M.C.H was supported by a NSERC Canadian Graduate Scholarships-PhD Scholarship.

Supplemental data – not included in publication

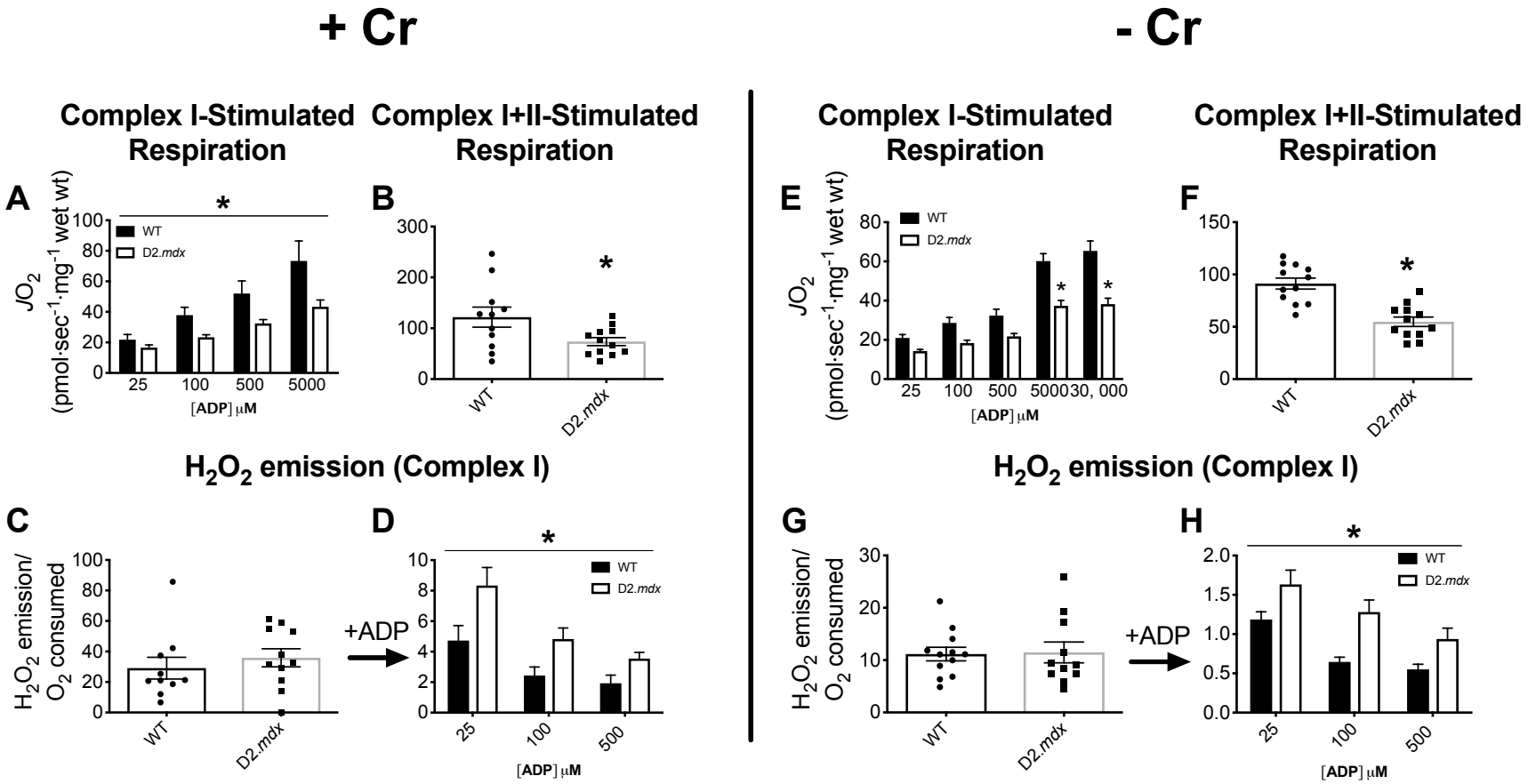

Supplemental Figure 7-2. Mitochondrial bioenergetics in WG PmFB. ADP-stimulated respiration supported by complex I (NADH from 5mM pyruvate/4mM malate) presence (A) and absence (E) of creatine (n=11-12) followed by complex II (FADH2 from 20mM succinate) in the presence (B) and absence (F) of creatine (n=11-12). H2O2 emission was stimulated at complex I (NADH from 10mM pyruvate/4mM malate) in the presence (C) and absence (G) of creatine (n=10-12) followed by an ADP titration (n=11-12). Results are reported as mean ± SEM, (*p<0.05).

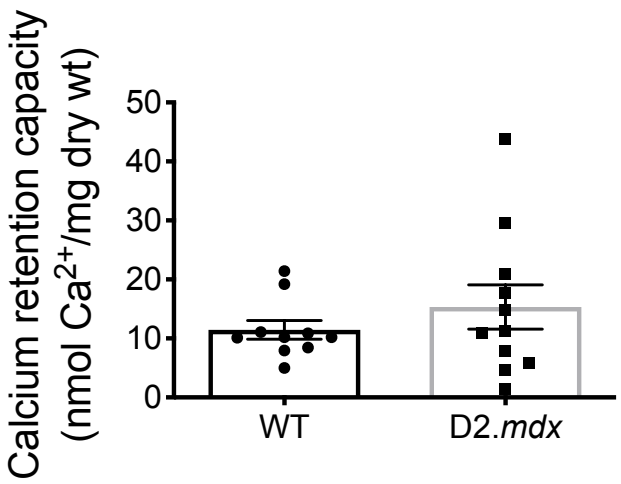

Supplemental Figure 7-3. Calcium retention capacity. (n=10-12) Results are reported as mean ± SEM.

Chapter 8

8.1 General Discussion

Emerging research posits that microtubules can regulate mitochondrial bioenergetics. This model is intriguing given it implicates the cytoskeleton as a direct regulator of energy homeostasis, oxidative stress and apoptotic pathways – all of which are linked to mitochondria. The application of this model is potentially wide spread given many disorders demonstrate considerable microtubule dynamics and a range of mitochondrial dysfunctions. Given the importance of mitochondria in supporting the wide range of energy demands and redox-dependent processes, this model may represent a new paradigm by which muscle function can be influenced through cytoskeletal-mitochondrial dynamics. The purpose of this thesis was to determine the degree to which manipulating microtubule networks alter mitochondrial function through the proposed tubulin-VDAC model of bioenergetic regulation.

Overall, the observations of this thesis suggest that the tubulin-VDAC model does not consistently predict the effect of altering microtubule organization on mitochondrial bioenergetics. Specifically, microtubule targeted chemotherapy significantly perturbs cellular microtubule organization causing a host of side effects including, mitochondrial dysfunction and muscle weakness (65, 74, 130, 169). Similarly, the lack of dystrophin in skeletal muscles from the mouse model of Duchenne muscular dystrophy results with a myriad of cellular impairments such as, mitochondrial dysfunction and sever muscle weakness (39, 51, 52, 60). These models allowed the examination of the tubulin-VDAC interaction through exogenous (the administration of paclitaxel and vinblastine) and endogenous/genetic (D2.*mdx* mouse) microtubule manipulations; uncovering the contribution of the tubulin-VDAC interaction to muscle mitochondria bioenergetics and skeletal muscle function. A summary of ADP-dependent

mitochondrial bioenergetics in the presence (Table 8-1) and absence (Table 8-2) of creatine can be found below.

Partially in line with our hypothesis, the chemotherapy model of microtubule stabilization with paclitaxel increased α- and βII-tubulin interaction with VDAC2 in isolated EDL single fibers, limiting the ability of ADP to attenuate H_2O_2 emission in an *in-vitro* model without limiting ADP-dependent respiration. *In-vitro* microtubule destabilization with vinblastine in the EDL does not support the tubulin-VDAC model. The amount of tubulin interacting with VDAC was unchanged, yet still increased respiration and impaired the ability of ADP to attenuate H_2O_2 emission. In cardiac tissues, *in-vitro* incubations with paclitaxel and vinblastine significantly reduced ADP-stimulated respiration and attenuation of H_2O_2 emission in the absence of a change in tubulin-VDAC interaction. These results were mirrored in the absence of creatine but not in the presence of creatine when analyzed *in-vivo*. 2-days of paclitaxel injections increased α- and βII-tubulin interaction with VDAC2 in soleus muscle without altering ADP-dependent bioenergetics. Vinblastine impaired the ability of ADP to attenuate H_2O_2 emission in both creatine dependent and independent conditions following 2-days of *in-vivo* injections. WG PmFB also yielded controversial results where respiration was only impaired following paclitaxel in the absence of creatine. Lastly, the Duchene muscular dystrophy model of known microtubule disorganization and severe mitochondrial dysfunction yielded no change in α-tubulin in the presence of impaired mitochondrial bioenergetics. Overall, these results do not fully fit the speculated model of tubulin regulation of VDAC permeability. Below, this thesis attempts to consolidate these findings with the current literature to broaden the understanding of the tubulin-VDAC model.

Table 8-1. Summary of changes to ADP-dependent mitochondrial bioenergetics in the <u>presence of creatine</u> under various conditions of microtubule organization.

Chapter	Approach	Tissue	Tubulin-VDAC interactions		ADP-dependent mitochondrial dysfunction: Respiration		ADP-dependent mitochondrial dysfunction: H_2O_2 + ADP		Relationship between tubulin-VDAC and mitochondrial function
			α-tubulin-VDAC2	βII-tubulin-VDAC2	Pac	Vin	Pac	Vin	
4	*In-vitro* glycolytic	EDL	⇑	⇑	⇔	⇑	⇓	⇓	✓ paclitaxel X vinblastine
5	*In-vitro* and *in-vivo* oxidative	Heart (*in-vitro*)	⇔	⇔	⇓	⇓	⇓	⇓	X Paclitaxel X vinblastine
		Heart (*in-vivo*)	N/A^	N/A^	⇔	⇔	⇔	⇔	N/A
		Soleus (*in-vitro*)	N/A^	N/A^	⇔	⇓	⇔	⇔	N/A^
6	*In-vivo* glycolytic vs. oxidative	Soleus	⇔	⇑	⇔	⇔	⇔	⇓	X paclitaxel X vinblastine
		WG	N/A^	N/A^	⇔	⇔	⇔	⇔	N/A^
7	*In-vivo* glycolytic (D2.*mdx*)	EDL	⇔	⇔	⇓		⇓		No relationship

^Proximity Ligation assay could not be performed in this tissue due to technical limitations as outlined in the respective chapters.
*Note: Refer to Chapter 3 – Methodological considerations to delineate between tissue distribution throughout studies

Table 8-2. Summary of changes to ADP-dependent mitochondrial bioenergetics in the absence of creatine under various conditions of microtubule organization.

Chapter	Approach	Tissue	Tubulin-VDAC interactions		ADP-dependent mitochondrial dysfunction: Respiration		ADP-dependent mitochondrial dysfunction: H_2O_2 + ADP		Relationship between tubulin-VDAC and mitochondrial function
			α-tubulin-VDAC2	βII-tubulin-VDAC2	Pac	Vin	Pac	Vin	
4	*In-vitro* glycolytic	EDL	N/A^	N/A^	N/A^	N/A^	N/A^	N/A^	✓ paclitaxel X vinblastine
5	*In-vitro* and *in-vivo* oxidative	Heart (*in-vitro*)	⇔	⇔	N/A^	N/A^	N/A^	N/A^	X Paclitaxel X vinblastine
		Heart (*in-vivo*)	N/A^	N/A^	⇓	⇔	⇓	⇓	N/A^
		Soleus (*in-vitro*)	N/A^	N/A	N/A^	N/A^	N/A^	N/A^	N/A^
6	*In-vivo* glycolytic vs. oxidative	Soleus	⇔	⇔	⇑	⇑	⇔	⇓	X paclitaxel X vinblastine
		WG	N/A^	N/A^	⇓	⇔	⇔	⇔	N/A^
7	*In-vivo* glycolytic (D2.*mdx*)	EDL	⇔	⇔	⇓		⇔		No relationship

^Proximity Ligation assay could not be performed in this tissue due to technical limitations as outlined in the respective chapters.
Note: Refer to Chapter 3 – Methodological considerations to delineate between tissue distribution throughout studies

8.2 Conclusions on tubulin regulation of VDAC permeability through microtubule manipulation

The work presented in this thesis is the first to determine the interaction between both α- and βII-tubulin and VDAC2 in cardiac and skeletal muscles. The current literature analyzing this interaction has been limited through methodology, where either the addition or removal of tubulin from cardiomyocytes and isolated mitochondria respectively, were the means of manipulating this potential interaction. This thesis challenges the current model of tubulin-VDAC interactions through *in-vitro* and *in-vivo* microtubule manipulation with microtubule stabilizing and destabilizing compounds, in an attempt to determine the resulting effect on ADP-dependent mitochondrial bioenergetics. While we are able to draw some conclusions from the presented work, no definitive conclusions can be made. This thesis encompassed *in-vivo* and *in-vitro* work (mimicking creatine dependent and independent conditions) in an attempt to mirror physiological conditions, yielding some contradictive results. As such, to speak to the current model of tubulin-VDAC interactions, this discussion will primarily focus on ADP-stimulated bioenergetics.

In both glycolytic EDL and oxidative soleus muscles, *in-vitro* and *in-vivo* microtubule stabilization with paclitaxel resulted with an increased tubulin-VDAC2 interaction. In glycolytic tissues, this increased interaction limits the ability of ADP to attenuate H_2O_2 emission while also reducing ADP-stimulated respiration in a creatine independent manner. In addition, the increased tubulin-VDAC2 interaction uncovered an increased H_2O_2 emission potential in the absence of creatine, surprisingly, not effecting any ADP-dependent bioenergetic pathways in the soleus muscle. These results are in partial support of the hypotheses made in chapter 3, whereby an increased interaction limits the ability of ADP to enter the mitochondria to either stimulate respiration or attenuate H_2O_2 emission. While these findings are intriguing, it raises the question

of the importance of experimental model selection and the differences in tissue types. Thus far, we can conclude that promoting microtubule stabilization through increased polymerization increases the amount of interactions between tubulin and VDAC2. This increased interaction may be altering ADP-dependent mitochondrial bioenergetics in EDL and soleus muscles but does not fully support the current model of tubulin regulation of VDAC permeability.

Tubulin exists in a state of dynamic stability where free tubulin should be readily available from newly depolymerized microtubules for polymerizing microtubules. To our knowledge, the architectural organization of the various tubulin isoforms has not been confirmed. α-tubulin is known to form an orthogonal network pattern often represented as what microtubules should look like in the literature, but the various tubulin isoforms are not represented, limiting the conclusions that can be drawn from microtubule manipulations. Confocal microscopy images of immunohistochemically stained βII-tubulin presented in chapter 4 show no apparent change in organization following stabilization and destabilization but resulted with an increased α- and βII-tubulin-VDAC2 interaction. Perhaps there is a conformational or structural change to the tubulin molecule in response to paclitaxel or vinblastine treatment that may be mediating the change in interaction observed. This work highlights the need to further understand the function of microtubules and tubulin in skeletal muscles.

8.3 Modeling *in-vivo* conditions with the absence and presence of creatine

The fundamental model of ADP/ATP flux through the mitochondria has been accepted to be through the efficient creatine dependent, and inefficient creatine independent pathways outlined in chapter 2 (Figure 2-3), where the transport of ADP/ATP and PCr/Cr is accepted to occur through VDAC. In chapter 5 and 6, the majority of ADP-dependent bioenergetic

impairments in response to paclitaxel and vinblastine occurred in the absence of creatine. This was particularly perplexing as this system is speculated to only contribute to 20% of energy exchange (4, 86, 165, 166). Perhaps, in an attempt to preserve efficient ADP/ATP transfer, muscle fibers allow the inefficient pathway to become compromised in the event of cytotoxicity preserving the pathway that the fiber is more reliant on. This may contribute to the measured impairments through the creatine independent pathway. The permeability of VDAC has been historically measured through reconstructed planar lipid membranes embedded with VDAC, where changes in membrane potential can mediate cation/anion selectivity (99, 123). This thesis has focused only on the physical interaction between tubulin and VDAC2 measured through the proximity ligation assay but does not discount the possibility that a change in the electrochemical gradient may have occurred as a result of microtubule stabilization and destabilization limiting the ability of ADP to diffuse through VDAC. An attempt was made to determine mitochondrial membrane potential in PmFB but our laboratory determined that the assay was not reliable when assessing membrane potential with the common tetraphenylophosphonium (TPP^+) probe. This method is currently optimized for isolated mitochondria and therefore pose a limitation as our aims are to maintain the intracellular integrity of the cell. Future studies could consider imaging live cells with intact microtubule architecture using fluorescent membrane potential probes to contribute to the elucidation of the current results.

8.4 Cumulative understanding of the tubulin-VDAC interaction and regulation of ADP permeability.

The current understanding of the tubulin-VDAC interaction has been developed by embedding VDAC to planar lipid membranes followed by the addition of tubulin (127, 145, 146). While this method has proven to be very useful in uncovering the physiological functions of VDAC and tubulin, *in-vivo* conditions differ significantly. Specifically, cardiac and skeletal

muscle contains the entire cytoskeletal network including microtubules, intermediate filaments, thick and thin filaments, costamers, intercalated discs (cardiac tissue), in addition to the abundance of proteins and organelles which may play a role in the overall metabolism of the cell. These features are not captured in the reconstructed planar membrane models. In addition, microtubules exist in a state of dynamic stability, where tubulin is constantly polymerizing and depolymerizing. It is important to consider the environment cells are in, in order to make accurate interpretations of what *in-vivo* conditions may be like.

Another limitation of the reconstructed planar membrane model is that tubulin is studied in the absence of MAP and EB binding proteins which may not truly capture how tubulin-VDAC interaction may be occurring under physiological conditions. This thesis aimed to capture the tubulin-VDAC interaction in its "natural environment" through paraformaldehyde fixation, securing all intracellular proteins and organelles in place, capturing the interaction under different physiological conditions (microtubule stabilization and destabilization). In addition, the use of PmFBs also maintains the integrity of the intracellular organelles which, in theory, should maintain the tubulin-VDAC interaction following microtubule stabilization and destabilization. This allows the accurate measurement of mitochondrial bioenergetics with the majority of the cell intact. Unfortunately, this method permeabilizes the cell membrane, where the cytosol is washed out. The cytosol may contain the free-tubulin pool, GTP/GDP, MAP and the EB family of proteins that would subsequently be washed out with the cytosol, placing a limitation to our interpretations. Concomitantly, this may be beneficial as during the incubation phase with paclitaxel and vinblastine, as all proteins required to maintain dynamic stability are present. The subsequent wash steps would then "freeze" the intracellular conditions so that when measured, microtubules would maintain a stabilized or destabilized condition during bioenergetic assays.

Another method of assessing the tubulin-VDAC interaction has been through the addition of tubulin to isolated mitochondria or through the removal of tubulin from cardiomyocytes to determine changes in ADP-stimulated respiration (40, 127, 135). While these two methods show a clear relationship between ADP-stimulated respiration and the presence of tubulin, some limitations exist. Homogenates undergo a series of differential centrifugation steps, breaking the microtubule network, reforming mitochondria into micelles that do not fully mimic *in-vivo* mitochondrial ultrastructure. In cardiomyocytes, the removal of βII-tubulin with trypsin does not discount the possibility of other tubulin isoforms from being removed in the process. The dynamic stability of microtubules and intricate organization of mitochondria poses methodological difficulties in the measurement of the tubulin-VDAC interaction. Research thus far has completed great strides in furthering the understanding of this novel interaction and its contribution to mitochondrial bioenergetics but further work is still required to fully deduce the mechanism.

8.5 The effect of cytotoxic drugs on mitochondrial bioenergetics

This thesis demonstrates that paclitaxel increases both α- and βII-tubulin interaction with VDAC2 which correlates with impaired H_2O_2 kinetics when measured *in-vitro* in PmFB from EDL muscles. An increased α- and βII-tubulin interaction was also measured in rats injected with paclitaxel, soleus PmFB resulting with an increased voluntary running and hind-limb torque frequency coupled with increased calcium retention capacity and activation of caspase 3. Portions of these *in-vitro* and *in-vivo* studies partially support the hypothesis stating that increased microtubule stabilization would increase the tubulin-VDAC interaction but the effect on ADP-stimulated bioenergetics appears to be selective in EDL and not applicable in soleus muscles. Instead, in soleus PmFBs, calcium retention capacity is increased and surprisingly,

caspase 3 activity is also increased suggesting the induction of apoptosis. As mentioned above, paclitaxel has been shown to induce apoptosis through alternative mechanisms. Calcium retention capacity was increased which, in theory would suggest an inhibition on apoptosis but the increased caspase activation suggests otherwise. Perhaps paclitaxel is disrupting normal mitochondrial activity by preventing calcium induced mPTP formation while still initiating apoptosis through caspase 3 activation. Due to tissue limitations, we were not able to measure caspase 9 activity which may have shed light on whether caspase 3 was initiated through the release of cytochrome c oxidase. These divergent data indicate that paclitaxel may be inducing apoptosis through an alternative mechanism in oxidative skeletal muscles when compared to glycolytic tissues.

Results from the glycolytic EDL and WG muscles appear follow somewhat of a similar response to paclitaxel treatment. This is exemplified in the ADP-dependent data collected. The ability of ADP to attenuate H2O2 emission in the EDL muscle was impaired while in the absence of creatine, there was significantly lower respiration when compared to control in the WG muscle. Due to time and cost of running the PLA assay, this measure was not completed in WG embedded tissues which limits the conclusions drawn regarding the tubulin-VDAC model. Both glycolytic EDL and WG PmFBs treated with paclitaxel did not elicit a response to calcium retention capacity or caspase activation. These data support the idea that the tubulin-VDAC model may illicit different responses in different skeletal muscle types.

In-vitro and *in-vivo* treatment with the microtubule destabilizer vinblastine did not elicit a change in both α- and βII-tubulin interaction with VDAC2. Interestingly, in the absence of a change in tubulin-VDAC interaction vinblastine treatment caused some mitochondrial bioenergetic changes. In the soleus muscles vinblastine produced divergent results when

comparing *in-vitro* and *in-vivo* approaches. ADP stimulated respiration was significantly decreased *in-vitro* while *in-vivo* this was statistically significantly increased. Similarly, H_2O_2 kinetics were similar to control under *in-vitro* conditions but in-vivo, H_2O_2 kinetics were significantly impaired in the presence and absence of creatine. This trend was mirrored in the CRC data where *in-vitro* resulted with trends for decreased CRC while *in-vivo* yielded increased CRC. This divergent data provides further evidence that the tubulin-VDAC model may not be as clear cut as once speculated. Further work in an oxidative tissue is required to understand the role of the tubulin-VDAC model in bioenergetic regulation.

In EDL PmFBs, vinblastine increased respiration while also impairing H_2O_2 kinetics and decreased calcium retention capacity. This was not mirrored under *in-vivo* conditions in the glycolytic WG muscle where vinblastine had no effect on ADP-stimulated respiration and H_2O_2 kinetics but appeared to limit the activation of apoptosis through increased CRC and decreased caspase activation. Here, we can speculate that vinblastine is preventing the induction of apoptosis as the mitochondrial may be attempting to "remove" its dysfunctional intracellular components to maintain overall functional mitochondria. Altogether, these data demonstrate that although microtubule destabilization with vinblastine did not alter the α- and βII-tubulin interaction, it may have 1) altered another tubulin-VDAC isoform interaction not measured in the current thesis, 2) caused a post-translational modification to either α- or βII-tubulin not measured or 3) altered mitochondrial membrane potential changing the ion selectivity independent of any tubulin involvement.

Chapter 5 explores both *in-vivo* and *in-vitro* effects of microtubule stabilization and destabilization in cardiac tissue yielding a host of ADP-dependent bioenergetic impairments independent of any change in both α- and βII-tubulin interaction. Here, both paclitaxel and

vinblastine significantly reduced ADP-stimulated respiration, reduced H_2O_2 emission potential while also reducing the ability of ADP to attenuate H_2O_2 emission. Mitochondrial bioenergetic impairments were not related with increased susceptibility to apoptosis induction as there was no change in calcium retention capacity or caspase activation in both *in-vitro* and *in-vivo* models. Similarly to soleus PmFBs, these results suggest that there may be other isoform combinations of tubulin and VDAC that may be limiting ADP diffusion. Paclitaxel and vinblastine are known to have a dose dependent effect where lower doses have shown to have beneficial effects to injured cardiac tissues while higher doses can activate various apoptotic pathways (28, 117, 168, 175). The *in-vitro* concentrations used in this thesis were in line with concentrations previously published (74, 101). To our knowledge, this thesis is one of the first to explore changes ADP-dependent mitochondrial bioenergetics following microtubule manipulation with cytotoxic compounds where this data may be capturing the initial impairments to mitochondria that may subsequently lead to mitochondrial dysfunction and cell death. This thesis has uncovered several questions which now provide the stepping stones towards designing new experimental models to elucidate the *in-vitro* and *in-vivo* contribution of the tubulin VDAC model to whole muscle and mitochondrial bioenergetic regulation.

8.6 Utilization of the proximity ligation assay to measure tubulin-VDAC interactions

Saetersdal and colleagues (1990) were the first to measure β-tubulin in close proximity to isolated cardiomyocyte mitochondria using immunogold labelling (131). Since discovering that tubulin may in fact bind to VDAC on the OMM, different laboratories have done extensive research trying to understand the purpose of this interaction, but limited work has been done to measure the physical interaction between tubulin and VDAC. Carre and colleagues (2002) were successful at using immunoprecipitation methodology to isolate VDAC and probe for both α-

and βII-tubulin in a variety of cancer cell culture (20). No other lab, including our own (unpublished previous experiments), has been able to successfully co-immuoprecipitate tubulin or VDAC in muscle tissues suggesting the need of an alternative protein interaction determination method. In 2018, Rostovtseva and colleagues were the first to publish the use of the proximity ligation assay to measure the interaction between βIII-tubulin-VDAC1 in human neuroblastoma cells. In addition, data presented in this thesis also measured α- and βII-tubulin interaction with VDAC2 in cardiac and skeletal muscles using the proximity ligation assay (126). More and more labs have been utilizing the proximity ligation assay as a tool to measure protein-protein interactions providing support for use as an adequate tool for this type of measurement.

The proximity ligation assay is a method similar to immunohistochemistry where the assay is predominately reliant on the molecular distance between the tubulin and VDAC antibodies. Oligonucleotide probes recognize the primary antibody, which when incubated with a ligase and followed by a polymerase, read and amplify a signal that can then be detected at a particular wavelength (Figure 8-1). The strengths of the proximity ligation assay are its ability to detect protein-protein interactions with a 40μm resolution, providing greater accuracy when compared to co-localization which only determines whether proteins are in the same relative area. In addition, the proximity ligation assay is relatively simple to use (once optimized), providing clear detection of protein interactions (82). In the current work, negative control experiments were used to ensure the specificity of the assay (Supplemental Figure 9-1). While the proximity ligation assay has proven to be a useful tool in detecting protein-protein interactions, it does have some limitations.

Optimization of the proximity ligation assay is highly dependent on the strength and accuracy of the primary antibody used. It is also crucial to perform sufficient washing between

steps as incubation of primary antibodies and oligonucleotide probes can provide a false positive response if the access antibodies are not properly washed away. In addition, over amplification with the polymerase incubation may result in a saturated signal limiting quantitative interpretations (82). Other methods of assessing protein–protein interactions include fluorescence resonance energy transfer (FRET), co-immunohistochemistry/precipitation and fluorescence complementation. While these methods are well established and more commonly used, they require the use of live cells, organelle specific fluorophores, specific equipment, and/or combination of fluorescent tags not compatible for tubulin or VDAC2 detection in our laboratory. The proximity ligation assay allowed the determination of a protein-protein interaction in isolated cardiomyocytes, EDL single fibers and embedded soleus muscles, without perturbing the intracellular environment.

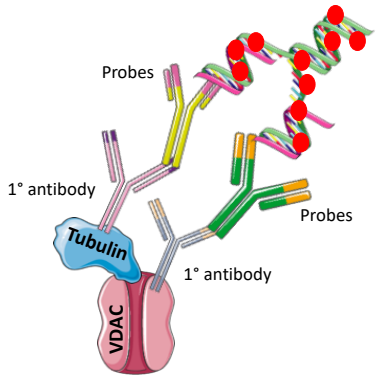

Figure 8-1. Representative schematic of the proximity ligation assay.

8.7 Limitations

In chapter 6 we explored an *in-vivo* model, injecting paclitaxel and vinblastine into 8-week old Wistar rats for 2 days to observe changes in tubulin-VDAC interactions and mitochondrial bioenergetics to then relate to muscle weakness. Adhering to the guidelines of the animal care facility at York University, we adapted our treatment schedule based on previous rodent literature where 2mg/ml/body weight was commonly used over 5-10 days (14, 55, 71). The initial intention for this study was to administer 2mg/ml/body weight of both paclitaxel and vinblastine for a duration of 5 days. Unfortunately, pilot studies revealed a severe negative phenotype following both paclitaxel and vinblastine injections where food consumption and voluntary movement significantly decreased following treatment. In addition, the rat's fur was constantly raised indicating pain and discomfort with the development of brown discharge around the mouth and nasal area. With the advice from the animal care committee and the campus veterinarian, the drug dose for both paclitaxel and vinblastine was reduced to 1mg/ml/body weight with a 2-day duration. While this was sufficient to still elicit mild

phenotypic change in behavior and physiological change in experiments, it is not completely in line with previously published rodent literature.

Another limitation faced in chapter 6 was the inability to complete the proximity ligation assay in both soleus and WG muscles. With the tubulin-VDAC interaction measured in both tissues, a direct comparison between protein interaction and bioenergetics for both tissues could have been made. As mentioned in chapter 2, microtubule density and organization differ in oxidative and glycolytic tissues and it has not been determined whether the tubulin-VDAC interaction would differ between the two fiber types. Inferring from the proximity ligation assay data collected in chapter 4 and 6, we can assume that the α- and βII-tubulin-VDAC interaction would yield a similar response (increased interactions) to paclitaxel in the WG muscle as well. The initial intention was to utilize embedded tissue as the single fiber isolation protocol used in chapter 4 requires the isolation of muscles from tendon to tendon rendering the soleus and WG unusable for these purposes. The last limitation in this chapter was the inability to determine whether microtubule organization was altered in response to *in-vivo* paclitaxel and vinblastine injections. Instead, we were reliant on previous literature, observations from chapter 4, and the rats' phenotypic response to injections to determine the effectiveness of our drug injections.

In chapter 7 we aimed to determine whether the tubulin-VDAC interaction contributed to the mitochondrial dysfunction seen in the mouse model of Duchenne muscular dystrophy. It is well known that microtubule organization is severely disrupted in mdx mice as dystrophin directly binds microtubules anchoring them to the sarcolemma providing stability throughout the cell (13, 66, 111). These studies explored α-tubulin as the only marker for microtubule organization which may be limiting as there are various tubulin isoforms that may be altered as a result of a lack of dystrophin. Previous literature has identified the disruption of α-tubulin in the

mdx model of Duchenne muscular dystrophy and therefore was the only tubulin isoform explored in this thesis. Secondly, microtubule density and organization differs in glycolytic and oxidative tissues, posing a limitation of not measuring both tissue types in the mouse model of Duchenne muscular dystrophy. Although the work presented in chapter 7 did not show a change in tubulin-VDAC interaction when comparing the mouse model of Duchenne dystrophy to wildtype control, a mitochondrial bioenergetic impairment were still present. Lastly, the contribution of other tubulin and VDAC isoforms were not explored which may be contributing to the ADP-dependent mitochondrial bioenergetic impairments seen.

8.8 Future directions

Tubulin regulation of VDAC permeability poses an exciting systematic mechanism whereby acute changes to the physiologic environment may cause a dynamic change in the tubulin-VDAC interaction to allow or inhibit the diffusion of energy through the mitochondria. Although a substantial amount of work has been done to understand this interaction, there is still much to clarify. Specifically, in cardiac and skeletal muscle, where little is known about the activity of microtubules and tubulin, further work should be done to explore the quantity of the different tubulin isoforms and isotypes. Uncovering each tubulin isoform contribution to overall microtubule architecture may assist in determining what roles they may play in the maintenance of muscle metabolism (126). This is of particular importance as previous literature revealed microtubule targeted compounds do not change mitochondrial membrane potential and that it is in fact the presence of microtubule that cause changes to mitochondrial function (74).

In addition to isoform/and isotype exploration, microtubules are known to undergo post-translational modifications where detyrosination has been shown to enhance the tubulin-VDAC interaction. Uncovering any further post-translational modifications that may occur to

microtubules may contribute to elucidating tubulin regulation of VDAC permeability. Similarly to tubulin, it is important to explore the contribution of VDAC1 and 3 to the tubulin-VDAC model. It may be that under certain cellular conditions, specific tubulin-VDAC interactions respond more than others. The complete elucidation of the potential combinations of tubulin isoform interactions with VDAC isoforms is required to advance the understanding of this interaction.

Chapter 6 investigated the contribution of muscle contraction following *in-vivo* paclitaxel and vinblastine injection to mitochondrial bioenergetics. Exercise is a potent stimulator of mitochondrial biogenesis and has been shown to improve mitochondrial and whole muscle function. An interesting route to further elucidate the contribution of the tubulin-VDAC interaction to ADP-dependent bioenergetics would be to explore the effect of an acute and chronic muscle contraction (endurance training) to determine whether this elicits a change in the tubulin-VDAC interaction. If completed in a healthy, untreated animal model, an increased or decreased interaction, coupled with improved muscle force, and mitochondrial bioenergetic may indicate that increased or decreased tubulin-VDAC interaction supports improved mitochondrial bioenergetics. This work would address some limitations presented in this thesis.

As mention above, results from chapter 6 in regard to ADP-dependent mitochondria bioenergetics in the presence and absence of creatine has raised many questions concerning the efficient and inefficient "phosphate shuttling" system. One such question is whether there is an electro-chemical change, in addition to a physical (tubulin-VDAC interaction) change, perturbing the diffusion of ADP/ATP? To address this question, similarly to chapters 4 and 5, PmFB incubated with mitochondrial uncouplers such as oligomycin and carbonyl cyanide-p-trifluoromethoxphenylhydrazone (FCCP) to perturb mitochondrial membrane potential in an in-

tact fiber (preserving microtubule architecture) prior to measurements of protein-protein interactions and ADP-dependent bioenergetics may reveal further insight into the tubulin-VDAC interaction.

8.9 Conclusions

This thesis highlights the complexity of what was initially believed to be a simple model of ADP/ATP regulation through VDAC. *In-vitro*, the model is partially met in EDL muscles with increased tubulin-VDAC interactions following only paclitaxel incubations relating to impaired H_2O_2 kinetics. Alternatively, the remaining findings in cardiac, EDL and soleus muscles (chapters 4 - 7) do not fit the model following both paclitaxel and vinblastine incubations. Perhaps it is the contribution of other tubulin and VDAC isoforms in these tissues that may be eliciting the mitochondrial bioenergetic impairments observed. Similarly, *in-vivo*, the tubulin-VDAC model did not explain the changes to mitochondrial function in the absence and presence of creatine but instead has now challenged the fundamental phosphate shuttling model. Future work should explore the effect of a higher dose and longer administration of microtubule targeted chemotherapies, attempting to mimic what is standard dosing in humans. Lastly, the disorganized microtubule architecture found in the mouse model of Duchenne muscular dystrophy does not contribute to an altered tubulin-VDAC interaction when compared to wildtype. Again, this suggests that other tubulin or VDAC isoforms should be explored. In addition, determining whether free or polymerized tubulin contributes to the mitochondrial bioenergetic impairments observed requires further exploration. Overall, this thesis has uncovered many potential avenues to explore to further elucidate the mechanism of tubulin regulation of VDAC permeability.

References

1. Biological Systems Relevant for Redox Signaling and Control. In: *Redox Signaling and Regulation in Biology and Medicine*.
2. **Aist JR, and Williams PH**. ULTRASTRUCTURE AND TIME COURSE OF MITOSIS IN THE FUNGUS FUSARIUM OXYSPORUM. *The Journal of Cell Biology* 55: 368-389, 1972.
3. **Albuquerque EX, Warnick JE, Tasse JR, and Sansone FM**. Effects of vinblastine and colchicine on neural regulation of the fast and slow skeletal muscles of the rat. *Experimental Neurology* 37: 607-634, 1972.
4. **Aliev MK, and Saks VA**. Compartmentalized energy transfer in cardiomyocytes: use of mathematical modeling for analysis of in vivo regulation of respiration. *Biophysical Journal* 73: 428-445, 1997.
5. **Allen DG, Whitehead NP, and Froehner SC**. Absence of Dystrophin Disrupts Skeletal Muscle Signaling: Roles of Ca2+, Reactive Oxygen Species, and Nitric Oxide in the Development of Muscular Dystrophy. *Physiological Reviews* 96: 253-305, 2016.
6. **Anderson EJ, Lustig ME, Boyle KE, Woodlief TL, Kane DA, Lin CT, Price JW, 3rd, Kang L, Rabinovitch PS, Szeto HH, Houmard JA, Cortright RN, Wasserman DH, and Neufer PD**. Mitochondrial H2O2 emission and cellular redox state link excess fat intake to insulin resistance in both rodents and humans. *J Clin Invest* 119: 573-581, 2009.
7. **Anflous-Pharayra K, Lee N, Armstrong DL, and Craigen WJ**. VDAC3 has differing mitochondrial functions in two types of striated muscles. *Biochimica et Biophysica Acta (BBA) - Bioenergetics* 1807: 150-156, 2011.
8. **Anmann T, Guzun R, Beraud N, Pelloux S, Kuznetsov AV, Kogerman L, Kaambre T, Sikk P, Paju K, Peet N, Seppet E, Ojeda C, Tourneur Y, and Saks V**. Different kinetics of the regulation of respiration in permeabilized cardiomyocytes and in HL-1 cardiac cells. Importance of cell structure/organization for respiration regulation. *Biochim Biophys Acta* 1757: 1597-1606, 2006.
9. **Baines CP**. The molecular composition of the mitochondrial permeability transition pore. *Journal of Molecular and Cellular Cardiology* 46: 850-857, 2009.
10. **Baines CP, Kaiser RA, Purcell NH, Blair NS, Osinska H, Hambleton MA, Brunskill EW, Sayen MR, Gottlieb RA, Dorn GW, Robbins J, and Molkentin JD**. Loss of cyclophilin D reveals a critical role for mitochondrial permeability transition in cell death. *Nature* 434: 658-662, 2005.
11. **Baines CP, Kaiser RA, Sheiko T, Craigen WJ, and Molkentin JD**. Voltage-dependent anion channels are dispensable for mitochondrial-dependent cell death. *Nature Cell Biology* 9: 550, 2007.
12. **Bates D, and Eastman A**. Microtubule destabilising agents: far more than just antimitotic anticancer drugs. *Br J Clin Pharmacol* 83: 255-268, 2017.
13. **Belanto JJ, Mader TL, Eckhoff MD, Strandjord DM, Banks GB, Gardner MK, Lowe DA, and Ervasti JM**. Microtubule binding distinguishes dystrophin from utrophin. *Proceedings of the National Academy of Sciences* 111: 5723-5728, 2014.
14. **Bennett GJ, Liu GK, Xiao WH, Jin HW, and Siau C**. Terminal arbor degeneration – a novel lesion produced by the antineoplastic agent paclitaxel. *European Journal of Neuroscience* 33: 1667-1676, 2011.

15. **Blandin G, Marchand S, Charton K, Danièle N, Gicquel E, Boucheteil J-B, Bentaib A, Barrault L, Stockholm D, Bartoli M, and Richard I**. A human skeletal muscle interactome centered on proteins involved in muscular dystrophies: LGMD interactome. *Skeletal muscle* 3: 3-3, 2013.
16. **Boudriau S, Vincent M, Côté CH, and Rogers PA**. Cytoskeletal structure of skeletal muscle: identification of an intricate exosarcomeric microtubule lattice in slow- and fast-twitch muscle fibers. *Journal of Histochemistry & Cytochemistry* 41: 1013-1021, 1993.
17. **Brand Martin D, Pakay Julian L, Ocloo A, Kokoszka J, Wallace Douglas C, Brookes Paul S, and Cornwall Emma J**. The basal proton conductance of mitochondria depends on adenine nucleotide translocase content. *Biochemical Journal* 392: 353-362, 2005.
18. **Bulfield G, Siller WG, Wight PA, and Moore KJ**. X chromosome-linked muscular dystrophy (mdx) in the mouse. *Proceedings of the National Academy of Sciences of the United States of America* 81: 1189-1192, 1984.
19. **Bushby K, Finkel R, Birnkrant DJ, Case LE, Clemens PR, Cripe L, Kaul A, Kinnett K, McDonald C, Pandya S, Poysky J, Shapiro F, Tomezsko J, and Constantin C**. Diagnosis and management of Duchenne muscular dystrophy, part 1: diagnosis, and pharmacological and psychosocial management. *The Lancet Neurology* 9: 77-93, 2010.
20. **Carre M, Andre N, Carles G, Borghi H, Brichese L, Briand C, and Braguer D**. Tubulin is an inherent component of mitochondrial membranes that interacts with the voltage-dependent anion channel. *J Biol Chem* 277: 33664-33669, 2002.
21. **Chaaban S, and Brouhard GJ**. A microtubule bestiary: structural diversity in tubulin polymers. *Molecular Biology of the Cell* 28: 2924-2931, 2017.
22. **Cheever MA, and Higano CS**. PROVENGE (Sipuleucel-T) in Prostate Cancer: The First FDA-Approved Therapeutic Cancer Vaccine. *Clinical Cancer Research* 17: 3520-3526, 2011.
23. **Chen JG, and Horwitz SB**. Differential mitotic responses to microtubule-stabilizing and -destabilizing drugs. *Cancer Res* 62: 1935-1938, 2002.
24. **Chen T-L, Lin Y-W, Chen Y-B, Lin J-J, Su T-L, Shen C-N, and Lee T-C**. A Low-Toxicity DNA-Alkylating N-Mustard-Quinoline Conjugate with Preferential Sequence Specificity Exerts Potent Antitumor Activity Against Colorectal Cancer. *Neoplasia* 20: 119-130, 2018.
25. **Cheng EH-Y, Sheiko TV, Fisher JK, Craigen WJ, and Korsmeyer SJ**. VDAC2 Inhibits BAK Activation and Mitochondrial Apoptosis. *Science* 301: 513-517, 2003.
26. **Chiu W-H, Luo S-J, Chen C-L, Cheng J-H, Hsieh C-Y, Wang C-Y, Huang W-C, Su W-C, and Lin C-F**. Vinca alkaloids cause aberrant ROS-mediated JNK activation, Mcl-1 downregulation, DNA damage, mitochondrial dysfunction, and apoptosis in lung adenocarcinoma cells. *Biochemical Pharmacology* 83: 1159-1171, 2012.
27. **Choo H-J, Saafir TB, Mkumba L, Wagner MB, and Jobe SM**. Mitochondrial calcium and reactive oxygen species regulate agonist-initiated platelet phosphatidylserine exposure. *Arterioscler Thromb Vasc Biol* 32: 2946-2955, 2012.
28. **Chu R, Upreti M, Ding WX, Yin XM, and Chambers TC**. Regulation of Bax by c-Jun NH2-terminal kinase and Bcl-xL in vinblastine-induced apoptosis. *Biochem Pharmacol* 78: 241-248, 2009.
29. **Coley WD, Bogdanik L, Vila MC, Yu Q, Van Der Meulen JH, Rayavarapu S, Novak JS, Nearing M, Quinn JL, Saunders A, Dolan C, Andrews W, Lammert C, Austin A,**

Partridge TA, Cox GA, Lutz C, and Nagaraju K. Effect of genetic background on the dystrophic phenotype in mdx mice. *Hum Mol Genet* 25: 130-145, 2016.
30. **Cortassa S, O'Rourke B, and Aon MA**. Redox-Optimized ROS Balance and the relationship between mitochondrial respiration and ROS. *Biochimica et Biophysica Acta (BBA) - Bioenergetics* 1837: 287-295, 2014.
31. **Crompton M, Virji S, and Ward JM**. Cyclophilin-D binds strongly to complexes of the voltage-dependent anion channel and the adenine nucleotide translocase to form the permeability transition pore. *European Journal of Biochemistry* 258: 729-735, 1998.
32. **Dam AD, Mitchell AS, Rush JWE, and Quadrilatero J**. Elevated skeletal muscle apoptotic signaling following glutathione depletion. *Apoptosis* 17: 48-60, 2012.
33. **Delp MD, and Duan C**. Composition and size of type I, IIA, IID/X, and IIB fibers and citrate synthase activity of rat muscle. *Journal of Applied Physiology* 80: 261-270, 1996.
34. **Fairclough RJ, Wood MJ, and Davies KE**. Therapy for Duchenne muscular dystrophy: renewed optimism from genetic approaches. *Nature Reviews Genetics* 14: 373, 2013.
35. **Fisher-Wellman KH, Gilliam LAA, Lin C-T, Cathey BL, Lark DS, and Darrell Neufer P**. Mitochondrial glutathione depletion reveals a novel role for the pyruvate dehydrogenase complex as a key H2O2-emitting source under conditions of nutrient overload. *Free radical biology & medicine* 65: 1201-1208, 2013.
36. **Fisher-Wellman KH, and Neufer PD**. Linking mitochondrial bioenergetics to insulin resistance via redox biology. *Trends Endocrinol Metab* 23: 142-153, 2012.
37. **Ghoreishi Z, Esfahani A, Djazayeri A, Djalali M, Golestan B, Ayromlou H, Hashemzade S, Asghari Jafarabadi M, Montazeri V, Keshavarz SA, and Darabi M**. Omega-3 fatty acids are protective against paclitaxel-induced peripheral neuropathy: A randomized double-blind placebo controlled trial. *BMC Cancer* 12: 355-355, 2012.
38. **Gilliam LAA, Fisher-Wellman KH, Lin C-T, Maples JM, Cathey BL, and Neufer PD**. The anticancer agent doxorubicin disrupts mitochondrial energy metabolism and redox balance in skeletal muscle. *Free radical biology & medicine* 65: 988-996, 2013.
39. **Godin R, Daussin F, Matecki S, Li T, Petrof BJ, and Burelle Y**. Peroxisome proliferator-activated receptor γ coactivator 1-α gene transfer restores mitochondrial biomass and improves mitochondrial calcium handling in post-necrotic mdx mouse skeletal muscle. *The Journal of Physiology* 590: 5487-5502, 2012.
40. **Gonzalez-Granillo M, Grichine A, Guzun R, Usson Y, Tepp K, Chekulayev V, Shevchuk I, Karu-Varikmaa M, Kuznetsov AV, Grimm M, Saks V, and Kaambre T**. Studies of the role of tubulin beta II isotype in regulation of mitochondrial respiration in intracellular energetic units in cardiac cells. *J Mol Cell Cardiol* 52: 437-447, 2012.
41. **Guerrero K, Monge C, Bruckner A, Puurand U, Kadaja L, Kaambre T, Seppet E, and Saks V**. Study of possible interactions of tubulin, microtubular network, and STOP protein with mitochondria in muscle cells. *Mol Cell Biochem* 337: 239-249, 2010.
42. **Guzun R, Gonzalez-Granillo M, Karu-Varikmaa M, Grichine A, Usson Y, Kaambre T, Guerrero-Roesch K, Kuznetsov A, Schlattner U, and Saks V**. Regulation of respiration in muscle cells in vivo by VDAC through interaction with the cytoskeleton and MtCK within Mitochondrial Interactosome. *Biochim Biophys Acta* 1818: 1545-1554, 2012.
43. **Guzun R, and Saks V**. Application of the principles of systems biology and Wiener's cybernetics for analysis of regulation of energy fluxes in muscle cells in vivo. *Int J Mol Sci* 11: 982-1019, 2010.

44. **Guzun R, Timohhina N, Tepp K, Monge C, Kaambre T, Sikk P, Kuznetsov AV, Pison C, and Saks V**. Regulation of respiration controlled by mitochondrial creatine kinase in permeabilized cardiac cells in situ. Importance of system level properties. *Biochim Biophys Acta* 1787: 1089-1105, 2009.
45. **Halestrap AP**. What is the mitochondrial permeability transition pore? *Journal of Molecular and Cellular Cardiology* 46: 821-831, 2009.
46. **Hammond JW, Cai D, and Verhey KJ**. Tubulin modifications and their cellular functions. *Current opinion in cell biology* 20: 71-76, 2008.
47. **Han Y, and Smith MT**. Pathobiology of cancer chemotherapy-induced peripheral neuropathy (CIPN). *Frontiers in Pharmacology* 4: 156, 2013.
48. **Hayes S, Battistutta D, and Newman B**. Objective and Subjective Upper Body Function Six Months Following Diagnosis of Breast Cancer. *Breast Cancer Research and Treatment* 94: 1-10, 2005.
49. **House KW, Simon SR, and Pugh RP**. Chemotherapy-induced myocardial infarction in a young man with hodgkin's disease. *Clinical Cardiology* 15: 122-125, 1992.
50. **Howarth FC, Calaghan SC, Boyett MR, and White E**. Effect of the microtubule polymerizing agent taxol on contraction, Ca(2+) transient and L-type Ca(2+) current in rat ventricular myocytes. *The Journal of Physiology* 516: 409-419, 1999.
51. **Hughes MC, Ramos SV, Turnbull PC, Edgett BA, Huber JS, Polidovitch N, Schlattner U, Backx PH, Simpson JA, and Perry CGR**. Impairments in left ventricular mitochondrial bioenergetics precede overt cardiac dysfunction and remodelling in Duchenne muscular dystrophy. *The Journal of Physiology* 0.
52. **Hughes MC, Ramos SV, Turnbull PC, Rebalka IA, Cao A, Monaco CMF, Varah NE, Edgett BA, Huber JS, Tadi P, Delfinis LJ, Schlattner U, Simpson JA, Hawke TJ, and Perry CGR**. Early myopathy in Duchenne muscular dystrophy is associated with elevated mitochondrial H2O2 emission during impaired oxidative phosphorylation. *Journal of Cachexia, Sarcopenia and Muscle* 0.
53. **Hughes MC, Ramos SV, Turnbull PC, Rebalka IA, Cao A, Monaco CMF, Varah NE, Edgett BA, Huber JS, Tadi P, Delfinis LJ, Schlattner U, Simpson JA, Hawke TJ, and Perry CGR**. Early myopathy in Duchenne muscular dystrophy is associated with elevated mitochondrial H2O2 emission during impaired oxidative phosphorylation. *Journal of Cachexia, Sarcopenia and Muscle* 10: 643-661, 2019.
54. **Iqbal S, and Hood DA**. Cytoskeletal regulation of mitochondrial movements in myoblasts. *Cytoskeleton* 71: 564-572, 2014.
55. **Jackson JK, Skinner KC, Burgess L, Sun T, Hunter WL, and Burt HM**. Paclitaxel-Loaded Crosslinked Hyaluronic Acid Films for the Prevention of Postsurgical Adhesions. *Pharmaceutical Research* 19: 411-417, 2002.
56. **Jacobsen PB, Hann DM, Azzarello LM, Horton J, Balducci L, and Lyman GH**. Fatigue in Women Receiving Adjuvant Chemotherapy for Breast Cancer: Characteristics, Course, and Correlates. *Journal of Pain and Symptom Management* 18: 233-242, 1999.
57. **Jemal A, Bray F, Center MM, Ferlay J, Ward E, and Forman D**. Global cancer statistics. *CA: A Cancer Journal for Clinicians* 61: 69-90, 2011.
58. **Johnstone TC, Park GY, and Lippard SJ**. Understanding and improving platinum anticancer drugs--phenanthriplatin. *Anticancer Res* 34: 471-476, 2014.
59. **Jones DP**. Radical-free biology of oxidative stress. *American journal of physiology Cell physiology* 295: C849-C868, 2008.

60. **JONES SW, HILL RJ, KRASNEY PA, O'CONNER B, PEIRCE N, and GREENHAFF PL**. Disuse atrophy and exercise rehabilitation in humans profoundly affects the expression of genes associated with the regulation of skeletal muscle mass. *The FASEB Journal* 18: 1025-1027, 2004.
61. **Jordan MA, Thrower D, and Wilson L**. Mechanism of Inhibition of Cell Proliferation by Vinca Alkaloids. *Cancer Research* 51: 2212-2222, 1991.
62. **Jordan MA, and Wilson L**. [22] Use of drugs to study role of microtubule assembly dynamics in living cells. In: *Methods in Enzymology*Academic Press, 1998, p. 252-276.
63. **Jorquera G, Altamirano F, Contreras-Ferrat A, Almarza G, Buvinic S, Jacquemond V, Jaimovich E, and Casas M**. Cav1.1 controls frequency-dependent events regulating adult skeletal muscle plasticity. *Journal of Cell Science* 126: 1189-1198, 2013.
64. **Juntunen J**. Effects of colchicine and vinblastine on neurotubules of the sciatic nerve and cholinesterases in the developing myoneural junction of the rat. *Zeitschrift für Zellforschung und Mikroskopische Anatomie* 142: 193-204, 1973.
65. **Kerr JP, Robison P, Shi G, Bogush AI, Kempema AM, Hexum JK, Becerra N, Harki DA, Martin SS, Raiteri R, Prosser BL, and Ward CW**. Detyrosinated microtubules modulate mechanotransduction in heart and skeletal muscle. *Nature Communications* 6: 8526, 2015.
66. **Khairallah RJ, Shi G, Sbrana F, Prosser BL, Borroto C, Mazaitis MJ, Hoffman EP, Mahurkar A, Sachs F, Sun Y, Chen Y-W, Raiteri R, Lederer WJ, Dorsey SG, and Ward CW**. Microtubules Underlie Dysfunction in Duchenne Muscular Dystrophy. *Science Signaling* 5: ra56-ra56, 2012.
67. **Kilgour RD, Vigano A, Trutschnigg B, Hornby L, Lucar E, Bacon SL, and Morais JA**. Cancer-related fatigue: the impact of skeletal muscle mass and strength in patients with advanced cancer. *Journal of Cachexia, Sarcopenia and Muscle* 1: 177-185, 2010.
68. **Kim J-S, Jin Y, and Lemasters JJ**. Reactive oxygen species, but not Ca2+ overloading, trigger pH- and mitochondrial permeability transition-dependent death of adult rat myocytes after ischemia-reperfusion. *American Journal of Physiology-Heart and Circulatory Physiology* 290: H2024-H2034, 2006.
69. **Kolomeichuk SN, Bene A, Upreti M, Dennis RA, Lyle CS, Rajasekaran M, and Chambers TC**. Induction of apoptosis by vinblastine via c-Jun autoamplification and p53-independent down-regulation of p21WAF1/CIP1. *Mol Pharmacol* 73: 128-136, 2008.
70. **Kolomeichuk SN, Terrano DT, Lyle CS, Sabapathy K, and Chambers TC**. Distinct signaling pathways of microtubule inhibitors – vinblastine and Taxol induce JNK-dependent cell death but through AP-1-dependent and AP-1-independent mechanisms, respectively. *The FEBS Journal* 275: 1889-1899, 2008.
71. **Konishi S, and Kishida S**. Studies on the morphological changes of skeletal muscle induced by vincristine, vinblastine and colchicine. *Bull Osaka Med Sch* 30: 19-40, 1984.
72. **Kottke M, Adams V, Wallimann T, Nalam VK, and Brdiczka D**. Location and regulation of octameric mitochondrial creatine kinase in the contact sites. *Biochimica et Biophysica Acta (BBA) - Biomembranes* 1061: 215-225, 1991.
73. **Kroemer G, Galluzzi L, and Brenner C**. Mitochondrial Membrane Permeabilization in Cell Death. *Physiological Reviews* 87: 99-163, 2007.
74. **Kumazawa A, Katoh H, Nonaka D, Watanabe T, Saotome M, Urushida T, Satoh H, and Hayashi H**. Microtubule disorganization affects the mitochondrial permeability transition pore in cardiac myocytes. *Circ J* 78: 1206-1215, 2014.

75. **Kuznetsov AV, Tiivel T, Sikk P, Kaambre T, Kay L, Daneshrad Z, Rossi A, Kadaja L, Peet N, Seppet E, and Saks VA**. Striking differences between the kinetics of regulation of respiration by ADP in slow-twitch and fast-twitch muscles in vivo. *Eur J Biochem* 241: 909-915, 1996.
76. **Kuznetsov AV, Winkler K, Wiedemann F, von Bossanyi P, Dietzmann K, and Kunz WS**. Impaired mitochondrial oxidative phosphorylation in skeletal muscle of the dystrophin-deficient mdx mouse. *Molecular and Cellular Biochemistry* 183: 87-96, 1998.
77. **Levy SE, Chen Y-S, Graham BH, and Wallace DC**. Expression and sequence analysis of the mouse adenine nucleotide translocase 1 and 2 genes. *Gene* 254: 57-66, 2000.
78. **Li L, Zhang Q, Zhang X, Zhang J, Wang X, Ren J, Jia J, Zhang D, Jiang X, Zhang J, Mei H, Chen B, Hu J, and Huang Y**. Microtubule associated protein 4 phosphorylation leads to pathological cardiac remodeling in mice. *EBioMedicine* 37: 221-235, 2018.
79. **Liu Y, and Chen XJ**. *Adenine Nucleotide Translocase, Mitochondrial Stress, and Degenerative Cell Death*. 2013, p. 10.
80. **Majewski N, Nogueira V, Bhaskar P, Coy PE, Skeen JE, Gottlob K, Chandel NS, Thompson CB, Robey RB, and Hay N**. Hexokinase-Mitochondria Interaction Mediated by Akt Is Required to Inhibit Apoptosis in the Presence or Absence of Bax and Bak. *Molecular Cell* 16: 819-830, 2004.
81. **Maldonado EN, Sheldon KL, DeHart DN, Patnaik J, Manevich Y, Townsend DM, Bezrukov SM, Rostovtseva TK, and Lemasters JJ**. Voltage-dependent anion channels modulate mitochondrial metabolism in cancer cells: regulation by free tubulin and erastin. *J Biol Chem* 288: 11920-11929, 2013.
82. **Maria-Magdalena M, Tímea V, János S, and Peter N**. Comparative analysis of fluorescence resonance energy transfer (FRET) and proximity ligation assay (PLA). *PROTEOMICS* 11: 2063-2070, 2011.
83. **Matthews H, Duffy CW, and Merrick CJ**. Checks and balances? DNA replication and the cell cycle in Plasmodium. *Parasites & Vectors* 11: 216, 2018.
84. **McKean PG, Vaughan S, and Gull K**. The extended tubulin superfamily. *Journal of Cell Science* 114: 2723-2733, 2001.
85. **Messina A, Reina S, Guarino F, and De Pinto V**. VDAC isoforms in mammals. *Biochimica et Biophysica Acta (BBA) - Biomembranes* 1818: 1466-1476, 2012.
86. **Meyer RA, Sweeney HL, and Kushmerick MJ**. A simple analysis of the "phosphocreatine shuttle". *American Journal of Physiology-Cell Physiology* 246: C365-C377, 1984.
87. **Mitchell P**. Chemiosmotic coupling in oxidative and photosynthetic phosphorylation. *Biochimica et Biophysica Acta (BBA) - Bioenergetics* 1807: 1507-1538, 2011.
88. **Moges H, Wu X, McCoy J, Vasconcelos OM, Bryant H, Grunberg NE, and Anders JJ**. Effect of 810 nm light on nerve regeneration after autograft repair of severely injured rat median nerve. *Lasers in Surgery and Medicine* 43: 901-906, 2011.
89. **Monaco CMF, Hughes MC, Ramos SV, Varah NE, Lamberz C, Rahman FA, McGlory C, Tarnopolsky MA, Krause MP, Laham R, Hawke TJ, and Perry CGR**. Altered mitochondrial bioenergetics and ultrastructure in the skeletal muscle of young adults with type 1 diabetes. *Diabetologia* 61: 1411-1423, 2018.
90. **Moos P, and Fitzpatrick F**. Taxanes propagate apoptosis via two cell populations with distinctive cytological and molecular traits. *Cell Growth Differ* 9: 687-697, 1998.

91. **Moreadith RW, and Jacobus WE**. Creatine kinase of heart mitochondria. Functional coupling of ADP transfer to the adenine nucleotide translocase. *Journal of Biological Chemistry* 257: 899-905, 1982.
92. **Moudi M, Go R, Yien CYS, and Nazre M**. Vinca alkaloids. *Int J Prev Med* 4: 1231-1235, 2013.
93. **Muroyama A, and Lechler T**. Microtubule organization, dynamics and functions in differentiated cells. *Development (Cambridge, England)* 144: 3012-3021, 2017.
94. **Muto A, Nakagawa A, Shimomura Y, Kitagawa Y, and Tsurusawa M**. Antineoplastic agents for pediatric anaplastic large cell lymphoma: Vinblastine is the most effective in vitro. *Leukemia & Lymphoma* 46: 1489-1496, 2005.
95. **Naghdi S, and Hajnóczky G**. VDAC2-specific cellular functions and the underlying structure. *Biochimica et Biophysica Acta (BBA) - Molecular Cell Research* 1863: 2503-2514, 2016.
96. **Needleman DJ, Ojeda-Lopez MA, Raviv U, Ewert K, Miller HP, Wilson L, and Safinya CR**. Radial Compression of Microtubules and the Mechanism of Action of Taxol and Associated Proteins. *Biophysical Journal* 89: 3410-3423, 2005.
97. **Nicholls DG**. *Bioenergetics*. Elsevier Science, 2013.
98. **Noble RL**. The discovery of the vinca alkaloids--chemotherapeutic agents against cancer. *Biochem Cell Biol* 68: 1344-1351, 1990.
99. **Noskov SY, Rostovtseva TK, and Bezrukov SM**. ATP Transport through VDAC and the VDAC–Tubulin Complex Probed by Equilibrium and Nonequilibrium MD Simulations. *Biochemistry* 52: 9246-9256, 2013.
100. **Oddoux S, Zaal KJ, Tate V, Kenea A, Nandkeolyar SA, Reid E, Liu W, and Ralston E**. Microtubules that form the stationary lattice of muscle fibers are dynamic and nucleated at Golgi elements. *The Journal of cell biology* 203: 205-213, 2013.
101. **Panda D, Jordan MA, Chu KC, and Wilson L**. Differential effects of vinblastine on polymerization and dynamics at opposite microtubule ends. *J Biol Chem* 271: 29807-29812, 1996.
102. **Parker AL, Kavallaris M, and McCarroll JA**. Microtubules and their role in cellular stress in cancer. *Frontiers in oncology* 4: 153-153, 2014.
103. **Pastorino JG, Shulga N, and Hoek JB**. Mitochondrial Binding of Hexokinase II Inhibits Bax-induced Cytochrome c Release and Apoptosis. *Journal of Biological Chemistry* 277: 7610-7618, 2002.
104. **Perry CG, Kane DA, Lanza IR, and Neufer PD**. Methods for assessing mitochondrial function in diabetes. *Diabetes* 62: 1041-1053, 2013.
105. **Perry CGR, Kane DA, Herbst EAF, Mukai K, Lark DS, Wright DC, Heigenhauser GJF, Neufer PD, Spriet LL, and Holloway GP**. Mitochondrial creatine kinase activity and phosphate shuttling are acutely regulated by exercise in human skeletal muscle. *The Journal of Physiology* 590: 5475-5486, 2012.
106. **Perry CGR, Kane DA, Lin C-T, Kozy R, Cathey BL, Lark DS, Kane CL, Brophy PM, Gavin TP, Anderson EJ, and Neufer PD**. Inhibiting Myosin-ATPase Reveals Dynamic Range of Mitochondrial Respiratory Control in Skeletal Muscle. *The Biochemical journal* 437: 10.1042/BJ20110366, 2011.
107. **Pinho RA, Sepa-Kishi DM, Bikopoulos G, Wu MV, Uthayakumar A, Mohasses A, Hughes MC, Perry CGR, and Ceddia RB**. High-fat diet induces skeletal muscle oxidative stress in a fiber type-dependent manner in rats. *Free Radic Biol Med* 110: 381-389, 2017.

108. **Pinz I, Zhu M, Mende U, and Ingwall JS**. An Improved Isolation Procedure for Adult Mouse Cardiomyocytes. *Cell Biochemistry and Biophysics* 61: 93-101, 2011.
109. **Plummer M, de Martel C, Vignat J, Ferlay J, Bray F, and Franceschi S**. Global burden of cancers attributable to infections in 2012: a synthetic analysis. *The Lancet Global Health* 4: e609-e616, 2016.
110. **Preau S, Montaigne D, Modine T, Fayad G, Koussa M, Tardivel M, Durocher A, Saulnier F, Marechal X, and Neviere R**. Macrophage Migration Inhibitory Factor Induces Contractile and Mitochondria Dysfunction by Altering Cytoskeleton Network in the Human Heart*. *Critical Care Medicine* 41: e125-e133, 2013.
111. **Prins KW, Humston JL, Mehta A, Tate V, Ralston E, and Ervasti JM**. Dystrophin is a microtubule-associated protein. *The Journal of Cell Biology* 186: 363-369, 2009.
112. **Raghavan A, Sheiko T, Graham BH, and Craigen WJ**. Voltage-dependant anion channels: Novel insights into isoform function through genetic models. *Biochimica et Biophysica Acta (BBA) - Biomembranes* 1818: 1477-1485, 2012.
113. **Ralston E**. Changes in architecture of the Golgi complex and other subcellular organelles during myogenesis. *The Journal of Cell Biology* 120: 399-409, 1993.
114. **Ralston E, Ploug T, Kalhovde J, and Lømo T**. Golgi Complex, Endoplasmic Reticulum Exit Sites, and Microtubules in Skeletal Muscle Fibers Are Organized by Patterned Activity. *The Journal of Neuroscience* 21: 875-883, 2001.
115. **Ramos SV, Hughes MC, and Perry CGR**. Altered skeletal muscle microtubule-mitochondrial VDAC2 binding is related to bioenergetic impairments after paclitaxel but not vinblastine chemotherapies. *American Journal of Physiology-Cell Physiology* 316: C449-C455, 2019.
116. **Ramos SV, Hughes MC, and Perry CGR**. Altered skeletal muscle microtubule-mitochondrial VDAC2 binding is related to bioenergetic impairments after paclitaxel but not vinblastine chemotherapies. *American Journal of Physiology-Cell Physiology* 0: null.
117. **Ren X, Zhao B, Chang H, Xiao M, Wu Y, and Liu Y**. Paclitaxel suppresses proliferation and induces apoptosis through regulation of ROS and the AKT/MAPK signaling pathway in canine mammary gland tumor cells. *Molecular medicine reports* 17: 8289-8299, 2018.
118. **Richter EA, and Hargreaves M**. Exercise, GLUT4, and Skeletal Muscle Glucose Uptake. *Physiological Reviews* 93: 993-1017, 2013.
119. **Rivera E, and Cianfrocca M**. Overview of neuropathy associated with taxanes for the treatment of metastatic breast cancer. *Cancer chemotherapy and pharmacology* 75: 659-670, 2015.
120. **Robinson-Hamm JN, and Gersbach CA**. Gene therapies that restore dystrophin expression for the treatment of Duchenne muscular dystrophy. *Hum Genet* 135: 1029-1040, 2016.
121. **Robison P, and Prosser BL**. Microtubule mechanics in the working myocyte. *The Journal of Physiology* 595: 3931-3937, 2017.
122. **Roskoski Jr. R**. Bioenergetics 3: Nicholls, David G., and Ferguson, Stuart J. *Biochemistry and Molecular Biology Education* 31: 215-216, 2003.
123. **Rostovtseva T, and Colombini M**. ATP Flux Is Controlled by a Voltage-gated Channel from the Mitochondrial Outer Membrane. *Journal of Biological Chemistry* 271: 28006-28008, 1996.

124. **Rostovtseva TK, and Bezrukov SM**. VDAC inhibition by tubulin and its physiological implications. *Biochimica et Biophysica Acta (BBA) - Biomembranes* 1818: 1526-1535, 2012.
125. **Rostovtseva TK, Gurnev PA, Chen M-Y, and Bezrukov SM**. Membrane Lipid Composition Regulates Tubulin Interaction with Mitochondrial Voltage-dependent Anion Channel. *The Journal of Biological Chemistry* 287: 29589-29598, 2012.
126. **Rostovtseva TK, Gurnev PA, Hoogerheide DP, Rovini A, Sirajuddin M, and Bezrukov SM**. Sequence diversity of tubulin isotypes in regulation of the mitochondrial voltage-dependent anion channel. *J Biol Chem* 293: 10949-10962, 2018.
127. **Rostovtseva TK, Sheldon KL, Hassanzadeh E, Monge C, Saks V, Bezrukov SM, and Sackett DL**. Tubulin binding blocks mitochondrial voltage-dependent anion channel and regulates respiration. *Proc Natl Acad Sci U S A* 105: 18746-18751, 2008.
128. **Rostovtseva TK, Tan W, and Colombini M**. On the Role of VDAC in Apoptosis: Fact and Fiction. *Journal of Bioenergetics and Biomembranes* 37: 129-142, 2005.
129. **Rowinsky EK, and Donehower RC**. The clinical pharmacology and use of antimicrotubule agents in cancer chemotherapeutics. *Pharmacology & Therapeutics* 52: 35-84, 1991.
130. **Rowinsky EK, and Donehower RC**. Paclitaxel (Taxol). *New England Journal of Medicine* 332: 1004-1014, 1995.
131. **Sætersdal T, Greve G, and Dalen H**. Associations between beta-tubulin and mitochondria in adult isolated heart myocytes as shown by immunofluorescence and immunoelectron microscopy. *Histochemistry* 95: 1-10, 1990.
132. **Saks V, Guzun R, Timohhina N, Tepp K, Varikmaa M, Monge C, Beraud N, Kaambre T, Kuznetsov A, Kadaja L, Eimre M, and Seppet E**. Structure-function relationships in feedback regulation of energy fluxes in vivo in health and disease: mitochondrial interactosome. *Biochim Biophys Acta* 1797: 678-697, 2010.
133. **Saks V, Kaambre T, Guzun R, Anmann T, Sikk P, Schlattner U, Wallimann T, Aliev M, and Vendelin M**. The creatine kinase phosphotransfer network: thermodynamic and kinetic considerations, the impact of the mitochondrial outer membrane and modelling approaches. *Subcell Biochem* 46: 27-65, 2007.
134. **Saks V, Kuznetsov AV, Gonzalez-Granillo M, Tepp K, Timohhina N, Karu-Varikmaa M, Kaambre T, Santos PD, Boucher F, and Guzun R**. Intracellular Energetic Units regulate metabolism in cardiac cells. *Journal of Molecular and Cellular Cardiology* 52: 419-436, 2012.
135. **Saks VA, Kuznetsov AV, Khuchua ZA, Vasilyeva EV, Belikova JO, Kesvatera T, and Tiivel T**. Control of cellular respiration in vivo by mitochondrial outer membrane and by Creatine Kinase. A new speculative hypothesis: possible involvement of mitochondrial-cytoskeleton interactions. *Journal of Molecular and Cellular Cardiology* 27: 625-645, 1995.
136. **Saks VA, Kuznetsov AV, Khuchua ZA, Vasilyeva EV, Belikova JO, Kesvatera T, and Tiivel T**. Control of cellular respiration in vivo by mitochondrial outer membrane and by creatine kinase. A new speculative hypothesis: possible involvement of mitochondrial-cytoskeleton interactions. *J Mol Cell Cardiol* 27: 625-645, 1995.
137. **Salerni BL, Bates DJ, Albershardt TC, Lowrey CH, and Eastman A**. Vinblastine Induces Acute, Cell Cycle Phase–Independent Apoptosis in Some Leukemias and Lymphomas and Can Induce Acute Apoptosis in Others when Mcl-1 Is Suppressed. *Molecular Cancer Therapeutics* 9: 791-802, 2010.

138. **Sato H, Nagai T, Kuppuswamy D, Narishige T, Koide M, Menick DR, and Cooper Gt**. Microtubule stabilization in pressure overload cardiac hypertrophy. *J Cell Biol* 139: 963-973, 1997.
139. **Schein SJ, Colombini M, and Finkelstein A**. Reconstitution in planar lipid bilayers of a voltage-dependent anion-selective channel obtained from paramecium mitochondria. *The Journal of Membrane Biology* 30: 99-120, 1976.
140. **Schlattner U, Dolder M, Wallimann T, and Tokarska-Schlattner M**. Mitochondrial Creatine Kinase and Mitochondrial Outer Membrane Porin Show a Direct Interaction That Is Modulated by Calcium. *Journal of Biological Chemistry* 276: 48027-48030, 2001.
141. **Schlattner U, Tokarska-Schlattner M, and Wallimann T**. Mitochondrial creatine kinase in human health and disease. *Biochimica et Biophysica Acta (BBA) - Molecular Basis of Disease* 1762: 164-180, 2006.
142. **Sébastien M, Giannesini B, Aubin P, Brocard J, Chivet M, Pietrangelo L, Boncompagni S, Bosc C, Brocard J, Rendu J, Gory-Fauré S, Andrieux A, Fourest-Lieuvin A, Fauré J, and Marty I**. Deletion of the microtubule-associated protein 6 (MAP6) results in skeletal muscle dysfunction. *Skeletal Muscle* 8: 30, 2018.
143. **Selimovic D, Badura HE, El-Khattouti A, Soell M, Porzig BBOW, Spernger A, Ghanjati F, Santourlidis S, Haikel Y, and Hassan M**. Vinblastine-induced apoptosis of melanoma cells is mediated by Ras homologous A protein (Rho A) via mitochondrial and non-mitochondrial-dependent mechanisms. *Apoptosis* 18: 980-997, 2013.
144. **Shachar SS, Deal AM, Weinberg M, Nyrop KA, Williams GR, Nishijima TF, Benbow JM, and Muss HB**. Skeletal Muscle Measures as Predictors of Toxicity, Hospitalization, and Survival in Patients with Metastatic Breast Cancer Receiving Taxane-Based Chemotherapy. *Clinical Cancer Research* 23: 658-665, 2017.
145. **Sheldon KL, Gurnev PA, Bezrukov SM, and Sackett DL**. Tubulin tail sequences and post-translational modifications regulate closure of mitochondrial voltage-dependent anion channel (VDAC). *J Biol Chem* 290: 26784-26789, 2015.
146. **Sheldon KL, Maldonado EN, Lemasters JJ, Rostovtseva TK, and Bezrukov SM**. Phosphorylation of voltage-dependent anion channel by serine/threonine kinases governs its interaction with tubulin. *PLoS One* 6: e25539, 2011.
147. **Shimizu S, Ide T, Yanagida T, and Tsujimoto Y**. Electrophysiological Study of a Novel Large Pore Formed by Bax and the Voltage-dependent Anion Channel That Is Permeable to Cytochrome c. *Journal of Biological Chemistry* 275: 12321-12325, 2000.
148. **Song E, Ramos SV, Huang X, Liu Y, Botta A, Sung HK, Turnbull PC, Wheeler MB, Berger T, Wilson DJ, Perry CGR, Mak TW, and Sweeney G**. Holo-lipocalin-2-derived siderophores increase mitochondrial ROS and impair oxidative phosphorylation in rat cardiomyocytes. *Proc Natl Acad Sci U S A* 115: 1576-1581, 2018.
149. **Sorensen JC, Cheregi BD, Timpani CA, Nurgali K, Hayes A, and Rybalka E**. Mitochondria: Inadvertent targets in chemotherapy-induced skeletal muscle toxicity and wasting? *Cancer Chemotherapy and Pharmacology* 78: 673-683, 2016.
150. **T. CB, L. WC, B. BH, J. WT, and J. CG**. Implantation of In Vitro Tissue Engineered Muscle Repair Constructs and Bladder Acellular Matrices Partially Restore In Vivo Skeletal Muscle Function in a Rat Model of Volumetric Muscle Loss Injury. *Tissue Engineering Part A* 20: 705-715, 2014.
151. **Tan W, and Colombini M**. VDAC closure increases calcium ion flux. *Biochimica et Biophysica Acta (BBA) - Biomembranes* 1768: 2510-2515, 2007.

152. **Tew WP, Radovich D, O'Reilly E, Schwartz G, Schrag D, Saltz LB, Kelsen DP, Kepler S, and Ilson DH**. Phase I trial of weekly cisplatin, irinotecan and paclitaxel in patients with advanced gastrointestinal cancer. *Investigational new drugs* 27: 366-373, 2009.
153. **Timohhina N, Guzun R, Tepp K, Monge C, Varikmaa M, Vija H, Sikk P, Kaambre T, Sackett D, and Saks V**. Direct measurement of energy fluxes from mitochondria into cytoplasm in permeabilized cardiac cells in situ: some evidence for mitochondrial interactosome. *Journal of Bioenergetics and Biomembranes* 41: 259-275, 2009.
154. **Timpani CA, Hayes A, and Rybalka E**. Revisiting the dystrophin-ATP connection: How half a century of research still implicates mitochondrial dysfunction in Duchenne Muscular Dystrophy aetiology. *Medical Hypotheses* 85: 1021-1033, 2015.
155. **Tombes RM, and Shapiro BM**. Enzyme termini of a phosphocreatine shuttle. Purification and characterization of two creatine kinase isozymes from sea urchin sperm. *Journal of Biological Chemistry* 262: 16011-16019, 1987.
156. **Tonkonogi M, Harris B, and Sahlin K**. Mitochondrial oxidative function in human saponin-skinned muscle fibres: effects of prolonged exercise. *The Journal of physiology* 510 (Pt 1): 279-286, 1998.
157. **Toth MJ, Callahan DM, Miller MS, Tourville TW, Hackett SB, Couch ME, and Dittus K**. Skeletal muscle fiber size and fiber type distribution in human cancer: Effects of weight loss and relationship to physical function. *Clinical Nutrition* 35: 1359-1365, 2016.
158. **Tsujimoto Y, and Shimizu S**. VDAC regulation by the Bcl-2 family of proteins. *Cell Death & Differentiation* 7: 1174-1181, 2000.
159. **Tsutsui H, Ishihara K, and Cooper G**. Cytoskeletal role in the contractile dysfunction of hypertrophied myocardium. *Science* 260: 682-687, 1993.
160. **Upreti M, Lyle CS, Skaug B, Du L, and Chambers TC**. Vinblastine-induced apoptosis is mediated by discrete alterations in subcellular location, oligomeric structure, and activation status of specific Bcl-2 family members. *J Biol Chem* 281: 15941-15950, 2006.
161. **Varikmaa M, Bagur R, Kaambre T, Grichine A, Timohhina N, Tepp K, Shevchuk I, Chekulayev V, Metsis M, Boucher F, Saks V, Kuznetsov AV, and Guzun R**. Role of mitochondria-cytoskeleton interactions in respiration regulation and mitochondrial organization in striated muscles. *Biochim Biophys Acta* 1837: 232-245, 2014.
162. **Veksler VI, Kuznetsov AV, Sharov VG, Kapelko VI, and Saks VA**. Mitochondrial respiratory parameters in cardiac tissue: A novel method of assessment by using saponin-skinned fibers. *Biochimica et Biophysica Acta (BBA) - Bioenergetics* 892: 191-196, 1987.
163. **Vicente JJ, and Wordeman L**. The quantification and regulation of microtubule dynamics in the mitotic spindle. *Current Opinion in Cell Biology* 60: 36-43, 2019.
164. **Wagner BK, Kitami T, Gilbert TJ, Peck D, Ramanathan A, Schreiber SL, Golub TR, and Mootha VK**. Large-scale chemical dissection of mitochondrial function. *Nature Biotechnology* 26: 343, 2008.
165. **Wallimann T, Tokarska-Schlattner M, and Schlattner U**. The creatine kinase system and pleiotropic effects of creatine. *Amino Acids* 40: 1271-1296, 2011.
166. **Wallimann T, Wyss M, Brdiczka D, Nicolay K, and Eppenberger HM**. Intracellular compartmentation, structure and function of creatine kinase isoenzymes in tissues with high and fluctuating energy demands: the 'phosphocreatine circuit' for cellular energy homeostasis. *The Biochemical journal* 281 (Pt 1): 21-40, 1992.

167. **Walsh B, Tonkonogi M, Söderlund K, Hultman E, Saks V, and Sahlin K**. The role of phosphorylcreatine and creatine in the regulation of mitochondrial respiration in human skeletal muscle. *The Journal of Physiology* 537: 971-978, 2001.
168. **Wang LG, Liu XM, Kreis W, and Budman DR**. The effect of antimicrotubule agents on signal transduction pathways of apoptosis: a review. *Cancer Chemotherapy and Pharmacology* 44: 355-361, 1999.
169. **Weaver BA**. How Taxol/paclitaxel kills cancer cells. *Molecular Biology of the Cell* 25: 2677-2681, 2014.
170. **Whitehead NP, Yeung EW, and Allen DG**. MUSCLE DAMAGE IN MDX (DYSTROPHIC) MICE: ROLE OF CALCIUM AND REACTIVE OXYGEN SPECIES. *Clinical and Experimental Pharmacology and Physiology* 33: 657-662, 2006.
171. **Wiernik PH, Schwartz EL, Strauman JJ, Dutcher JP, Lipton RB, and Paietta E**. Phase I Clinical and Pharmacokinetic Study of Taxol. *Cancer Research* 47: 2486-2493, 1987.
172. **WONG H-S, Dighe PA, Mezera V, Monternier P-A, and Brand MD**. Production of superoxide and hydrogen peroxide from specific mitochondrial sites under different bioenergetic conditions. *Journal of Biological Chemistry* 2017.
173. **Woods CM, Zhu J, McQueney PA, Bollag D, and Lazarides E**. Taxol-Induced Mitotic Block Triggers Rapid Onset of a p53-Independent Apoptotic Pathway. *Molecular Medicine* 1: 506-526, 1995.
174. **Wuerker RB, and Bodley HD**. Changes in muscle morphology and histochemistry produced by denervation, 3,3′-iminodipropionitrile and epineurial vinblastine. *American Journal of Anatomy* 136: 221-234, 1973.
175. **Xiao J, Cao H, Liang D, Liu Y, Zhang H, Zhao H, Liu Y, Li J, Yan B, Peng L, Zhou Z, and Chen Y-H**. Taxol, a microtubule stabilizer, prevents ischemic ventricular arrhythmias in rats. *J Cell Mol Med* 15: 1166-1176, 2011.
176. **Ydfors M, Hughes MC, Laham R, Schlattner U, Norrbom J, and Perry CGR**. Modelling in vivo creatine/phosphocreatine in vitro reveals divergent adaptations in human muscle mitochondrial respiratory control by ADP after acute and chronic exercise. *The Journal of Physiology* 594: 3127-3140, 2016.

Appendix

A1. Histology preparation – single fiber isolation

Equipment

- 50ml falcon tubes
- water bath (maintained at 37°C)
- Incubator (maintained at 37°C with 5% CO_2)
- Transfer pipettes (5) of various sizes
- Glass transfer pipette + bulb
- Hydrophobic pen
- Microscope slides
- Microscope cover slips

Reagents

- 0.2% collagenase
- High glucose DMEM
- Low glucose DMEM
- Horse serum low glucose DMEM
- Paraformaldehyde
- PBS

Protocol

1. Coat 6-9 60mm dishes with horse serum and fill to approximately ½ with LG DMEM.
    a. Assign 2 dishes as "good fibers" to store viable fibers
2. Combine 2mL of horse serum and 10mL of LG DMEM in a 50mL falcon tube to coat pipettes of various diameters
    a. Use transfer pipettes to create a range in mouth sizes. Prepare one glass pipette by using a flame to smooth sharp edges
3. Store in an incubator at 37°C (can make all dishes for 1 week and leave in incubator).
    a. Horse Serum can be reused for coating until finished
4. Prepare 2 50ml tubes with 0.2% collagenase solution on day of harvest. Store in a water bath at 37°C until tissue is collected.
5. Harvest muscle and directly place in warmed 0.2% collagenase and keep in a water bath at 37°C for approximately 90 (mouse) to 120 (rats) minutes.
    a. Periodically swirl tissues to ensure maximum diffusion
6. Ensure all pipettes are coated with HS LG DMEM solution
7. Following collagenase digestion, using the largest pipette transfer muscle to a warmed HS HG DMEM dish.
8. Triturate the muscle until viable fibers are released
    a. Transfer viable fibers into "good fibers" dish and transfer remaining muscle to a new dish and continue to triturate/transfer/switch to new dish until desired amount of fibers are collected.

    b. Never leave fibres at room temp for more than 10 minutes, put back in incubator to allow them to re-equilibrate if taking longer than 10 minutes
9. Once viable fibers have been collected, carefully replace media with fresh PBS until the solution is clear.
    a. Insure the dish always has fluid in it as to not dry out fibers
10. Fixation: fill dish with ½ 4% PFA and ½ PBS and place in fridge for 5-10 minutes for fixation
11. Transfer fixed fibers into a final dish and store at °C
    a. Fibers can be used up to 1 week

http://www.jove.com/video/50074/isolation-culture-individual-myofibers-their-satellite-cells-from

A2. Histology preparation – embedded muscle and slicing

Equipment

- Metal bowl
- Styrofoam container
- String
- Thumb tacks
- Weigh spatula
- Foil or 1.5mL tube

Reagents

- Methybutane
- Liquid nitrogen
- OCT embedding compound

Protocol

1. Use string to secure metal bowl in suspension within Styrofoam container
2. Cool Styrofoam container and metal bowl with lipid nitrogen
3. Add methybutane to cooled bowl and allow to cool
    a. Listen carefully, will hear a first sizzle but wait for a second sizzle to know methybutane is cool enough
4. Lightly coat the flat end of the weighing spatula with OCT compound and gently place tissue in desired orientation. Apply another coat of OCT compound over the muscle covering it completely and immediately place into liquid nitrogen cooled methybutane
5. Let tissue freeze for approximately 30-60 seconds
6. Remove and quickly detach from spatula and cover with labelled foil or 1.5mL tube.
7. Store at -80°C until ready for use
    a. Best to use embedded samples within 1 year of collection.

<u>Sectioning embedded muscle protocol:</u>

1. Cool cryostat to -22°C
2. Remove stored muscle (at -80°C) to equilibrate in cryostat for ~ 1hour
3. Adjust blade angle to 0° and folding shield to an appropriate position to prevent the muscle from rolling on itself (will have to slice and adjust as you go)
4. Once at the muscle, slide 3 transverse sections (serial if possible) at a 10μm thickness
5. Allow slices to dry for 30min before storage (-80°C)

A3. Histology – Immunohistochemical staining

Equipment

- Microscope slides
- Microscope coverslips
- Hydrophobic pen
- Light blocking container
- Glass pipettes (flamed tipped)

Reagents

- Primary and secondary antibodies of interest
- PBS
- Clear nail polish
- 0.01% (single fibers) or 0.05% (muscle sections) tritonX-100

Protocol – single fibers

1. Using a hydrophobic pen, outline the perimeter of the microscope slide to create a barrier
2. Place several drops of PBS on to slide and transfer desired amount of fixed single fibers (approximately 8-10)
3. Remove PBS with a 200μL pipette and add approximately 2mL of 0.01% tritonX-100
    a. Incubate for 10 min to permeabilize
4. Wash fibers with PBS by removing and then re-adding PBS until all triton has been removed
5. Incubate with primary antibody for desired length of time
    a. For proximity ligation assay (PLA), both α- and βII-tubulin primary antibodies were incubated for 4 hours at room temperature RT) followed by a wash as outlined in step 4 and incubation with VDAC2 primary antibody overnight at 4°C
    b. For PLA protocol stop here and see section A3.1 – 3.3
6. Wash fibers as indicated in step 4
7. Incubate with secondary antibody for 1 hour RT
    a. For fluorescent secondary's, ensure slides with fibers are kept out of the light.
8. Wash fibers as indicated in step 4
9. Using a 200μL pipette, remove all liquid from microscope slide and carefully use a kim wipe to remove remaining access liquid.
10. Pipette 2.5-5μL of anti-fade reagent over each fiber
11. Gently place coverslip over fibers
12. Secure with nail polish and let dry overnight
13. Images should be acquired within ~2weeks of staining.

A3.1 Histology – Immunohistochemical staining: Proximity ligation assay: Rat single fibers

Reagents

- Proximity ligation assay kit including
    - Plus, and minus probes – matching primary antibodies
    - Antibody diluent
    - Detection reagents
    - Wash buffers A and B

Equipment

- Incubator maintained at 37°C

Protocol

1. Follow protocol "A3 – immunohistochemical staining" stopping at step 5 to prepare for PLA
2. Following incubations with primary antibodies, wash fibers 3x with buffer A
3. Incubate fibers with both plus and minus probes (1:10 dilution) diluted with antibody diluent (provided in kit) for 1 hour in incubator
4. Wash fibers with 3x in buffer A
5. Prepare ligation buffer
    a. Dilute 5x ligation buffer with ddH_2O)
    b. Add ligase (1:40 dilution) *vortex buffer to ensure it is well mixed
6. Incubate with ligation buffer for 30min in cubator
7. Wash fibers 3x 5minutes with buffer A
8. Prepare amplification buffer
    a. Dilute 5x amplification buffer with ddH2O
    b. Add polymerase (1:80) * vortex buffer to make sure it is well mixed
9. Incubate fibers with amplification buffer for 1 hour and 40 min in an incubator
    a. Protect fibers from light from this point
10. Wash fibers 2x 4minutes with Buffer B
    a. Dilute a small about of Buffer B to make 0.5% Buffer B
11. Wash fibers with 0.5% Buffer B 1x for 5 minute
12. Using a 200µL pipette, remove all liquid from microscope slide and carefully use a kim wipe to remove any remaining liquid.
13. Pipette 2.5-5µL of anti-fade reagent over each fiber
14. Gently place coverslip over fibers
15. Secure with nail polish and let dry overnight
16. Images should be acquired within ~2weeks of staining.

A3.2 Histology – Immunohistochemical staining: Proximity ligation assay: Rat sectioned muscle

Reagents

- Proximity ligation assay kit including
    - Plus, and minus probes – matching primary antibodies

    - Antibody diluent
    - Detection reagents
    - Wash buffers A and B
- 4% Paraformaldehyde
- hydrophobic pen
- 0.5% triton X-100

Equipment

- Incubator maintained at 37°C

Protocol

1. Thaw frozen muscle sections for 15 minutes RT
2. Outline squares with a hydrophobic pen around each or all sections
3. Pipette 4% paraformaldehyde over each section, ensuring to cover the entire fiber and let fix for 1 hour RT
4. Wash fiber 3x 5min with PBS
5. Follow protocol "A3 – immunohistochemical staining" stopping at step 5 to prepare for PLA
6. Following incubations with primary antibodies, wash fibers 3x with buffer A
7. Incubate fibers with both plus and minus probes (1:7.5 dilution) diluted with antibody diluent (provided in kit) for 1 hour in incubator
8. Wash fibers with 3x 10minutes in buffer A
9. Prepare ligation buffer
    a. Dilute 5x ligation buffer with ddH_2O)
    b. Add ligase (1:40 dilution) *vortex buffer to ensure it is well mixed
10. Incubate with ligation buffer for 1 hour in an incubator
11. Wash fibers 3x 10 minutes with buffer A
12. Prepare amplification buffer
    a. Dilute 5x amplification buffer with ddH2O
    b. Add polymerase (1:80) * vortex buffer to make sure it is well mixed
13. Incubate fibers with amplification buffer for 2 hour and 30 min in an incubator
    a. Protect fibers from light from this point
14. Wash fibers 3x 10 minutes with Buffer B
    a. Dilute a small about of Buffer B to make 0.5% Buffer B
15. Wash fibers with 0.5% Buffer B 3x 5 minutes
16. Using a 200µL pipette, remove all liquid from microscope slide and carefully use a kim wipe to remove any remaining liquid.
17. Pipette 2.5-5µL of anti-fade reagent over each fiber
18. Gently place coverslip over fibers
19. Secure with nail polish and let dry overnight
20. Images should be acquired within ~2weeks of staining.

A3.3 Histology – Immunohistochemical staining: Proximity ligation assay: Mouse single fibers

Reagents

- Proximity ligation assay kit including
    - Plus, and minus probes – matching primary antibodies
    - Antibody diluent
    - Detection reagents
    - Wash buffers A and B
- hydrophobic pen
- 0.5% triton X-100

Equipment

- Incubator maintained at 37°C

Protocol

1. Follow protocol "A3 – immunohistochemical staining" stopping at step 5 to prepare for PLA
2. Following incubations with primary antibodies, wash fibers with buffer A
3. Incubate fibers with both plus and minus probes (1:10 dilution) diluted with antibody diluent (provided in kit) for 1 hour in incubator
4. Wash fibers with in buffer A
5. Prepare ligation buffer
    a. Dilute 5x ligation buffer with ddH_2O)
    b. Add ligase (1:40 dilution) *vortex buffer to ensure it is well mixed
6. Incubate with ligation buffer for 30 minutes in an incubator
7. Wash fibers 3x 5 minutes with buffer A
8. Prepare amplification buffer
    a. Dilute 5x amplification buffer with ddH_2O
    b. Add polymerase (1:80) * vortex buffer to make sure it is well mixed
9. Incubate fibers with amplification buffer for 1 hour and 40 min in an incubator
    a. Protect fibers from light from this point
10. Wash fibers 3x 5minutes with Buffer B
    a. Dilute a small about of Buffer B to make 0.5% Buffer B
11. Wash fibers with 0.5% Buffer B 1x 1 minute
12. Using a 200µL pipette, remove all liquid from microscope slide and carefully use a kim wipe to remove any remaining liquid.
13. Pipette 2.5-5µL of anti-fade reagent over each fiber
14. Gently place coverslip over fibers
15. Secure with nail polish and let dry overnight
16. Images should be acquired within ~2weeks of staining.

A4. Permeabilized muscle fiber bundle (PmFB) preparation

Equipment

- Ice blocks
- Dissecting microscope
- Anti-magnetic fine tipped forceps (1 large, 1 small)
- 18mm cell culture dish
- 1.5ml tubes
- gel loading tips

Reagents

- Biops buffer
- MIR05 buffer
- saponin

Protocol

1. Prepare a Styrofoam container with ice and 5ml tubes filled with biops buffer (see section for preparation instructions)
2. Prepare 40μg/ml saponin dissolved in biops (saponin tubes)
    a. Dilute 7μL of 10mg/mL saponin into 1.5mL of biops
3. Prepare equal amounts of 1.5mL tubes 1) with 40μg/mL saponin + biops and 2) MIR05 buffer (see section for preparation instructions) (wash tubes)
4. Harvest tissue and immediately submerge into ice cold biops buffer
5. Decant tissue with biops into a 18mm dish and place on an ice block under a dissecting microscope
6. Cut all connective tissues and remove blood and fat
7. Gently begin separating fibers ~1-3mg wet weight fiber bundles
8. Place muscle bundles into saponin tubes and rock at 4°C for 30 minutes
9. Transfer permeabilized muscle fiber bundles (PmFB) to wash tubes and rock at 4°C for 15 minutes
10. PmFB are ready for bioenergetic assays
    a. See appendix for respiration experimental protocols (A4.1) and buffer preparation (A4.2-A4.3)
    b. See appendix for H_2O_2 emission experimental protocols (A4.4) and buffer preparation (A4.5 – 4.8)
    c. See appendix for calcium retention capacity experimental protocols (A4.7) and buffer preparation (A4.8)

A4.1 Sample respiration protocol

Sample respiration protocol				
Substrate	**Event Code**	**STOCK**	**Titration Volume (µl)**	**Final Concentration in chamber**
Miro5 BLEB Lights out Fibre	 5uM BLEB F10 Fibre	20mM Cr 10mM	1uL	5uM
Stop stir bar, turn on lights and verify fibre is in chamber/not stuck on side wall **Hit F10 (Lights out)**				
100% O_2	O		Injection	325-350 µM
Pyruvate Malate	P M	**2M** **1M**	**5** **4**	5 mM 2 mM
ADP	25 µM D	**5 mM**	**10**	25 µM D
ADP	50 µM D	**5 mM**	**10**	50 µM D
ADP	100 µM D	**50 mM**	**2**	100 µM D
ADP	250 µM D	**50 mM**	**6**	250 µM D
ADP	500 µM D	**50 mM**	**10**	500 µM D
ADP	5 mM D	**500 mM**	**18**	5 mM D
Cytochrome c oxidase	Cyt C	**4mM**	**5**	10uM
Glutamate	GLU	**2M**	**5**	5mM
Succinate	Succ	**2M**	**20**	20mM

A4.2 Biops Buffer

Chemical	Stock Solution	Molecular Weight	Final Concentration	Addition to *2 Litre* final volume
CaK_2EGTA*	100mM		2.77mM	55.4mL
K_2EGTA*	100mM		7.23mM	144.6mL
Na_2ATP		555.1	5.77mM	6.28g
$MgCl_2 \bullet 6H_2O$		203.3	6.56mM	2.67g
Taurine		125.1	20mM	5.02g
Na_2Phosphocreatine		327.14	15mM	9.81g
Imidazole		68.1	20mM	2.72g
Dithiothreitol (DTT)		154.2	0.5mM	0.154g
MES Hydrate		195.2	50mM	19.52g

** prepare stock solutions (see instructions below)*

CaK_2EGTA: Dissolve 2.002g $CaCO_3$ in 100mM hot (80°C) solution of EGTA (7.608g of EGTA in 200mL ddH_2O). Add 2.3g of KOH and adjust pH to 7.0 using KOH. Freeze unused portions

K_2EGTA: dissolve 7.608g EGTA and 2.3g KOH into 200mL ddH_2O. Adjust pH to 7.0 using KOH. Freeze unused portions

Protocol

1. Add approximately 1500mL of ddH_2O to 2000mL beaker
2. While constantly stirring add stock solutions of CaK_2EGTA and K_2EGTA
3. Weigh and add all powder chemicals
4. Adjust pH to 7.1 using KOH pellets
5. Using graduated cylinder, bring total volume to 2000mL
6. Filter and then aliquot into 50mL falcon tubes
    a. Leave some room at the top of the tube to allow for expansion when buffer is freezing
7. Freeze falcon tubes

A4.3 MiRO Buffer

Chemical	Stock Solution	Molecular Weight	Final Concentration	Addition to *2 Litre* final volume
EGTA		380.4	0.5mM	0.38g
$MgCl_2 \bullet 6H_2O$		203.3	3mM	1.22g
K-Lactobionate*	0.5M	358.3 free acid	60mM	240mL
Taurine		125.1	20mM	5.02g
KH_2PO_4		136.1	10mM	2.72g
HEPES		238.3	20mM	9.54g
Sucrose		342.3	110mM	75.3g
BSA		154.2	1g/L	2g

** prepare stock solution (see instructions below)*

K-Lactobionate: Dissolve 71.6g lactobionic acid in 300mL ddH_2O, adjust pH to 7.0, adjust final volume to 400mL with ddH_2O

Protocol

1. Add approximately 1500mL of ddH_2O to 2000mL beaker
2. While constantly stirring add stock solution of K-Lactobionate
3. Weigh and add all powder chemicals
4. Adjust pH to 7.1 using KOH pellets
5. Using graduated cylinder, bring total volume to 2000mL
6. Filter and then aliquot into 50mL falcon tubes
    a. Leave some room at the top of the tube to allow for expansion when buffer is freezing
7. Freeze falcon tubes

A4.4 Sample H_2O_2 protocol

Treatment in Saponin Solution	In Cuvette Prior to Experiment	Volume to Add	Substrate added to induce H_2O_2	Volume to add
NONE	Amplex Red 0.2U/mL HRP	1mL 2uL of 10U/ml	10mM Succinate	5µL of 2M
Mouse: 35µM CDNB Rat: 100µM CDNB	Amplex Red 0.2U/mL HRP 0.5uM Rotenone	1mL 2uL of 10U/ml 2uL of 250uM	10mM Pyruvate	5µL of 2M
Mouse: 35µM CDNB Rat: 100µM CDNB	Amplex Red 0.2U/mL HRP	1mL 2uL of 10U/ml	10mM Pyruvate 2mM Malate	5µL of 2M 2µL of 1M

ADP titration		
Final concentration	**Amount to add**	**ADP stock**
15uM	3ul	5uM ADP
50uM	7uL	5uM ADP
100uM	1uL	50uM ADP
250uM	3uL	50uM ADP
500uM	5uL	50uM ADP

A4.5 Buffer Z

Chemical	Molecular weight	Final concentration (mM)	Addition to 500mL final volume (g)
K-MES	233.33	105	12.26
KCL	74.55	30	1.12
KH_2PO_4	136.08	10	0.7
$MgCL_2$ $6H_2O$	203.3	5	0.51
EGTA	380.35	1	0.19
BSA		5mg/mL	2.5

Protocol

1. Add ` 400mL of ddH2O to 1000mL beaker
2. Weigh and add powder chemicals
3. Adjust pH to 7.4 using KOH pellets
4. Using graduated cylinder, bring total volume to 500mL
5. Filter and then aliquot into 50mL falcon tubes
    a. Leave some room at the top of the tube to allow for expansion when buffer is freezing
6. Freeze falcon tubes

A4.6 Amplex ultra Red buffer preparation

Stock A = Amplex ultra red without creatine Stock B = Amplex ultra red + 20mM creatine

Stock A and B ingredients required:

Amplex Ultra-Red (Invitrogen A36006)
5000 IU/ml Cu/Zn Superoxide dismutase (SOD1; Sigma S9697)
10mM Blebbistatin (BLEB; Cayman)
DMSO
Buffer Z (0.5mg/ml BSA)
0.5M EGTA (aliquots in freezer)

Stock B additional ingredients:

20mM Creatine hydrate

Final concentrations for both AUR Stock A and AUR Stock B:

10μM AUR
1μM BLEB
25U/ml Cu/Zn SOD1
1mM EGTA

Work fairly quickly given AUR and BLEB should not be stored on ice. Best to prepare with lights out in lab as AUR and BLEB are light sensitive.

Preparation of AUR Stock A (No Creatine):

Step 1: Prepare 5mM AUR. Add 666.6ul of DMSO to 1mg AUR. Vortex gently. Prepare in black tube but do not place on ice (DMSO will freeze).

Step 2: Prepare 10mM BLEB. Add 1.71 mL DMSO to 5mg bottle of BLEB. Prepare in black tube but do not place on ice.

Step 3: Prepare 10uM AUR stock. Mix the following:

- 160.6 ml of Buffer Z (0.5mg/ml BSA). Note: sucrose buffers lower oxidant emission.
- 325μL of 5mM AUR
- 812.5μL of 5000 IU/ml SOD1
- 16.24μL of 10mM BLEB
- 325μL of 0.5M EGTA

Aliquot 1.050 μL in black tubes. Store at -80°C.

Preparation of AUR Stock B (20mM Creatine):

Prepare 10μM AUR stock as in Stock A but with 20mM creatine monohydrate. Mix the following:

- 160.6 ml of Buffer Z (0.5mg/ml BSA)
- 484.74 mg creatine monohydrate
- 325μL of 5mM AUR
- 812.5μL of 5000 IU/ml SOD1
- 16.24μL of 10mM BLEB
- 325μL of 0.5M EGTA

Aliquot 1.050 μL in black tubes. Store at -80°C.

A4.7 Calcium retention capacity – sample protocol

Substrate	Stock Concentration	Addition to cuvette	Final Concentration in Cuvette
CRC Assay Buffer		300µL	
Glutamate	2M	1.5µL	10mM
Malate	1M	1.5µL	5mM
** make sure fibre is at the bottom of cuvette attached to stir bar**			
Collect 400 second background to establish "F-Min"			
$CaCl_2$	5mM	2.5µL	8nmol
Wait 5 minutes or until steady state			
$CaCl_2$	5mM	1.25µL	12nmol (4nmol pulse)
Wait 5 minutes in between pulses and continue pulsing until pore opens			
$CaCl_2$	50mM	3µL	0.5mM Pulse (F-Max)
Wait 3 minutes before final addition, this should establish F-Max but last addition is to make sure			
$CaCl_2$	50mM	3µL	0.5mM Pulse (F-Max)

A4.8 Buffer Y

Chemical	Final Concentration	Addition to *500mL* final volume
Sucrose	250mM	42.78g
Tris-HCl	10mM	0.788g
Tris Base	20mM	1.21g
KH_2PO_4	10mM	0.68g
BSA	0.5mg/mL	0.25g

**Due to high sugar content buffer may being to precipitate within 3-4 weeks, even when stored at 4°C. Be sure to check buffer periodically to insure clarity

Protocol

1. Add 300mL of ddH_2O to 1000mL beaker
2. Weigh and add powder chemicals
3. Using graduated cylinder, bring total volume to 500mL
4. Filter and store at 4°C

Calcium retention capacity assay buffer

Chemical	Final Concentration	Addition to *120mL* final volume
Buffer Y (freshly made)		120mL
Creatine	20mM	0.358g
EGTA	40uM	9.6µL of 0.5M
2-Deoxyglucose	5mM	0.0984g
Hexokinase	2U/mL	160µL of 1500U/mL
BLEB	5µM	60µL of 10mM
Calcium Green*	1µM	400µL of 0.3mM
Tharpsigargin**	2µM	160µL of 1.5mM

Protocol

1. Dissolve 0.5mg calcium green-5N in 1.398mL water
2. Add 100mL of ddH_2O to 200mL beaker
3. Weigh and add powder and liquid chemicals
4. Bring to volume with ddH_2O
5. aliquot into 165µL stocks and freeze

A5 Western blotting – Tissue homogenization

Equipment

- 1.5mL tubes
- motor and pestle
- centrifuge

Reagents

- CHAPS buffer (see A8.3 for buffer ingredients)
- Phosphatase inhibitor cocktail 2 and 3
- Protease inhibitor cocktail

Protocol

1. Chip ~15-20mg of frozen muscle tissue (on liquid nitrogen) and weigh
2. Prepare a 1.5mL tube with 200µL of Chaps buffer with:
    a. Phosphatase inhibitor 2 (1:100)
    b. Phosphatase inhibitor 3 (1:100)
    c. Protease inhibitor (1:200)
3. Add weighed muscle to tube and correct volume to match (20mg of tissue:400µL buffer) dilution
4. Homogenize with a motorized Teflon pestle 3x 10 seconds with 10 second rests
    a. **always maintain on ice during homogenization
5. Centrifuge samples at 1500g for 10 minutes at 4°C
6. Collect supernatant and store samples at -80°C

A5.1 Western blotting

Equipment

- Thick and thin glass plates
- Green stands
- Gel holder cassetts + foam

Reagents

- See appendix (A8.1) for buffer recipes

Protocol

1. Place clean plates washed in methanol in green stands on foam and make sure there is a tight seal
2. Prepare running gel (1 column makes 2 gels) ***DO NOT ADD TEMED UNTIL READY TO LOAD***
3. Using transfer pipette transfer running gel (with TEMED) until top of green door
4. Using new transfer pipette on opposite end of plate add water to top of plate removing any bubbles
5. Let set until left over running gel is hard
6. Make Stacking Gel ***DO NOT ADD TEMED UNTIL READY TO LOAD***
7. Make 1X RUNNING BUFFER (990mL dH_20, 110mL 10X Running Buffer) in graduated cylinder
8. Go get samples in liquid nitrogen and thaw on ice
9. Turn on heat block to 95°C
10. After 30 minutes, turn over gel holder to remove excess water, using square paper towel remove water from corner of gel and wipe plate clean
11. Using Transfer pipette add stacking gel (with TEMED) to top of plate
12. Insert comb starting from one end on angle, careful of splash
13. Let set until left over stacking gel is hard
14. Put standard on bench
15. Vortex thawed samples
16. In fumehood mix Laemmeli's buffer and 2-mercaptoehtanol (100ul 2-mer: 900uL Lam)
17. In new labeled tubes mix given quantites of water, Lam buffer mix and protein (see excel sheet)
18. Boil for 5 minutes in heat block
19. Remove combs from gels and transfer to tank
20. Fill holders with 1X Running Buffer and then tank
21. Load wells with given volume based on excel sheet with standard in first well always
22. Put lid on at set volts to 1**60** and time to **40 min**, press run
23. Transfer Gels following steps
24. Block for 1 hour at room temp in 15ml Odyssey Blocking Buffer (50% BB,50%TBS)
25. Pour out blocking buffer into falcon tube and keep in fridge
26. Cover membrane in Primary in fridge overnight
27. Do 4x5min washes in TBST
28. Cover membrane box in foil and wash in secondary at room temp for 1 hour
29. 4x5min washes in TBST

30. Rinse in TBS then pour out and put fresh TBS to detect

A5.2 Western blotting: Buffer preparation

10 X Running Buffer:

	500 ml	**1 L**	**2 L**
Tris	15 g	30 g	60 g
Glycine	72 g	144 g	288 g
SDS	5 g	10 g	20 g

1 X Running Buffer: 10 X Running buffer 100 ml
dH_2O 900 ml

---

10 X Western Transfer Buffer:

	500 ml	**1 L**
Glycine	52.5 g	105 g
Tris Base	22.5 g	45 g

1 X Western Transfer Buffer: 10 X Tranfer buffer 80 ml
Methanol 160 ml
dH_2O 560 ml

---

10 X TBS (Tris Buffered Saline):

	500 ml	**1 L**
Tris	12.1 g	24.2 g
NaCl	40 g	80 g
Adjust to pH 7.6 with HCl		

1 X TBST:

	1 L	**2 L**
10 X TBS	100 ml	200 ml
dH_2O	900 ml	1800 ml
Tween 20	1ml	2 ml

Note: Ensure solution is stirring when adding Tween

Primary antibody preparation
- Blocking Buffer
- .1% Tween
- .01% SDS

Secondary antibody preparation
- Blocking Buffer
- .1% Tween

- .01% SDS

Running and stacking gel preparation

	Stacking	**Running**				
		5%	**6%**	**8%**	**10%**	**12%**
dH_2O	6.8 ml	11.4	10.6 ml	9.4 ml	8 ml	6.7 ml
1.5M Tris-Base, pH 8.8	***	5 ml	5 ml	5 ml	5 ml	5 ml
1M Tris-HCl, pH 6.8	1.25 ml	***	***	***	***	***
30 % Acrylamide	1.70 ml	3.4 ml	4 ml	5.3 ml	6.7 ml	8 ml
10 % SDS	100 µl	200 µl	200 µl	200 µl	200 µl	200 µl
10 % APS	100 µl	200 µl	200 µl	200 µl	200 µl	200 µl
Temed	**20 µl**	**20 µl**	**20 µl**	**20 µl**	**20 µl**	**20 µl**

A6. Caspase activity assay

Equipment

- 1.5mL tubes
- Motorized Teflon pestle
- Centrifuge

Reagents

- Caspase 3: AC-DEVD-AMC (Enzo - ALX-260-031-M001)
    - 1mg into 1.48 mL DMSO for 1mM Stock
- Caspase 3 Inhibitor: AC-DEVD-CHO (Enzo - ALX-260-030-M001)
    - 1mg into 2mL DMSO for 1mM Stock
- Caspase 8: AC-IETD-AMC (Enzo - ALX-260-042-M001)
    - 1mg into 1.48 mL DMSO for 1mM Stock
- Caspase 8 Inhibitor: AC-IETD-CHO (Enzo - ALX-260-043-M001)
    - 1mg into 2mL DMSO for 1mM Stock
- Caspase 9: AC-LEHD-AMC (Enzo - ALX-260-080-M001)
    - 1mg into 1.45 mL DMSO for 1mM Stock **different MW from 3 and 8
- Caspase 9 Inhibitor: AC-LEHD-CHO (Enzo - ALX-260-079-M001)
    - 1mg into 1.86mL DMSO for 1mM Stock
- Caspase homogenization buffer (see A9.2 for buffer ingredients)
- Caspase incubation buffer (see A9.2 for buffer ingredients)

Protocol

1. Homogenize ~15-20mg of frozen tissue with motorized Teflon pestil for 3x 10 seconds with 10 seconds rests inbetween
    a. Prepare 1.5mL tube with ~75µL of caspase homogenization buffer and then add weighed tissue
    b. Bring to final volume based on tissue weight (10:100)
2. Centrifuge samples at 4°C
    a. Spin at 700x g for 10 minutes and retain supernatant
    b. Spin at 16300x g for 20 minutes and retain supernatant (**this fraction contains proteasomes)
3. Aliquot samples and store at -80°C
    a. Thaw each sample only once
4. Determine protein concentration with the reducing agent compatible kit
5. Dilute 1mM stock of each substrate into 100µM using incubation buffer – make up total volume needed for all samples plus 20µL extra (see loading table in excel)
6. Add 30ug of protein from frozen and spun homogenate into the wells (total of 6 wells for each sample)
7. Add x µl of diluted substrate (110- amount added for 30ug protein) for Caspase 3 to 2 wells
8. Repeat step 3 using Caspase 8 and Caspase 9 substrate
9. Add 3uL of Caspase 3 inhibitor to 1 of 6 wells
10. Repeat step 5 for Caspase 8 and 9 inhibitor
11. Read every 2 minutes for 1 hour

a. Excitation = 360nm, emission = 460nm at 37°C

A6.1 Caspase homogenization buffer

Chemical	Molecular Weight	Concentration	Amount added
Sucrose	342.3	250 mM	42.8g
Tris	121.14	50 mM	3.03g
DTT	154.25	1 mM	0.077g
EDTA	372.24	1 mM	0.186g
$MgCl_2$	203.3	5 mM	0.51g
Glycerol		10%	50mL

**total volume = 100mL

A6.2 Caspase incubation buffer

Chemical	Molecular Weight	Concentration	Amount added
HEPES	283.3	100 mM	2.38g
Sucrose	342.3	10%	10g
DTT	154.25	1 mM	0.015g

**total volume = 100mL

A7. Rat *In-vivo* muscle function system – Plantar flexion hind-limb force production

Equipment

- Aurora scientific 1305A: 3-in-1 whole animal system – Rat
    - 305C-FP: Dual-mode footplate
    - 605A: Dynamic muscle data acquisition and analysis system
    - 608C: LCD monitor
    - 701C: Electrical stimulator and micro-electrodes
    - 806D: In-situ rat apparatus
- Clippers
- Medical gauze

Reagents

- Iodine solution (Providone-iodine)
- Saline
- Isoflurane

Protocol

1. Anaesthetize rat with 5% isoflurane and maintain at 3%
    a. Throughout entire procedure ensure body temperature is maintained at 37°
2. Shave entire hind-limb with clippers and sterilize with iodine solution (3x washes with saline)
3. Secure foot to footplate with tape, adjust and secure knee at 90°
    a. Ensure heel is flush to the bottom of the footplate and the foot is extremely secured. Monitor foot/heel and knee placement during protocol.
4. Place electrodes as shown in image below

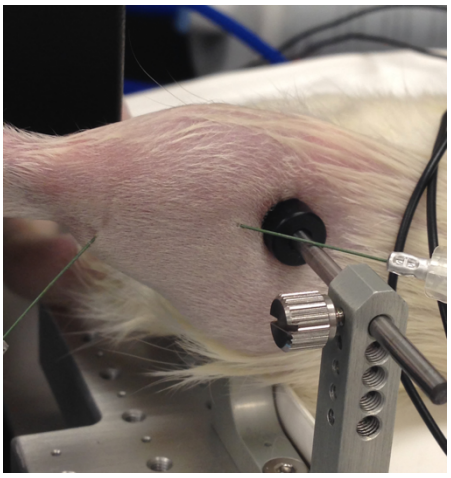

** electrode placement requires optimization to ensure user consistency. Recommend practicing entire protocol for minimum 1 week to determine whether consistent results are obtained.

5. Determine twitch and length

    a. Run twitch stimulation and adjust amperage and length to ensure all muscle fibers are recruited
    b. Should obtain 3 consecutive maximal twitches
6. Run Torque frequency protocol
    a. 25, 50, 75, 100, 125, 150, 175, 200, 225, and 250 Hz
    b. Rest for 10 minutes
7. Determine maximum torque
8. Run fatigue protocol
    a. Rest for 15 minutes total: measure max torque at 5, 10 and 15 minutes

**Torque protocol

- Pulse width: 0.2ms, train duration: 300ms, delay: 200ms

**Fatigue protocol

- Frequency: 60Hz/second for 120 seconds, stimulation: 300ms with 700ms rest at 119 repeats